

AEROSOLS IN THE TROPICAL MIDDLE ATMOSPHERE

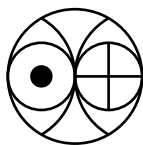
A Thesis Submitted to
The Maharaja Sayajirao University of Baroda

for

THE DEGREE OF DOCTOR OF PHILOSOPHY
IN
PHYSICS

by

S. RAMACHANDRAN

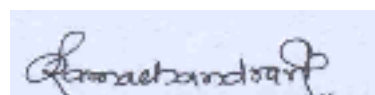


PHYSICAL RESEARCH LABORATORY
AHMEDABAD 380 009
INDIA

NOVEMBER 1995

CERTIFICATE

I hereby declare that the work presented in this thesis is original and has not formed the basis for the award of any degree or diploma by any University or Institution.

A handwritten signature in black ink on a light blue rectangular background. The signature appears to be 'S. Ramachandran' in a cursive script.

S. Ramachandran

(Author)

Certified by:

Dr. A. Jayaraman

(Guide)

Physical Research Laboratory

Ahmedabad 380 009, India.

Dr. (Ms.) M. S. Shah

(Co-Guide)

The M. S. University of Baroda

Baroda 390 002, India.

For
my sweet and loving Mom
and
the cherished memory of my Dad

Contents

Acknowledgements	iv
Abstract	vii
1 Introduction	1
1.1 Atmospheric aerosols: Classification, production and removal processes and effects	1
1.2 Need for aerosol studies	4
1.3 Importance of tropical aerosols	6
1.4 Indian scene	7
1.5 Objective and Scope of the present investigation	8
2 Physical and Optical properties of aerosols	10
2.1 Size distributions	10
2.1.1 Junge power law size distribution	11
2.1.2 Lognormal distribution	12
2.1.3 Modified Gamma distribution	14
2.2 Optical properties	16
2.2.1 Scattering processes	16
2.2.2 Mie scattering	17
2.2.3 Mie scattering of individual particle	19
2.2.4 Angular distribution of the scattered light intensity of single particle	22
2.2.5 Mie scattering for many particles	23
2.2.6 Size range of aerosols for optical investigations	30
2.2.7 Spectral dependence of aerosol extinction coefficients and its dependence on relative humidity	31

3	Tropospheric aerosols	35
3.1	Introduction	35
3.2	Ground based Sun-tracking photometer observations over Ah- medabad	38
3.2.1	Instrumentation	38
3.2.2	Theory	40
3.2.3	Experiment and Data analysis	42
3.2.4	Determination of $I_o(\lambda)$ and Optical depth τ	44
3.3	Results and Discussion	48
3.3.1	Diurnal, day to day and monthly variations in aerosol optical depths over Ahmedabad	48
3.3.2	Spectral dependence of aerosol optical depth	53
3.3.3	Variations in wavelength exponent α	55
3.3.4	Variations in ozone optical depth	56
3.3.5	Variations in aerosol optical depth with relative humidity and temperature	57
4	Stratospheric aerosols	60
4.1	Formation, Physical, Chemical, Radiative and Optical effects	60
4.2	Volcanic aerosols: An assessment of the effects	64
4.3	Measurement techniques	70
4.4	Balloon-borne optical studies of Pinatubo aerosols over tropical India	73
4.4.1	Instrumentation	74
4.4.2	Experiment	77
4.5	Results and Discussion	81
4.5.1	Aerosol extinction coefficients	81
4.5.2	Aerosol number density and size distribution parameter	87
4.5.3	Ångström coefficient	91
4.5.4	Mode radius	93
4.5.5	Asymmetry factor	95
4.5.6	Mass density of Pinatubo aerosols	100
4.5.7	Comparison of Pinatubo results with previous major eruptions	100
4.5.8	Synthesis of results	102
4.6	Nd:YAG backscatter lidar measurements	106
4.6.1	Lidar system specifications and Data collection	106
4.6.2	Data analysis	109

4.6.3	Lidar observations	110
4.7	Results and Discussion	110
4.7.1	Scattering ratios	110
4.7.2	Aerosol extinction coefficients	111
4.7.3	Decay of Pinatubo aerosol layer mass	114
4.7.4	Aerosol mass decay at three stratospheric altitude regions	117
4.7.5	Peak scattering ratio	118
4.7.6	Comparison of results with El Chichon data	119
4.8	Modeling studies of aerosol characteristics	120
4.8.1	A brief survey of existing aerosol models	120
4.8.2	Aerosol microphysical processes responsible for the formation and decay of stratospheric aerosol layer	124
4.9	A time dependent stratospheric aerosol layer model: Present work	125
4.9.1	Model specifications	126
4.9.2	Results and Discussion	128
5	Summary and Scope for future work	135
5.1	Summary of results obtained	135
5.1.1	Tropospheric aerosols	135
5.1.2	Stratospheric aerosols	136
5.2	Scope for future work	139
5.2.1	Tropospheric aerosols	139
5.2.2	Stratospheric aerosols	140
	References	142
	List of Publications	159

Acknowledgements

At the outset, I wish to express my thanks and gratitude to Dr. A. Jayaraman under whose direction the work contained in this thesis has been carried out. His enthusiasm, positive outlook, encouraging attitude and meticulous guidance have made the years working with him pleasant and memorable. I am deeply grateful for all the knowledge and experience that I have gained from him during the course of this work through very many useful discussions and for his personal kindness at every stage.

I am grateful to Prof. B.H. Subbaraya, who is a great inspiration to me, for his guidance, encouragement and care and for many beneficial discussions throughout this work. His sincere advice on the many facets of life will go a long way in shaping my career.

It is a pleasure to thank Mr. Y.B. Acharya for his concern and encouragement throughout this work. I thank him for developing the instruments used for balloon-borne and ground based observations. I am immensely grateful for his help and cheerful presence during the balloon experiments and lidar observations. I wish to acknowledge Messrs. J.T. Vinchhi and S.M. Shukla for their involvement in the fabrication and testing of the payload. My special thanks are due to Mr. Vinchhi for his help during the balloon-borne and ground based observations.

I am profoundly thankful to Dr. M.S. Shah for her concern and encouragement throughout this work.

I thank Dr. Shyam Lal for the concern he showed about the progress of this work and my personal well-being. Many enlightening and delightful discussions I had with him still linger in my mind.

I was greatly benefitted by my working with Dr. B.R. Sitaram, a storehouse of knowledge, without whose help the model calculations presented in this thesis would not have been possible. I express my sincere thanks to him.

I accord my thanks to Profs. Harish Chandra and Vijay Kumar for their comments and remarks during my assessment reviews. I am grateful for the encouragement given to me during my Ph. D. tenure by Profs. R. Sridharan, J.N. Goswami, S.K. Bhattacharya, A.C. Das and R.K. Varma.

My interactions at various stages with the faculty members of our area Profs. R. Raghavarao, S.P. Gupta, Drs. G. Subramanian, D.K. Chakrabarty, H.S.S. Sinha, R. Sekar, K.P. Subramanian, S.A. Haider, Mr. R. Narayanan and with Prof. J.N. Desai, Drs. T. Chandrasekhar and N.M. Ashok were beneficial and I thank them for the same. I thank Profs. B.G. Anandarao, S. Krishnaswami, A.K. Singhvi, Dr. R. Ramesh and the late Mr. C.S.R. Murthy for their encouragement.

I thank all my area colleagues for providing me a pleasant working atmosphere during the course of this work. I acknowledge the secretarial assistance rendered by Messrs. N.P.M. Nair, Philip Samuel and N.R. Pillai.

I am indebted to the staff of the Hyderabad balloon facility for the successful balloon launches, in particular to Mr. M.N. Joshi, the Scientist-in-Charge and Messrs. R. Vasudevan and S. Sreenivasan. I thank Prof. S.V. Damle of Tata Institute of Fundamental Research and Mr. P. Rajaratnam of ISRO HQs for helping in various stages in planning and conduct of the balloon experiments.

My thanks are due to Dr. Sai Iyer for the knowledge I gained from his expertise in computers.

This acknowledgement would be incomplete if I do not recall with fond memory, the various other facilities that I have availed and the people associated with them. To mention a few, this includes Mr. Ghanashyam Dholakia, Mr. P.S. Shah and all other staff members of the computer centre, Mrs. Rhoda Bharucha, Mrs. Urmila Ghiya, Mrs. Rohini Patil and all other staff members of the library and Mr. D.R. Ranpura of the photography section. I remember them with deep gratitude for the support and service I have obtained from them during the course of my thesis work. The functional block diagrams found in this thesis are due to courtesy: Dr. A. Jayaraman and Mr. S.K. Bhavsar. I thank them for their sincere efforts.

Words are perhaps inadequate to express my thanks to my dear and wonderful friends Sam Ragland, Ravi Bhushan, Venkataramani, Krishnan, Gurubaran, Devashis Banerjee, Debasish Majumdar, Sivakumaran, Manish, Tarun, Santhanam, Janardhan and Seema, whose persistent cooperation and vivacious company was a source of strength, joy and refreshment. My friendship with them has been unique and unforgettable. I wish to place on record my thanks to all my other friends, to name a few, Subrat, Anjan, Pandey, Navin, Dipankar, Jitesh, Manohar Lal, Supriya, Srinivasan, Himadri, Vijaykumar, Dinanath, Biswajoy, Varun, Pallam Raju, Prahlad, Gautam, Mitaxi, Sushma, Poullose, Watson, Sandeep, Abhijit, Debabrata, Prashant, Biju, Prabir, Jyoti, Chetan, Ratan, Muthu, Anandmayee, Aparna, Nanda Kumar and Prosenjit, for their warm and affectionate company. Jagadheesha's efforts in data collection are greatly acknowledged.

My special thanks are due to my parents who by their relentless support, encouragement and understanding made it all possible. Letters from my mom showering love and affection had been inspiring me all through the years. I deeply express my thanks to my dad, who was more a friend, for his enthusiasm and patience, which have left a deep indelible impression in my mind. I am in dearth of words to thank my sisters Mrs. Visalakshi and Ms. Mathanghi

for their love and care and for being a source of emotional support through their letters. It is indeed a pleasure to thank my brother-in-law Mr. Karthikeyan and his family for the moral support and encouragement. I express my deep sense of gratitude to the families of my uncle Mr. Venkataraman, my sister Mrs. Rathna, my aunt Mrs. Jayanthi and my brother Mr. Ganesan for their boundless love and encouragement.

At times, if I was bored or felt lonely during my stay in Ahmedabad, it was due to being faraway from home. The long and beautiful letters from my nieces Padmapriya, Anupama, Jaishri, Kanchana, Chitra and my friend Chandra gave me the required pep and encouragement to work with renewed vigour and enthusiasm. I thank them for their untiring efforts. I thank all my relatives and family friends for their constant queries about the progress of my work and my well-being.

Abstract

Optical investigations using ground based and balloon-borne photometers and lidar are the means by which the present work on tropospheric and stratospheric aerosols is carried out and reported herein. The thesis focuses on the optical properties of tropospheric aerosols, their day to day and seasonal variations and of stratospheric aerosols, their formation, evolution and decay.

A quantitative treatment of the role of aerosols in the Earth-atmosphere system continues to be a challenging task because of the wide variety of aerosol particles exhibiting different optical properties and large variations in aerosol abundances over different geographical areas and with respect to seasons. The composition of the atmospheric aerosol is exceedingly complex and our knowledge of the physical and chemical properties, which govern the aerosol size distribution and concentration, is still poor, because the measurements exhibit a wide range of uncertainty. In recent years, there has been a significant activity in developing comprehensive global models based on the observed features of tropospheric and stratospheric aerosols. However, at low and equatorial latitudes, there has been a scarcity of data for a long time. Even if the data exist, the data will be available only on one parameter and other aerosol parameters have to be assumed or calculated on that basis and as many of the aerosol parameters are not directly related to each other, makes aerosol modeling a tough assignment. Ground based and balloon-borne measurements form the heart of this work, the results of which have given a comprehensive data set and enabled us to understand various aerosol properties in troposphere and in stratosphere and the relative importance of the various processes which control the size parameter and number density responsible for the formation of stratospheric aerosol layer and its decay. The results are useful in climate models and for modelers developing radiation parametrisation schemes to study quantitatively the impact of aerosols on the atmospheric radiation balance.

The thesis comprises of five chapters.

- Chapter 1 gives a background for the thesis. Description of aerosols, aerosol characteristics such as their sources, residence times, sinks and the effects are outlined. The present day understanding about aerosols is summarised. Some key issues relating to aerosols are discussed. The need for aerosol studies and the importance of tropical aerosols is stressed. A very brief history of Indian measurements is also outlined. The scope and the importance of

the present work is presented.

- Chapter 2 gives a general description of the various physical and optical properties of aerosols and their consequences which are covered in this work. Aerosol size distributions, results on Mie scattering theory both for a single aerosol particle and for an ensemble of particles representing an aerosol size distribution, extinction, scattering and absorption coefficients, important radius range for optical investigations, aerosol phase functions, asymmetry factor and single scattering albedo are explained and their importance is discussed in detail.

As the thesis is divided thematically, the following two chapters have in them the work done on tropospheric and stratospheric aerosols, alongside the instrumentation, data analysis and the results obtained.

- Chapter 3 deals with the features of aerosols over Ahmedabad observed with a Sun-tracking photometer. An automatic Sun-tracking photometer was developed and employed to measure the aerosol optical depths at selected wavelength bands. A brief description of the instrumentation, calibration procedure, measurements, data analysis and the results obtained on the diurnal, day to day and seasonal variations of aerosols observed over a period of 5 years, from 1991 to 1995 which covers the Gulf oil fires in early 1991 and Pinatubo eruption in mid-1991 are explained and discussed. From the measurements of transmitted solar radiation intensities the aerosol optical depths are obtained. The relation between the aerosol optical depths and other meteorological parameters is explored.

- Chapter 4 can broadly be classified on the basis of experimental and modeling work carried out by the author.

The experimental part describes the two high altitude balloon flights, conducted from Hyderabad during October 1991 and April 1992 to study the stratospheric aerosol layer formed due to Pinatubo volcanic eruption in June 1991. Sun-tracking and Sun-scanning photometers were employed onboard the balloons to measure the vertical profiles of direct and scattered solar radiation intensities. From the direct solar radiation intensities, the aerosol extinction coefficients, mode radius, mass of the layer and from the scattered radiation intensities the aerosol size parameter, number density and asymmetry factor are determined. A newly set up Nd:YAG lidar system is described and measurements conducted to study the Pinatubo

layer over Ahmedabad for over a period of 3 years from April 1992 to May 1994, data analysis, results obtained on scattering ratios, aerosol backscatter and extinction coefficients, the time evolution of the mass of the Pinatubo layer, peak scattering ratio and comparison of the results with El Chichon eruption are presented and discussed.

A simple model is developed to study the decay of volcanic aerosol layer formed at stratospheric altitudes and changes in the aerosol size distribution, taking into account the aerosol microphysical processes of growth, coagulation and sedimentation. Model results on the time evolution of aerosol optical depths at stratospheric altitudes, for different initial aerosol amounts, corresponding to eruptions of widely varying magnitudes are presented and discussed. The experimental lidar results obtained on Pinatubo (present work) and El Chichon (data available in literature) are compared with the model results and discussed.

- The summary of the results obtained and suggestions for future research are envisioned in Chapter 5.

Chapter 1

Introduction

Earth's atmosphere is predominantly a nitrogen-oxygen atmosphere, these two gases occupying about 99% by volume. A whole host of minor and trace constituents contribute to the remaining 1% which include argon, carbon dioxide, water vapour, ozone, methane, oxides of nitrogen, carbon monoxide, hydrogen sulphide, ammonia etc. which occur in minute quantities - parts per million to parts per trillion by volume and more importantly aerosols vie with each other in playing a vital role in determining the conditions on the Earth's surface and in the biosphere. In spite of their small proportion by volume the mankind is concerned about these minor constituents because of their distinctive but very important roles in the physico-chemical and related activities in the atmosphere. The sources and sinks of atmospheric particulate matter (*aerosols*), their physical and chemical properties and their residence times are of special interest, primarily because their size and composition can be readily noticed than gaseous pollutants and they are a link in the chain of the removal process which returns gaseous pollutants to the Earth's surface.

1.1 Atmospheric aerosols: Classification, production and removal processes and effects

Atmospheric aerosols are a mixture of solid or liquid particles suspended in the medium of air. Their physical (size, shape and texture) and chemical properties vary over a wide range and consequently their removal processes and hence their residence times vary greatly. Aerosol particles of different sizes and composition play a vital role in many atmospheric processes such as visibility, radiation balance, atmospheric electricity, air pollution, cloud formation etc. The sizes of aerosols extend over several orders of magnitude from $0.001\ \mu\text{m}$

to 100 μm , sweeping from a cluster of molecules at one end to hailstones at the other end. They are in general divided into three categories based on their sizes:

- (i) Aitken nuclei ($0.001 \mu\text{m} < r < 0.1 \mu\text{m}$)
- (ii) Large particles ($0.1 \mu\text{m} < r < 1.0 \mu\text{m}$)
- (iii) Giant particles ($r > 1.0 \mu\text{m}$)

Particles in the size range below 1.0 μm are formed mostly through gas-to-particle conversion process, while particles larger than 1.0 μm are formed directly by mechanical processes such as wind blown dust, sea salt droplets produced by breaking bubbles on the sea surface, pollen grains etc. The fine particles size mode (which incorporates both Aitken nuclei and large particles) is made up of two distinct populations. The particles at the lower end of the size spectrum (Aitken nuclei or transient nuclei) have a short residence time in the atmosphere as they are chemically active and also due to their physical mobility. These particles will eventually get transformed into 0.1 - 1.0 μm size particles, generally referred to as accumulation mode, through processes such as nucleation, condensational growth and coagulation. The coarse mode accommodates particles larger than 1.0 μm . The production source of aerosols determines the chemical composition while the formation mechanisms determine the size spectrum and shape of the particles. Chemical composition, size range and shape decide the ability of a particle to interact with electromagnetic radiation. The source strength of any particle determines by and large the importance of a component by virtue of its mass concentration and number density. The sources of aerosols can be classified into *primary* and *secondary*. The primary or direct sources which are mostly of natural origin include, the world oceans (covering two thirds of the Earth's surface, sea salt particles), arid and semiarid regions (wind blown soil dust), terrestrial biota (biological material of plant origin), smoke from burning of land biota and direct anthropogenic particle emissions, for example soot, smoke, road dust etc., terrestrial ejecta (volcanic effluvia, which includes direct particle emissions and products derived subsequently from reactions of emitted gases) and meteorites (extraterrestrial and interplanetary dust). The secondary or indirect source, which is the major source of particles below 1 μm in radius, is the conversion of the available natural and man-made atmospheric trace gases into solid and liquid particles. This process called as *gas-to-particle conversion mechanism* depends on a number of precursors which include sulphur and nitrogen bearing gases among others.

While due to above processes aerosols are incessantly created and transformed, the existing ones are also regularly removed from the atmosphere by a wide variety of dry and wet removal processes. Dry deposition include settling of particles by gravitation and impaction and diffusion of particles to surfaces and wet removal is by rainwash. The removal efficiencies are a function of the particle size. Hence when a specific aerosol is subjected to a large number of conversion and removal mechanisms which are size dependent, the overall residence time of that particle will be governed by the competing effects of all the conversion and removal processes acting on the particle. For particles in the size range of 0.01 to 10 μm the residence time in the lower troposphere is about a week, while in the upper troposphere they reside up to a few months. In stratosphere the residence time extends to few years. The variation in the residence times of aerosols with respect to altitude stems from a variety of factors, principal being the distribution of water vapour which affects conversion and removal processes and the vertical distribution of a number of reactant gases which include SO_2 , COS , CS_2 etc. The aerosol number density shows variations with altitude and as well with seasons in the troposphere. For example, over the Indian subcontinent, the aerosol number density in the lower troposphere is about a few thousands of particles during the pre-monsoon period, while after the monsoon their number is reduced to a few hundreds, due to rainwash. In the stratosphere, in volcanically quiescent i.e. background conditions the aerosol number density is about a few particles, while after major volcanic eruptions the number can go up by more than one order of magnitude. Most of the aerosols are concentrated between 0 and 35 km in the atmosphere, while the bulk of them are in the troposphere which vary with seasons and locations and subsequently produce regional effects, the stratospheric aerosols are longlived and can produce global effects.

The atmospheric aerosol plays a vital role, in many processes which impact our lives either directly (health) or indirectly (climate), the most obvious manifestation being haze. Scattering and absorption of solar radiation and the formation of clouds and fog by cloud condensation nuclei are of more fundamental importance. The aerosol particles by capturing the small ions influence the electrical conductivity of air.

The size distribution of stratospheric aerosols generally is a unimodal distribution as they are formed mainly due to gas-to-particle conversion mechanism, while the tropospheric aerosols are made up of two to three modes depending on their production environments i.e. whether urban, continental, maritime, desert etc. and are further influenced by meteorological phenomena. Thus as the properties of tropospheric aerosols are much more variable on

time and space scales because of the great diversity and wide distribution of sources and their short residence times, in many ways it is more difficult to study tropospheric aerosols than stratospheric aerosols, which have a residence time of about a few years.

1.2 Need for aerosol studies

The study on aerosols can be broadly classified into two leagues, though they are inter-related.

(i) As a group of atmospheric constituents that can be defined chemically and physically, aerosols themselves. Basic questions of characteristics of aerosols, their composition, their residence times, their major sources and sinks and their size distributions fall under this category. Just as in any other field of science, basic information about aerosols is warranted.

(ii) The other genre of study involves the associated processes of aerosols and their effects in the radiative transfer and climate.

Some key issues regarding aerosols and their effects about which the scientific community is apprehensive are as follows:

Recent study of *Charlson et al.* [1992] suggests that tropospheric aerosol, contributes substantially to radiative forcing and anthropogenic sulphate aerosol in particular has imposed a major perturbation to this forcing. This perturbation is comparable in magnitude to the current anthropogenic greenhouse gas forcing but opposite in sign. So it is essential to take aerosol effects into account while evaluating anthropogenic influences on past, current and future climate. As a number of aerosol related phenomena depend nonlinearly on aerosol concentrations, the influence of the anthropogenic aerosols depends nonlinearly on their emissions and their interactions with the natural background aerosol. Also as aerosols are shortlived in atmosphere unlike the principal greenhouse gases and as the aerosol forcing is greatest in daytime and in summer, whereas greenhouse forcing acts over the full diurnal and seasonal cycles, the anthropogenic aerosols perturb radiative forcing differently than greenhouse gases in many important ways. Some of the key questions which remain unanswered regarding the climatic influence of anthropogenic aerosol and its relation to the increased concentrations of greenhouse gases are, how these forcings compensate each other physically, altitudinally, geographically and temporally and to what degree, among others. In

addition to the tropospheric aerosols, as the concentration of sulphate aerosol in the lower stratosphere is also increasing due to aircraft emissions [Hofmann, 1990], sporadic volcanic eruptions etc., which inject lot of SO₂ into the stratosphere, stratospheric changes must also be taken into account while considering climate trends.

Recent model calculations by Alkezweeny [1995] on the anthropogenic sulphur dioxide emissions and sulphate concentrations indicate that the cooling effect of sulphate aerosols overwhelms the greenhouse warming. He also suggests that the increase in the sulphate aerosols of the past one hundred years may have caused a global cooling of about 2°C and he recommends more measurements of sulphate mass concentrations and cloud condensation nuclei to prove this trend. Kaufman *et al.* [1991] reached a similar conclusion from the analysis of fossil fuel and biomass burning impact on the global climatic change. Alkezweeny also established a nonlinear relationship between the sulphate concentration and sulphur emission and this nonlinearity was explained in terms of the difference in the tropospheric residence times of sulphur gases and aerosols. While SO₂ stays up to one to three days in the atmosphere, the aerosols in the size range of 0.1 - 1 μm in diameter can stay a week in the troposphere. It's important to mention that nearly all sulphate aerosols are in this size range [Whitby, 1978]. In the recent past during the post-industrial era, as the number of power plants and industry is on the rise and due to fossil fuel and biomass burning escalation, anthropogenic aerosols have increased near the source regions and majority of these aerosols are sulphate aerosols. A detailed analysis of temperature and aerosol emission records for large areas of the northern hemisphere indicates a persuasive evidence of aerosol cooling [Kerr, 1995] and the aerosol cooling effect is found to be strongest where aerosol pollution is heaviest and it changes with time depending on emissions. These results show that now there is a substantial evidence which points out a cooling effect due to aerosols and to assess and understand the regional and global climate changes, aerosols are an essential ingredient. In the light of these results now it has become clear that sulphate aerosols from volcanic eruptions and fossil fuel combustion exert a cooling influence on the climate. While this effect is an established one, estimates of magnitude, trends and extent of cooling effects are uncertain. This uncertainty mainly arises from limitations in the observations of aerosol amount and composition both in the troposphere and stratosphere globally, limitations in the models used to simulate the aerosol system and the indirect influence of sulphate aerosols in cloud extent and character.

Atmospheric aerosols affect indirectly the cloud microphysical characteristics. Cloud dro-

plets are formed in the lower atmosphere by condensation of water on existing aerosol particles. Sulphate aerosols, being water soluble, act as good condensation nuclei and seem to dominate the anthropogenic influence on cloud condensation nuclei. They take part in the cloud formation and wield an influence on the cloud droplet size distributions. By affecting the amount, type and distribution of clouds, aerosols could alter the radiation balance of the Earth.

Volcanic aerosols can cause warmings (of about 3-4°C) in the stratosphere primarily due to the absorption of upwelling terrestrial radiation and by reducing the amount of total solar radiation reaching the troposphere, can cause cooling (of about 0.5°C) globally [Ackerman, 1988] and also these aerosols by backscattering (as these aerosols are efficient scatterers but only weak absorbers at visible wavelengths) more amount of solar radiation into space, increase the planetary albedo. Major development during the recent years has been the finding of active participation of volcanic aerosols in heterogeneous chemistry, which accelerates stratospheric ozone depletion. Also the transport caused by heating of the aerosols and the resultant lofting of the stratospheric air mass has been identified as one of the key players in ozone depletion, in the post-volcanic period [Grant *et al.*, 1994]. Significantly the order of importance of these two phenomena is not yet ascertained. Though it was found initially that the processes which are responsible for ozone depletion in mid and higher latitudes [Hofmann and Solomon, 1989] are not active in the tropics, recent observations on ozone depletion in the tropics by Grant *et al.* [1992, 1994] and Hofmann *et al.* [1994] have proved the other way. The continued decrease of stratospheric ozone till mid-1992 (an year after Pinatubo eruption) raises a question whether the ozone loss mechanisms are continuing to operate or whether the ozone recovery mechanisms are not as rapid as had been estimated [Grant *et al.*, 1994], as tropics is the source region for ozone.

These issues can be addressed if a reliable data base exists, so that more realistic aerosol parameters can be used instead of scalable parameters while modeling as well as to assess the impact of these aerosols.

1.3 Importance of tropical aerosols

It has been shown that the tropical lower stratosphere and tropical tropopause are more sensitive to perturbation in radiative heating rates than at other latitudes [Ramaswamy, 1988a]. Further, arid and semiarid regions of the world, which are the major sources for the wind blown mineral particles and most of these regions lie along the tropical belt, making it im-

portant to study about these particles as well their transport inland. The optical properties of these particles can help in the assessment of their impact on the radiation balance and hence on climate.

Volcanic eruptions, though are a disaster for those living nearby, provide an exceptional opportunity for atmospheric scientists to understand the various processes involved in the formation of stratospheric aerosol layer, its decay and the climate effects and hence should be studied in greater detail as a valuable experiment on the nature and should be exploited as a natural resource to enhance our knowledge of the working of this complex atmosphere and climate system. Documentation of the scientific data and assessment of the impacts form the first crucial step in the process of evaluating the radiative, dynamical, chemical and climatic effects due to volcanic aerosols, to provide us with a glimpse into the future. As most of the active volcanoes lie along the tropical belt and also as the ejecta from an equatorial volcano can have a wider global coverage, the tropical stratosphere becomes a very vital region to study the optical and physical properties of volcanic aerosols.

1.4 Indian scene

Observations of solar radiation and atmospheric turbidity started in late 1950s in India during the International Geophysical Year (1957) using pyrhelimeters over Pune and Delhi [*Mani and Chacko*, 1963]. In the 1970s using Sun photometers haze extinction coefficients were obtained for over an year and turbidity coefficients and Ångström wavelength exponent α were determined over Pune [*Rangarajan*, 1972]. Though the measurement of aerosol properties started about 4 decades before in Pune, not until 1980s an immense need was felt to study these properties systematically, on a long term basis over the Indian subcontinent. With this in view Indian Middle Atmosphere Programme was established in 1980s and multiwavelength radiometers to study tropospheric aerosols over various Indian stations were established [*Krishna Murthy*, 1988; *Krishna Moorthy et al.*, 1989] and aerosol number density and size parameter measurements were made using rocket- and balloon-borne Sun photometers [*Subbaraya and Jayaraman*, 1982; *Jayaraman et al.*, 1987] up to stratospheric altitudes. Chemical composition and size distribution of aerosols in the size range of 0.4 to 10.0 μm were studied using an Andersen particle sampler over Pune [*Khemani et al.*, 1982] and other locations over India [*Negi et al.*, 1987; *Khemani*, 1989]. Aerosol characteristics could be determined up to 28 km with a pulsed ruby lidar over Trivandrum [*Parameswaran et al.*, 1991] and a helium-neon lidar was operated over Pune to study aerosol characteristics up to a few

hundreds of metres, which then later was extended up to about 5 km using argon ion laser [Raj and Devara, 1989; Devara and Raj, 1991]. However, for an assessment of the effect of aerosols on the Earth-atmosphere radiation budget, both, columnar aerosol optical depth, a measure of the amount of aerosol in the atmosphere, which is a function of wavelength, air-mass, season, altitude, latitude and proximity to source, is vital in studying the tropospheric climate changes relevant to the location of measurement, and vertical profiles of aerosol extinction, size parameter, number density and asymmetry factor are important in studying the radiative effects of stratospheric aerosols, at various altitudes, especially after major volcanic eruptions and these data on various parameters will go a long way in addressing some of the key issues of aerosols.

1.5 Objective and Scope of the present investigation

The objective of this work has been to study the characteristics of tropospheric and stratospheric aerosols in the tropical middle atmosphere. Optical investigations using ground based and balloon-borne photometers and lidar are made and the results are reported herein. The thesis focuses on the optical properties of tropospheric aerosols, their day to day and seasonal variations and of stratospheric aerosols, their formation, evolution and decay, after the Mt. Pinatubo eruption as observed over the tropical locations Hyderabad (17.5°N) and Ahmedabad (23°N).

The scope of the present work can be broadly classified topicwise into tropospheric and stratospheric aerosols.

- Using a newly developed Sun-tracking photometer the temporal variations of tropospheric aerosols over Ahmedabad, from 1991 to 1995, the day to day variations, diurnal variations, spectral dependence of aerosol optical depths, variations in wavelength exponent and the relation of aerosol optical depths to the day's maximum temperature and relative humidity are studied and the results are discussed. The results obtained include the effects of Gulf oil fires of 1991 and Mt. Pinatubo eruption in 1991 on the aerosol optical depths.

- Two high altitude balloon flights were conducted from Hyderabad (17.5°N, 78.6°E) during October 1991 and April 1992 to study *in situ* the optical properties of aerosols at the stratospheric altitudes produced due to the Pinatubo volcanic eruption occurred in June 1991. Sun-scanning and Sun-tracking photometers were employed to measure the scattered and the

direct solar radiation intensities and the results obtained on the vertical profiles of aerosol extinction coefficients, number density, size distribution parameter, mode radius, asymmetry factor and mass of Pinatubo aerosols are presented and discussed.

- Using a newly set up Nd:YAG backscatter lidar system at the Physical Research Laboratory (PRL), Ahmedabad (23°N, 72.5°E) the Pinatubo aerosol layer was studied from April 1992 to May 1994. Results obtained on the vertical profiles of scattering ratios, aerosol extinction coefficients and aerosol mass are discussed and their time evolutions are studied.

- A simple model taking into account the aerosol microphysical processes of growth, coagulation and sedimentation was developed to study the time evolution of a volcanic aerosol layer in the stratosphere. The model results are compared with balloon, lidar and satellite data for Pinatubo as well as with El Chichon data available in literature.

Chapter 2

Physical and Optical properties of aerosols

2.1 Size distributions

As the sizes of aerosols span over a wide range of magnitudes, from about $0.001\ \mu\text{m}$ to $100\ \mu\text{m}$ an individual description of aerosols becomes an arduous task. The spread in the sizes of aerosols is due to intricate processes that create the particles, the interactions among themselves and processes that remove these particles from the atmosphere. The spread of the aerosol particle population over the vast size range is described by a *size distribution function*, in which the sizes of particles are represented by their radii. Essentially a size distribution function describes the number of particles per specified interval of radius. Size distribution is perhaps the basic aerosol parameter used in determining other properties of aerosols, provided their composition and physical state are known. Though many size distribution representations are possible, the discretion of opting for a harmonious size distribution function rests mainly on the considerations of the property to be emphasised apart from the preference of the researcher, limited by measurement techniques. There exist atleast three major size distributions for characterising atmospheric aerosols, namely,

- (1) Junge power law size distribution
- (2) Lognormal size distribution and
- (3) Modified Gamma distribution.

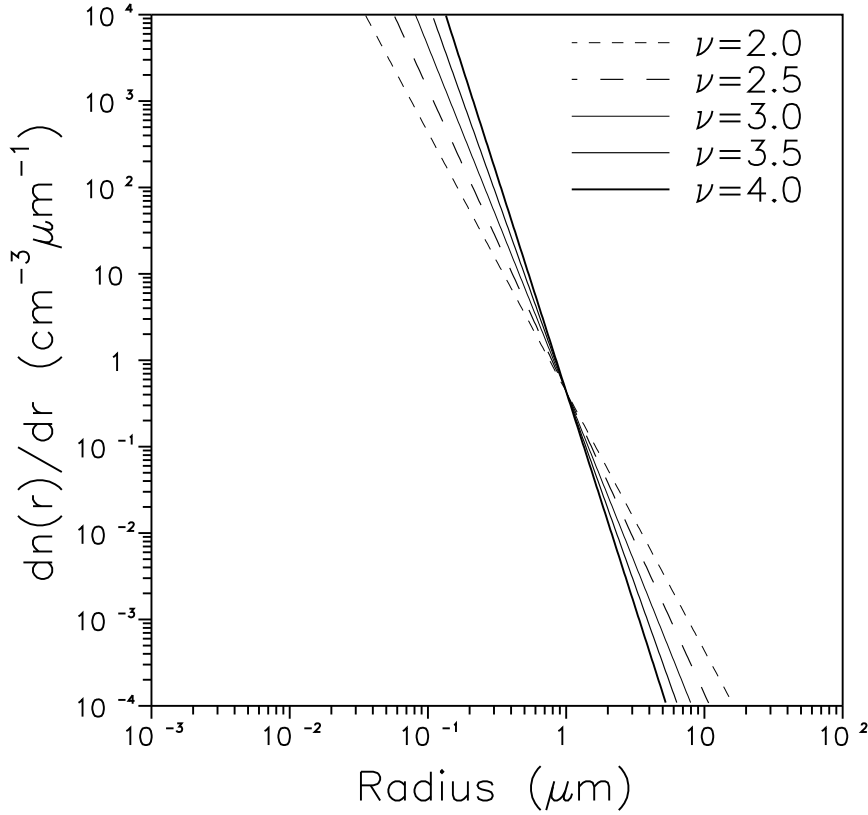


Figure 2.1: Aerosol size distributions obeying Junge power law for exponents ν varying from 2 to 4.

2.1.1 Junge power law size distribution

Junge was among the first scientists to have recognised the need for using logarithmic scales for the illustration of size distributions. *Junge* [1958] based on experimental observations, proposed a power law size distribution function of the form

$$\frac{dn(r)}{d(\log r)} = cr^{-\nu} \quad (2.1)$$

where $dn(r)$ represents the number of particles with radii between r and $r+dr$, c is a constant, depending on the number of particles in one cubic centimetre and the exponent ν , determines the slope of the curve (Figure 2.1). As ν value decreases the number of larger particles increases compared to the number of smaller particles. For typical hazes ν takes a value of about 3 and fogs are characterised by $\nu = 2$. The smallest aerosol particles are the molecular complexes of the small and intermediate ions. These, however do not play an important role in light scattering because of their small size and relatively low concentrations. The size

range of interest however starts from $0.04 \mu\text{m}$ where normally the bulk of the aerosol particles is found. From this radius up to $10 \mu\text{m}$ the aerosol size distribution more or less follows a power law. The physical explanation of the lower boundary radius is that according to Smoluchowsky's theory, a greater coagulation rate is caused due to increasing number of particles and consequently the small particles coagulate more quickly than the larger ones so that within half a day, the number of particles of the size $0.01 \mu\text{m}$ is reduced to a negligible amount and hence the number of larger particles is increased. The upper boundary radius ($10 \mu\text{m}$) falls in the range of giant nuclei and particles of larger size are more effectively removed mainly through sedimentation and rainwash [Bullrich, 1964]. The advantage of this size distribution resides in the possibility of describing a size distribution from the knowledge of ν only.

Though it's claimed that this law does not explain or accommodate the smaller particle range as well as the larger particle range adequately, in a given volume of aerosol the number of large particles is orders of magnitude less compared to that of small particles and hence particles of size $10 \mu\text{m}$ and above have relatively insignificant contribution to the total scattered intensity or to the extinction. Similarly in the lower size range even though the number densities are large, the scattering efficiency is much less and they tend to behave more like air molecules. It is found that in the 'optically effective' particle size range of $0.05 \mu\text{m}$ to $10 \mu\text{m}$, Junge power law can be taken as a good representation of aerosol size distribution as the Mie scattering contribution of the smaller particles (less than about $0.05 \mu\text{m}$) to the total integrated intensity is marginal. It has also been found that the total aerosol extinction coefficient is found to increase by 0.4% or less if the power law is truncated at r_{\min} of $0.01 \mu\text{m}$ instead of $0.05 \mu\text{m}$ [Ramachandran et al., 1994c].

2.1.2 Lognormal distribution

The lognormal distribution [Davies, 1974] developed on the basis of the distribution of particles originating from a single source through a single production mechanism can be written as

$$\frac{dn(r)}{dr} = \frac{A}{\sqrt{2\pi} \ln \sigma} \frac{1}{r} \exp \left[-\frac{\ln^2 \left(\frac{r}{r_m} \right)}{2 (\ln \sigma)^2} \right] \quad (2.2)$$

where A is the total number concentration (cm^{-3}), σ is the width of the lognormal curve and r_m is the mode radius. For a mixture of particles originating from multiple independent sources, the resulting size distribution is a combination of all individual sources.

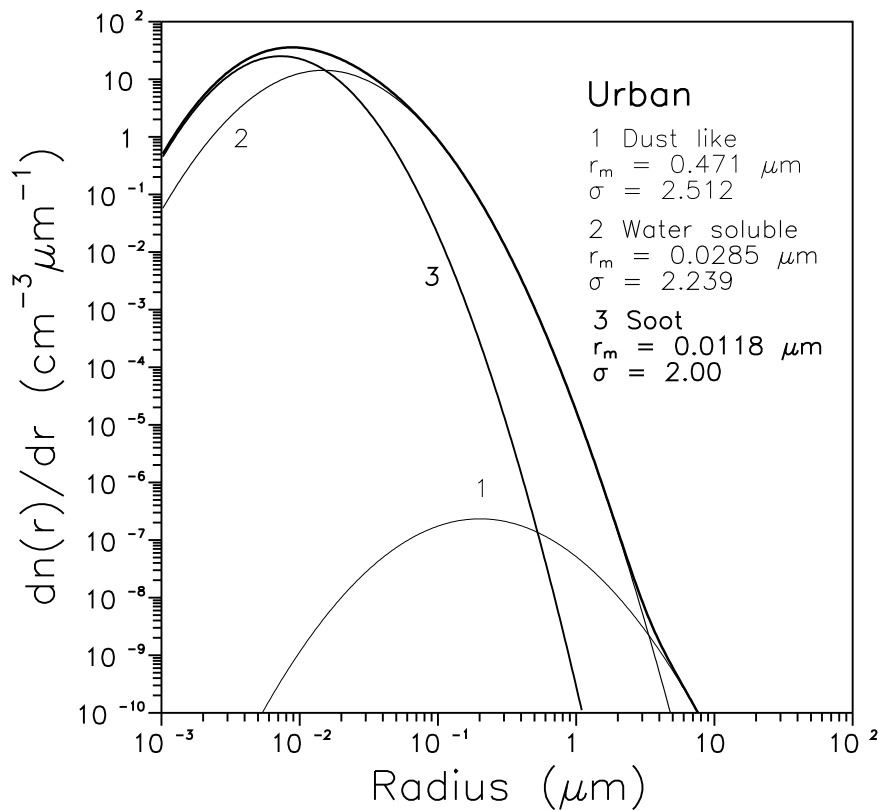


Figure 2.2: A typical lognormal aerosol size distribution for an urban aerosol model which encompasses three different modes, representative of three individual sources. The values are taken from *d'Almeida et al. [1991]*.

The lognormal distribution (LND) function lays emphasis on the individual components in a mixture of particles originating from different sources. Each component has its specific mode radius and standard deviation (σ) and its assigned refractive index. For example the size distribution of an urban aerosol model which is made up of dust like, water soluble and soot components is plotted in Figure 2.2.

The geographical importance of each component depends on the distance from its source of production as well as its ability to remain airborne and travel long distances [*d'Almeida et al., 1991*]. For these reasons, it becomes clear that lognormal distributions are best suited to characterise the aerosol components, the aerosol types and their spatial and temporal variability and hence it is widely used for tropospheric studies.

While in the Junge power law distribution ν alone is sufficient to describe the aerosol characteristics, in the lognormal distribution the width of the size distribution σ and mode radius

r_m are vital.

A simplified version of the lognormal distribution is zero order logarithmic distribution (ZOLD). This size distribution is used normally after a major volcanic eruption, when the aerosol particles are nonsoluble and is written as

$$\frac{dn(r)}{dr} = A \exp \left[-\frac{\ln^2 \left(\frac{r}{r_m} \right)}{2 (\ln \sigma)^2} \right] \quad (2.3)$$

where A is an arbitrary constant and $\sigma = 1.8$ [Pinnick *et al.*, 1976].

It is a property of the ZOLD that a change in the mode radius r_m does not affect the width of the distribution or in other words for all σ s the r_m value will not change as the radius of maximum concentration or the geometric mean radius $r_g = r_m$ in the case of ZOLD, while in LND $r_g = r_m \exp [-(\ln \sigma)^2]$ (Figures 2.3a and 2.3b).

2.1.3 Modified Gamma distribution

The modified Gamma distribution was originally proposed for clouds. In its general form the function may be written as

$$\frac{dn(r)}{dr} = A r^\alpha \exp (-b r^\gamma) \quad (2.4)$$

representing a family of size distributions with A , α , b and γ positive constants which depend on each other. The integration of the above equation over the entire radius range yields the total number of particles per unit volume. The function owes its name to the presence of γ . In the original Gamma distribution $\gamma = 1$.

Deirmendjian [1964] used this function and computed scattering and polarisation properties of clouds and hazes in the visible as well as in the infrared and he observed that the results compared fairly well with measurements both on natural water clouds and aerosols. The mode radius r_m was obtained by setting the derivative of the equation to 0. The modified Gamma distribution has great adaptability and can be fitted to various models of haze, cloud and rain, as it contains four adjustable parameters. However, while the slope ν in the Junge power law is often correlated with the Ångström's wavelength exponent α as $\nu = \alpha + 2$, which essentially specifies the behaviour of the aerosol extinction and hence the atmospheric turbidity, both Gamma and modified Gamma distribution functions are not very popular, as there is no definitive correlation with aerosol extinction and also the physical meaning of the parameters A , α , b and γ is not well understood. Above all, the flexibility of adjusting four parameters, itself turns out to be a drawback as it makes these distributions difficult to handle.

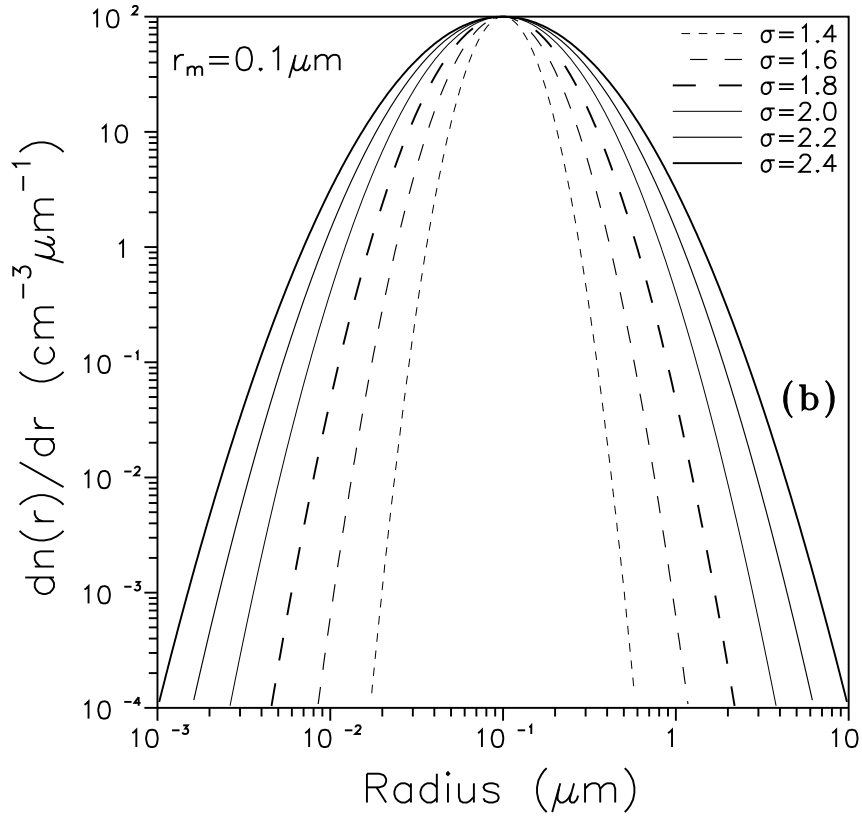
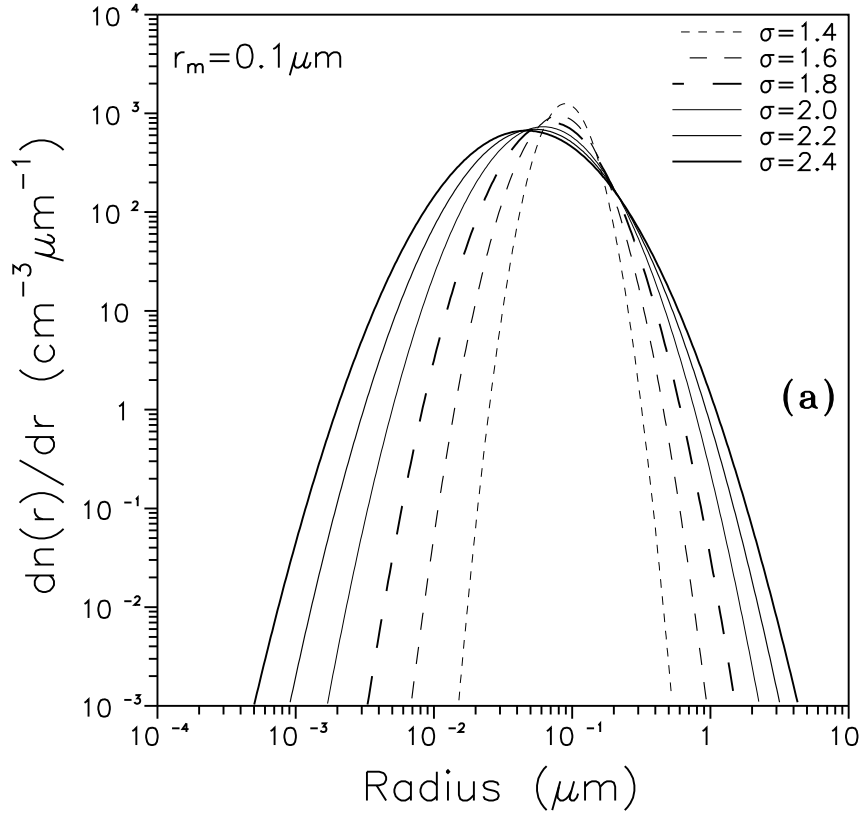


Figure 2.3: Lognormal (top) and zero order logarithmic (bottom) distributions for a mode radius of $0.1 \mu\text{m}$ and for various widths of size distributions σ , from 1.4 to 2.4.

2.2 Optical properties

2.2.1 Scattering processes

Scattering is the process by which a particle in the path of an electromagnetic wave continuously extracts energy from the incident wave and reradiates that energy in all the 4π directions.

Scattering can be broadly classified into two categories (i) the elastic scattering, in which the wavelength of the scattered radiation is same as the incident radiation and (ii) inelastic scattering, in which the wavelength of the scattered radiation is different from that of the incident radiation. The elastic scattering can further be classified into two, *Rayleigh scattering* and *Mie scattering* depending on the size of the particle as compared to the wavelength of the incident radiation. When the particle radius is much smaller than the incident wavelength ($< 0.03\lambda$, λ being the wavelength), the scattering is called Rayleigh scattering, named after the scientist who first developed the theory of scattering by very small isotropic particles. Air molecules are the chief Rayleigh scatterers in the atmosphere. Rayleigh scattering varies inversely as the fourth power of the wavelength, with equal amount of fluxes scattered in both forward and backward hemispheres.

Scattering is explained in terms of the electromagnetic theory. The electric field of the incident wave sets in oscillation of electric charges in the particle. When the particle is smaller than the wavelength of the incident radiation, as in the case of Rayleigh scattering, an electric dipole is set up and the scattering is symmetric as an electric dipole radiates equal amount of fluxes in both forward and backward directions (Figure 2.4).

As the particle dimensions become appreciable to the incident wavelength the scattering process can no longer be explained by merely an induced dipole, a three dimensional charge distribution is set up within the particle with higher moments like quadrupole, octupole, hexadecapole etc. and the scattering process becomes complex. The exact solution to the scattering problem was given by Gustav Mie in 1908 in terms of Maxwell equations and encompasses Rayleigh scattering as a special case. The most notable feature in Mie scattering is the development of forward peak. As the particle size increases the scattering is no more symmetric and more and more radiation is scattered in the forward direction than in the backward direction (Figure 2.4).

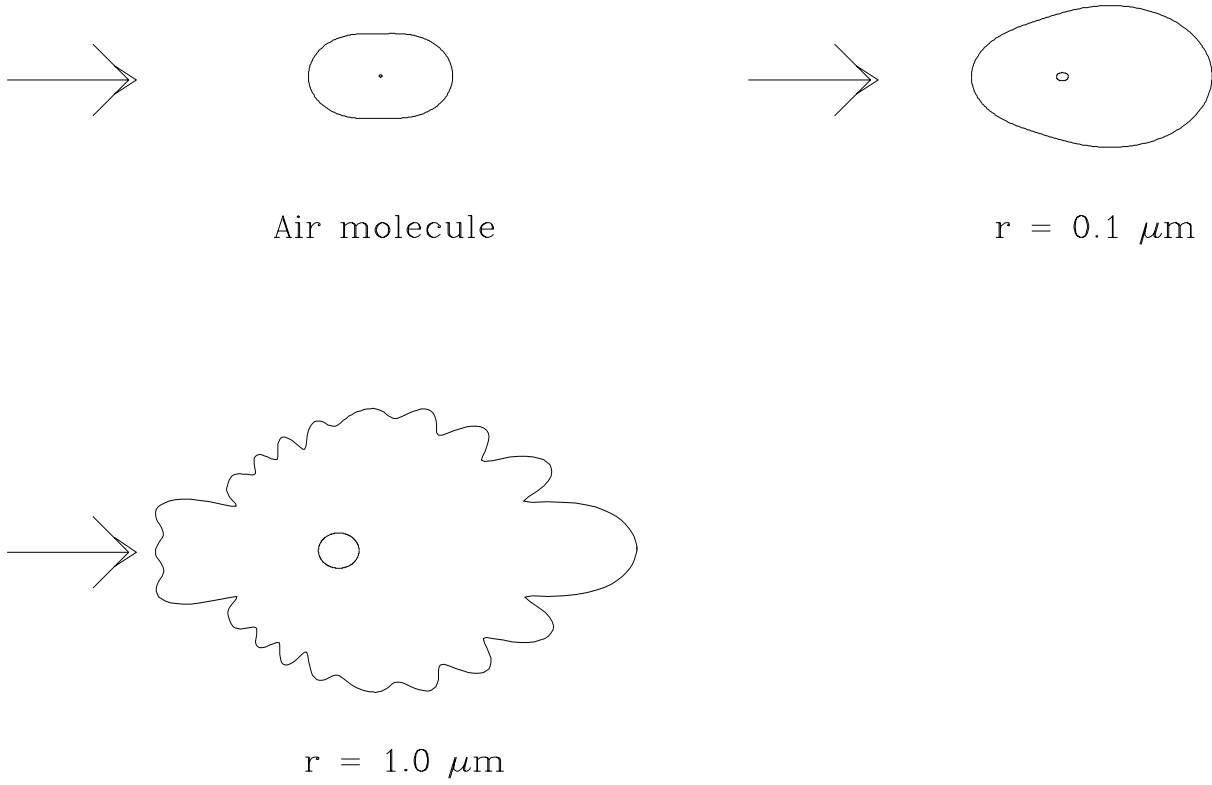


Figure 2.4: Schematic diagrams of the angular distribution of the scattered radiation intensities for particles of different sizes at $\lambda = 0.55 \mu\text{m}$.

2.2.2 Mie scattering

If i_1 and i_2 are the polarised components of the scattered intensity resolved perpendicular and parallel to the plane of scattering, then

$$i_1(\alpha, m, \theta) = |S_1|^2 = \left| \sum_{n=1}^{\infty} \frac{2n+1}{n(n+1)} (a_n \pi_n(\cos\theta) + b_n \tau_n(\cos\theta)) \right|^2 \quad (2.5)$$

$$i_2(\alpha, m, \theta) = |S_2|^2 = \left| \sum_{n=1}^{\infty} \frac{2n+1}{n(n+1)} (b_n \pi_n(\cos\theta) + a_n \tau_n(\cos\theta)) \right|^2 \quad (2.6)$$

where S_1 and S_2 are the amplitudes of the scattered radiations i_1 and i_2 . The complex numbers a_n and b_n are the Mie coefficients. The functions π_n and τ_n depend only on the scattering angle θ , the derivatives of Legendre polynomials having an order n and argument $\cos\theta$. α is the size parameter $2\pi r/\lambda$ where λ is the wavelength of the incident radiation.

Mie coefficients a_n and b_n determine the optical properties such as efficiency factors for extinction (Q_{ext}), scattering (Q_{sca}) and absorption (Q_{abs}).

$$Q_{\text{ext}} = \left(\frac{2}{\alpha^2}\right) \sum_{n=1}^{\infty} (2n+1) \text{Re}(a_n + b_n) \quad (2.7)$$

$$Q_{\text{sca}} = \left(\frac{2}{\alpha^2}\right) \sum_{n=1}^{\infty} (2n+1) (|a_n|^2 + |b_n|^2) \quad (2.8)$$

$$Q_{\text{abs}} = Q_{\text{ext}} - Q_{\text{sca}} \quad (2.9)$$

The extinction coefficient β_{ext} indicates the fraction of energy removed, per unit path length, from an incident wave with energy flux density 1 by a collection of aerosol particles characterised by the particle size distribution. The energy that then reappears as the scattered energy is the scattering coefficient β_{sca} and the energy absorbed produces the absorption coefficient β_{abs} . The sum of scattering and absorption yields the extinction.

$$\beta_{\text{ext,sca,abs}}(\lambda) = \int_{r_1}^{r_2} \frac{dn(r)}{dr} Q_{\text{ext,sca,abs}}(m, \lambda, r) \pi r^2 dr \quad (2.10)$$

where $dn(r)/dr$ is the number of particles per cm^3 whose radii are between r and $r+dr$, $Q_{\text{ext,sca,abs}}(m, \lambda, r)$ is the Mie extinction /scattering/absorption efficiency factor and m is the refractive index of aerosol particle.

The single scattering albedo ω_0 is defined as the fraction of energy removed from the incident beam which reappears as scattered radiation. ω_0 is equal to 0 for a perfectly absorbing aerosol and is 1 for a pure scatterer and is written as,

$$\omega_0(\lambda) = \frac{\beta_{\text{sca}}(\lambda)}{\beta_{\text{ext}}(\lambda)} = 1 - \frac{\beta_{\text{abs}}(\lambda)}{\beta_{\text{ext}}(\lambda)} \quad (2.11)$$

The aerosol scattering phase function $P_a(\lambda, \theta)$ is computed using Mie algorithm as

$$P_a(\lambda, \theta) = \frac{\lambda}{(2\pi)^2} \int_{r_1}^{r_2} i(r, \theta) \frac{dn(r)}{dr} dr \quad (2.12)$$

and normalised to unity such that

$$2\pi \int_0^\pi P_a(\lambda, \theta) \sin\theta d\theta = 1. \quad (2.13)$$

The phase function represents the angular distribution of the scattered energy i.e. the angular dependence of scattering. The ‘normalised phase function’ describes what fraction of scattered radiation appears per unit solid angle in the direction θ .

The asymmetry factor g is defined as the average of the cosine of the scattering angles for scattered radiation such that,

$$g = \frac{\int_0^\pi \cos\theta P_a(\lambda, \theta) d(\cos\theta)}{\int_0^\pi P_a(\lambda, \theta) d(\cos\theta)} \quad (2.14)$$

Theoretically, g can vary between -1 and $+1$. For particles with isotropic scattering properties $g = 0$. When scattering is entirely in the forward direction asymmetry factor equals one. The more the particles scatter in the forward direction, which is the case with larger particles the higher is the asymmetry factor.

The integration of extinction coefficient over a path length through the atmosphere yields the optical depth, τ .

2.2.3 Mie scattering of individual particle

Variation of Mie scattering parameters with size of the particle

By and large, the refractive indices of atmospheric particles and molecules are constituted of a real part m_r and an imaginary part m_i corresponding, respectively to the scattering and absorption properties. In the solar visible spectrum, as the imaginary parts of the refractive indices of air molecules are insignificantly small, they can be neglected in the scattering discussion.

The behaviour of Q_{ext} , Q_{sca} and Q_{abs} for single particle of various sizes and various types of aerosols, with varied imaginary refractive indices and their implications will be discussed here. Figures 2.5a-d show the behaviour of Q_{ext} , Q_{sca} and Q_{abs} for different aerosol types. All these calculations are done for $\lambda = 550$ nm. The real and imaginary parts of the refractive index are specified in the diagrams. As soot has an imaginary refractive index of 0.44 at 550 nm, the extinction is only due to absorption till about $0.06 \mu\text{m}$ and the scattering contribution is orders of magnitude less and the curves are very smooth, throughout the radius range. In dust like particle, though initially the contribution comes from only absorption till $0.02 \mu\text{m}$, beyond this radius, scattering contributes most to the extinction. In stark contrast, in both 75% H_2SO_4 and oceanic type particles, the extinction is only due to scattering throughout from $0.001 \mu\text{m}$ to $10 \mu\text{m}$, while the absorption is orders of magnitude less, as they have very low imaginary refractive indices. In 75% H_2SO_4 and oceanic, the curves of extinction and scattering, which are one and the same, tend to oscillate from about $0.2 \mu\text{m}$ about a smooth curve that approaches $Q_{\text{ext}} = 2$. The largest oscillations about this curve are those associated with nonabsorbing particles ($m_i \sim 0$) and the amplitude of these oscillations decreases as the value of m_i increases, which is very clearly seen in the soot and dust like particles as compared to 75% H_2SO_4 and oceanic particles. In oceanic and 75% H_2SO_4 particle profiles the absorption curve exhibits several peaks and troughs, while in soot and dust like particles they are relatively smooth.

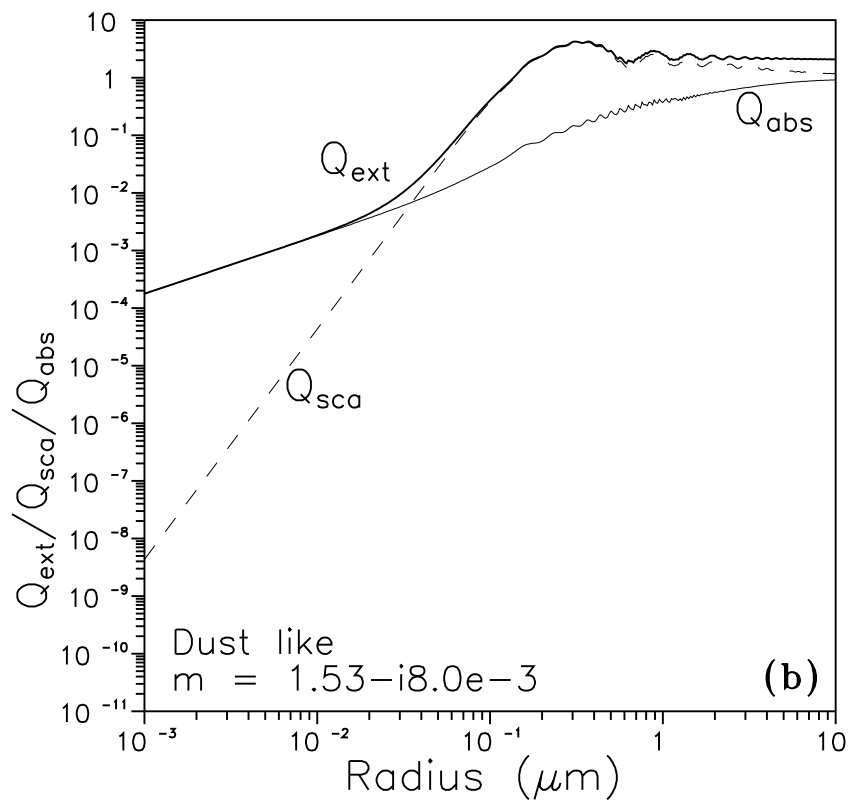
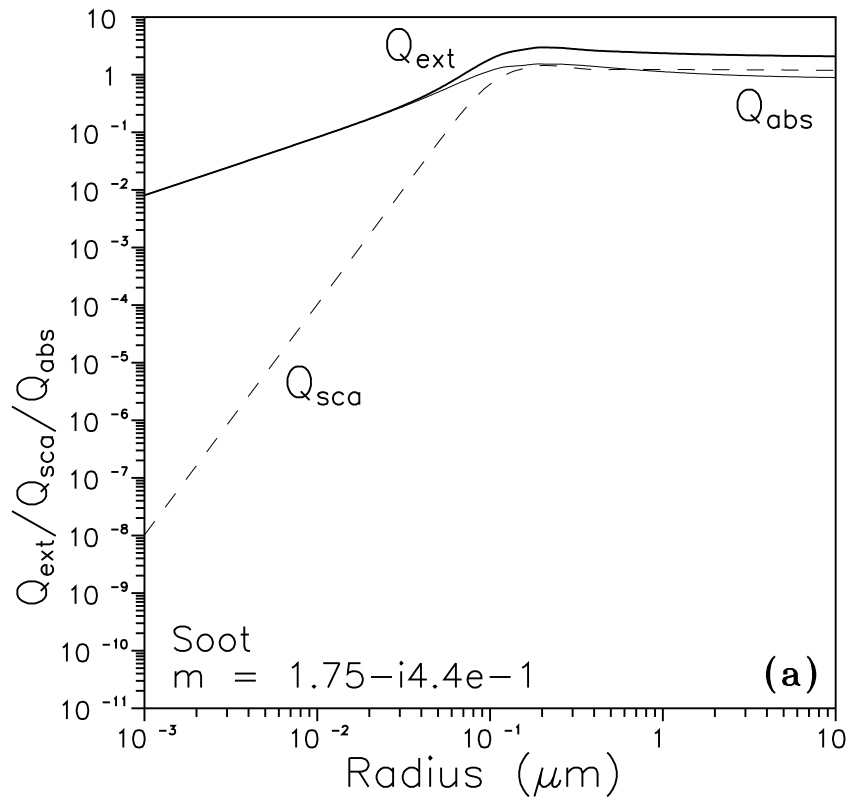
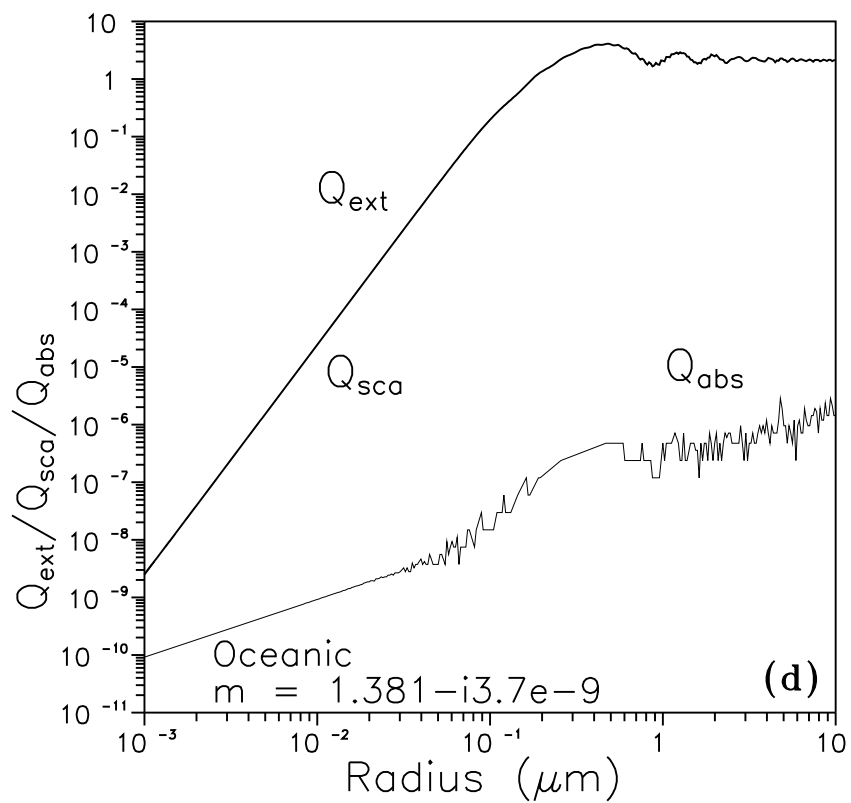
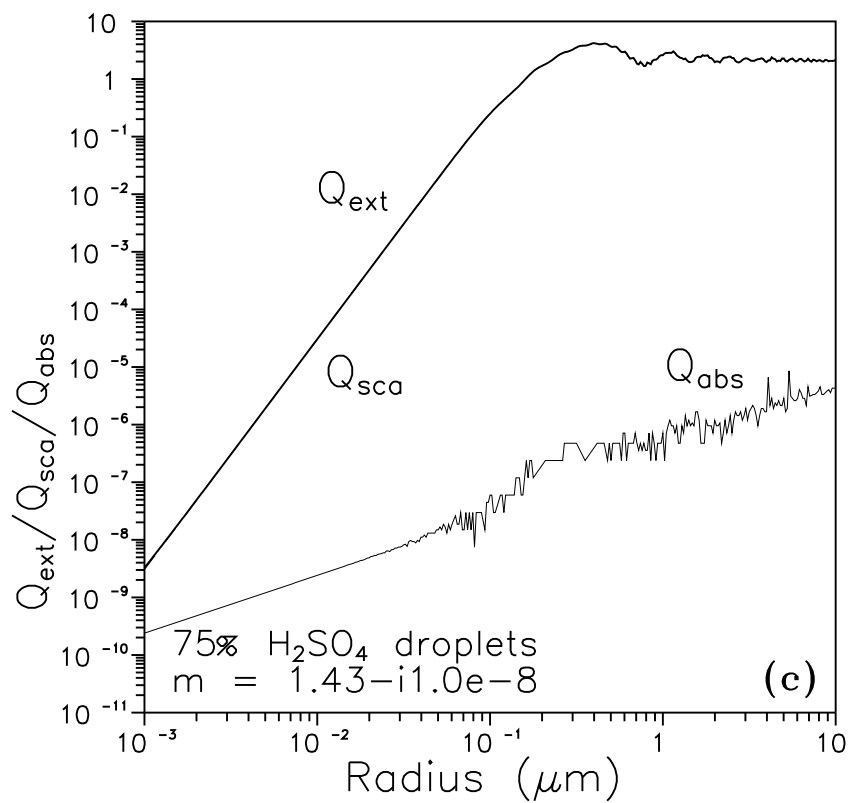


Figure 2.5: Extinction efficiency (Q_{ext}), scattering efficiency (Q_{sca}) and absorption efficiency (Q_{abs}) at $\lambda = 550 \text{ nm}$ for (a) soot (b) dust like (c) 75% H_2SO_4 droplets and (d) oceanic aerosol particles.



It is seen that $Q_{\text{sca}} = Q_{\text{ext}}$ for nonabsorbing particles and with increasing particle size, Q_{sca} approaches 2, indicating that the scattering cross section is twice the geometric cross section of the particle. In this case, as we are in the realm of geometric optics, the problem can be discussed in the known terms of reflection, refraction and diffraction. It may seem at first surprising that Q_{sca} is 2 rather than unity. This is known as ‘extinction paradox’. It is seen that, except for the infinitesimal fraction of the energy that propagates along the axis of the sphere, all of the geometrically intercepted radiation will undergo a change in direction because of reflection and/or refraction and thus half of the predicted magnitude of Q_{sca} can be explained. The other half arises from the radiation that is diffracted by the periphery of the sphere. The ‘edge’ of the sphere is identical to the edge of a hole of the same diameter in an opaque screen, as far as the diffraction effects go. This is known as *Babinet’s principle*. The diffraction pattern is the result of the interference of wave fronts from the edges and therefore it is not essential to know whether the outer edge of the disc is considered or the inner edge of the hole. The total scattered light comes from the light geometrically intercepted by the particle (reflected and refracted) plus from an equal amount of edge-diffracted light. Hence, $Q_{\text{sca}} = 2$ for nonabsorbing particles in the larger size limit. But as m_i increases, the amount of light absorbed by the particle increases and the fraction of the intercepted light refracted by the particle gets decreased and in that case major contribution to Q_{sca} comes from the light diffracted by the edge and it therefore approaches unity in the large size limit for absorbing particles [Cadle and Grams, 1975].

2.2.4 Angular distribution of the scattered light intensity of single particle

The angular distribution of the scattered intensity is described by the phase function. In case of Rayleigh scattering, no angular variation in the scattered radiation intensity is observed along the scattering plane perpendicular to the electric vector of an incident polarised light beam and a $\cos^2\theta$ variation is observed in the parallel plane (Figure 2.6a).

The angular distribution of the scattered radiation intensities for aerosol particle of radius 0.01, 0.1, 1.0 and 10.0 μm are plotted in Figures 2.6b-e, where i_{total} refers to the total intensity and is $(\frac{i_{\text{perpendicular}} + i_{\text{parallel}}}{2})$, $i_{\text{perpendicular}}$ refers to the intensity scattered in the perpendicular plane to the electric vector of the incident beam and i_{parallel} refers to the intensity in the parallel plane. These figures illustrate the effect of increasing particle size, from a smoothly varying function at 0.01 μm to a highly distorted function with troughs and peaks at 10.0 μm . Although these calculations have been done for $\lambda = 550 \text{ nm}$ and for a dust like

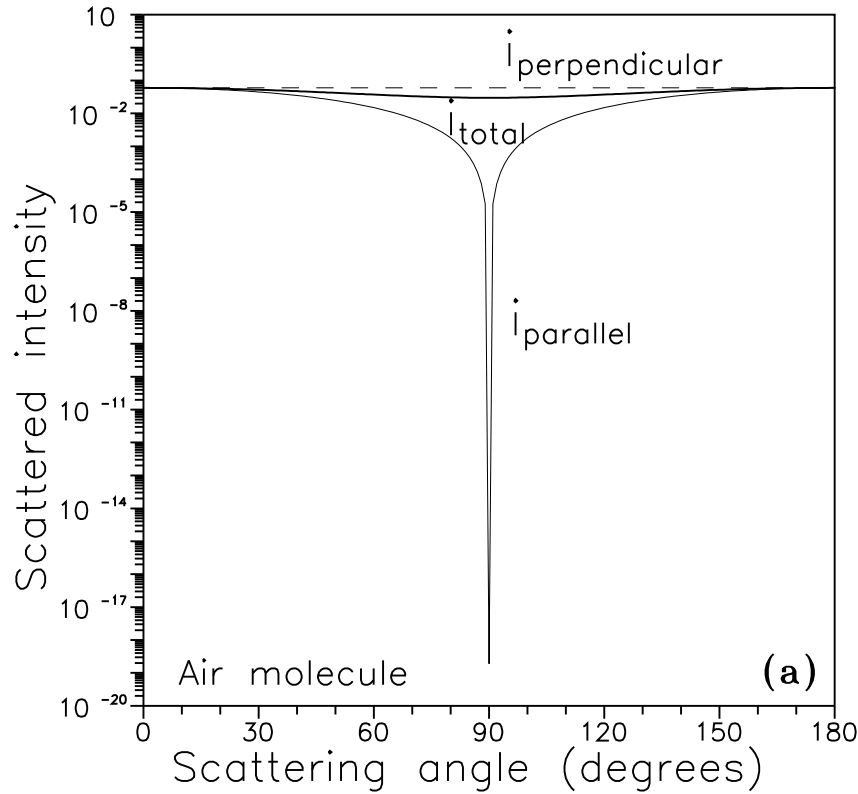


Figure 2.6: *The angular distribution of the scattered radiation intensity for an air molecule.*

particle ($m = 1.53 - i8 \times 10^{-3}$), the behaviour shown in the graphs is representative of the general behaviour of most of the commonly observed aerosols. It is evident that a larger portion of the energy is scattered in the forward direction as the particle size increases. It is also noticeable that a great deal of structures can exist in the angular distribution of the scattered radiation and the structures are prominent as the particle size increases. Practically, much of these strongly marked structures disappear when we consider the results of a polydispersed aerosol i.e. when applied to a size distribution consisting particles of all sizes.

2.2.5 Mie scattering for many particles

Q_{ext} , Q_{sca} and Q_{abs} determined for individual particle using Mie theory when integrated over the entire particle range of an aerosol size distribution, β_{ext} , β_{sca} and β_{abs} are obtained and the integration of the scattered intensities gives the aerosol phase function. Aerosol phase function essentially determines the fraction of intensity scattered at an angle. The aerosol phase functions calculated for 75% H_2SO_4 droplets are shown in Figure 2.7 as examples. The phase

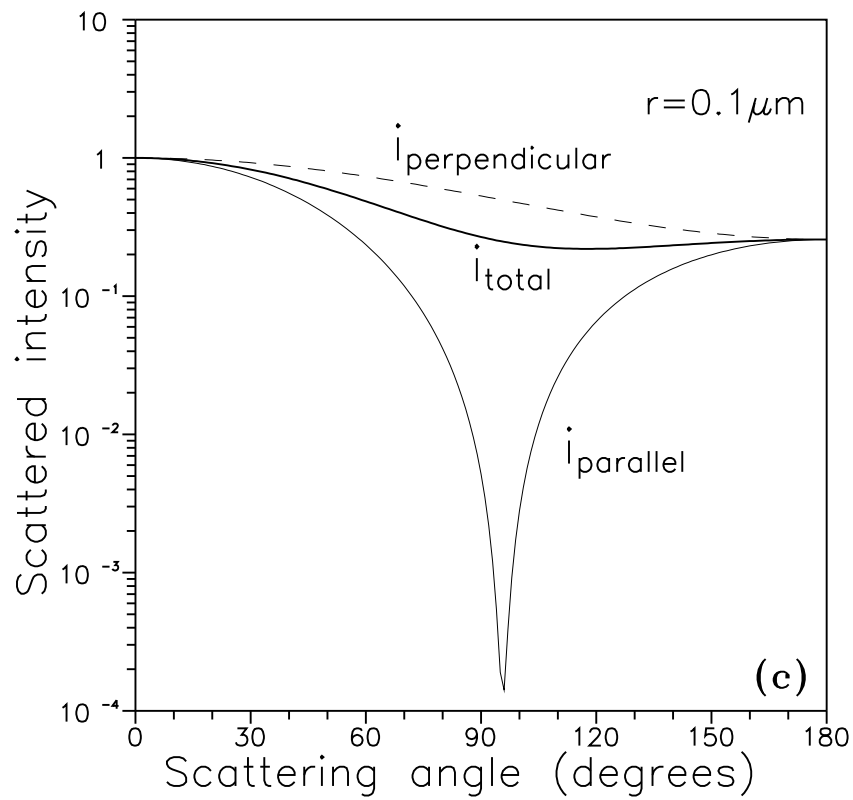
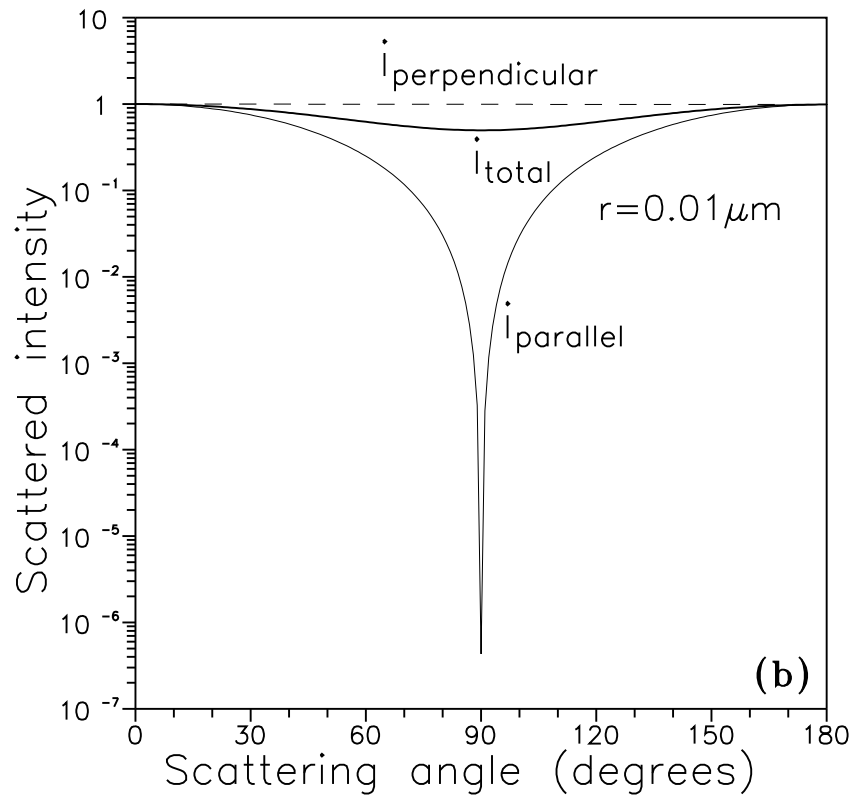
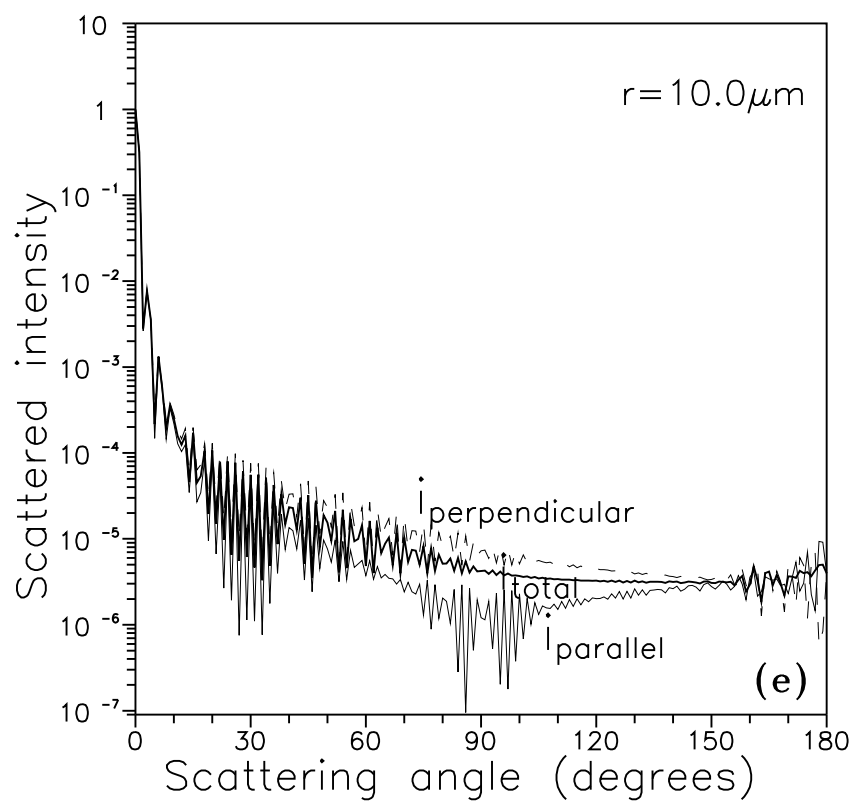
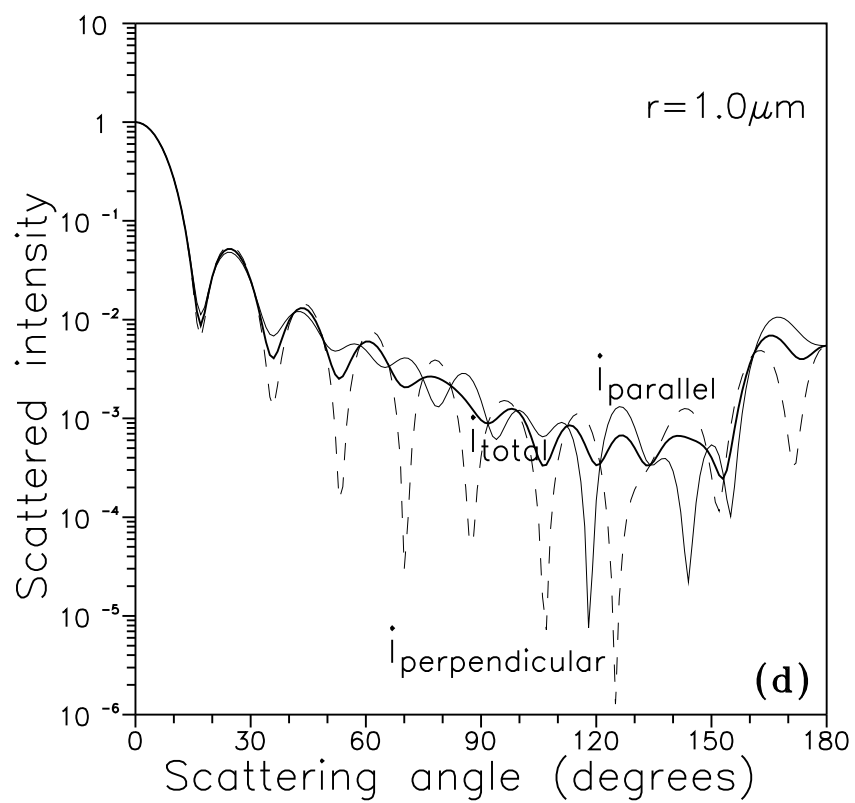


Figure 2.6: The angular distribution of the scattered radiation intensities for dust like aerosol particles of various sizes in both perpendicular and parallel directions and the total intensities.



functions for different size distributions are normalised at 0° scattering angle for comparison. In Junge size distributions (Figure 2.7a) the aerosol phase functions are smooth while in lognormal distributions (Figure 2.7b) the aerosol phase functions develop small disturbances when mode radius is $1.0 \mu\text{m}$ while for all the mode radii ranging from $0.07 \mu\text{m}$ to $0.5 \mu\text{m}$, the aerosol phase functions are smooth. This difference is mainly due to the assumed lower and upper radii limits used in the integration which are different.

Junge size distributions for various ν values are calculated for $r_{\min} = 0.04 \mu\text{m}$ and $r_{\max} = 10.0 \mu\text{m}$ while in lognormal distributions r_{\min} and r_{\max} are chosen such that the aerosol number density falls by 1×10^{-6} with respect to the maximum value in the size distribution. Even in the case of Junge size distribution, for $\nu = 2.0$, the aerosol phase function shows some disturbances although they are not as marked as in the case of lognormal distribution, for $r_m = 1.0 \mu\text{m}$. So as the mode radius increases and ν decreases the size distributions encompass more and more large particles and the cumulative phase function also develops some fluctuations due to structures in the individual scattered intensity distribution, as we have seen above. And also it is evident that as the number of large particles increases in a size distribution more and more radiation is scattered in the forward direction when compared to backward direction.

To investigate the dependence of aerosol phase functions on the type of particles i.e. on the refractive index, computations were done for four aerosol types exhibiting a wide range of refractive index values and for different ν values. The results of computations are shown in Figure 2.8. For comparison the aerosol phase functions have been normalised at 0° scattering angle. Results indicate that the aerosol phase function depends more on size parameter than on different aerosol types. Though the results of Junge size distributions are shown as an example, the above fact is valid for lognormal distributions also. Also the phase functions for $\nu = 2.0$ and 4.0 are shown for various models and for the sake of clarity, for $\nu = 3.0$, only the dust like particle's phase function is shown.

Aerosol phase functions obtained for g values varying from 0.6 to 0.9 at 550 nm are plotted in Figure 2.9. As asymmetry factor is an average of the cosine of the scattering angles, the disturbances in the phase functions derived using ν are not present in these curves and a smooth picture is obtained. With decreasing ν , the relative number of larger particles increases, which results in an increase in g as can be seen in Figure 2.9.

Mie scattering theory assumes that scattering particles in the atmosphere are homogeneous spheres. But in reality particles can have aspherical shapes such as ellipsoid, spheroids,

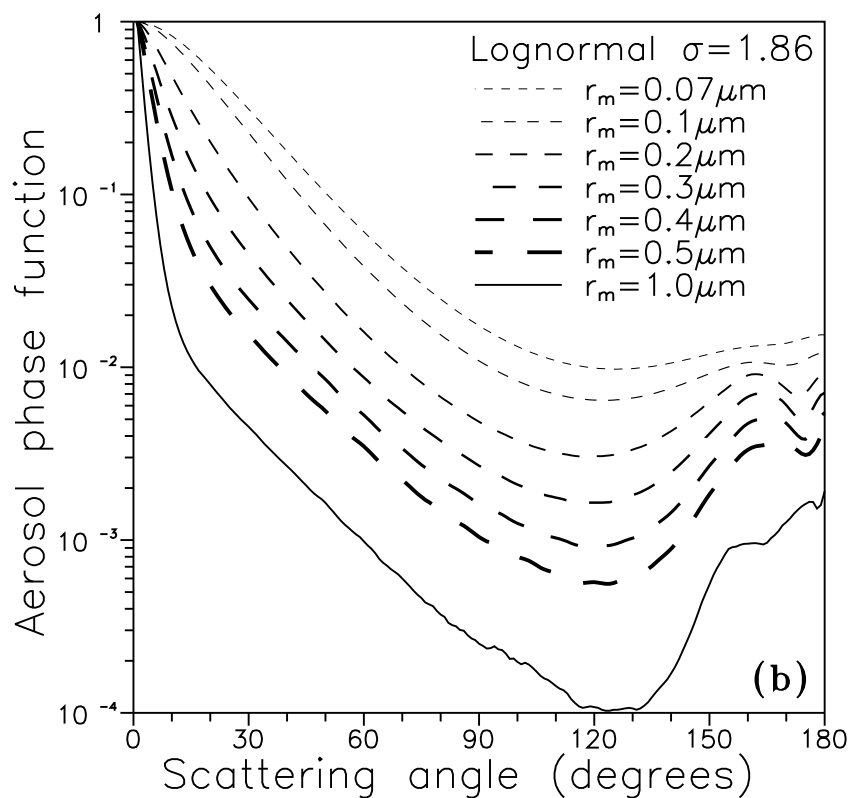
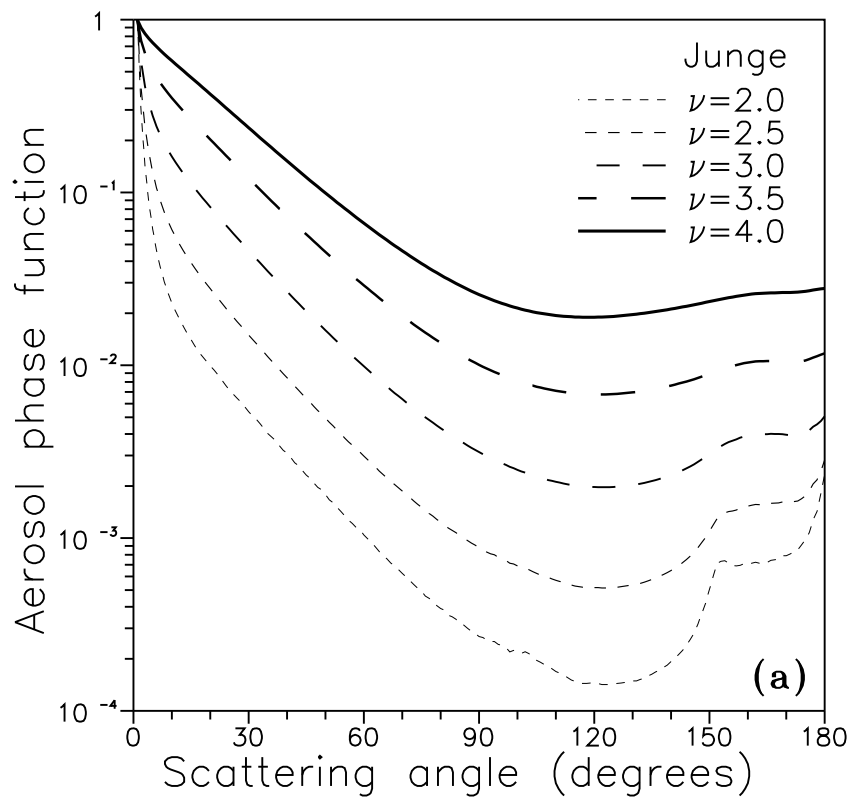


Figure 2.7: Aerosol phase functions $P_a(\lambda, \theta)$ for (a) Junge size distributions having exponents from 2 to 4 in steps of 0.5 for an ensemble of particles from $0.04 \mu\text{m}$ to $10.0 \mu\text{m}$ and (b) lognormal distributions for various mode radii from $0.07 \mu\text{m}$ to $1.0 \mu\text{m}$.

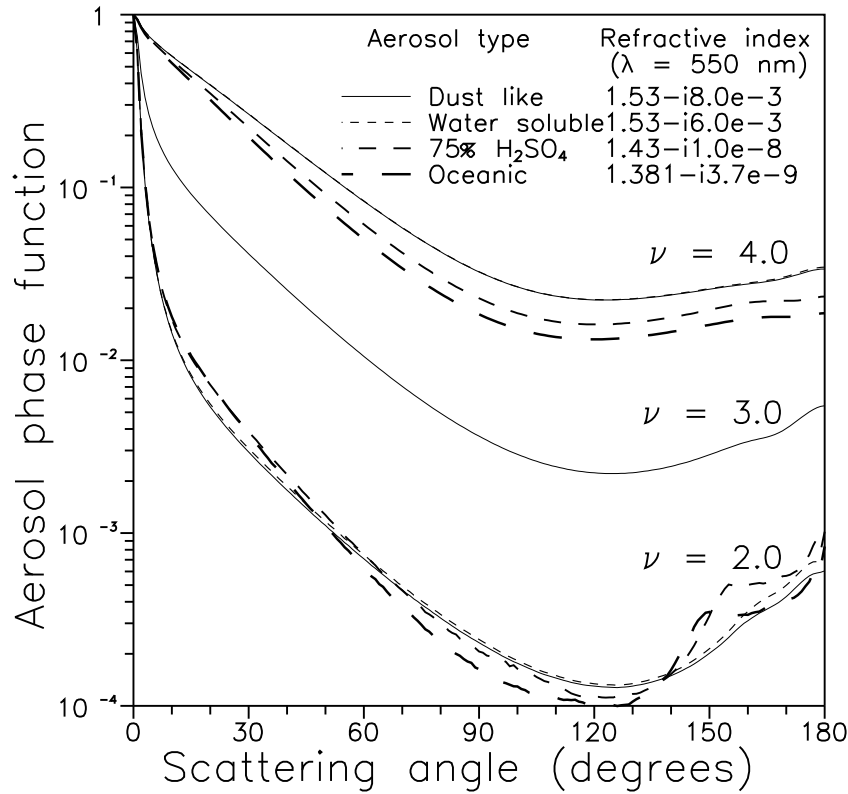


Figure 2.8: Aerosol phase functions for various aerosol types for $\nu = 2, 3$ and 4. The curve shows the dependence of aerosol phase function more on ν than on various aerosol types.

oblate etc. and so the implications of the assumption of all the scattering particles to be spheres needs investigation. *Holland and Gagne* [1970] used a polar nephelometer to study scattering from irregularly shaped particles with an emphasis on the differences between the measured scattering parameters and those calculated from Mie solution for homogeneous spheres. In the forward direction (i.e. for angles $< 90^\circ$) a good agreement was found but in the backward scattering (i.e. for scattering angles $> 90^\circ$) the scattered intensity was found to be less than that predicted for spherical particles. Recently *Koepke and Hess* [1988] found that the scattering functions of nonspherical particles compared with those of equivalent spheres show differences with increasing particle size. They also found that for aerosol types with a relatively low amount of large particles such as continental and urban aerosols, the effect due to uncertainty about particle shape can be ignored. For desert aerosols, which are larger in size an appreciable difference in the scattering functions was found beyond 120° . However, as in the present work aerosol scattering phase functions have been compared only between

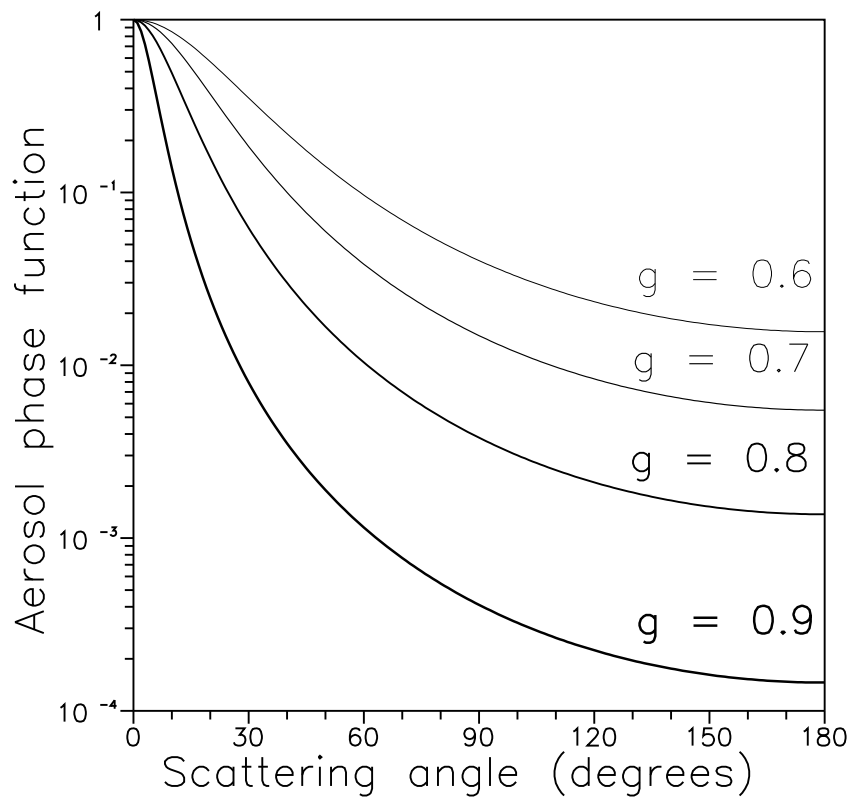


Figure 2.9: *Aerosol phase functions obtained for asymmetry parameter g varying from 0.6 to 0.9. g is defined as the average of the cosine of the scattering angles for scattered radiation.*

0° and 90° the question of effect of nonsphericity on the derived aerosol parameters does not arise.

Using LOWTRAN 7 code multiple scattering calculations were performed for solar zenith angles varying from 0° to 80° from 300 to 1000 nm for a model atmosphere which was made up of Urban (0-2 km), Tropospheric (2-10 km), High/Aged volcanic (10-30 km) and Meteoric dust (30-100 km) aerosol models. The results indicate that multiple scattering is important only at low altitudes between 0 and 4 km for 300 nm and at 500 nm. However, above about 5 km the influence of multiple scattering on the scattered radiation is almost nil. The irradiance at any point in the atmosphere is a combination of direct solar radiation and radiation scattered more than once. Thus the inclusion of multiple scattering will only enhance the estimated radiation values. However, this increase in intensity to the direct radiation is negligibly small. In the balloon-borne measurements as the observations are done above 5 km and in ground based Sun photometry measurements as only the total loss of radiation in the

medium is only measured i.e. optical depth, the effect of multiple scattering is neglected, in the present work.

2.2.6 Size range of aerosols for optical investigations

In a size distribution there is a tendency for number of particles to increase rapidly with decreasing particle size, making small particles the most important ones as they are numerous, while studying the optical effects. Though in a given volume of aerosol, the number of larger particles is orders of magnitude less when compared to smaller particles, as the cross section increases with the square of radius, the large particles can still dominate aerosol optical effects because their cross section per particle is significantly larger than that of smaller particles. The shape of the size distribution function (i.e. the relative number concentrations of large and small particles) obviously is important for establishing the size ranges that must be measured to draw any conclusion concerning the optical properties of aerosols.

To determine the size range of aerosols suitable for optical investigations, Junge size distribution ($\nu = 3$) and lognormal distribution function ($r_m = 0.3 \mu\text{m}$, $\sigma = 1.86$) for 75% H_2SO_4 droplets ($1.43 - 11.0 \times 10^{-8}$) and dust like particle ($1.53 - 18.0 \times 10^{-3}$) at $\lambda = 550 \text{ nm}$ are considered. The lower (r_1) and upper radii (r_2) limits are set as $0.01 \mu\text{m}$ and $10.0 \mu\text{m}$ in the calculations of β_{ext} , β_{sca} and β_{abs} and these quantities were calculated as a function of r_1 varying from $0.01 \mu\text{m}$ to $10.0 \mu\text{m}$ for both the size distributions and for both aerosol types. The results obtained were normalised by dividing all the intermediate values of β_{ext} , β_{sca} and β_{abs} , by the values obtained for the $r_1 = 0.01 \mu\text{m}$, $r_2 = 10.0 \mu\text{m}$ case. The results of β_{ext} are shown in Figure 2.10.

For both the size distributions it is seen that the major contribution to β_{ext} occurs in the size range from 0.1 to 2.0 - $3.0 \mu\text{m}$ radius. The same is true for β_{sca} and β_{abs} also and hence are not plotted. So depending on the experimental technique employed and the parameter of interest, say ν in Junge size distribution and r_m and σ in LND, both the size distributions can adequately be used, provided they cover the important aerosol range of 0.1 - $3.0 \mu\text{m}$. Though in general, this is the range suitable for optical investigations, observations have shown that desert and sea salt aerosols can have radius of $20 \mu\text{m}$ and above, but the number density of these aerosols is small and also their residence times are very short [*d'Almeida et al.*, 1991]. It is not ascertained how long particles above $20 \mu\text{m}$ can remain in the atmosphere in an urban

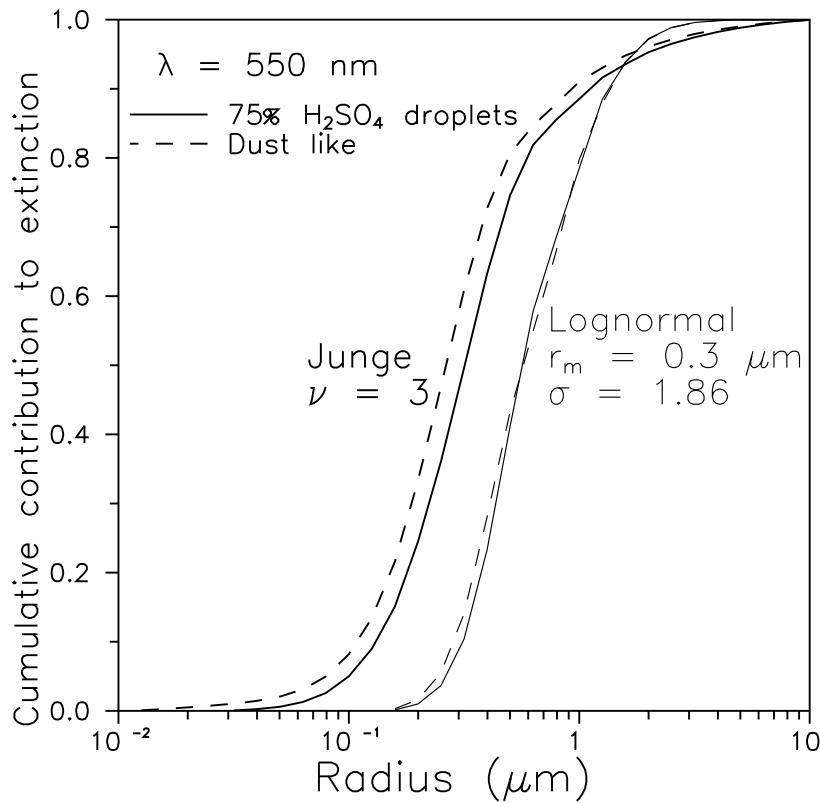


Figure 2.10: Cumulative contribution of Q_{ext} to β_{ext} by particles of sizes from 0.01 to 10.0 μm for Junge and lognormal size distributions for 75% H_2SO_4 droplets and dust like particles.

environment and whether can take part in the radiative transfer process.

2.2.7 Spectral dependence of aerosol extinction coefficients and its dependence on relative humidity

The spectral (wavelength) exponent α defined by Ångström as

$$\beta_{ext} = k \lambda^{-\alpha} \quad (2.15)$$

where k is Ångström coefficient can be obtained by plotting the aerosol extinction coefficients with respect to wavelength on a log-log scale wherein the slope of the curve determines α . In this section an attempt is made to determine α for various aerosol types and models in the visible wavelength and near infrared ranges and the results are discussed.

The aerosol extinction coefficients are calculated for various models and aerosol types obeying lognormal distributions given by *d'Almeida et al.* [1991] for the wavelength region 300 to 1050 nm and α is determined.

In Figure 2.11 β_{ext} obtained for a 75% H_2SO_4 particle for different mode radii are plotted. It is apparent that the extinction coefficients increase for a size distribution when the mode radius is large whereas they decrease for a small mode radius. This in general is valid for all types of particles. α varies from 1.5 for 0.07 μm to about -0.1 for 1.0 μm , which clearly shows that as the mode radius increases, keeping the width of the size distribution constant, it encompasses more and more large particles, which leads to a lower α value and also the extinction coefficient shows almost a linear dependence with respect to wavelength. The same result is found to be true for various widths of the size distribution, keeping the mode radius r_m constant. So in general, it becomes essential to know two different quantities in order to adequately describe aerosol extinction in the atmosphere. They are refractive index of the particle, especially the imaginary part of it, as it conveys the absorption characteristics of the particle and particle size distribution. Apart from these two, it is essential to know the particle shapes, which we assume to be spherical.

The permanent presence of water vapour in the atmosphere, except in the arid and semi-arid regions, affects the aerosol by aiding it to grow bigger or shrink in size. The growth of aerosol particle results in a change in the size, shape and chemical composition of the particle and affects the radiative characteristics owing to changes in the radius and refractive index [*Hänel*, 1976].

The aerosol extinction coefficients from 300 to 1000 nm for various relative humidity classes ranging from 0% to 99% given by *d'Almeida et al.* [1991] have been used to determine α . The aerosol extinction coefficients are found to increase in general with increasing relative humidity, but in a distinct way, representative of the various components present in the model. But α values give interesting results. In Figure 2.12 the variation of α with relative humidity is plotted for six aerosol models.

For Polluted maritime, Clean continental, Average continental and Urban aerosol models, the α values decrease with increasing relative humidity and the effect is more prominent when the relative humidity is higher than 80%. Interestingly Clean maritime shows almost no change in α value with increasing relative humidity. Mineral maritime model which consists of larger particles has a $-\alpha$ value at 0% relative humidity and then approaches toward $+\alpha$ as the relative humidity increases.

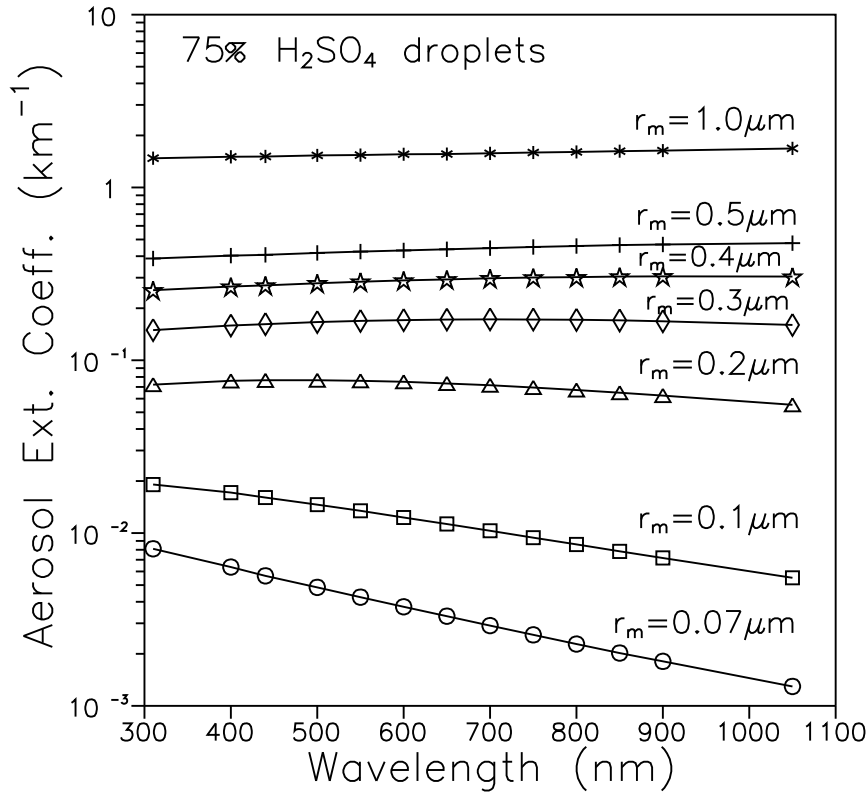


Figure 2.11: *Aerosol extinction coefficients for a lognormal size distribution having mode radius varying from 0.07 to 1.0 μm show that as the mode radius increases the size distribution encompasses more and more larger particles and the dependence of extinction on the particle size becomes less.*

Single scattering albedo (ω_0) is a parameter which has application in climate modeling studies and in satellite inversions while using the radiative transfer code. Essentially single scattering albedo determines whether the Earth-atmosphere system gets cooler or warmer because of the presence of aerosols. Weakly absorbing aerosols ($\omega_0 \sim 1$) which predominantly scatter radiation, increase the amount of energy backscattered to space. As the energy input to the Earth-atmosphere system gets reduced, it results in a net cooling of the system. The magnitude of this increase in planetary albedo is a function of particle size, optical depth and the location of the aerosol layer [Ackerman, 1988]. The asymmetry factor g at a given wavelength increases with increasing particle size for a fixed aerosol composition, thus the smaller particles tend to increase the planetary albedo in comparison to large particles for the same optical depth. Absorbing aerosols ($\omega_0 \leq 0.8$) tend to reduce the solar energy lost from

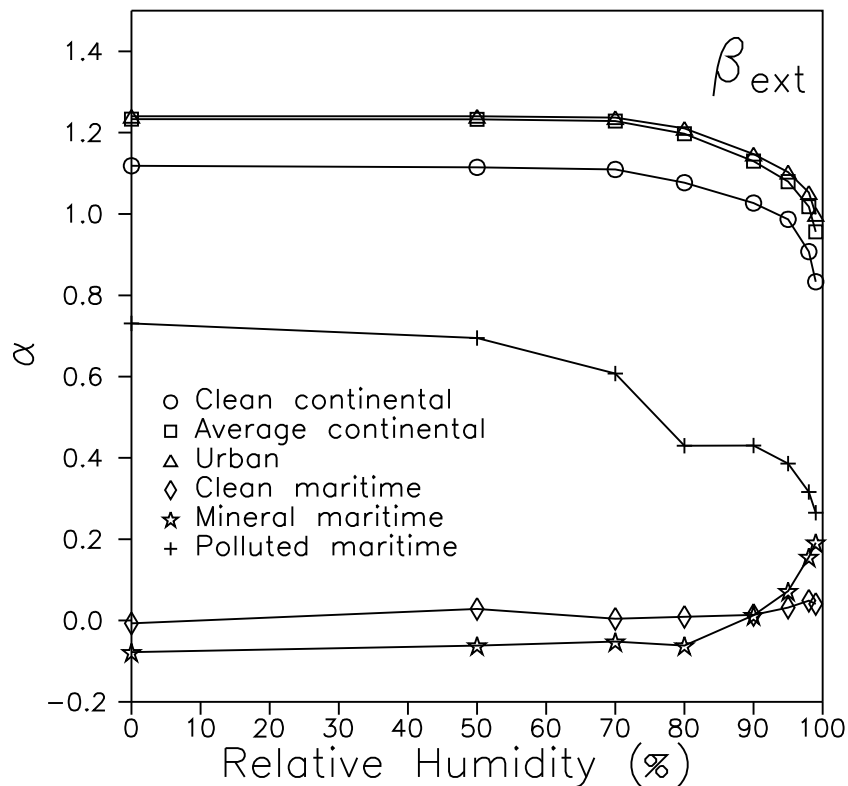


Figure 2.12: The variation of Ångström's wavelength exponent α with respect to change in relative humidity for six aerosol models.

the Earth-atmosphere system by absorbing solar radiation that otherwise would be reflected from clouds and from the surface. The Earth-atmosphere system would then get warmed up as the energy input gets increased. But after large volcanic eruptions, large amount of sulphate particles are present in the stratosphere. Though ω_0 is nearly 1 for these particles in the visible wavelength range, in the infrared region they are highly absorbing, leading to a heating due to the absorption of solar radiation as well as the upwelling thermal radiation. This effect is seen where the aerosol layer is present and as the layer scatters the incoming solar radiation a cooling effect will occur in troposphere, as was seen after El Chichon and Mt. Pinatubo eruptions. Pollack *et al.* [1981] estimated that when ω_0 becomes ≤ 0.98 it would change the sign of climate forcing from cooling to heating. Various aerosol types can have ω_0 varying from 0.1 to about 0.9 depending on wavelength and season [d'Almeida *et al.*, 1991].

Chapter 3

Tropospheric aerosols

3.1 Introduction

The sources of tropospheric aerosols vary from gas-to-particle conversion process to mechanical processes such as wind blown dust, volcanic emissions, soot from industries, vehicle exhaust, sea spray etc. Accordingly their residence times and removal processes vary greatly. Depending on the parameter of interest the measurement techniques employed to study aerosol characteristics can vary from ground based to space borne. In this chapter a brief summary of the measurement techniques employed for determining aerosol characteristics with an emphasis on the troposphere is provided and a description of various other measurement techniques relevant to stratospheric aerosol study is deferred to Chapter 4. Measurement of aerosol characteristics can be done by ground based techniques such as Sun photometer [Volz, 1970], lidar (laser radar) [Fiocco and Grams, 1964; Jäger and Hofmann, 1991; Takamura *et al.*, 1994], particle impactors [Junge, 1963; Jaenicke and Schütz, 1978] or air borne techniques such as balloons, either with optical particle counters [Hofmann, 1993] or impactors [Bigg, 1976] and satellites [Griggs, 1983; Quenzel, 1983; Kaufman *et al.*, 1990; Kent *et al.*, 1991].

Lidar makes use of the scattered radiation from particles in the medium being probed. Based on the configuration there are two types of lidars. The monostatic lidar [Fiocco and Grams, 1964; Jäger and Hofmann, 1991] is a system in which the transmitter and the receiver are collocated, whereas in the bistatic lidar system [Herman *et al.*, 1971; Parameswaran *et al.*, 1984; Devara *et al.*, 1994] the transmitter and the receiver are separated by a distance. While the monostatic lidar is capable of obtaining vertical profile of aerosols up to higher altitudes, the bistatic lidar can be used to study the angular distribution of the scattered intensity from

a desired altitude by changing the orientation of the transmitter and the receiver, but the altitude coverage is limited to lower altitudes. The transmitter-receiver configuration determines the scattering volume. From the monostatic lidar the vertical profiles of aerosol extinction coefficients can be obtained [Parameswaran *et al.*, 1991] and in the bistatic mode the aerosol size distribution and number density can be obtained [Parameswaran *et al.*, 1984].

Sampling of particles is one of the most widely used methods to determine the physical and chemical characteristics of aerosols [Junge, 1963; Khemani *et al.*, 1982]. From the mass of aerosols collected in the various size ranges, the aerosol size distribution and the chemical composition can be determined.

Quenzel [1983] and Griggs [1983] determined the total optical depth of the medium from the scattered solar radiation intensity measurements over low albedo surfaces such as oceans. Kaufman *et al.* [1990] using the NOAA/AVHRR visible and near infrared channels determined the aerosol optical depth and particle radius from the satellite images of the surface (land and water). The aerosol optical depths were determined with an error of about 0.08-0.15 when the optical depth was in the range of 0.5-1.5. The satellite derived values were found to agree well with the Sun photometer measurements made from the ground. Determination of the aerosol optical depth using satellite data requires an apriori knowledge of the type of aerosol, aerosol phase function and single scattering albedo (ω_0). In their absence the results can only be qualitative and are useful for studying the variations in the aerosol loading [Jayaraman and Koepke, 1992]. However, the natural variability of the aerosol size distribution even at one place can create variations in the radiance measured by the satellite (for example over the Atlantic off West Africa, both maritime background aerosol and Saharan dust aerosol are present simultaneously) [Quenzel, 1983]. The next difficulty arises from the noninclusion of the multiple scattering processes in the computations of the radiation field. Especially in cases such as desert dust outbreaks the aerosol optical depths become too high to neglect the multiple scattering effect [Jayaraman and Subbaraya, 1993b]. The satellite-borne, Stratospheric Aerosol Gas Experiments (SAGE I, SAGE II) of NASA are meant for monitoring stratospheric and tropospheric aerosols. In these measurements Sun photometers are used to determine aerosol characteristics [Kent *et al.*, 1991; Kent *et al.*, 1994]. Kent *et al.* [1994] compared the SAGE I and II data with the surface radiometer data and the results showed good agreement. Also in these experiments vertical profiles of aerosol extinction coefficients are obtained which are integrated to determine the aerosol optical depths. The presence of high-altitude clouds adversely affect the satellite borne studies on tropospheric aerosols.

Using balloonborne optical particle counters *Hofmann* [1993] studied tropospheric aerosol number density from 2 km above the ground, over a period of 2 decades, over Laramie, Wyoming (41°N) starting from 1971.

Sun photometry is one of the most widely used techniques for measuring aerosol properties by which the aerosol optical depths can be directly obtained, unlike other remote sensing techniques, where the data have to be analysed using complex inversion algorithms to evaluate the optical depths. The other methods require a knowledge of the type of aerosols in the medium. Also, no absolute calibration of the instrument is necessary in case of Sun photometers and comparison of results with other measurements is relatively easy, as the optical depths are directly derived. Volz sun photometry [Volz, 1970] is one of the most widely used techniques for atmospheric turbidity [Ångström, 1961; Flowers *et al.*, 1969] measurement. From the turbidity measurements attempts were also made to draw an inference on the aerosol properties [Ångström, 1961].

Direct-Sun photometry at multiple wavelengths is a useful method to characterise aerosols in the Earth's atmosphere. The technique is based on the principle of sunlight attenuation by scattering and absorption of aerosols. Generally by measuring the absolute value of ground level direct solar irradiance and comparing it to the known value of incident solar irradiance, the aerosol induced optical attenuation of the atmosphere in a narrow wavelength band is derived [Shaw, 1976]. The information on the aerosol size distribution can be obtained from the spectral variation of the extinction of light through the atmosphere, as particles of different sizes scatter light differently. An advantage of such multiwavelength Sun photometry as compared to 'point' collections of aerosols, is its relevance to the column integrated atmospheric quantities, that is, the assessment of amount of aerosol in the entire atmosphere, a quantity likely to be much more valuable to climatic investigations than surface parameters only [Shaw, 1983].

In this chapter the features of aerosol optical depths observed over Ahmedabad (23°N, 72.5°E) located in western India, an urban station with several industries, the possible aerosol type over the station is a mixture of water soluble, dust like and soot aerosols, are discussed. Soil dust, vehicle and industrial exhausts are the major sources of aerosols in Ahmedabad.

3.2 Ground based Sun-tracking photometer observations over Ahmedabad

An automatic Sun-tracking multichannel photometer was developed at the Physical Research Laboratory for aerosol measurements both at Ahmedabad (23°N , 72.5°E) as well as onboard balloons from Hyderabad (17.5°N , 78.6°E). The experimental programme was initiated to study the day to day and seasonal variations in aerosol optical depths induced due to natural and anthropogenic phenomena, for over a period of 5 years from 1991 to 1995. The observation period encompasses some of the devastating events that had strong influence on the atmosphere, namely the Gulf oil fires in early 1991 and Pinatubo volcanic eruption in mid-1991. The 'Operation Desert Storm' left about 600 naturally pressurised oil wells aflame in Kuwait in late February 1991 injecting large quantities of smoke, sulphur dioxide etc. into the atmosphere [Johnson *et al.*, 1991]. As Ahmedabad is located in the same zonal belt as Kuwait and also as the wind direction during the period is in general eastward, perturbation, if any, in the aerosol optical depth should be detectable over Ahmedabad. As the residence time of tropospheric aerosols is of the order of few months [Prospero *et al.*, 1983] measurements were repeated in 1992 during the same period in order to bring out the difference between the two data sets as a consequence of the fires. However, the Mt. Pinatubo eruption, which occurred in Philippines in June 1991 had a greater impact on the aerosol characteristics all around the globe [Stowe *et al.*, 1992] and marred the post Gulf oil fire effects. Several interesting features in aerosol optical depths and their temporal variations, revealed by the Sun-tracking photometer observations over Ahmedabad for a period of about 5 years will be discussed in this chapter.

3.2.1 Instrumentation

A six channel Sun-tracking photometer was used to measure the direct solar radiation intensities in the selected spectral bands, centered at 319, 441, 491, 736, 852 and 952 nm. However, since 1992 the 736 nm channel has been converted into 1051 nm in order to extend the spectral coverage of measurements. The data corresponding to 319 and 952 nm are used to obtain ozone and water vapour optical depths respectively, while the data corresponding to other photometers are used for aerosol studies.

Figure 3.1 shows the block diagram and photograph of the Sun-tracking photometer system. The instrument consists of a sensor assembly containing six photometers, the tracking

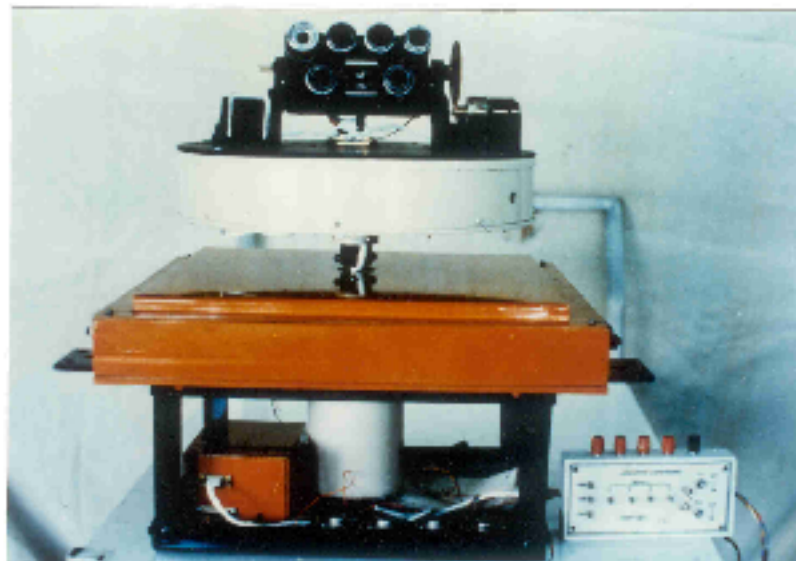
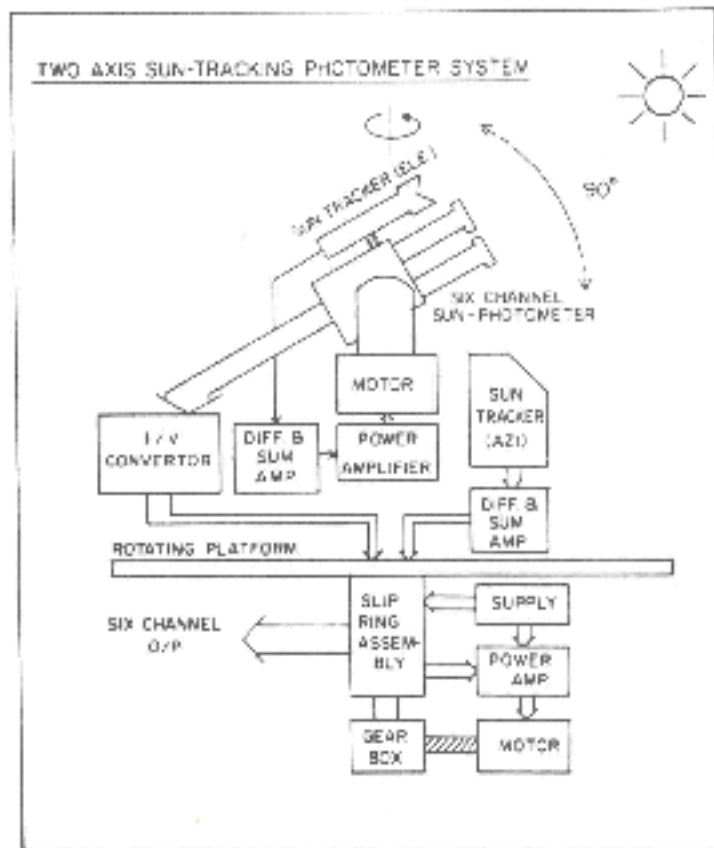


Figure 3.1: Block diagram and photograph of the six channel two-axis Sun-tracking photometer system.

mechanism for the zenith orientation of the photometers and a mechanical assembly consisting of a motor, gear box and slip rings to enable azimuthal tracking. Each photometer is a combination of a photodiode or a phototube and an interference filter. The field of view of the photometers is restricted to about 9° , using baffles. Hamamatsu R 765 solar blind phototube having spectral sensitivity only in the UV range has been used in the 319 nm photometer. For other wavelengths UV-100 photodiodes (EG&G) having spectral response from 200-1150 nm are used. The optical characteristics of the photometers used are given in Table 3.1. The filters are calibrated with a Beckman UV-Visible spectrophotometer (Model 3600, USA). As the performance of the filters can deteriorate with time, routine calibrations of the filters are made. The tracking of the Sun in elevation is achieved using two photodiodes mounted perpendicular to each other in the vertical direction. The freedom of rotation of the photometer assembly in the vertical direction is restricted between 0° and 90° , by means of two micro switches. The difference in the photodiode currents is amplified by means of a difference and sum amplifier. The amplified output is fed to a motor which orients the sensor assembly towards the Sun. A similar arrangement of photodiodes has been used for tracking in azimuth. Two 'view sensors' (solar cells) are mounted with an angular separation of 120° at the rear side of the tracking platform to bring the photometer assembly into the field of view of the azimuthal tracking sensors. The output currents from the photometers are converted into voltages using current to voltage convertor and the data are stored in computer through a PC add-on A/D card.

3.2.2 Theory

The atmospheric transmission T at any wavelength λ takes the general form

$$T_i = e^{-[\sigma_i(\lambda) n_i m]} \quad (3.1)$$

for any species i under consideration, be it air, aerosol, ozone or water vapour, $\sigma_i(\lambda)$ is the corresponding absorption/scattering cross section of the species, n_i is the column density of the species and m is the air mass expressed as

$$m = \left[\frac{\sqrt{(r^2 \cos^2 \theta + 2rH + H^2)} - r \cos \theta}{H} \right] \quad (3.2)$$

where r is the radius of the Earth at the latitude of observation, H is the scale height and θ is the solar zenith angle.

Table 3.1: *Optical characteristics of the Sun-tracking photometer system.*

Channel	Center Wavelength λ_{\max} (nm)	FWHM* nm	Transmission at λ_{\max} (%)	Photodetector
1	319	15	15.4	R 765 phototube
2	441	9	33.0	UV 100 photodiode
3	491	11	34.5	-do-
4	736	17	28.0	-do-
5	852	14	21.0	-do-
6	952	20	40.0	-do-
7	1051	25	39.8	-do-

* Full Width at Half Maximum

However in photometry technique, measurements are taken for a wavelength band from λ_1 to λ_2 and hence an effective transmission $T_i(\text{eff})$ is to be defined to average out the variations in σ , solar flux (SF) and the detector response functions such as the filter transmission (FT) and photodiode efficiency (PE) which are all functions of λ .

$$T_i(\text{eff}) = \frac{\int_{\lambda_1}^{\lambda_2} T_i(\lambda) FT(\lambda) PE(\lambda) SF(\lambda) d\lambda}{\int_{\lambda_1}^{\lambda_2} FT(\lambda) PE(\lambda) SF(\lambda) d\lambda} \quad (3.3)$$

The transmission due to Rayleigh scattering and Rayleigh optical depths are calculated following *Penndorf* [1957]. The aerosol optical depths are calculated from the *Elterman* [1970] model. The column density of ozone over Ahmedabad was taken from the Dobson ozone data [*Angreji*, 1989] and the ozone optical depths were calculated. The water vapour optical depth is calculated from the absorptance of water vapour reported in literature [*Tanaka et al.*, 1982]. The columnar number density n of water vapour can be obtained using the relation

$$n = n_o \left(\frac{p}{760} \right) \left(\frac{273}{T} \right) \quad (3.4)$$

where n_o is Loschmidt's number = 2.687×10^{19} molecules cm^{-3} . p (= 63 torr) and T (= 296°K) are the laboratory values of pressure and temperature at which the absorptance ($1 - T$) values are measured [*Tanaka et al.*, 1982]. From the *Water vapour atlas of India* [*Sarkar et al.*, 1982] the model humidity profiles are converted [*Hudson*, 1969] into total precipitable water content (in mm km^{-1}) or in other words, the column density of water vapour from the ground

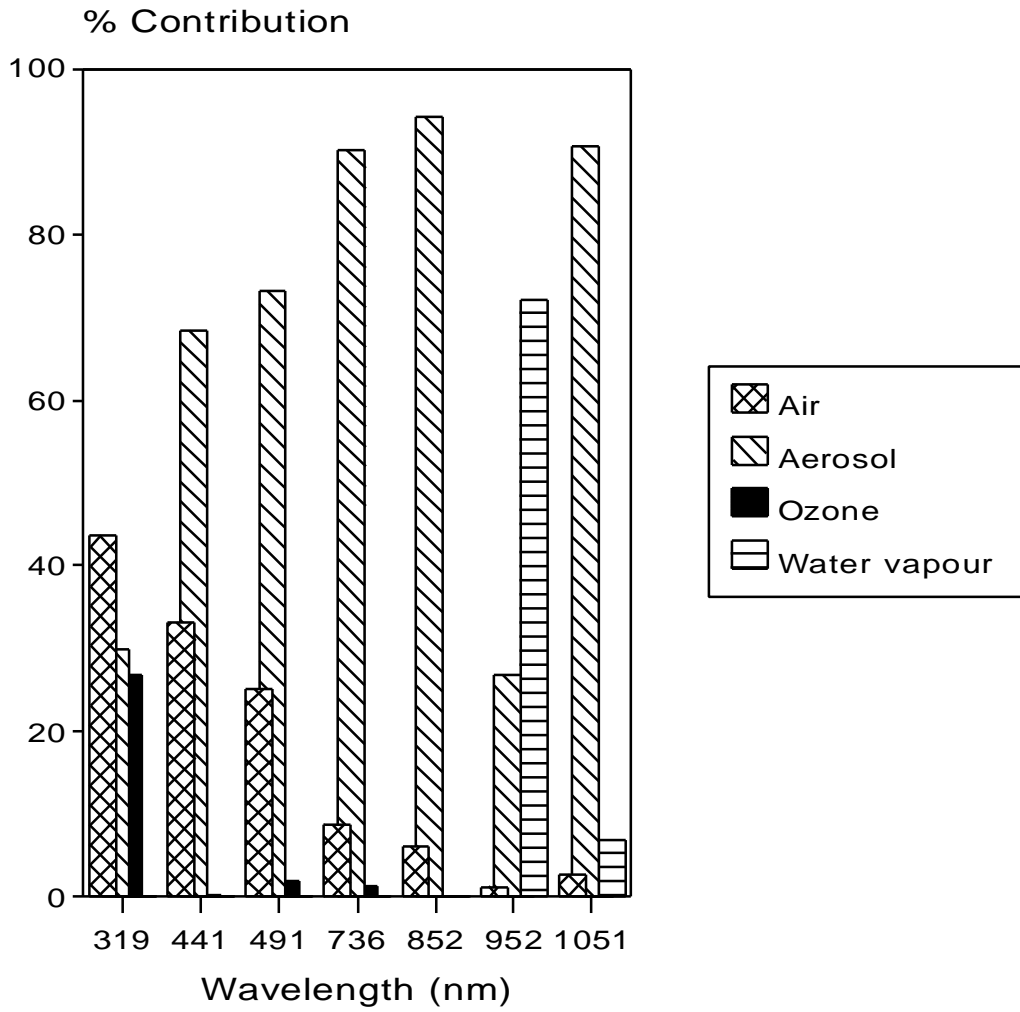


Figure 3.2: Diagram illustrating the relative contributions of air, aerosol, ozone and water vapour to the total optical depth for the respective photometers (Table 3.1) used in the present study.

to the top of the atmosphere is obtained and used to estimate the optical depth due to water vapour absorption. The values of the solar flux at the top of the atmosphere are taken from Nicolet [1989] and Thekaekara and Drummond [1971] between 280 nm and 1100 nm. These values are multiplied by respective transmissions due to air, aerosol, ozone and water vapour in order to get the solar flux values (SF in Eqn. 3.3) at the ground.

The relative contributions of Rayleigh scattering optical depth (τ_{rs}), aerosol optical depth ($\tau_{aerosol}$), ozone optical depth (τ_{ozone}) and water vapour optical depth (τ_{water}) to the total optical depth in all the wavelength bands are shown in Figure 3.2.

3.2.3 Experiment and Data analysis

The period of measurements of the transmitted solar radiation intensities taken over Ahmedabad is listed in Table 3.2. (✓ indicates the months, for which the data are available for at least

Table 3.2: *The period of Sun-tracking photometer observations over Ahmedabad.*

Year	Months											
	J	F	M	A	M	J	J	A	S	O	N	D
1991	✓	✓	✓				Monsoon					
1992	✓	✓	✓									
1993		✓	✓	✓	✓	✓	Overcast				✓	✓
1994				✓	✓	✓				✓	✓	✓
1995	✓	✓	✓	✓	✓		sky					

10 days and more.)

The observations are taken at an interval of 10 minutes from sunrise to sunset, for various solar zenith angles. Following Beer-Lambert's law, the total integrated columnar optical depth of the atmosphere can be written as

$$\tau = \frac{-1}{m} \left[\ln \left(\frac{I}{I_0} \right) - 2 \ln \left(\frac{r_0}{r} \right) \right] \quad (3.5)$$

where I is the instantaneous solar radiation intensity measured by the photometer and I_0 is the solar radiation intensity obtained from Langley plot for zero airmass, m is the atmospheric airmass, r is the instantaneous value of the Sun-Earth distance and r_0 is the Sun-Earth distance when I_0 values are obtained. The total integrated columnar optical depth of the atmosphere

$$\tau = \tau_{rs} + \tau_{aerosol} + \tau_{ma} \quad (3.6)$$

where τ_{rs} is the Rayleigh scattering optical depth (scattering due to air molecules), $\tau_{aerosol}$ is the aerosol optical depth and τ_{ma} is the optical depth due to molecular absorptions such as ozone, water vapour or nitrogen dioxide. The aerosol optical depth $\tau_{aerosol}$ can be obtained by subtracting τ_{rs} and τ_{ma} from τ . An average air column density of 2.14×10^{25} molecules cm^{-2} derived from a series of rocket experiments [Sasi and Sengupta, 1979] is used in the estimation of τ_{rs} . The annual variation in the air column density inclusive of seasonal dispersion from January to December is not considered as it is found to be less than 2% [Sasi and Sengupta, 1986]. Differences in the total column density of air between the various reference atmospheres such as the Reference Atmosphere for Equatorial Zone [Sasi and Sengupta,

1979] and the *U. S. Standard Atmosphere* [1966] are in the range of 1% and not considered in the present work. τ_{ma} for ozone absorption is estimated using the available mean ozone column concentrations derived from Dobson measurements at Ahmedabad for over 30 years [Angreji, 1989]. The monthly mean variations in the ozone column density, which is found to be about 3 to 4% from autumn to spring is also not considered here. τ_{ma} for water vapour is estimated for each month from the monthly mean values of total column density of water vapour [Sarkar *et al.*, 1982]. The contribution by NO_2 to the total optical depth around 440 nm where it has the maximum absorption cross section is in the range of 0.5% and less and is not considered in the present study.

The atmospheric airmass (m) is calculated from corresponding time information by converting it to local mean time using the equation of time and solar declination angle (δ) for the day from the Astronomical Ephemeris using the equation

$$m = (\sin\delta \sin\phi + \cos\delta \cos\phi \cos H)^{-1} \quad (3.7)$$

where ϕ is the latitude of the place and H is the hour angle. For solar zenith angle greater than 60° , m is calculated taking into account the curvature of the Earth (Eqn. 3.2).

3.2.4 Determination of $I_o(\lambda)$ and Optical depth τ

$I_o(\lambda)$ values are obtained using Langley plot technique. In this technique, the natural logarithm of the photometer outputs measured for various solar zenith angles are plotted with respect to airmass. Through the experimentally observed points a least square fitted straight line is drawn and is extrapolated to meet zero airmass in the abscissa. The intercept gives $I_o(\lambda)$ of a particular photometer. Similarly, Langley plots are made to obtain $I_o(\lambda)$ for all individual photometers. The voltage $I_o(\lambda)$ obtained for zero airmass is a constant in time for a particular photometer, if the response of the instrument is constant and if the value is corrected for the mean solar distance. Since $I_o(\lambda)$ values are constant for each photometer, they can be used together with each individual photometer output I to obtain the corresponding optical depth τ using Eqn. 3.5.

To draw Langley plots observations are to be taken in a cleaner and stable atmosphere where the effects of local pollutants are minimum. These conditions are best met at high altitude mountain sites. In the present case observations are taken for a period of about one week from sunrise to sunset, at Gurushikhar (24.6°N , 72.72°E) in Mt. Abu, at a height of about 1680 metres above the mean sea level, once in a year. Mt. Abu is preferred because

Table 3.3: $I_o(\lambda)$ values obtained at Mt. Abu using Langley plot technique.

Date	Wavelength (λ) nm					
	319	441	491	736	852	952
11 May 1991	68.84	6.97	3.23	4.07	3.04	4.40
12 May 1991	72.32	7.55	3.39	4.05	3.00	4.35
13 May 1991	79.90	7.36	3.46	4.10	3.28	4.48
14 May 1991	72.26	7.06	3.07	4.00	2.94	4.06
Mean	73.33	7.23	3.29	4.05	3.07	4.32
Sigma	4.05	0.23	0.15	0.04	0.13	0.16

at Ahmedabad, industrial pollutants, vehicle smoke etc. not only pollute the atmosphere but also introduce diurnal variations in aerosol optical depth as could be seen in the Langley plot (Figure 3.3a). Drawing Langley plots and finding $I_o(\lambda)$ for individual photometer helps to calibrate the instrument once and for all. The $I_o(\lambda)$ values obtained for various photometers are given in Table 3.3. Due to technical difficulties during 1992, the photometers could not be calibrated at Gurushikhar but were calibrated in Hyderabad (17.5°N, 78.6°E), at the balloon launch station well away from the Hyderabad city.

A typical Langley plot obtained for 852 nm at Mt. Abu on 11 May 1991 is shown as an example (Figure 3.3b). In an idealised Langley plot the natural logarithm of all the observed solar radiation intensities will fall in a straight line when plotted versus airmass (m). In order to study the difference, if any, between the data collected between morning and evening hours a detailed analysis was made as suggested by *Kremser et al.* [1984], in which morning and afternoon data points are treated separately. The observations made before noon i.e. between 0700 and 1130 hrs are taken as morning data and observations made before sunset but between 1400 and 1800 hrs are taken as evening data. Langley plots are drawn for each of these data sets on all the days. The $I_o(\lambda)$ values obtained for the morning and evening data sets for each photometer are shown in Table 3.4. These values are found to compare well (within $\pm 1\sigma$) with the $I_o(\lambda)$ values obtained taking into account all the data points, indicating the stability of the atmosphere over Gurushikhar when the observations are made. The $I_o(\lambda)$ values thus obtained are used in determining the total columnar optical depths over Ahmedabad. The accuracy of the optical depths depends on the accuracy of the solar radiation intensity data with which it is measured. Due to Sun-tracking mechanism, the I values

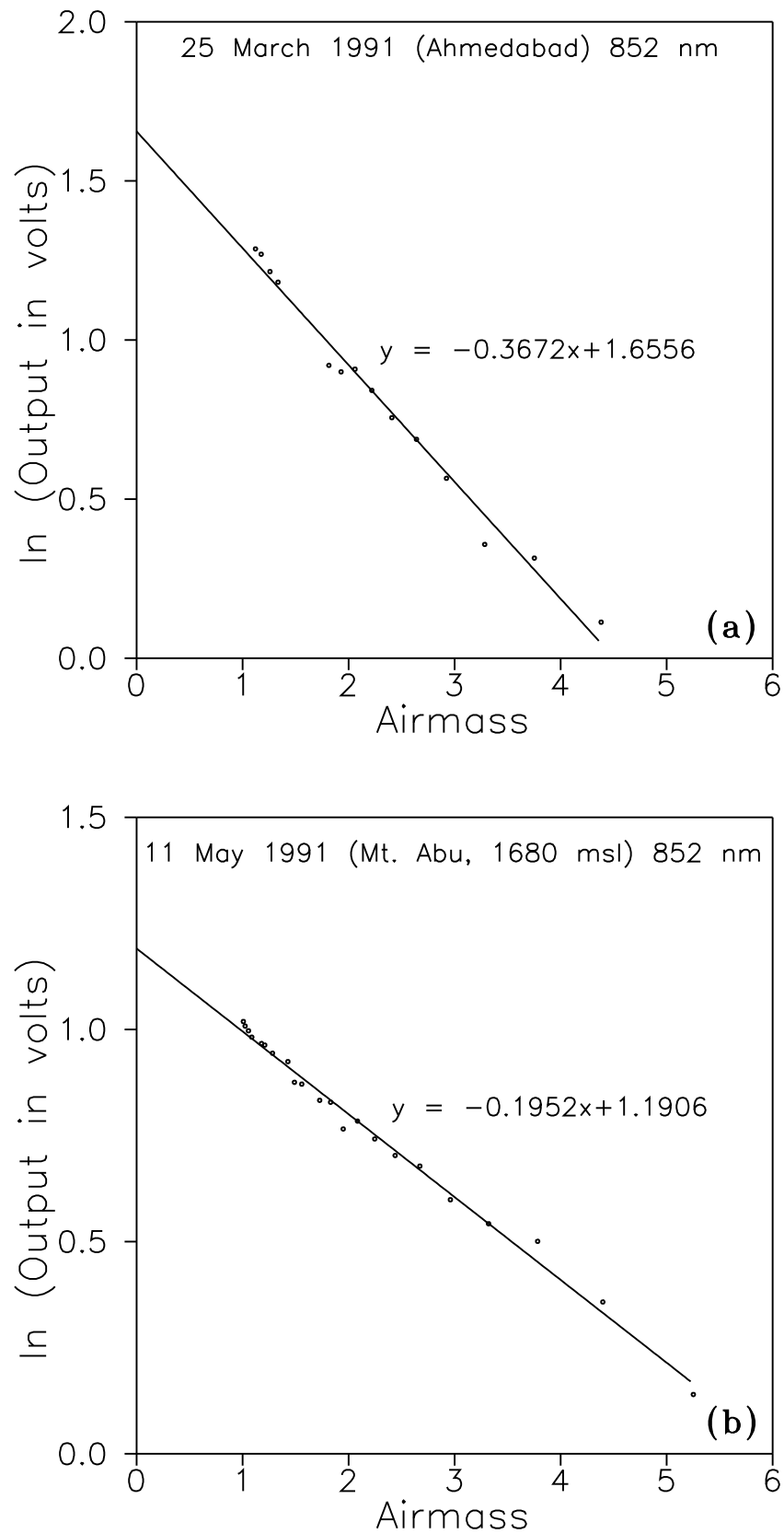


Figure 3.3: A typical Langley plot using Sun-tracking photometer data obtained at (a) Ahmedabad and (b) Mt. Abu (1680 m above msl).

Table 3.4: Comparison of $I_o(\lambda)$ values obtained using Langley plot technique for morning and evening and the $I_o(\lambda)$ values used in calculation.

Date	Session	Wavelength (λ) nm					
		319	441	491	736	852	952
11 May 1991	Morning		6.34	3.09	3.97	2.95	4.19
	Evening		7.13	3.38	4.36	3.18	4.49
12 May 1991	Morning		6.50	3.56	4.08	2.79	4.82
	Evening		7.96	3.47	4.36	3.17	4.25
13 May 1991	Morning		6.22	3.31	4.38	3.18	3.85
	Evening	72.38	7.51	3.48	4.34	3.28	4.26
14 May 1991	Morning		5.74	2.97	3.86	2.90	3.79
	Evening	66.39	6.17	3.00	3.78	2.90	3.16
	Mean	69.38	6.70	3.28	4.14	3.04	4.10
	Sigma	2.99	0.71	0.22	0.23	0.17	0.47
$I_o(\lambda)$ values used		73.33	7.23	3.29	4.05	3.07	4.32

are measured with an accuracy better than 1% and as the values are digitised through an A/D card, there is no further error in retrieving I values. However, as the aerosol optical depths are obtained after correcting for the molecular contributions and ozone and water vapour optical depths, the accuracy of the derived optical depths will depend on the model values used. Also it should be noted that the $I_o(\lambda)$ values determined for each photometer have a variation around the mean value as shown in Table 3.3. This uncertainty in $I_o(\lambda)$ can introduce an error as high as 70% in the derived optical depth values, depending on the Sun position (solar zenith angle variation) as well as the turbidity on a particular day. It is noted that for high optical depth values (as it is encountered over Ahmedabad in most of the cases) the uncertainty in the optical depths will be less (less than 30%).

Since the same instrument was flown later on balloon in October 1991, some changes had to be done to accommodate one more gain level and the electronics was also changed and

Table 3.5: $I_o(\lambda)$ values obtained during 1992 to 1995 and corrected for the Sun - Earth distance.

Year	Wavelength (λ) nm					
	319	441	491	852	952	1051
1992	1.69	2.42	2.01	2.15	1.00	2.39
1993	1.57	2.59	2.15	2.12	0.98	2.30
1994	1.54	2.60	1.97	2.03	0.93	2.20
1995	1.73	2.76	2.27	1.87	0.98	2.50

hence the difference in I_o values between 1991 and the rest of the years. Though the differences in $I_o(\lambda)$ values are of the order of $\pm 10\%$ during 1992 to 1995 (Table 3.5), between two successive years, the aerosol optical depths are calculated using the $I_o(\lambda)$ values as appropriate for each observation period.

The aerosol optical depths obtained are further analysed using Ångström's power law

$$\tau_{\text{aerosol}} = \beta \lambda^{-\alpha} \quad (3.8)$$

where β and α are Ångström parameters commonly used to describe the columnar distribution of aerosols. The wavelength exponent α describes the size distribution parameter of aerosols. Higher the α value smaller the aerosol particle size and vice versa. β is directly proportional to the amount of aerosol particles along the Sun path [Ångström, 1961].

Though observations are taken at Ahmedabad throughout the day, aerosol optical depths obtained between 1100 and 1200 hrs only are used to derive the wavelength exponent and their day to day variations are studied. A fixed time was chosen in preference to the daily average since the aerosol optical depths normally show a diurnal variation.

3.3 Results and Discussion

3.3.1 Diurnal, day to day and monthly variations in aerosol optical depths over Ahmedabad

About 40 observations of solar radiation intensities are made each day over Ahmedabad and aerosol optical depths are derived using the procedure outlined above. On most of the occasions the obtained aerosol optical depths are found to show diurnal type variation. In Fig-

ure 3.4 the diurnal variations of aerosol optical depths obtained on three typical days in the months of January, February and March, for the 491 nm channel, during the year 1991 are shown as an example.

As discussed earlier no separate attempts have been made to obtain I_o on individual days, instead the I_o values derived for individual channels from Mt. Abu/Hyderabad are used. Hence the observed diurnal type variations could be due to the uncertainty in the derived I_o values. However, actual diurnal variation in aerosol optical depths in an urban situation can also not be ruled out as discussed by *Shaw* [1976], in which case the apparent zero air-mass intercept I_o can be lower than the true I_o , with a resultant decrease in τ . It has been argued that in an urban situation, τ can increase in morning hours, when urban pollutants are emitted under a capping radiative inversion. However after noon hours, under solar heating, the inversion breaks down and convection currents which set in can ventilate the trapped pollutants out of the city limits and hence a reduction in the total columnar aerosol optical depth. This feature is seen at all wavelengths and on almost all days [*Ramachandran et al.*, 1994a]. The same feature was seen by *Pinker et al.* [1994] during the 'Harmattan' season in sub-Saharan Africa. This season brings in Saharan dry and dust laden air. But sometimes, the aerosol optical depths were found to be quite stable with little diurnal variability. The diurnal variability was explained on the basis of diurnal wind effects which could have brought in more dust laden air. The optical depths are high, of the order of 0.9-1.6 at 500 nm due to very dense dust. Over Vienna and Santiago de Chile the daily patterns of aerosol optical depths are different [*Horvath*, 1993]. In Vienna the aerosol optical depth peaks at 0800 and 1800 hrs very close to the peak traffic hours, indicating the influence of the vehicular traffic on the light absorption of aerosol. But in Santiago de Chile the aerosol optical depth peaks at around 0830 hrs and then decreases, the decrease has been attributed to the continuous increase in the height of the mixing layer during the daytime. The measurements of aerosol optical depths by *Weller and Leiterer* [1988] using a Sun-calibrated spectrophotometer off the Crimea Black Sea coast also show diurnal variations. But the measurements over Tsumeb (18°E, 19°S, a semiarid region in Namibia) revealed that the aerosol optical depths are quite stable during the day [*Kremser et al.*, 1984].

The aerosol optical depths also exhibit large day to day variations as shown in Figure 3.5. (As an example, to depict the daily variations in aerosol optical depths, data obtained during 1991 and 1992 are shown.) As 319 nm and 952 nm photometer data are used for ozone optical depth and water vapour optical depth calculations, they are not included in the figure, but

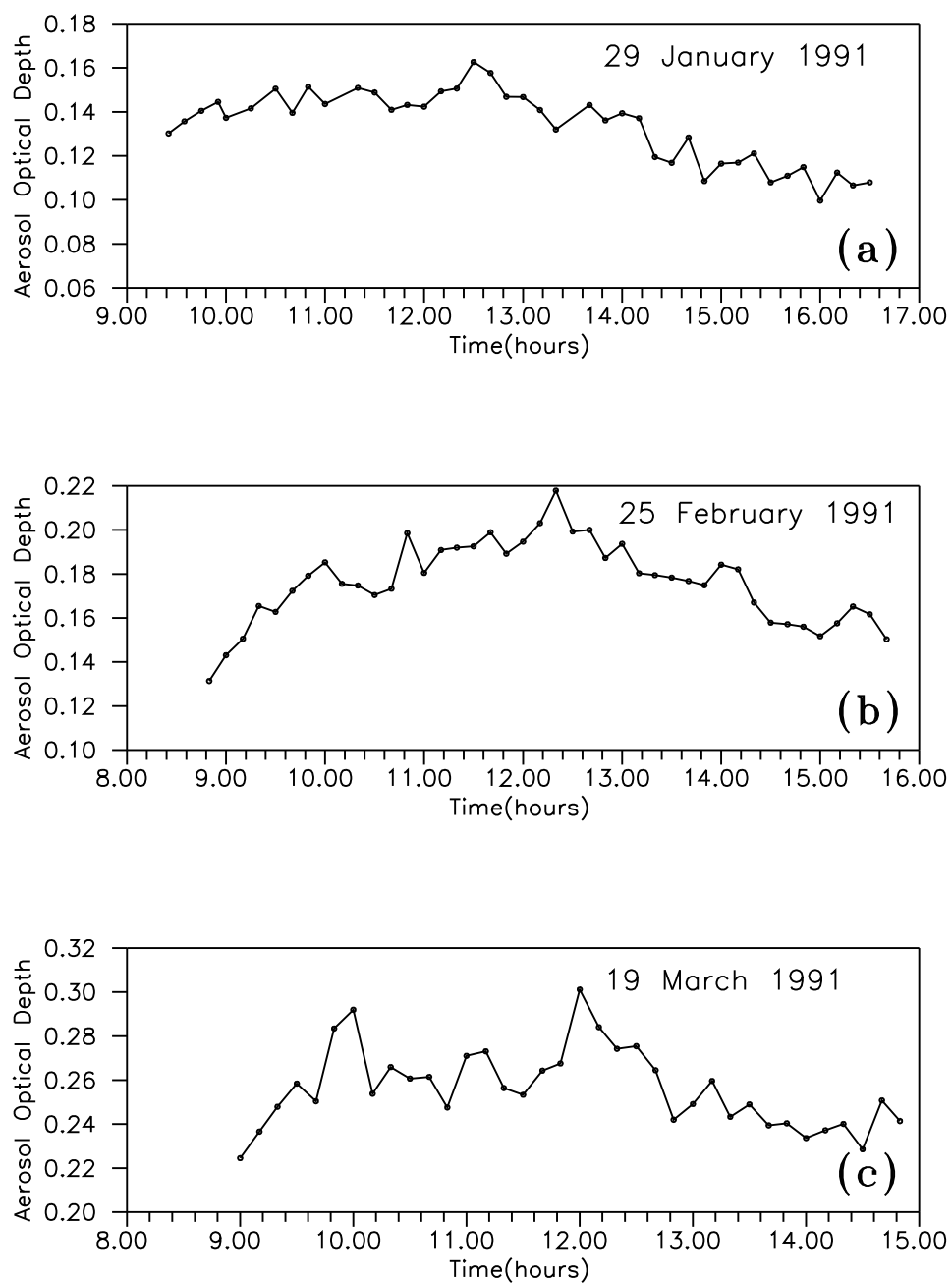


Figure 3.4: Diurnal variation of aerosol optical depths obtained over Ahmedabad for 491 nm channel during 1991.

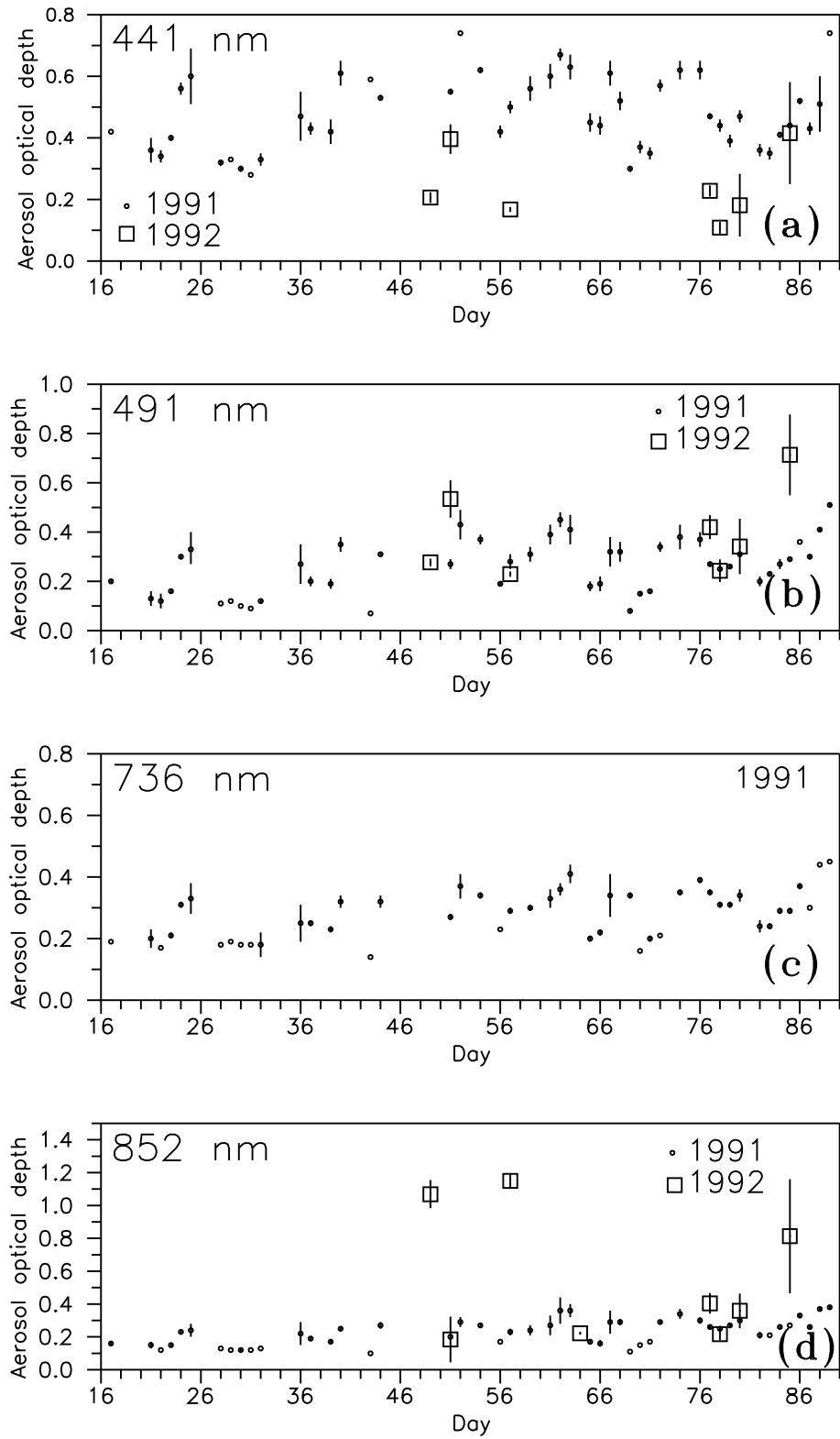


Figure 3.5: Day to day variation of aerosol optical depths for 441, 491, 736 and 852 nm. Mean of the data obtained during 1100 to 1200 hrs are shown. Vertical error bars represent two standard deviations ($\pm 1\sigma$) of the mean.

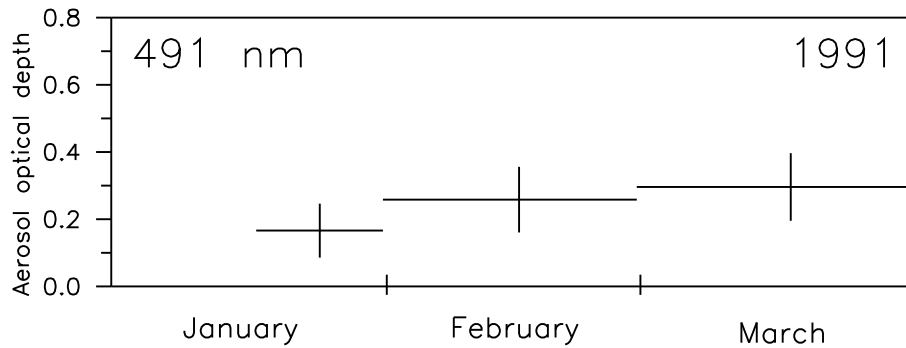


Figure 3.6: Variation of the monthly mean aerosol optical depth for the 491 nm channel. Vertical bars represent $\pm 1\sigma$ of the mean.

are shown separately. The day to day variations in optical depths are found to be associated with changes in meteorological parameters such as temperature and surface wind speed and direction. The aerosol optical depth values are also found to increase in general from January to March. As an example the 491 nm data, are shown in Figure 3.6 where the monthly mean values of the aerosol optical depth are plotted for the January to March 1991 period. This feature is seen at all the wavelengths in 1991 as well as in subsequent years' data sets. Similar feature has been reported earlier [Flowers *et al.*, 1969; Krishna Moorthy *et al.*, 1993] for other locations. The increase in optical depth is in general due to the increased surface temperature and low soil moisture content which can induce injection of more soil derived particles into the atmosphere. Photochemical activities [Pueschel *et al.*, 1972] can also play a role in producing aerosols *in situ* at lower tropospheric altitudes, but their seasonal dependence, if any, is not well known. The monthly mean aerosol optical depths obtained at 441 nm for the year 1993 are plotted in Figure 3.7.

By and large the aerosol optical depths are found to increase from January to May, all the years and after the monsoon rains, during which the particles get rainwashed, the aerosol optical depths are found to decrease during October to December period. As the aerosols over Ahmedabad are mainly wind blown dust particles, mechanically generated by the action of wind on dry land, the aerosol optical depths are found to increase from winter (December, January, February) to summer (April, May, June), by a factor of 4. The increase is attributed to the increased convective activity due to the increased surface heating in summer, which

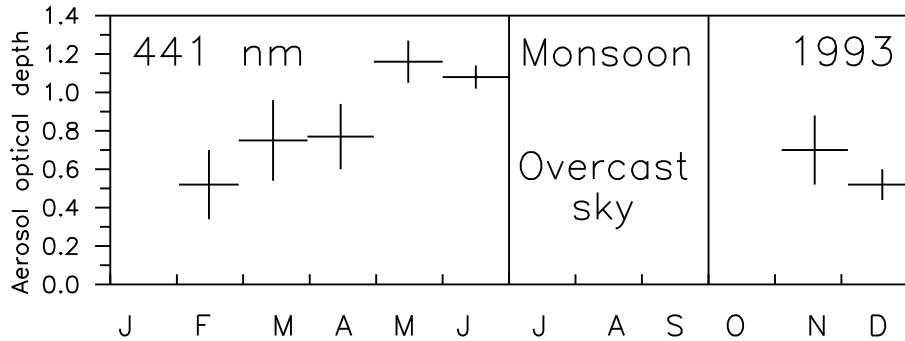


Figure 3.7: Variation of the monthly mean aerosol optical depths for the 441 nm channel for the year 1993. Vertical bars represent $\pm 1\sigma$ of the mean.

reduces the soil moisture content, thus inducing more soil derived particles into the atmosphere. Also, as these aerosols are large, about $1 \mu\text{m}$, they are confined to the lower troposphere and are not lifted to higher altitudes, but are removed by sedimentation and monsoon rains, during the June-September period. Though these features in general are seen in all the years, 1993 data are shown for illustration. Similar features have been observed by *Krishna Moorthy et al.* [1993] using multiwavelength radiometers at different locations in India, representing different geographical areas, comprising of coastal stations, arid regions and urban stations.

3.3.2 Spectral dependence of aerosol optical depth

The spectral dependence of the aerosol optical depth is mainly governed by the aerosol columnar size distribution. Using matrix inversion methods, multiwavelength radiometer measurements of τ_{aerosol} could be analysed to find the total columnar size distributions, when the spectral dependence is nonmonotonic. *King et al.* [1978] developed a method for such inversion. Using multiwavelength radiometer data, they deduced the columnar size distributions. The distributions are classified into three types. A monotonically decreasing $\tau_{\text{aerosol}} - \lambda$ variation gives an inverse power law size distribution as

$$\frac{dn(r)}{d(\log r)} = cr^{-\nu} \quad (3.9)$$

where $n(r)$ is the total number density of aerosols between r and $r+dr$, r is the radius of aerosol particle, c is a constant and ν is the power law exponent. The value of ν is the slope of the fitted straight line. This distribution is referred to as Type 1 (Junge distribution). Type 2 size distribution is a monomodal type distribution with a distinct maximum in the number density at a particular value of r . Type 2 results from a $\tau_{\text{aerosol}} - \lambda$ variation with a negative curvature. The size where $dn(r)/d(\log r)$ peaks depends upon the maximum in the $\tau_{\text{aerosol}} - \lambda$ variation. Type 3 results from a $\tau_{\text{aerosol}} - \lambda$ variation with a positive curvature. This distribution resembles a bimodal type distribution with 2 peaks, one in the smaller radius range and the other in the larger radius range [Krishna Moorthy *et al.*, 1991].

As the present observations of aerosol optical depths are available only at four wavelengths, it is not possible to use a detailed inversion method which requires observations at more wavelengths (six or more), to obtain quantitatively reliable size distributions. However, the nature of aerosol size distributions can be inferred as follows: the spectral dependence of τ_{aerosol} plots showed a positive curvature in 1991 indicating bimodal type size distribution, with one radius peaking below $0.5 \mu\text{m}$ and the other at $0.75 \mu\text{m}$. But in 1992 the spectral dependence showed a negative curvature indicating a monomodal type distribution, peaking at a radius of $0.5 \mu\text{m}$. Asano *et al.* [1993] using ground based Sun photometry have also shown that at Tsukuba (36.1°N , 140.1°E) during 1991 the volume size spectra exhibit a bimodal feature with enhancements at smaller and larger radii above $0.5 \mu\text{m}$ which they attributed to tropospheric aerosols and the 1992 data exhibit a monomodal size distribution similar to the present results with the maximum radius at around $0.6 \mu\text{m}$ compared to $0.5 \mu\text{m}$ in the present case. Considering the aerosol production mechanisms, particles with sizes $\leq 0.5 \mu\text{m}$ are produced by a combination of nucleation from the gas phase and coagulation processes, whereas particles with sizes $\geq 1 \mu\text{m}$ are mainly the result of mechanical and wind stresses at the Earth's surface [King *et al.*, 1978]. The urban aerosol particles are in the size range from $0.1 \mu\text{m}$ to $1 \mu\text{m}$ (wind blown dust). A combination of the different production mechanisms may result in a bimodal distribution because of the distinct nature of these sources. A monomodal distribution would result when a strong source dominates over other sources. From the above discussion, it is seen that in 1991 (bimodal), there are two dominating sources, of which one could be of the smoke particles derived from the Gulf oil fires and the other could be the local wind derived mineral particles. In the case of 1992 data, the effect of post-volcanic aerosols due to Mt. Pinatubo can not be ruled out as also shown by Asano *et al.* [1993].

But the spectral variation curves obtained during February 1993 show a monomodal dis-

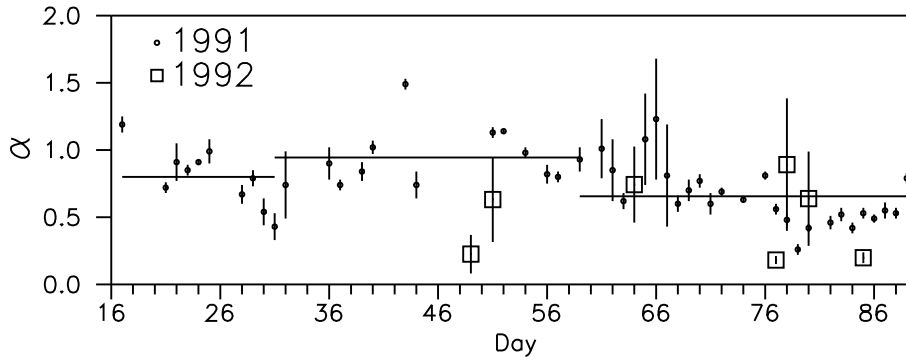


Figure 3.8: Variation in wavelength exponent, α from January to March in 1991 and 1992. The horizontal bars represent the monthly mean α values for the January-March, 1991 period.

tribution, March 1993 data shows a bimodal distribution, while during summer months of May and June two peaks are seen, one at $0.44 \mu\text{m}$ and the other at $1.05 \mu\text{m}$, which indicates the presence of larger particles, during summer. In the absence of a continuous data set, over this region, these results can only be taken as qualitative. Similar features of spectral variations have been observed by *Weller and Leiterer* [1988] and *Krishna Moorthy et al.* [1993]. The 1994 data in all the months, exhibit a peak at $0.5 \mu\text{m}$ and the aerosol optical depth remains almost the same for the other wavelengths. The aerosol optical depths are found to exhibit similar variations in 1995 also.

3.3.3 Variations in wavelength exponent α

The aerosol optical depth values when plotted against wavelength on a log-log scale, then the slope of the fitted line yields the wavelength exponent (α). It should be noted that while the 1991 τ_{aerosol} values could be fitted with λ with goodness of fit greater than 0.9, no simple function is found between τ_{aerosol} and λ in the 1992 data on most of the occasions. This holds good for the 1993, 1994 and 1995 data sets also. The α values in the case of 1992 are limited to only a few occasions. The wavelength exponent α when plotted with respect to days (Figure 3.8) shows an oscillating behaviour. The monthly mean α values of 1991 data are also shown.

The mean α value for February is found to be higher than that of January but decreases in March. While for Rayleigh scattering $\alpha = 4$, for aerosol or Mie scattering α decreases with the increasing size of particles. Low α values in March indicate the predominance of bigger particles which can be attributed to wind blown dust. Dust storm activity also shows an increase

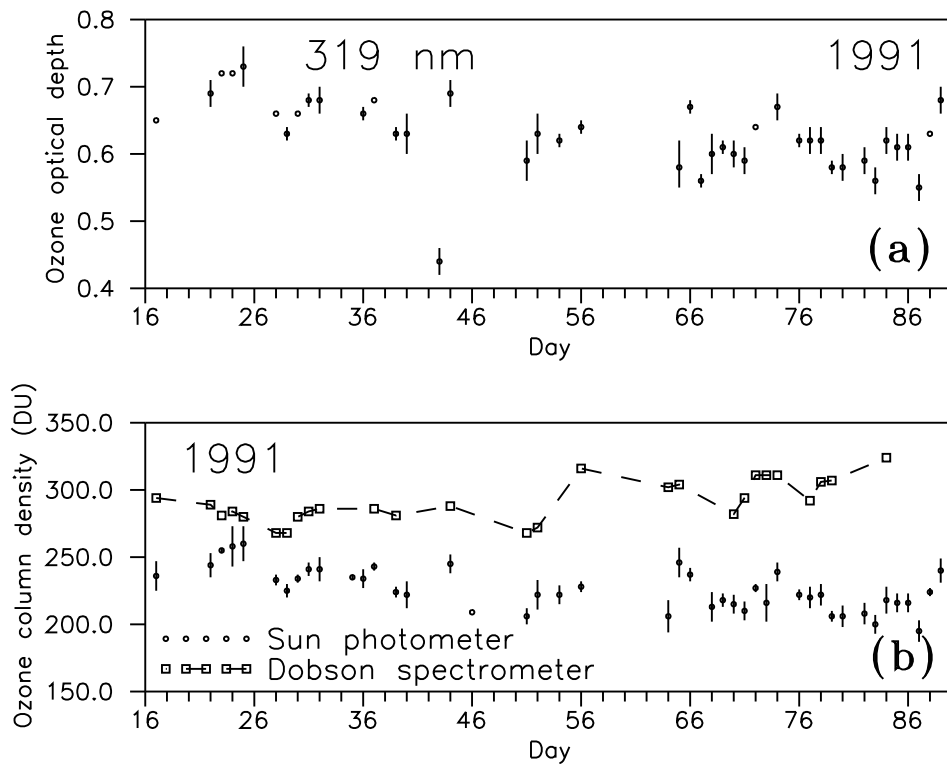


Figure 3.9: (a) Variations in ozone optical depth at 319 nm. Mean of the data obtained during 1100 to 1200 hrs are shown. Vertical bars represent $\pm 1\sigma$ of the mean. (b) Total column density of ozone, expressed in Dobson Units (DU) obtained during January-March, 1991 from Sun photometer measurements are compared with that of Dobson spectrophotometer measurements, both made at Ahmedabad. Mean of the data obtained during 1100 to 1200 hrs are shown. Vertical bars represent $\pm 1\sigma$ of the mean.

during this period in the arid and semiarid regions of Gujarat and Rajasthan.

3.3.4 Variations in ozone optical depth

The daily mean ozone optical depth for the January to March 1991 period is plotted in Figure 3.9a. The vertical bars represent two standard deviations ($\pm 1\sigma$). The ozone optical depth values are then converted into ozone column density values in Dobson units and compared (Figure 3.9b) with the ozone column density values measured using the Dobson spectrophotometer available in PRL. The photometer derived values are consistently lower than the Dobson spectrophotometer values. The difference varies from day to day and is generally between 40-50 Dobson units, but occasionally as large as 80 Dobson units.

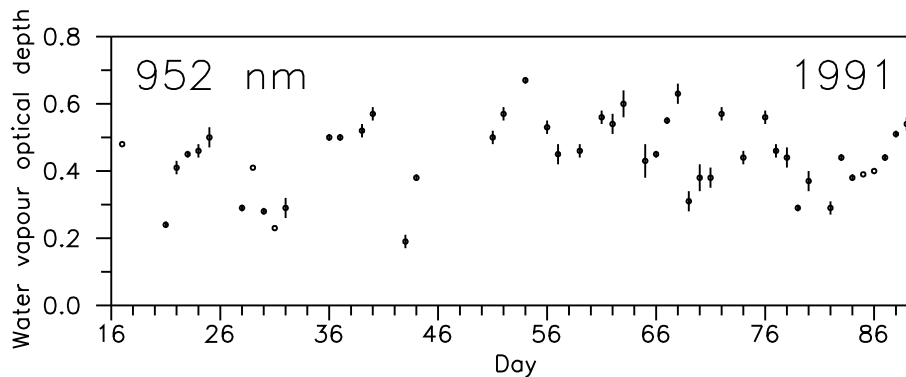


Figure 3.10: Variations in water vapour optical depth (at 952 nm) obtained during January-March, 1991. Mean of the data obtained during 1100 to 1200 hrs are shown. Vertical bars represent $\pm 1\sigma$ of the mean.

Similar findings are reported earlier [Shaw, 1979; Acharya *et al.*, 1985] with observations made in the Chappuis band of ozone absorption, in which the ozone values are consistently lower than the Dobson spectrophotometer values by about 40 Dobson units. Shaw [1979] discusses sources of error in the ozone measurements done in ultraviolet region due to changes in the solar output. While discussing the systematic errors Shaw [1979] reports that errors could arise due to the wrong assumption of atmospheric airmass or from diurnal variations of aerosol optical depth. Also he concludes that if ozone is to be measured using the Chappuis band method to anywhere near the accuracy obtainable with a Dobson spectrometer, the experiments would have to be made from high altitude locations with low turbidity. Computations show that the percentage contributions of ozone absorption is about 27% and the aerosol extinction is about 30% to the total optical depth at 319 nm wavelength region, which are comparable. Hence, reliable estimation of ozone column amounts from UV extinction measurements is possible only in locations of low turbidity, unlike Ahmedabad.

3.3.5 Variations in aerosol optical depth with relative humidity and temperature

To investigate the effect of meteorological parameters on the aerosol optical depths, the optical depths are studied with respect to relative humidity and temperature. Figure 3.10 shows the water vapour optical depths obtained at 952 nm during 1991.

Water vapour in the atmosphere affects the aerosol, by aiding it to grow bigger or shrink in size. The growth of aerosol particle results in a change in the size distribution of the aerosol

particles and changes the overall refractive index of the aerosol particle, thereby affecting the optical depth by altering the scattering characteristics [Hänel, 1976]. At a coastal station where maritime aerosols are predominant, the aerosol optical depth increases as the relative humidity increases [Krishna Moorthy *et al.*, 1993] as shown by the Shettle and Fenn [1979] model. But in Ahmedabad, the aerosols are of urban type and mineral dust forms the prime component, which are nonhygroscopic. The scatter plot (Figure 3.11a) of the daily mean (1100 to 1200 hrs data) of the aerosol optical depth with the corresponding relative humidity does not show any positive increase in the optical depth with relative humidity as it has been the case with maritime aerosols, but a general decreasing trend is seen with increasing humidity probably due to the fact that a rise in humidity increases the soil moisture content which inhibits the production of soil derived particles. Similarly the aerosol optical depths are found to increase as the day's maximum temperature increases (Figure 3.11b), which further proves the above conclusion that the rise in temperature promotes further input of soil derived particles into the atmosphere. These results are seen in all the photometers, but the results of 491 nm photometer for the year 1991 are shown here as an example. Similar results are obtained for the 1993, 1994 and 1995 years data. The trend indicates that for an increase of about 10°C in the surface temperature, the aerosol optical depth increases by about 0.2, whereas for an increase of 10% in relative humidity, the aerosol optical depth decreases by less than 0.01, showing no significant dependence.

The Ångström wavelength exponent (α) values obtained in 1991 were analysed for variations in relative humidity and are shown in Figure 3.12. As in Ahmedabad, aerosols are of urban type and mineral dust is the prime component we see a very feeble dependence of α on the varying relative humidity. As shown in Chapter 2 for Urban and Average continental models, α values almost remained the same throughout the relative humidity range of 0% to 80% and variations could be found beyond that range.

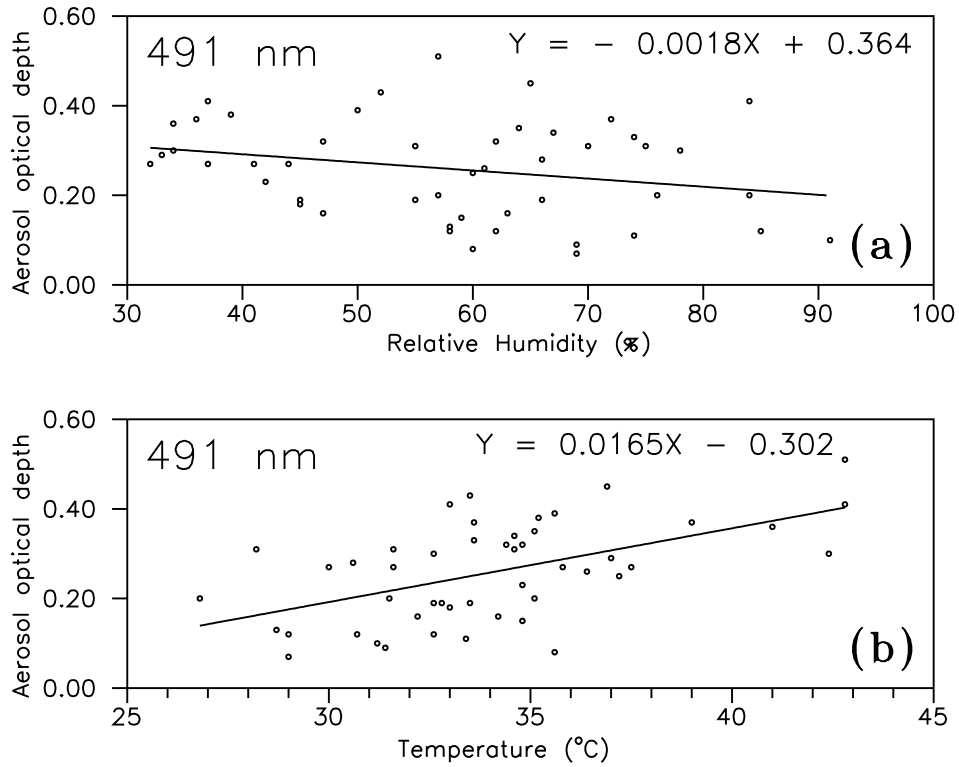


Figure 3.11: *Dependence of aerosol optical depth (at 491 nm) on (a) relative humidity and (b) on the day's maximum temperature, during 1991. (Relative humidity and temperature data source: India Meteorological Department.)*

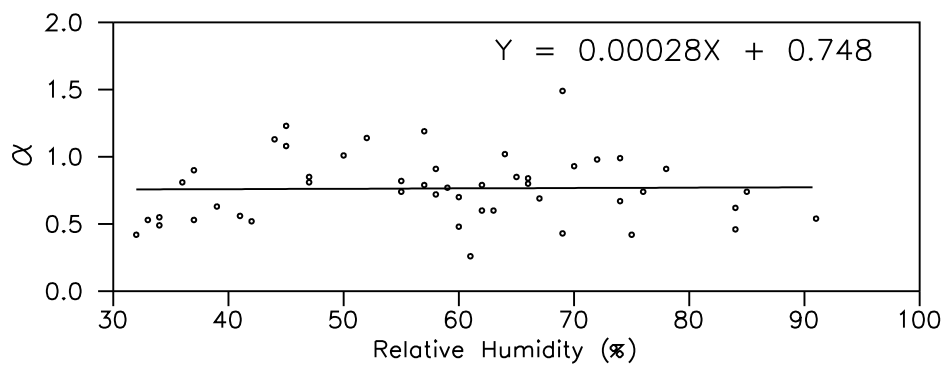


Figure 3.12: *Wavelength exponent, α obtained during 1991 is plotted against measured relative humidity values. No significant dependence between the two parameters is found over Ahmedabad.*

Chapter 4

Stratospheric aerosols

4.1 Formation, Physical, Chemical, Radiative and Optical effects

Research on stratosphere grew into a separate discipline and developed a great deal after 1970s, which till then was an unexplored region in space. The concern in 1970 [Crutzen, 1970] that supersonic transports which produce water vapour and oxides of nitrogen and the discovery of *Molina and Rowland* [1974] in 1974 that chlorine compounds produced by the chemical industry, commonly known as CFCs or Freons could disturb the protective ozone layer brought a large number of scientists from the adjacent fields to this sphere. But not until recently that the role stratosphere plays in global climate and in global change was recognised adequately. Stratosphere suffers from a variety of issues, some of them being the ozone depletion, changes in thermal structure and how effective are the stratospheric aerosols in wrecking the ozone abundances, especially after a major volcanic eruption when the depletion gets more deeper due to the availability of abundantly large number of aerosols and how these aerosols play a role in the radiative and climatic impacts.

Stratospheric aerosols exist in a stratified layer beginning near the tropopause and extending up to 30 km. The height and thickness of the layer exhibit temporal and latitudinal variations and exhibits an apparent correlation with tropopause height [Rosen *et al.*, 1975]. The background stratospheric aerosol layer has a mode radius of about 0.05-0.1 μm and has a number density of about 1-10 particles cm^{-3} . But immediately after volcanic eruptions the mode radius can increase to 1.0 μm in the stratosphere and the number density can go up by more than an order of magnitude, when compared to the background conditions.

Stratospheric aerosols are formed after major volcanic eruptions and diffusion of natural gases such as H_2S , COS , CS_2 , SO_2 , etc. from troposphere. Most of the sulphur present in the

Earth's atmosphere ends up as sulphate, as it is the thermodynamically stable form of sulphur in the presence of oxygen. Sulphur bearing gases are generated both naturally and anthropogenically. *Charlson et al.* [1987] estimate that marine flora and terrestrial biota account for 50% of the total natural flux of the sulphur present in the atmosphere. The only significant nonbiological natural flux is the emission of SO₂ and H₂S by volcanoes and fumaroles, which account for 10-20% of the total natural flux of gaseous sulphur in the atmosphere. The anthropogenic counterpart arises from combustion processes such as coal burning, oil burning, smelting and petroleum refining and traffic and their relative contributions are 70%, 8.4%, 21% and 0.6% respectively [*d'Almeida et al.*, 1991].

The marine emissions are almost exclusively in the form of dimethyl sulphide (DMS), the chemical formula being CH₃SCH₃. The highest production of DMS occurs in the warmest, most saline and most intensely illuminated regions of the ocean i.e. the tropical regions [*Charlson et al.*, 1987]. The terrestrial emissions occur from a variety of species, including H₂S, DMS, CS₂, COS among others. SO₂ is mainly produced by fossil fuel combustion, biomass burning and volcanic eruptions. While the SO₂ emitted from fossil fuel combustion and biomass burning are the major sources of sulphate aerosols in the troposphere, SO₂ from volcanic eruptions and other sources of SO₂ from troposphere by diffusion accounts for sulphate aerosols in the stratosphere.

Stratospheric aerosols are mostly sulphate particles (70-75% H₂SO₄ and 30-25% H₂O with some traces of other sulphates, nitrates etc.). They are formed due to conversion from gaseous sulphur dioxide. The key process is the reaction with OH which initiates the oxidation.



The sulphur trioxide so produced gets converted into sulphuric acid particles, through condensation and coagulation.



The sulphuric acid particles finally get converted into sulphate aerosols. The detailed mechanism has several uncertainties but the presence of clouds and other chemicals like NH₃ seem to help. Typical life times for conversion of SO₂ to H₂SO₄ is estimated to be 24 days [*McPeters.*,

1993]. Volcanic eruptions pump in large quantities of SO_2 into the atmosphere. But the reaction scheme from (4.1) to (4.3) which converts SO_2 to H_2SO_4 and sulphate aerosols is valid even in the background (nonvolcanic) conditions. In the background case SO_2 comes from oxidation of carbonyl sulphide (COS) and carbon disulphide (CS_2) which are of biospheric origin. The oxidation is either through O^1D or through photodissociation.



Further oxidation gives rise to SO_2 .



More important at the tropospheric altitudes are the following reactions.



Crutzen [1976] has estimated that the above scheme can give rise to SO_2 in the range of 10^6 - 10^7 molecules $\text{cm}^{-2} \text{sec}^{-1}$ in the free troposphere.

Volcanic aerosols can cause warmings (of about $3\text{-}4^\circ\text{C}$) in the stratosphere primarily by the absorption of upwelling terrestrial radiation and by reducing the amount of total solar radiation reaching the troposphere, can cause cooling (of about 0.5°C) globally [*Ackerman*, 1988] and also these aerosols by backscattering (as these aerosols are efficient scatterers but only weak absorbers at visible wavelengths) more amount of solar radiation into space, increase the planetary albedo. For example, following El Chichon the transmission of direct solar radiation was found reduced by about 15% and did not recover for about 3 years [*Hofmann*, 1988] and after the more recent Mt. Pinatubo, the transmission was found decreased by about 25-30%, resulting in a cooling of the troposphere by 0.5°C , globally [*Dutton and Christy*, 1992]. The major development during the recent years has been the recognition that heterogeneous chemistry, in which aerosols play a key role, is the dominant process responsible not only for the polar spring time ozone depletion (Antarctic and Arctic ozone holes) but also for global ozone depletion [*Hofmann and Solomon*, 1989], the only difference being

the medium on which the depletion occurs i.e. the polar stratospheric clouds in the former, which is replaced by the increased number of large size aerosols offering large surface area formed after the volcanic eruption, in the latter. Aerosols added to the stratosphere can affect ozone concentrations in other ways, such as by absorbing the sunlight can heat the stratosphere and alter its usual circulation patterns [Kinne *et al.*, 1992]. In the atmosphere the aerosol characteristics are altitude dependent [Subbaraya and Jayaraman, 1982] and the stratospheric aerosols are quite different from the lower tropospheric aerosols. Unlike tropospheric aerosols, which are shortlived due to gravitational settling and rainwash and produce only local and seasonal effects, stratospheric aerosols on the other hand are long lived [Prospero *et al.*, 1983] and can produce long term global effects.

The location, time of the year, injection altitude and the amount of SO₂ injected by the eruption are important not only in determining the global impact, but also in determining the eventual stratospheric aerosol particle size [Hofmann, 1987]. In general, low latitude eruption can have a larger impact because of the global coverage it can provide. However, generalisation and extrapolation of the effects, from one eruption to the other, is not possible. Even though qualitatively the effects have been known for a long time, it is the recent volcanic eruptions after Mt. St. Helens (1980), especially the El Chichon (1982) and now the Mt. Pinatubo (1991) that have given opportunities to determine the detailed physical characteristics of volcanic aerosols and enable a study of their impact in the middle atmosphere.

The size distribution of volcanic aerosols typically shows a trimodal structure that varies with time. The principal size modes are: the nucleation mode, which is most prominent within one month after the eruption having particles of size around 0.01 μm ; the sulphate accumulation mode, which evolves initially from the nucleation mode (by condensation and coagulation) and increases in size to about 0.3 μm after about an year; the large particle 'ash' mode (of silicate mineral and possibly salt particles) of micron size that settles out of the layer within the first month of an eruption [Turco *et al.*, 1993]. Figure 4.1 schematically illustrates the time evolution of the stratospheric aerosol size distribution, after a major volcanic eruption. The evolution process involves a variety of physico-chemical interactions such as H₂SO₄ vapour nucleation, condensational growth and evaporation, coagulation, gravitational sedimentation and dynamical process such as diffusion (Figure 4.2). While the dust or silicate particulate matter settles out rapidly and does not play an important role after a few months, the sulphurous gases which are injected get converted into sulphuric acid droplets (as explained above) while other gases may affect the ozone layer. The 'optically effective' aerosols

are in the size range from $0.05\ \mu\text{m}$ to $10\ \mu\text{m}$ which can alter the Earth's radiation budget by scattering away the incoming solar radiation and to some extent by absorbing the outgoing Earth's longwave radiation. The possible consequences are heating of the stratosphere and a cooling effect at the Earth's surface. Ice core data show a clear record of the sulphur emissions from major historical eruptions [Delmas, 1992]. The sulphur dioxide after conversion to sulphate is transported to high latitudes in the stratosphere, from where it is deposited on glacial ice sheets over a period of several years. Ice core data provides the much needed information on the time and magnitude of major eruptions that have disturbed the stratosphere [Legrand and Delmas, 1984; Kirchner and Delmas, 1988] and gives an opportunity for gaining a more profound understanding of the relation between volcanic eruptions and climate change.

4.2 Volcanic aerosols: An assessment of the effects

Our awareness on the effects of volcanic eruptions on the stratosphere appreciably improved after the eruption of Mt. St. Helens in 1980. This is mainly due to the availability of techniques for measuring these effects by both direct and remote sensing, at our disposal. It was also clear that the large quantities of SO_2 injected into the stratosphere, after conversion to sulphate aerosols can have a chemical, physical, radiative and climatic influence on a global scale, due to the prevailing atmospheric circulation.

Mt. St. Helens volcano (46.2°N , 122.2°W) erupted on 18 May 1980 injecting about 0.6 megatons (Mt) of SO_2 into the atmosphere, with the debris reaching up to 24 km in the atmosphere [Turco *et al.*, 1983]. The average optical depth at $1.0\ \mu\text{m}$ over the midlatitudes was about 0.006 following the eruption [Kent and McCormick, 1984] as compared to a prevolcanic, background value of 0.001. The condensation nuclei concentration had increased by more than one order of magnitude and the mode radius was found to be around $0.1\ \mu\text{m}$ between 10 and 25 km, few months after the eruption [Hofmann and Rosen, 1982]. The aerosol mixing ratios (particles per milligram ambient air) in the two size ranges ($r \geq 0.15\ \mu\text{m}$, $r \geq 0.25\ \mu\text{m}$) over Laramie, Wyoming (41°N), increased by about more than one order of magnitude, as compared to the background conditions [Hofmann, 1987]. As the St. Helens eruption was from midlatitude and also as the amount of SO_2 injected was comparatively less, the global effects were small and had little influence on climate and can not be classified as a major eruption in terms of stratospheric aerosol effects.

This century witnessed two of the strongest volcanic eruptions ever recorded namely El Chichon in April 1982 and Mount Pinatubo in June 1991. El Chichon (17.3°N , 93.2°W) in

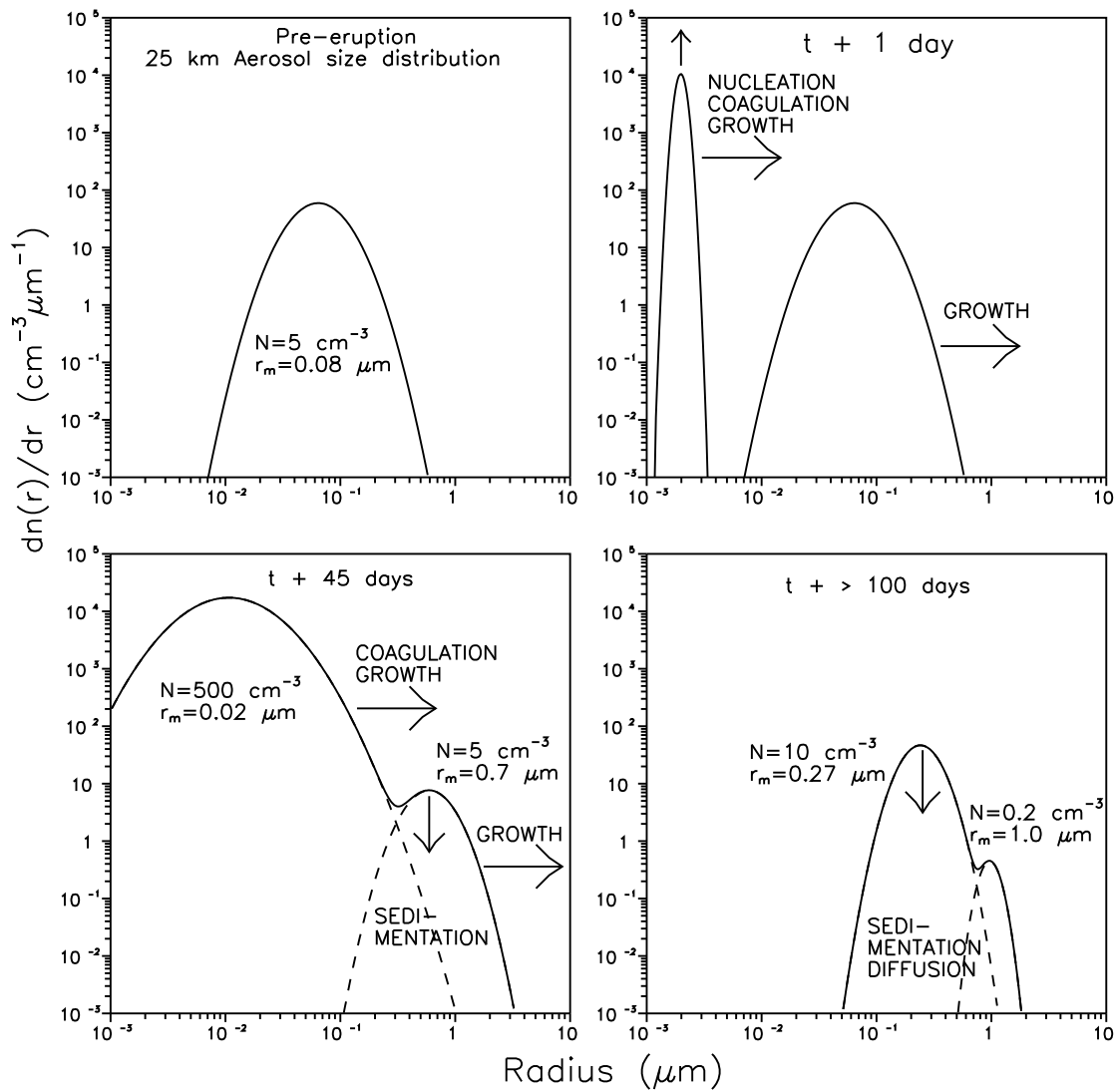


Figure 4.1: Schematic illustration of the time evolution of the stratospheric aerosol size distribution after a major volcanic eruption, due to various physico-chemical and dynamical processes in the atmosphere (adopted from Hofmann, 1988).

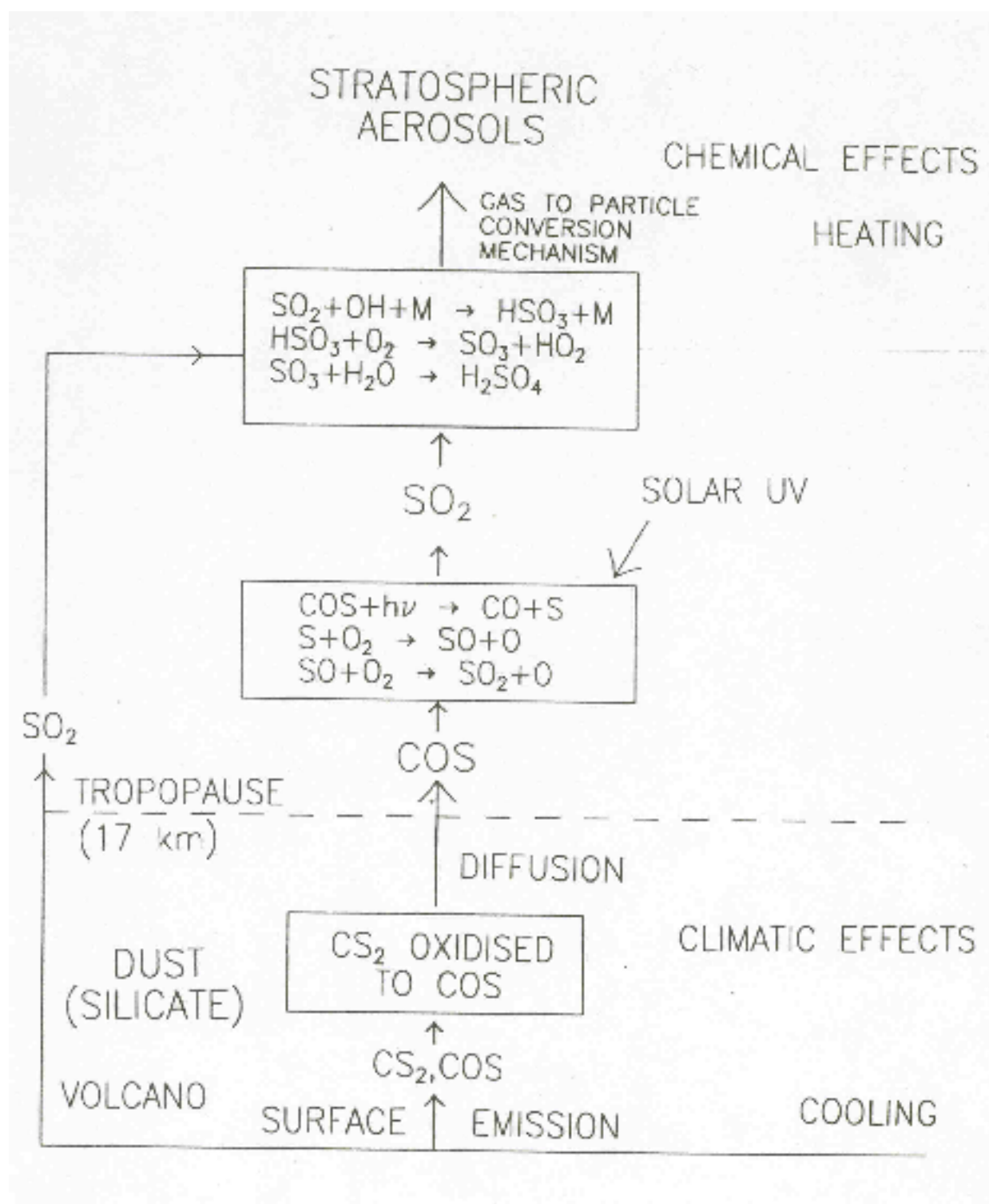


Figure 4.2: Schematic representation of the formation, importance and effects of stratospheric aerosols (adopted from Hofmann, 1987; Jayaraman, 1993).

Mexico erupted on 4 April 1982 injecting about 10 megatons of SO_2 which penetrated altitudes in excess of 25 km [Hofmann, 1987]. The 500 nm aerosol optical depth measured at Mauna Loa (19.53°N) in Hawaii increased from a preeruption value of 0.02 to about 0.3 by the middle of 1982, indicating the magnitude of the eruption. The aerosol cloud was found confined over the tropics in the early months after the eruption. Lidar results on scattering ratio obtained immediately after the eruption showed an increase of about 2 orders of magnitude in the scattering ratios. Hofmann and Rosen [1983] have shown using balloonborne optical particle counters at Laramie, Wyoming (41°N), that the aerosol ($r \geq 0.15 \mu\text{m}$) concentration at the stratosphere has increased by about an order, from about a few particles (during background, volcanically quiescent periods) to a few tens of particles in May 1982, 45 days after the eruption. The mean radius of aerosols in the 17-25 km altitude region was found to be around 0.2 to 0.3 μm even after an year of eruption, whereas the background mean radii are around 0.1 μm . Also for the first time a correlation between the increased aerosol loading and ozone depletion at the stratospheric altitudes over midlatitudes was found [Hofmann, 1987]. But the role of aerosols in altering the ozone abundances through heterogeneous chemistry, was demonstrated later, in 1989 [Hofmann and Solomon, 1989]. While a stratospheric heating of around 3-4°C has been observed after the El Chichon eruption, a surface cooling was not very apparent.

On 15 June 1991 Mt. Pinatubo (15.14°N, 120.35°E) in the Philippines, after being dormant for about 635 years, erupted producing the largest impact at the stratospheric altitudes [McCormick and Veiga, 1992; Bluth *et al.*, 1992]. This colossal eruption gave an opportunity to study the various physico-chemical processes involved in the formation of stratospheric aerosol layer and its decay and predict the impending climatic effects. Stratospheric Aerosol and Gas Experiment (SAGE) II extinction measurements of the Pinatubo aerosols in the stratosphere during June, July and early August 1991 show that aerosols in the tropics reached altitudes as high as 29 km. At altitudes above 20 km, the aerosol cloud moved rapidly to the west with the leading edge circling the globe in about 3 weeks [McCormick and Veiga, 1992]. Figure 4.3 shows the 6.5 year record of SAGE II optical depth at 1020 nm over the altitude range from 3 km above the tropopause to 40 km. The time series shows aerosol perturbations caused by the eruptions of Nevado del Ruiz (November, 1985), Kelut (February, 1990) and the first indication of Pinatubo (June, 1991). The stratospheric optical depth following Pinatubo has increased by about 2 orders of magnitude.

A number of investigations have been carried out by several groups on the globally dis-

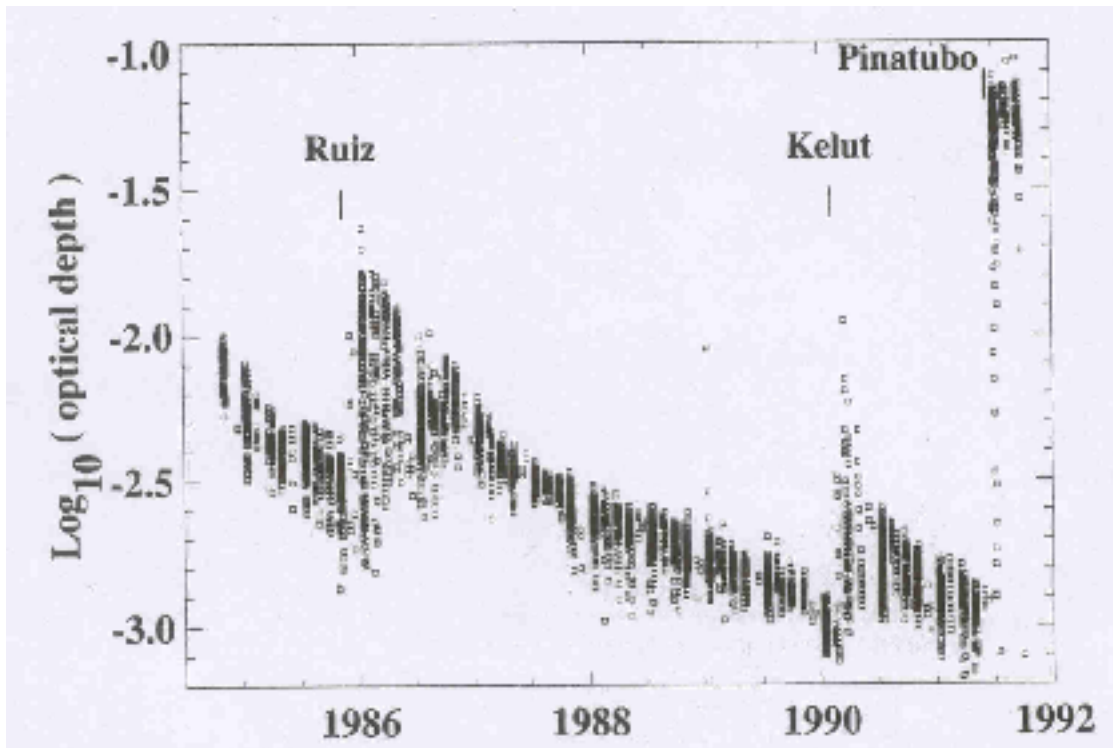


Figure 4.3: SAGE II aerosol optical depths computed from integration of the 1020 nm extinction profiles over the altitude range from 3 km above the tropopause to 40 km (from McCormick and Veiga, 1992).

persed aerosol due to the Pinatubo eruption using airborne lidar [Winker and Osborn, 1992], particle counters [Deshler *et al.*, 1992, 1993], ship-borne and stationary lidars in the northern hemisphere [Avdyushin *et al.*, 1993; Nardi *et al.*, 1993]. Thomason and Osborn [1992] have reported on the vertical profiles of aerosol extinction using SAGE II data. All these results in general show that the eruption has put as much as 2 to 3 times more material (about 15 to 30 megatons of SO_2 [McPeters, 1993; Bluth *et al.*, 1992]) into the stratosphere compared to the El Chichon eruption in Mexico in 1982, which resulted in a global stratospheric aerosol mass load of about 20-30 Mt [McCormick and Veiga, 1992]. Also for the first few months after the eruption the bulk of the material was confined over the tropics [Stowe *et al.*, 1992; Trepte *et al.*, 1993] from the tropopause level to about 28 km [DeFoor *et al.*, 1992]. Labitzke and McCormick [1992] using analyses of rawinsonde-derived temperature profile data have shown that warming occurred at 30 mb and 50 mb (approximately 24 and 20 km, respectively) at latitudes over the tropics and the warming at the equator in September 1991 was as high as 4°C . Stowe *et al.* [1992] state that the globally averaged net radiation may be reduced by about 2.5 Wm^{-2} (equivalent to a cooling effect of at least 0.5°C) at the surface once the aerosol is

distributed globally over the next 2 to 4 years. *Minnis et al.* [1993] determined from the radiative flux anomalies derived from the Earth Radiation Budget Experiment measurements that the radiative cooling caused due to Mt. Pinatubo eruption during August-September 1991 was $2.7 \pm 1.0 \text{ Wm}^{-2}$. After a volcanic eruption, the large ash particles settle out during the first few months and the sulphuric acid droplets and sulphate aerosols become important in determining the radiative forcing. *Pollack et al.* [1981] have demonstrated that the radiative forcing varied as a function of aerosol composition, size and altitude. For example, the size distributions of stratospheric aerosols measured after El Chichon eruption showed that the particle size decreased from an effective radius of about $1.4 \mu\text{m}$ after 1.5 months after the eruption to about $0.5 \mu\text{m}$ after 6.5 months [*Hofmann and Rosen*, 1983], hence such a drastic change in the size of the aerosol particle will have a considerable effect on the volcanic aerosol forcing. Recently *Lacis et al.* [1992] showed that though the climate forcing is a function of the aerosol size distribution, the size dependence can well be described by a single parameter namely effective radius r_{eff} . When the effective radius r_{eff} , defined as the mean radius of the size distribution weighed by the cross sectional area, becomes greater than $2 \mu\text{m}$ the global average of the greenhouse effect of the aerosols is found to exceed the albedo effect, causing a surface heating [*Lacis et al.*, 1992].

Krueger et al. [1992] using TOMS data have found that the 1991 Antarctic springtime ozone decline was the maximum, when the columnar ozone concentration values were 8 DU less than 1987 and 1990 springtime declines, earlier deep ozone hole years. Recent report [*Ozone Trends Panel*, 1994] shows that both the 1992 and 1993 springtime ozone values are still lower than that of the 1991 values. This has been attributed to the presence of Pinatubo aerosols. The fact that the 1994 ozone loss is not as severe compared to the previous years further substantiates this view. Using electrochemical concentration cell sondes, airborne UV differential absorption lidar system and SAGE II measurements, *Grant et al.* [1994] have found ozone decreases of up to 33%, over the tropics, in the 16 and 28 km altitude region, which coincided with enhanced aerosol loading due to Pinatubo eruption. *Hofmann et al.* [1994] using the aerosol backscatter lidar data at 532 nm, the aerosol concentrations using particle counters and the ozone vertical profiles, have found ozone deficits as large as 30% between 14 and 20 km over Laramie, Wyoming (41°N) (Figure 4.4). This figure also shows the close correspondence between the region of maximum ozone deficit and the location of Pinatubo aerosol layer. The large ozone depletion in the Antarctic as well as in the tropics is attributed to the presence of large amount of Pinatubo aerosols, which aided the heteroge-

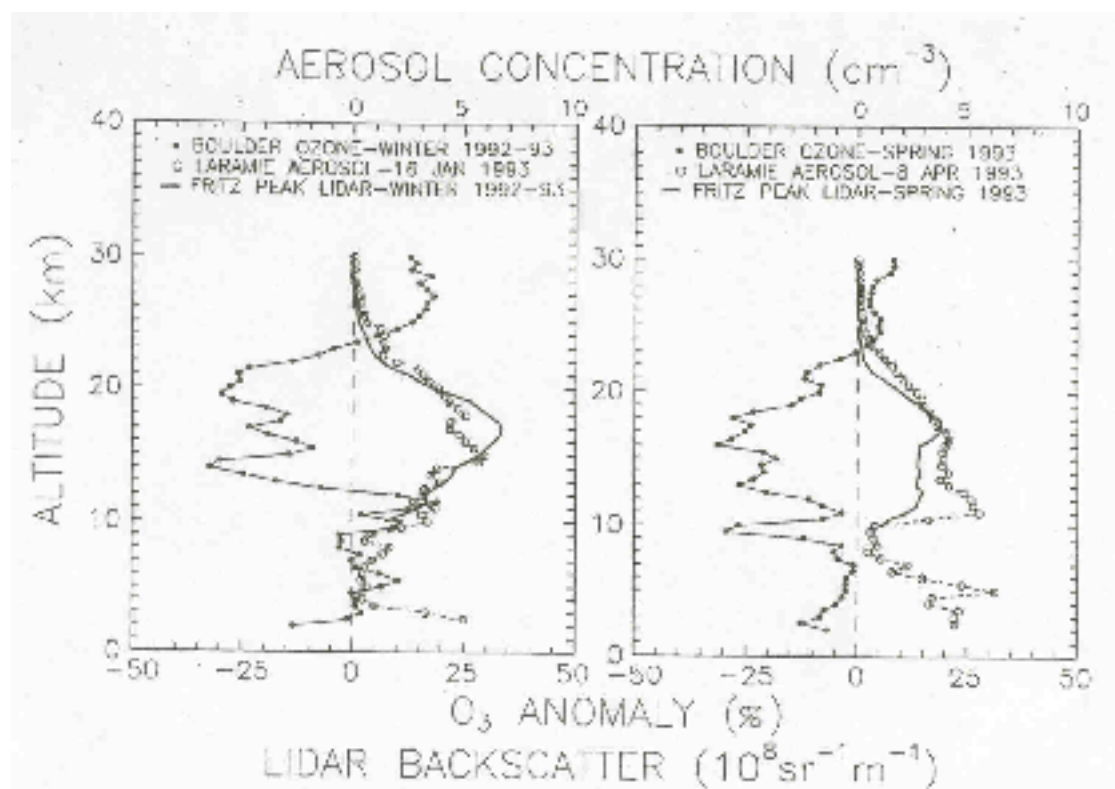


Figure 4.4: Profiles of ozone anomaly (as compared to 1985-1988 average), lidar backscatter and aerosol concentration as measured during the winter (December, January and February) and spring (March, April and May) of 1992-93 at Boulder, Fritz Peak and Laramie respectively, indicating a close relation with the enhanced aerosol loading which through heterogeneous phase chemistry has lead to ozone depletion (from Hofmann *et al.*, 1994).

neous chemistry to take place much faster. Using differential absorption lidar measurements D'Altorio *et al.* [1993] have found that the aerosol surface area densities have increased by about 20 times over midlatitudes, between 17 and 22 km. At Laramie, Wyoming (41°N) the surface areas have increased by a factor of 10 to 20 in the stratosphere, below 25 km, during the June 1991 - January 1993 period [Deshler *et al.*, 1993].

4.3 Measurement techniques

Much of what we know today about stratospheric aerosols, started with the pioneering work of Junge [Junge *et al.*, 1961] about 4 decades ago, who by *in situ* measurements collected aerosol samples using balloonborne cascade impactors and discovered the existence of the stratospheric aerosol layer, which is also referred to as 'Junge' layer. Soon after, the availability of high-altitude research aircraft made more spatial and altitude coverage possible [Junge and

Manson, 1961]. The measurement of stratospheric aerosols by collecting samples improved with the development of new techniques such as palladium wire impactors [*Bigg*, 1976; *Farlow et al.*, 1979], cascade impactors [*Sheridan et al.*, 1992] and jet impactors [*Goodman et al.*, 1994]. A different application of the impactor technique was evolved, in which each impaction plate is a tuned piezoelectric quartz crystal oscillator and the change in frequency determines the mass accumulated on each impactor stage [*Chuan*, 1976].

In all the above methods, the samples collected have to be analysed in the laboratory to determine the physical and chemical characteristics of aerosols, for example the concentration, size distribution and composition which in turn gives the refractive index. These techniques suffer from the drawbacks of contamination or evaporation of samples collected before the laboratory analysis. Also, the microscopic examination of the impaction samples is tedious and time consuming and the accuracy and efficiency of the measurement, are questionable [*Bigg*, 1976].

Rosen [1964] developed an *in situ* optical particle counter having a light source, a photomultiplier tube and a pulse height analyser. As the particles enter the system, the scattered radiation is converted to electrical pulses and are counted for the number density and analysed for the particle sizes. This system was simple, reliable and could be easily mounted on a balloon gondola and the estimation of the particle density and size distribution could be obtained, altitude wise [*Hofmann and Rosen*, 1983; *Deshler et al.*, 1993].

Attempts were made in the late 1970s to determine the stratospheric aerosol characteristics by using polar nephelometer [*Grams*, 1981] and retrieve the aerosol phase functions.

Remote optical sensing of aerosols has the advantage of not disturbing the medium of investigation. Several ground based, balloon and satellite based techniques have been developed and are being used extensively. One of the first techniques was the use of intensity-modulated search lights [*Elterman*, 1966], in which the search light was pointed vertically upwards or at different elevations and the characteristics of aerosols could be obtained up to about 35 km. This principle could be more effectively used with the availability of lasers to study the vertical profiles of aerosols on a continuous basis and now are being extensively used worldwide [*Fiocco and Grams*, 1964; *Thomas et al.*, 1981; *Parameswaran et al.*, 1991; *Jäger and Hofmann*, 1991; *Jayaraman et al.*, 1995a] to determine the aerosol characteristics. In backscatter lidar systems, the transmitter and the receiver are collocated and the backscattering coefficient of aerosols is measured.

Measurements of the direct solar radiation and the scattered radiation intensities is an

other modest and a refined way of obtaining the aerosol characteristics, such as the aerosol optical depth. The wavelength dependence of the optical depth can be used to infer the size distribution function [Ångström, 1961; Rangarajan, 1972; Michalsky *et al.*, 1990]. However, in this technique knowledge about the total content of the absorbing gases such as ozone and water vapour are essential. Measurements of twilight radiations [Volz and Goody, 1962; Ashok *et al.*, 1982] and on the intensity distribution around solar aureole [Deepak and Adams, 1983] have been made to determine the aerosol characteristics. Scattering measurements have been done using balloons, aircrafts and rockets [Newkirk and Eddy, 1964; de Bary and Rossler, 1966; Subbaraya and Jayaraman, 1982]. These *in situ* measurements have been successfully used to determine the altitude variation of aerosol characteristics such as, extinction coefficient, mode radius, concentration and size distribution.

Though large information about aerosols can be obtained from ground based and *in situ* measurements, they are usually restricted both in time and space. Also, the balloon-borne measurements are quite costly. For an extensive period of observation and for global coverage, satellites are best suited. The SAM II (Stratospheric Aerosol Measurement II) experiment onboard NASA's NIMBUS 7 satellite launched in October 1978 and the SAGE (Stratospheric Aerosol and Gas Experiment) onboard NASA AEM-2 satellite launched in February 1979 and later SAGE II launched in October 1984, have provided an excellent source of data of aerosol characteristics, for about 2 decades [McCormick *et al.*, 1979; Kent and McCormick, 1984; Lenoble and Brogniez, 1985; McCormick and Veiga, 1992; Trepte *et al.*, 1994]. The SAM II and SAGE satellite sensors consist of Sun photometers designed to measure atmospheric extinction in certain wavelength bands during satellite sunrise and sunset [McCormick *et al.*, 1979]. While SAM II is a one channel instrument providing aerosol extinction profiles at $1.0\ \mu\text{m}$, SAGE has four wavelength bands centered at $0.385\ \mu\text{m}$, $0.45\ \mu\text{m}$, $0.6\ \mu\text{m}$ and $1.0\ \mu\text{m}$, to measure aerosol extinction profiles as well as ozone and nitrogen dioxide profiles. SAGE II launched in October 1984 aboard the Earth Radiation Budget Satellite has been continuously measuring gas and aerosol extinction profiles at the Earth's limb during each solar occultation experienced by the satellite, by Sun photometers at the seven wavelength bands centered at $0.385\ \mu\text{m}$, $0.448\ \mu\text{m}$, $0.453\ \mu\text{m}$, $0.525\ \mu\text{m}$, $0.6\ \mu\text{m}$, $0.94\ \mu\text{m}$ and $1.02\ \mu\text{m}$, since its launch [McCormick and Veiga, 1992]. All the above data put together have become an exhaustive and an important data set for the study of both nonvolcanic, background and volcanically perturbed conditions and the decay of stratospheric aerosols, connected throughout in time and space, on a global scale. More recently, the Improved Stratospheric and Mesospheric Sounder (ISAMS)

onboard the Upper Atmospheric Research Satellite (UARS), launched in September 1991, was used to study the spatial and temporal evolution of the volcanic stratospheric aerosol from Mt. Pinatubo [*Lambert et al.*, 1993].

4.4 Balloon-borne optical studies of Pinatubo aerosols over tropical India

In situ measurements have the distinct advantage of giving a detailed insight into the various physical processes involved in the formation of sulphate aerosols and their evolution at stratospheric altitudes, especially after large volcanic eruptions as compared to satellite measurements. Though satellite measurements can give a global view of the volcanic impact and have the advantage of not disturbing the medium of investigation, the solar intensity passing through the volcanic aerosol layer will not be often high enough to obtain a transmission measurement reliably and so the measurements are to be truncated at certain altitudes. Especially when the opacity of the atmosphere is large, as when occurred during the Pinatubo time frame, extinction measurements at lower altitudes (near and below the peak of the extinction profile) were not possible.

With this in view two balloon experiments were conducted from the National Balloon Facility at Hyderabad (17.5°N, 78.6°E), one in October 1991 and the other in April 1992, 4 and 10 months respectively after the eruption, to study the impact of the Pinatubo eruption over a tropical site as well as its time evolution.

The two balloons carried identical payloads of multiwavelength filter photometers to obtain the vertical profiles of aerosol extinction as well as the aerosol number density and size distribution parameter from the direct and the scattered radiation intensity measurements. The balloons carried a Sun-scanning and a Sun-tracking photometer systems. While the Sun-scanning photometer system is used to obtain the direct as well as the scattered radiation intensities, the direct solar radiation intensities are also measured using the Sun-tracking photometer system uninterruptedly. While the measurement of extinction coefficients gives details about the scattering and absorption properties, thus their effect on the radiative budget, the study on the size distribution parameter and the number density of aerosols gives details about the formation, evolution and decay of stratospheric aerosols. As the balloon programme for atmospheric aerosol studies under Indian Middle Atmosphere Programme was in the formative stage and also as the instrument was under fabrication during 1982, the

opportunity given by the El Chichon eruption to study the characteristics of volcanic aerosols could not be utilised, though two balloon experiments in the decaying phase of the El Chichon volcanic aerosol layer could be conducted. Hence, these two balloon experiments conducted in 1991 and 1992, have yielded for the first time, the almost complete set of volcanic aerosol parameters needed to study quantitatively their impact on atmospheric radiation balance. Moreover these are the only *in situ* optical measurements made in India and to the best of knowledge anywhere in the tropics around the globe and most of the other measurements of Pinatubo aerosols have been from high latitudes.

While the balloon-borne measurements are the best suited to study the role of various physical processes going on at the stratospheric altitudes which control the aerosol size distribution and the number density, Lidar technique is useful in monitoring the decay of the aerosols, as conducting balloon experiments often, proves costly. Also, as the vertical profiles of aerosol extinction are obtained, a detailed study on the vertical dispersion and sedimentation of aerosols is possible, using the lidar data.

4.4.1 Instrumentation

The Sun-scanning multichannel photometer system, developed [Acharya *et al.*, 1985] to measure the direct as well as the angular distribution of the scattered radiation intensities during balloon ascent, has been in use since 1983 and results on the stratospheric aerosols obtained before the Mt. Pinatubo eruption have been previously reported [Jayaraman *et al.*, 1987]. Previous results show that large variations are found in the aerosol concentrations obtained over Thumba and Hyderabad at all altitude levels, with few hundreds of particles at 10 km and decreasing to a few particles at the stratospheric altitudes. Also, the derived aerosol size distribution parameter (the slope of the Junge power law size distribution) was found to be in the range of 2.8 to 3.4 in the 18 to 30 km altitude region [Jayaraman and Subbaraya, 1988; Jayaraman, 1991].

Figure 4.5 shows the functional block diagram and photograph of the Sun-scanning multichannel filter photometer system. The instrument consists of a sensor assembly containing six filter photometers, a Sun-tracking mechanism and a motor assembly for scanning the sky along the solar almucantar, $\pm 90^\circ$ with respect to the Sun for scattered sky radiation measurements. The photometer is a combination of a photodiode/phototube and an interference filter. Baffles are used to restrict the total field of view of photometers to about 9° . The central wavelengths of the photometers used in the Sun-scanning system are 276, 310, 494,

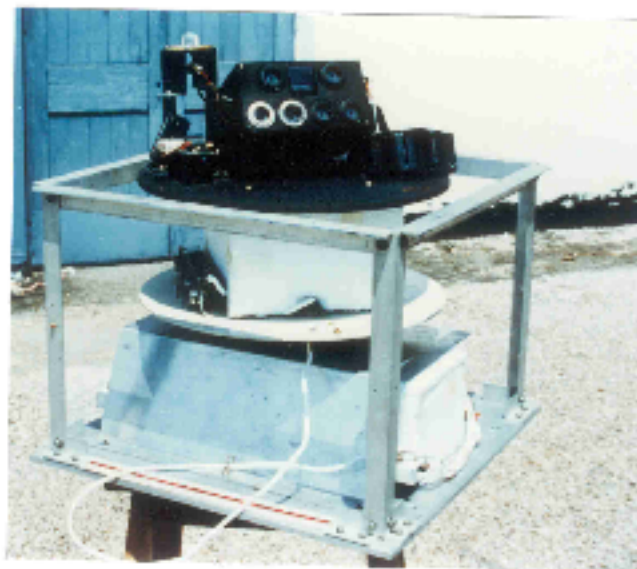
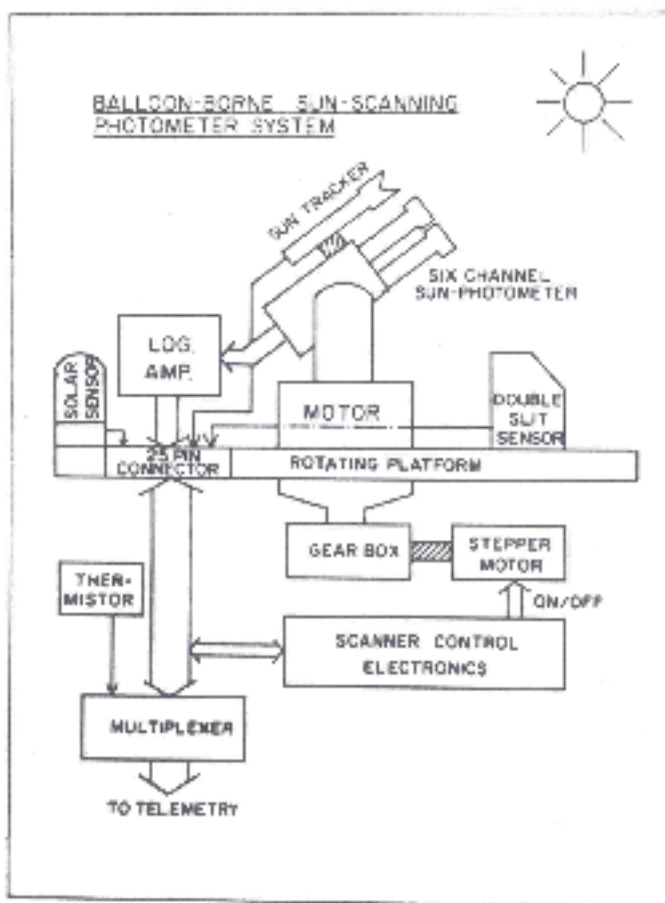


Figure 4.5: *Functional block diagram and photograph of the Sun-scanning photometer assembly used onboard balloons for the measurement of the angular distribution of the scattered solar radiation intensities.*

744, 845 and 952 nm having bandwidths (Full Width at Half Maxima) of 10, 9, 10, 14, 20 and 20 nm, respectively. However, in figures and further discussions these photometers are designated to the round off wavelengths as 280, 310, 500, 750, 850 and 950 nm. As the same photometers are used to measure both direct and scattered radiation intensities, the detector and the amplifier should have low noise level and large dynamic range. Hamamatsu R 765 phototube which has a spectral response between 160 and 320 nm is used for 280 and 310 nm and UV-100 (EG & G) photodiodes are used for other wavelengths. The photodiodes are so chosen to have dark currents in the picoampere range which is 2 orders of magnitude less than the minimum expected signal. Current generated by these photodetectors are fed to six temperature compensated logarithmic current to voltage amplifiers which have a dynamic range of six orders of magnitude from 1 nA to 1 mA. During each rotation of the platform, the tracking mechanism is switched on for $\pm 30^\circ$ near the vicinity of the Sun using a double slit sensor, consisting of two photodiodes and slits separated by an angle of 60° . The scanning is achieved in 18 seconds corresponding to an altitude ascent of about 90 metres by the balloon, which sets the lower limit of the altitude resolution of the various quantities, the aerosol extinction, number density and size distribution parameter, that are measured.

In addition to the Sun-scanning photometer system an automatic two-axis stabilised continuous Sun-tracking photometer system (described in detail in Chapter 3) was also employed in order to get the altitude profiles of the direct solar radiation intensities uninterruptedly. The central wavelengths of the photometers used in the Sun-tracking system are 310, 440, 494, 848, 952 and 1051 nm having bandwidths of 9, 10, 12, 14, 20 and 25 nm, respectively. In figures and further discussions these photometers are referred to as 310, 440, 500, 850, 950 and 1050 nm. Four of the wavelengths are similar to the Sun-scanning system in order to cross validate the data. The two other spectral bands (440 and 1050 nm) are used in the Sun-tracking system to increase the spectral resolution and extent of the measurements. Linear amplifiers are used in the Sun-tracking photometer for the direct solar radiation intensity measurements.

The tracking of the Sun in elevation is achieved using two photodiodes mounted perpendicular to each other in the vertical plane. The difference signal is amplified and fed to a servo motor which orients the sensor assembly towards the Sun. The vertical tracking mechanism corrects for the change in the solar elevation during the balloon flight. In Sun-scanning photometer assembly a solar sensor has been used to activate the system only in the presence of the Sun. The solar sensor switches on the power to stepper motor, which is used for azimuthal

scanning. A thermistor is used to monitor the temperature inside the detector assembly. The outputs are multiplexed with a 5V and 0V square wave marker to indicate the scanning direction of the photometer. While the data corresponding to 280 nm and 950 nm are aimed at retrieving the vertical profiles of ozone and water vapour number densities, data from the other channels are used for aerosol studies, the results of which are presented here.

4.4.2 Experiment

The hydrogen inflated zero pressure balloons are designed to reach a ceiling altitude exceeding 30 km. Figure 4.6 shows the loadline of the balloon experiment, consisting of the payload, radiosonde, radar reflector, apex valve, parachute etc. The length of the loadline is adjusted such that the balloon shadow does not fall on the instrument at higher solar elevation. The balloon has a volume of about 54,000 m³ and is made from 'stratofilm' having a thickness of about 20 μ m. The balloon is filled with the lifting gas hydrogen to about 1% of its volume, just before the launch. The preflight activity involves among other things, studying the prevailing winds at ceiling altitude by conducting wind sounding flights and logistics associated with launching of a balloon including liaison with local Civil Aviation authorities [Joshi, 1991]. The balloon along with the instruments is launched by dynamic launch method [Damle *et al.*, 1983]. Till 1976, onboard recording of the scientific data was in practice in most of the experiments. But at present a 25 kbit/sec standard PCM telemetry encoder is in use. The telemetry flight data are recorded on high speed tape recorders. The outputs of the photometers are digitised at a rate of 25 samples/sec using onboard A/D convertor. Also in these experiments the data are recorded on paper charts for quick look analysis. A PDM/FM/AM telecommand system is used both for inflight control of the scientific experiments and balloon flight control/operation, such as ballast dropping, apex valve control and flight termination. There are three main aspects of the balloon flight control, namely, the balloon tracking, ballast release system and a flight termination device. Additionally, in some flights, balloon apex valve control for slow controlled balloon descent from the ceiling altitude down to about 20 km which enables to get additional data for the important altitude region at which the volcanic aerosol layer resides is also involved. During the balloon flight the temperatures can go as low as -20°C inside the gondola, especially near the tropopause and hence the instrument and the associated electronics setup are given thermal protection. Figure 4.7 shows the picture of the payload assembly on the launch truck, launch balloons for the radar target, radiosonde and the balloon at the far end of the photograph, minutes before the launch. The first balloon

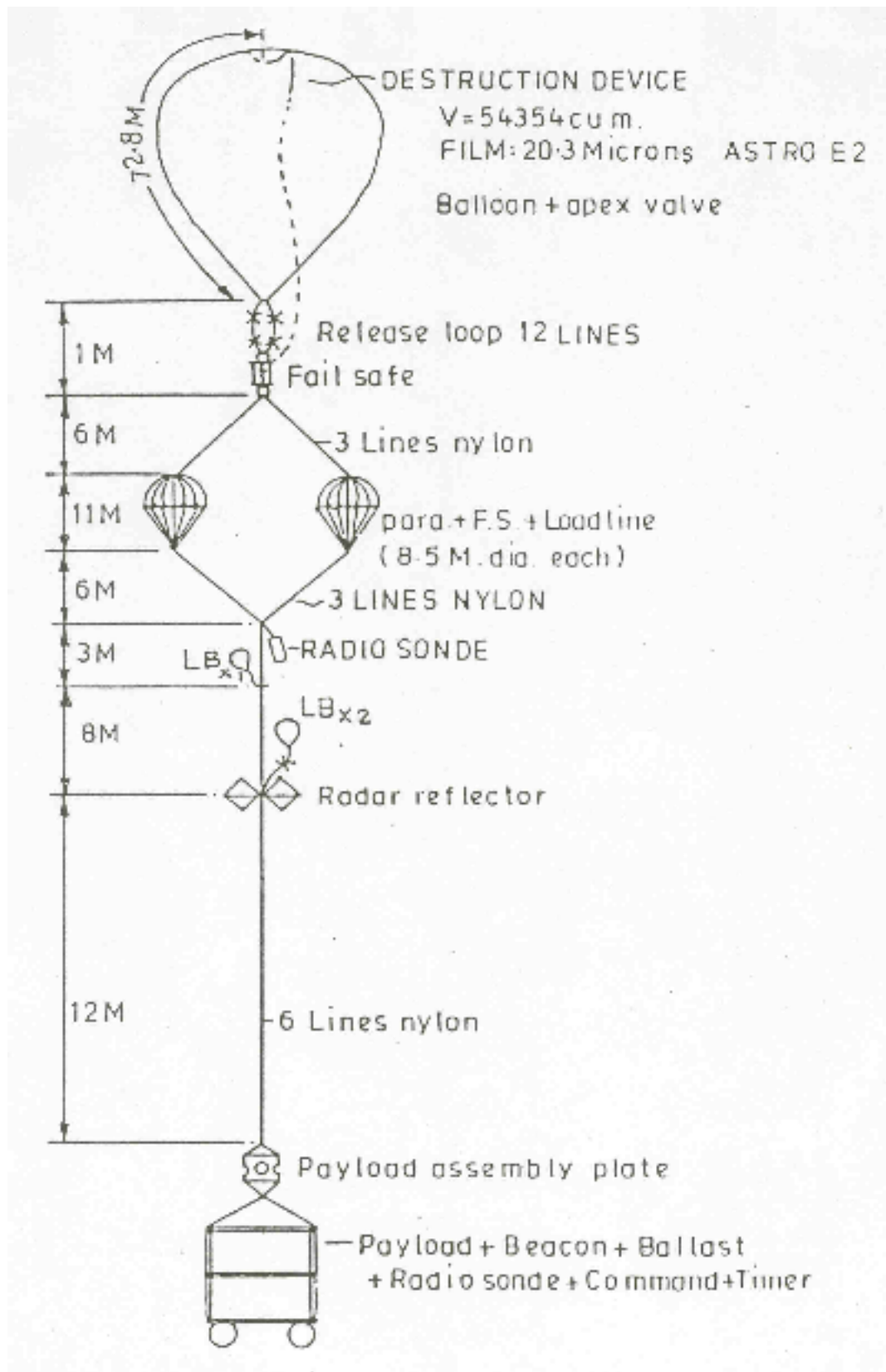


Figure 4.6: Loadline of the 26 October 1991 balloon flight (not to scale).



Figure 4.7: *Picture showing the payload assembly on the launch truck, alongwith the radar target, radiosonde etc. and the launch balloon, minutes before the launch.*

was launched on 26 October 1991 (henceforth referred to as the October flight) at 0608 hrs (local time), close to the local sunrise time. Figure 4.8 shows the balloon ascent a few minutes after take off. The balloon reached the expected ceiling altitude of about 34 km at about 0810 hrs with an average ascent rate of about $280 \text{ m minute}^{-1}$. A ground based radar of the India Meteorological Department (IMD), Hyderabad was used for balloon tracking. This provided continuous information on balloon position (latitude, longitude of the balloon) and its height in kilometres above the mean sea level during all important phases of the flight. A steerable 2.5 m dish antenna and also a 'radio theodolite' unit that receives 375 MHz balloon telemetry signal provided rough balloon position and the radiosonde gave information on the balloon altitude. A special airborne pressure-altitude (baratron) sensor was also included to determine the balloon altitude more accurately. After about two hours of float duration, the balloon could be brought down to about 26 km by releasing the gas through an apex valve incorporated in the balloon, in about two hours. A ballast release system operating through telecommand was used, when required, to accelerate the balloon during the ascent phase and also to maintain the ceiling altitude by a controlled release of magnetic ballast, which was carried as an additional but controllable load. The flight was terminated at 1300 hrs and the instruments were released on a parachute and recovered. An anti-air collision radio beacon is used which forewarns an approaching aircraft of the descending payload train in space,



Figure 4.8: *Balloon carrying the gondola, a few minutes after take off.*

by transmitting an electrical signal. A specially developed fail-safe device, which is a spring-loaded switch on the balloon loadline, was incorporated in the flight train. It operates instantaneously in case of an accidental balloon burst in flight and separates the parachute-payload system from the balloon [Damle, 1991]. The entire sequence of the balloon flight operation conducted on 26 October 1991 is shown in Figure 4.9a. The same instruments were flown again on 20 April 1992 (henceforth referred to as the April flight) with an advanced launch time of 0558 hrs to accommodate the earlier sunrise in April (Figure 4.9b). Also the balloon was made to float only an hour at the ceiling level of 33.5 km which helped to get additional descent data for the stratospheric region. The results presented are the average of the ascent and descent data wherever applicable. In both the experiments all the scientific as well as technical instruments such as baratrons for pressure monitoring, radiosonde and telecommands worked satisfactorily. Data corresponding to the altitude region of 10 to 34 km in the case of the October 1991 flight and from 5 to 34 km in the case of the April 1992 flight are presented. The low-altitude data correspond to high solar zenith angles and hence are affected by the curvature of the Earth and multiple scattering through the long optical paths. In the

case of the October flight, low-altitude clouds are also found to contaminate the data below 10 km.

4.5 Results and Discussion

4.5.1 Aerosol extinction coefficients

The data analysis essentially involves the estimation of the attenuation of the incoming solar radiation at each altitude. If I is the intensity of the solar radiation at altitude z , then the total atmospheric extinction coefficient β (km^{-1}) at z could be written using Beer-Lambert's law as,

$$\beta(z) = \frac{dI}{I(z) dz \sec \chi} \quad (4.11)$$

where χ is the solar zenith angle at the time of observation and $\sec \chi$ gives the atmospheric airmass. Vertical profile of the direct solar radiation intensity obtained on 26 October 1991 at 500 nm is given in Figure 4.10, as an example.

The total atmospheric extinction coefficient β is made up of

$$\beta = \beta_{\text{ma}} + \beta_{\text{rs}} + \beta_{\text{aerosol}} \quad (4.12)$$

where β_{ma} is the absorption coefficient due to molecular gases such as ozone, nitrogen dioxide, water vapour etc., β_{rs} is the Rayleigh scattering coefficient (scattering due to air molecules) and β_{aerosol} is the aerosol extinction coefficient. The air density profile (Figures 4.11a and 4.11b) constructed from the temperature and pressure data obtained from the meteorological balloon soundings on the flight days and the mean ozone density profile available for Hyderabad [Lal *et al.*, 1989] are further used to correct extinction coefficient profiles for Rayleigh scattering and ozone absorption. Absorptions due to nitrogen dioxide in the 400 to 450 nm region, as well as by water vapour at 800 nm, are less than 1% of the total extinction coefficient in the wavelength bands used [Jayaraman and Subbaraya, 1993a]. For the altitudes where measured air density values are not available, *U.S. Standard Atmosphere* [1966] for 15°N is used. Further, the aerosol extinction profiles could be obtained from the direct solar radiation up to about 30 km. Above 30 km, as the altitude increment of the intensities is small, the extinction profiles are calculated from the aerosol number density and ν , derived from the scattered sky radiation measurements.

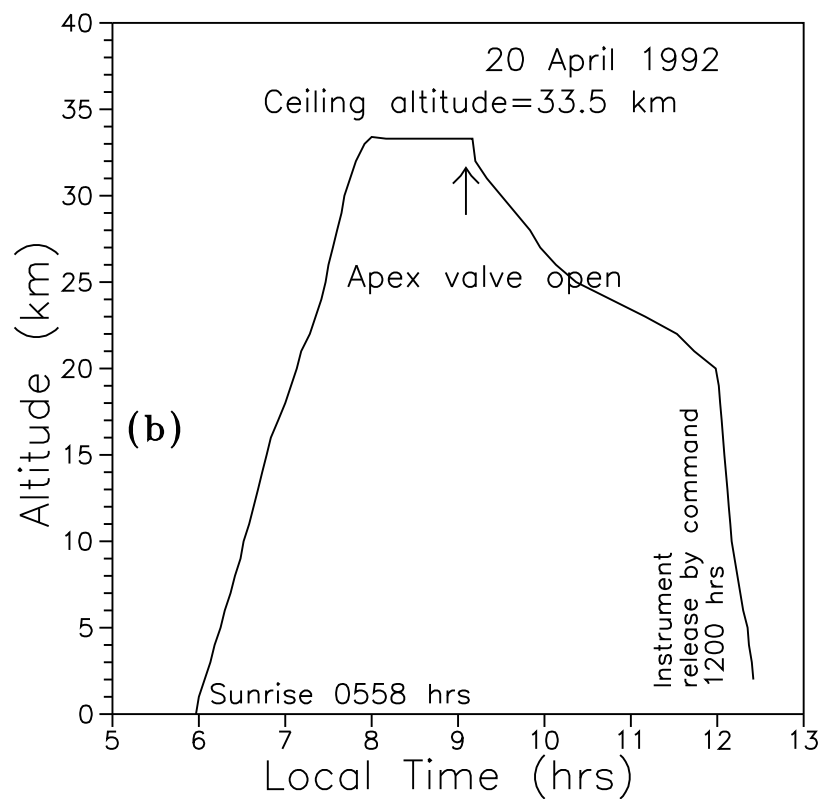
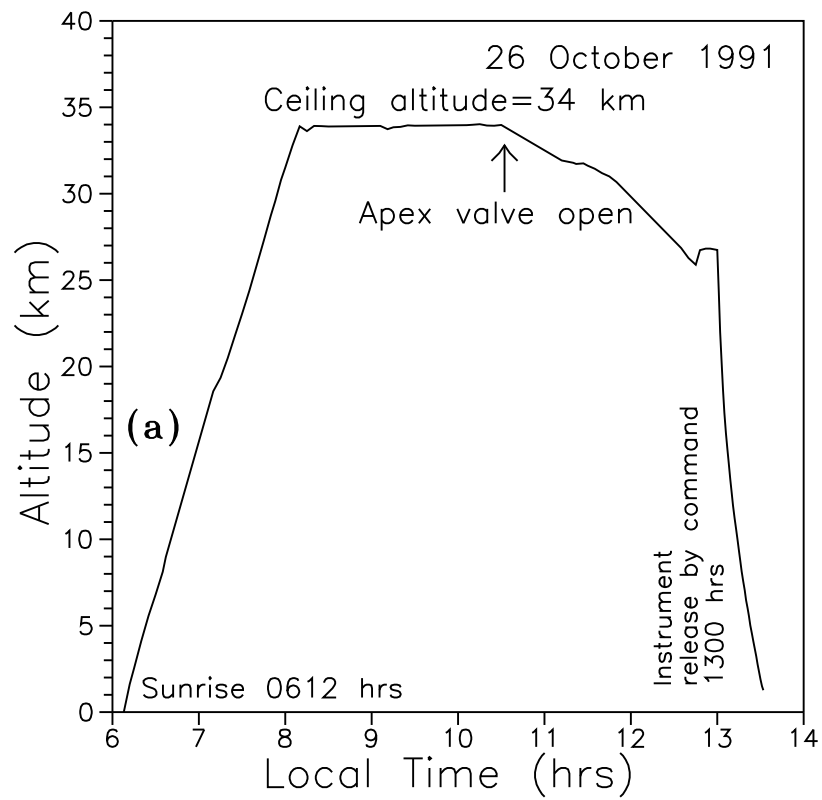


Figure 4.9: History of the (a) 26 October 1991 and (b) 20 April 1992 balloon flights.

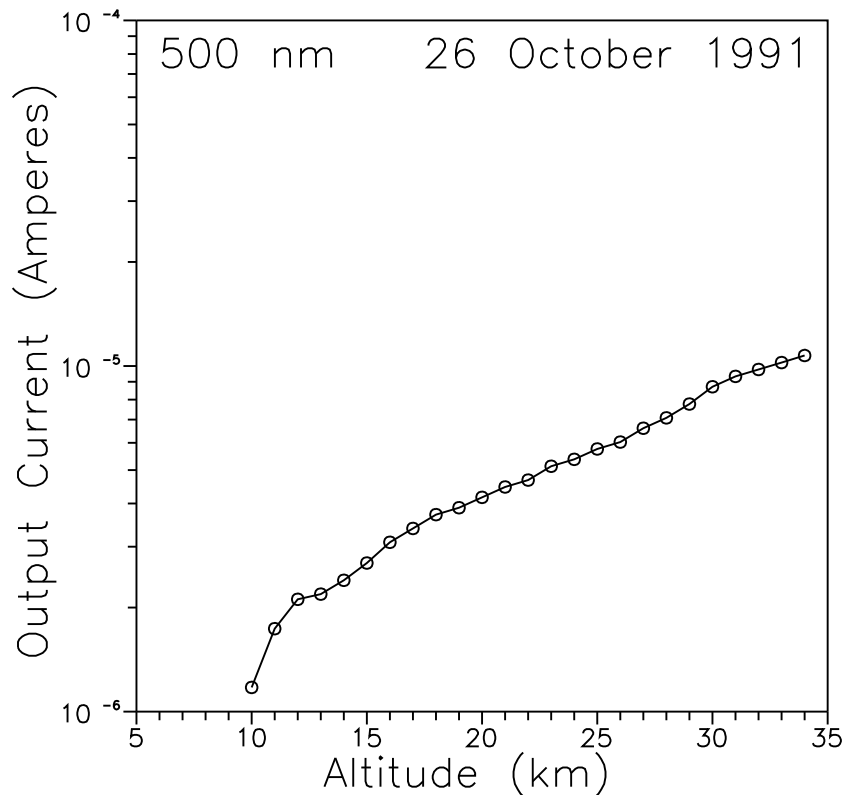


Figure 4.10: Vertical profile of the direct solar radiation intensity obtained on 26 October 1991 at 500 nm.

Using Sun-tracking mechanism the solar radiation intensities, $I(\lambda)$ are measured with an accuracy better than 1%. The analog I values are digitised and recorded on magnetic tapes for detailed analysis. However, as the aerosol extinction coefficients are derived from the total extinction coefficients after correcting for the contribution due to scattering and absorption by the molecular species, the accuracy of the final results depends on the accuracy of the input parameters. In the absence of meteorological radiosonde data on the air density profile, model values [U.S. *Standard Atmosphere*, 1966] are used. In general, the derived aerosol extinction coefficient profiles have a maximum uncertainty of 10% in the lower altitudes which increases to about 30% at the stratospheric altitude levels.

Figures 4.12a-d show the aerosol extinction coefficient profiles after correcting for molecular scattering and absorption at 310, 440, 500, 750, 850 and 1050 nm for the October and April flights. The Pinatubo aerosol layer is seen as an increase in the extinction values above the tropopause between 16 and 30 km altitude region. The peak of the aerosol layer is seen at 23 km in October 1991 with an aerosol extinction coefficient of about 10^{-2} km^{-1} . Typically an

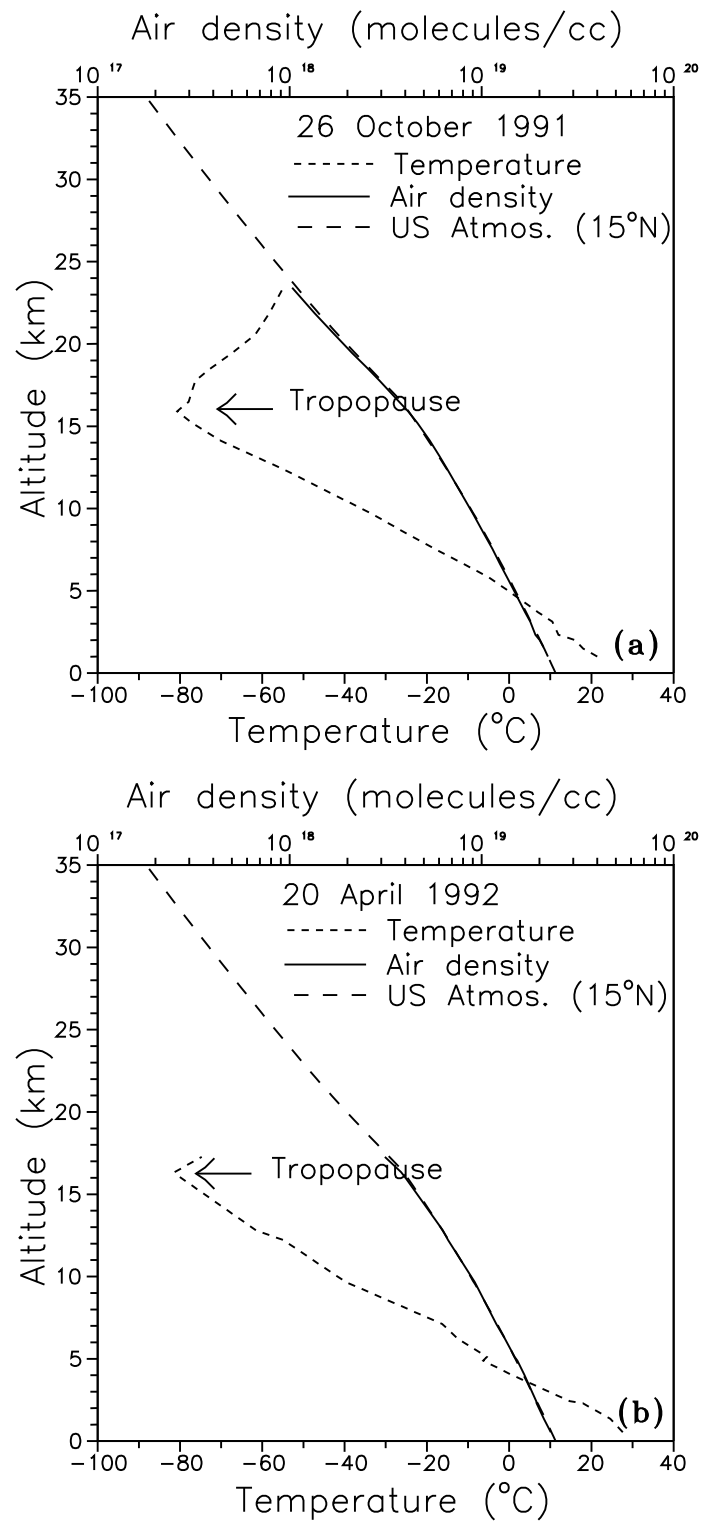


Figure 4.11: The meteorological parameters obtained two hours prior to the aerosol experiments over Hyderabad. The U.S. Standard Atmosphere for 15°N is used in the analysis at altitudes where data are not available.

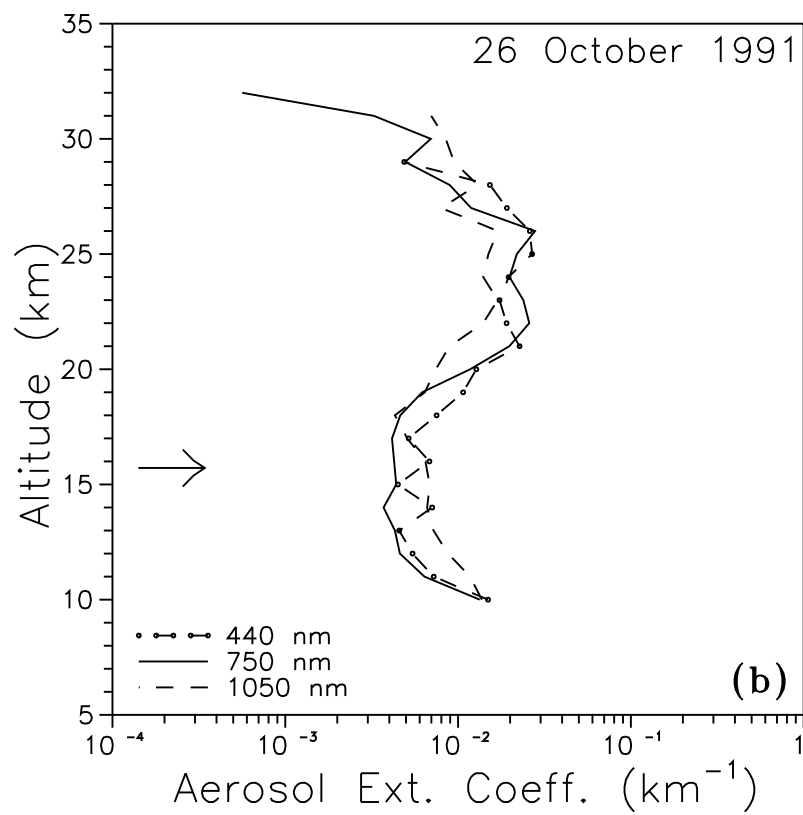
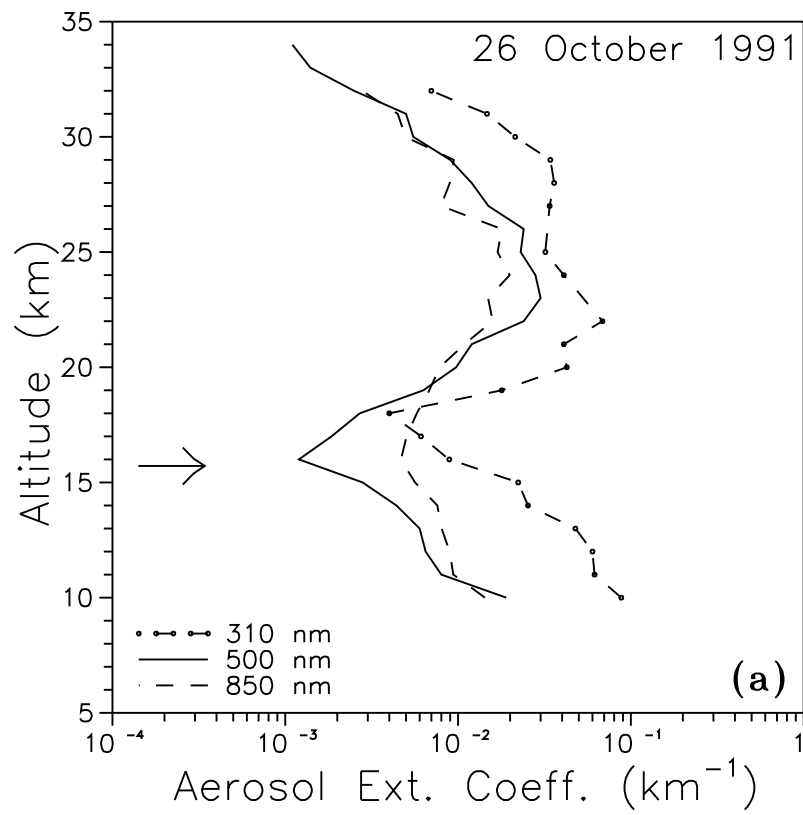
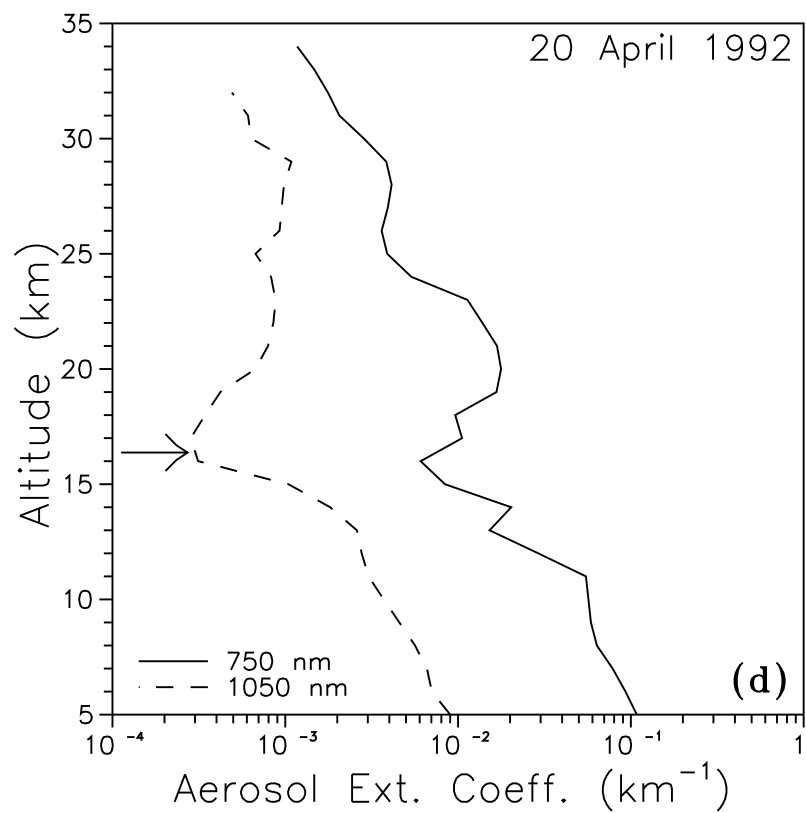
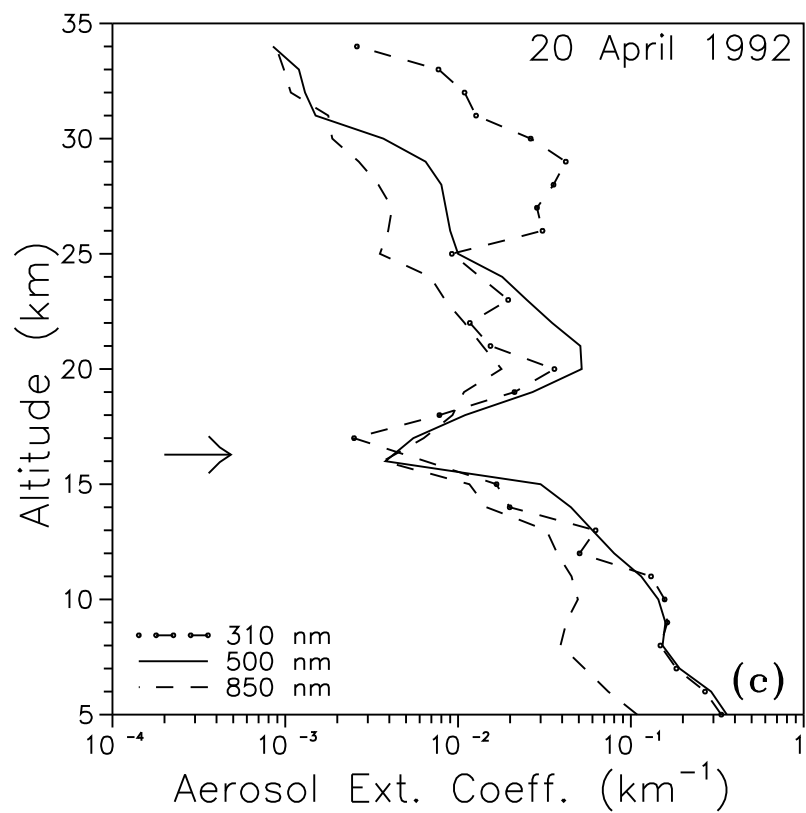


Figure 4.12: Profiles of aerosol extinction coefficients obtained over Hyderabad (17.5°N) during October 1991 and April 1992 balloon experiments. The arrows indicate tropopause level.



order of magnitude increase in the extinction is seen between the tropopause and the aerosol peak layer altitudes. Above about 30 km the aerosol extinction gradually decreases to about 10^{-3} around 33 km. In general, the features observed are the same at all wavelengths. In the April 1992 measurement the extinction profiles are characterised by two layers, one between 16 and 24 km and the other between 25 and 30 km. While the features observed are similar at all the wavelengths, the 310 nm aerosol extinction profile shows a predominant hump structure at the 25 to 30 km region in both the measurements. The 310 nm profiles are corrected for the ozone absorption using the mean ozone profile constructed from several individual ozone measurements made over Hyderabad [Lal *et al.*, 1989]. Interestingly, if the Pinatubo aerosols had an effect on ozone it could have been a decrease in the ambient ozone concentration by about 5% at these altitudes as shown by Grant *et al.* [1992] and hence the use of a mean ozone profile is expected to overestimate the ozone correction and as a consequence a decreased aerosol extinction. In general, the extinction coefficients at all wavelengths are about 2 orders higher in magnitude at the peak altitude when compared with that of the 1985 values measured over Hyderabad [Ramachandran *et al.*, 1994b]. The 1985 aerosol extinction coefficient values are the lowest values ever obtained at stratospheric altitudes during a decade of stratospheric aerosol observations over Hyderabad. The 1985 measurement was made 3.5 years after the El Chichon eruption but before the Nevado del Ruiz eruption in November 1985 and therefore can be considered relatively a volcanically quiescent period. The recent results showing the highest values ever obtained over the same site indicate the magnitude of Pinatubo eruption which is estimated to be the strongest in this century [Bluth *et al.*, 1992].

4.5.2 Aerosol number density and size distribution parameter

The aerosol size parameter ν , defined as the slope of the power law size distribution is determined by comparing the experimentally observed aerosol scattering phase function with the results of the Mie scattering computation for various ν values. The scattering angle θ at which the radiation reaches the photometer can be expressed as,

$$\cos \theta = \cos \chi_o \cos \chi + \sin \chi_o \sin \chi \cos \phi \quad (4.13)$$

where χ_o is the solar zenith angle, χ is the zenith angle of the optical axis of the photometer measured from the vertical and ϕ is the azimuthal rotation of the photometer from the Sun. Measurements are performed for the solar almucantar i.e. $\chi = \chi_o$. In Figure 4.13 the typical

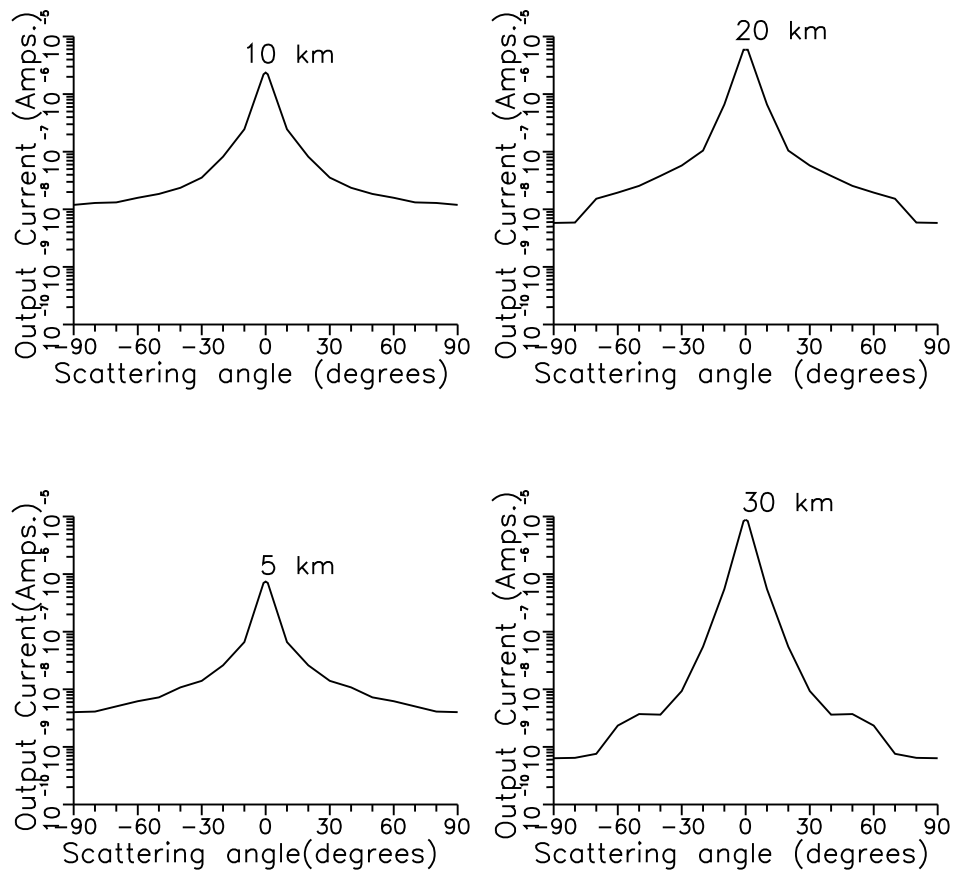


Figure 4.13: *Scattered radiation intensities measured at 5, 10, 20 and 30 km on 20 April 1992 at 500 nm.*

angular distribution of the scattered radiation intensities measured at 5, 10, 20 and 30 km on 20 April 1992 at 500 nm are given, which are further used in determining the aerosol scattering phase functions.

Though the use of a lognormal size distribution may best describe the stratospheric aerosol size distribution, for optically effective particles, in the size range from 0.05 to 10 μm , power law can be taken as a good representation [Volz and Sheehan, 1971; Bigg, 1976]. Though, the power law has a tendency to overestimate the number density of smaller particles, their Mie scattering contribution to the total integrated intensity is however marginal [Jayaraman, 1991]. From the ratio (ϕ) between the measured aerosol scattering function and the computed Rayleigh scattering function the aerosol number density N_z can be derived as,

$$N_z = \frac{3 \sigma_R (1 + \cos^2 \theta) \phi \rho_z}{8 \pi \left(\frac{2\pi}{\lambda}\right)^{\nu-2} \eta \nu r_1 \nu \rho_0} \quad (4.14)$$

where σ_R is the Rayleigh scattering cross section at wavelength λ , θ is the scattering angle and η is the Mie angular function [Bullrich, 1964]. ρ_0 and ρ_z are the air densities at the ground level and at altitude z , respectively. Sensitivity of the assumed refractive index of aerosol (taken as $1.43 - i1 \times 10^{-8}$ at 550 nm corresponding to 75% H_2SO_4 droplets) and the lower limit of the particle size, taken as $0.04 \mu m$ in the Mie scattering computations are found to introduce an error of about ± 0.2 in the derived ν values and an uncertainty of about 20% to 35% in the derived aerosol number density.

Figures 4.14a and 4.14b show the derived aerosol number density profiles for the October and April flights. A large increase in the aerosol number density is seen above the tropopause and up to about 30 km. In October 1991 the aerosol number density is found to decrease from about 500 particles per cm^3 at 10 km to about 8 particles at 19 km. The aerosol layer peak occurs at 23 km with about 40 particles per cm^3 . Using balloonborne optical particle counters *Deshler et al.* [1992] have reported that the particle concentration over Wyoming ($41^\circ N$) which was less than 1 particle per cm^3 before the volcanic impact in June 1991 had increased to few tens of particles by July 1991. By the end of August and mid-September a broad volcanic aerosol layer is seen above the local tropopause up to an altitude of about 30 km. A period of about 24 days is found typical [McPeters, 1993] for the chemical conversion of SO_2 to H_2SO_4 droplets. The observed increase in aerosol concentration is the result of the H_2SO_4 vapour formed after the Pinatubo eruption. Hence, these results obtained about 4 months after the eruption represent the fully grown aerosol particles. Also, the higher aerosol concentration observed over Hyderabad compared to Wyoming results confirm the fact that the aerosols were confined over the equatorial region during the initial period after the eruption. In April 1992 the aerosol number densities (Figure 4.14b) have already shown a decline, with a peak aerosol number density of about 20 particles per cm^3 at an altitude of about 20 km. The enhancement of particle number density below the tropopause is due to local effects [Jayaraman and Subbaraya, 1993a] where there is an accumulation of wind derived dust particles till summer, which however will get rainwashed after the Indian monsoon which is active during the June-September period.

Figures 4.15a and 4.15b show the altitude variation of the size parameter ν , the slope of the power law curve for the aerosol size distribution for the October and April flights. The size distribution of the optically effective aerosol particles well above the submicron size range

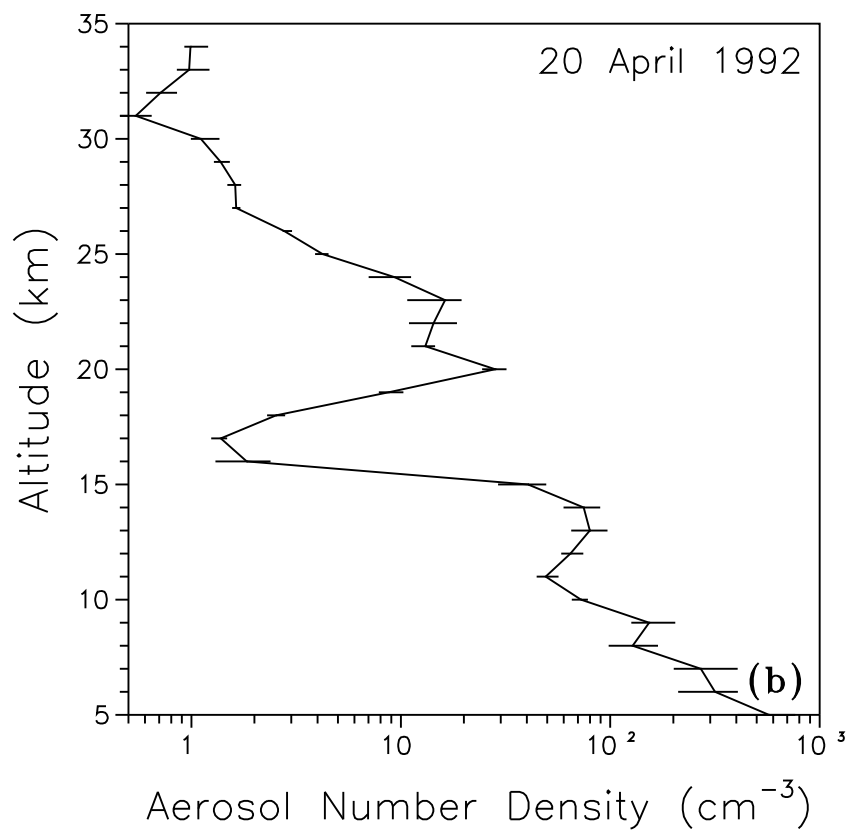
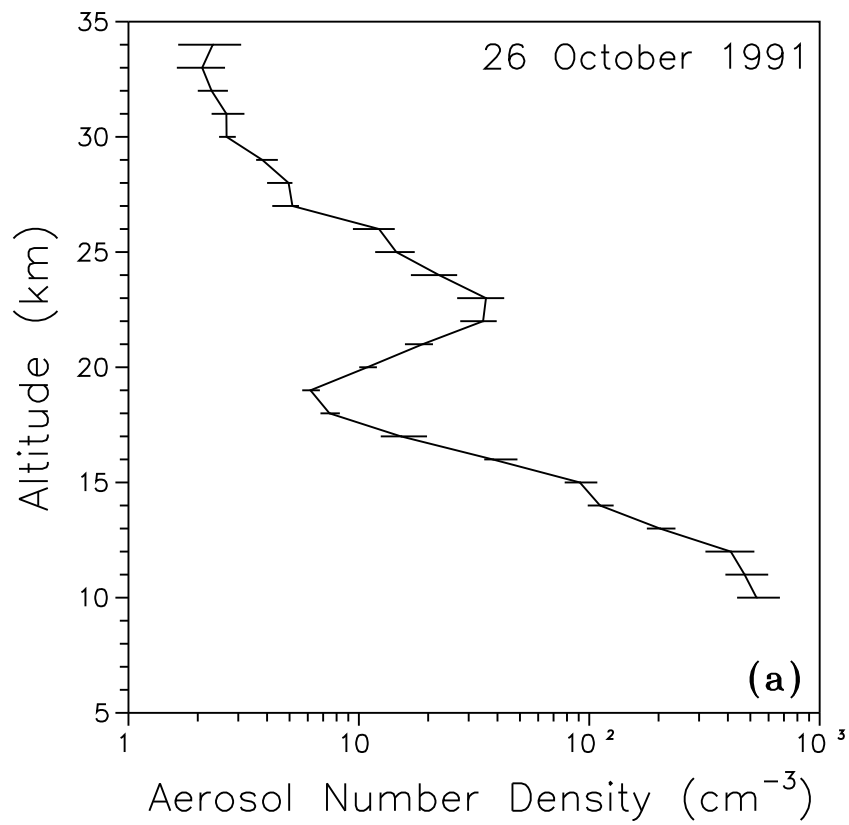


Figure 4.14: The aerosol number density profiles obtained from the scattered radiation intensity data with the lower limit of the particle size taken as $0.04 \mu\text{m}$.

could be described by a simple power law, the stooping edge in the case of a lognormal curve, such that a low value of the slope, represented by a low ν value, indicates a greater number of larger particles compared to a higher ν value. A value of 3 is found typical for ν which represents background aerosol particles. In October 1991 the region between 17 and 23 km shows a marked decrease in the ν value which is around 1.8 compared to all other altitudes. This result, derived from the scattered radiation measurement complements the obtained extinction profiles (Figures 4.12a-d) derived independently from the direct solar radiation intensity measurements. Though the extinction profiles show a broad maximum above the tropopause which extends to about 30 km, only the lower part of the layer, between 17 and 23 km, contains the larger sized particles. However, the April results show two distinct layers above the tropopause with ν less than 2. One layer lies between 16 and 22 km and the other between 25 and 30 km. However, the number density (Figure 4.14) in the 25 to 30 km altitude region shows no corresponding increase. On the contrary, a decrease in density of about 2 particles per cm^3 is seen during April 1992 compared to about 6 particles in October 1991 in the 25 to 30 km region. This apparent decrease could have been caused both by meridional displacement to higher latitudes and by a coagulation of smaller particles into larger particles and subsequently a reduction in the total number of particles. Any loss of particles due to sedimentation would be insignificant at these altitudes, as a particle of size $0.5 \mu\text{m}$ having a typical settling velocity of about 0.015 cm s^{-1} [Lamb, 1970] takes around 2 years time to be removed from the stratosphere. Deshler *et al.* [1992] using optical particle counters found that at 22-23 km the typical mode radius of aerosols was about $0.35 \mu\text{m}$, during July 1991. Since, the experiments were conducted within an year, sedimentation would not have affected significantly the number density of aerosols. The third layer seen in the ν profile of April flight, with a corresponding increase in aerosol number density in the 10 to 13 km region, could be due to locally produced dust particles from the arid and semiarid regions of central India. This layer, typical of the Indian region, has been found to exhibit an annual cycle similar to the Indian monsoon [Jayaraman and Subbaraya, 1993a].

4.5.3 Ångström coefficient

With an attempt to get further insight into the problem of aerosol size variation with respect to altitude, the parameter α , defined as

$$\tau = \beta \lambda^{-\alpha} \quad (4.15)$$

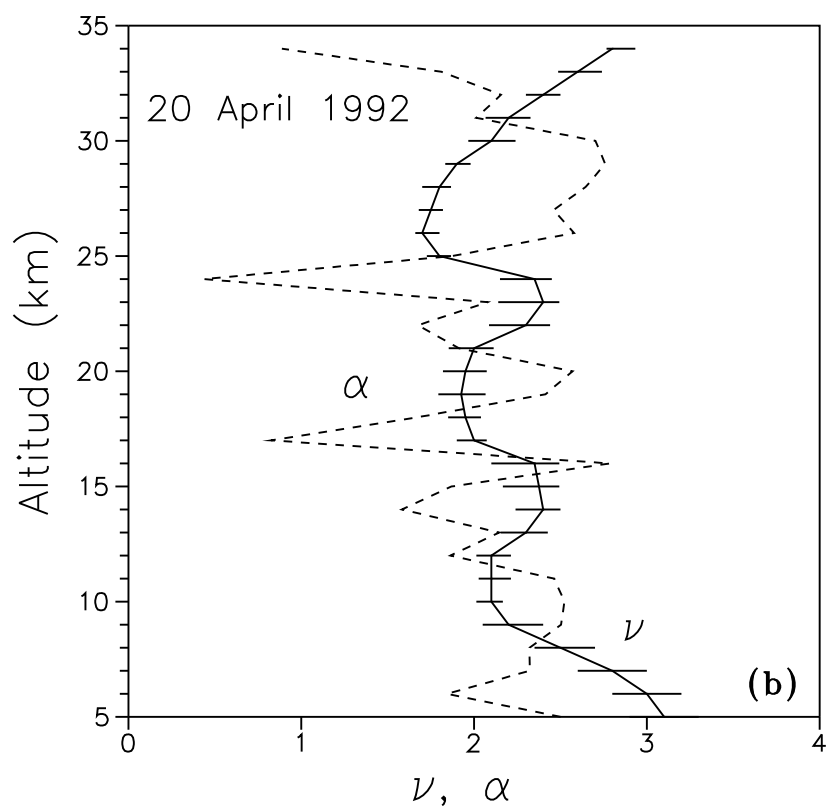
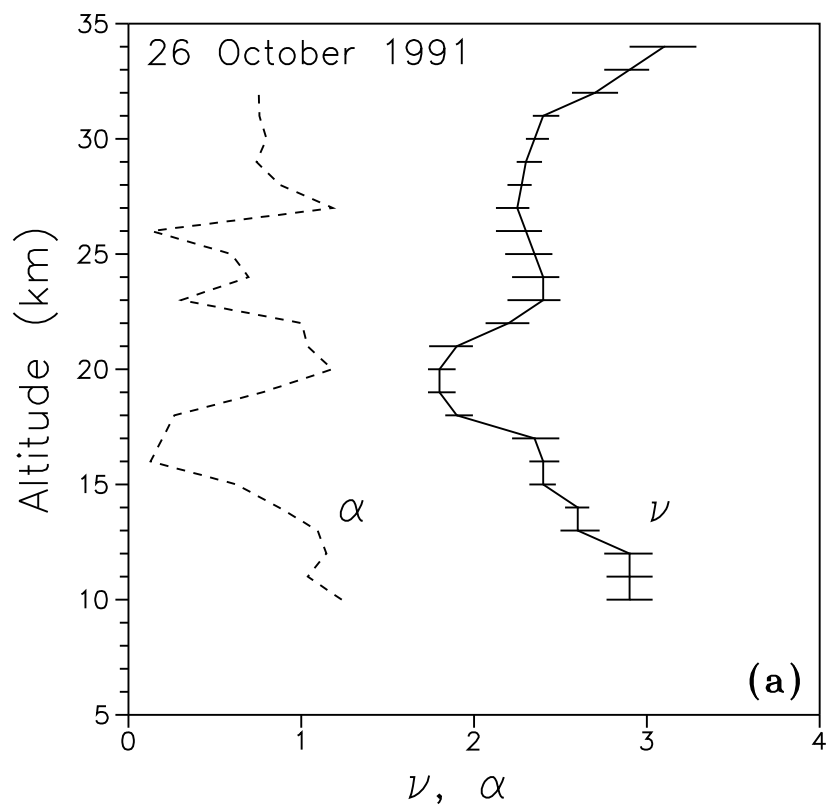


Figure 4.15: Profiles of the aerosol size parameter ν , defined as the slope of the Junge power law curve and the wavelength exponent α , of Eqn. 4.15.

where τ , the aerosol optical depth and β the so called Ångström coefficient, is derived from the aerosol extinction values, independent of the scattered sky radiation measurement used for deriving ν . The obtained α values are also plotted along with ν in Figures 4.15a and 4.15b. The α values obtained during October 1991 are found to be less than or equal to 1 at most altitudes and satisfy the relation $\alpha = \nu - 2$, as proposed by *Bullrich* [1964]. In April 1992 however, such a relation is not found to be valid because of the increase in α values by about 2 at all altitudes while there is no corresponding change in ν . While fitting a curve through the extinction coefficients through a limited number of wavelength points, about five in this case, it is not clear why there should be a systematic increase in α at all altitudes during April, while the error in fitting α (the error in α values in general, is in the range of 0.2-0.4), is same in both flights. Another interesting feature observed is the apparent anticorrelation which exists between the α and ν profiles in both flights. The α and ν profiles, in principle should correlate with each other, at least qualitatively, because as the relative size of the particle increases, the slope of the power law curve decreases, as well as does α , indicating that the aerosol scattering is less dependent on λ . The absence of such a correlation on the experimentally observed data sets indicates that determining α directly from the extinction coefficients and inferring about the size distribution could be erroneous as it has the inherent assumption that the aerosol absorption is absent and extinction is purely due to scattering. However, in the determination of ν , only the measured scattered radiation intensities are used which are compared with the computed scattered radiation intensities.

4.5.4 Mode radius

Yue and Deepak [1983, 1984] have proposed a method of retrieving aerosol mode radius from the aerosol extinction coefficients β at two wavelengths. Assuming that the stratospheric aerosol size distribution can be best fitted using a lognormal distribution (LND) function of the form

$$\frac{dn(r)}{dr} = \frac{A}{\sqrt{2\pi \ln \sigma}} \frac{1}{r} \exp \left[-\frac{\ln^2 \left(\frac{r}{r_m} \right)}{2 (\ln \sigma)^2} \right] \quad (4.16)$$

where A is the total number concentration (cm^{-3}), σ is the width of the lognormal curve and r_m is the mode radius, one can retrieve r_m . A value of 1.86 for σ is considered acceptable in literature [*Pinnick et al.*, 1976] for the stratospheric aerosol layer. On the other hand, if the measurements are made after a major volcanic eruption, such as Mt. Pinatubo, one may decide to choose zero order logarithmic distribution (ZOLD) [*Toon and Pollack*, 1976] of the

form

$$\frac{dn(r)}{dr} = A \exp \left[-\frac{\ln^2 \left(\frac{r}{r_m} \right)}{2 (\ln \sigma)^2} \right] \quad (4.17)$$

where A is an arbitrary constant and $\sigma = 1.8$. The method involves computing β as a function of r_m for $A = 1$ using Mie theory, given by the expression

$$\beta_\lambda = \int_{r_1}^{r_2} \frac{dn(r)}{dr} Q(m, \lambda, r) \pi r^2 dr \quad (4.18)$$

where $dn(r)/dr$ is the number of particles per cm^3 whose radii are between r and $r+dr$, $Q(m, \lambda, r)$ is the Mie extinction efficiency factor and m is the refractive index of the aerosol particle. Mie computations are made for the selected photometer wavelengths of 440 and 1050 nm taking the m values as $1.432 - i1 \times 10^{-8}$ and $1.423 - i1.5 \times 10^{-6}$ for the two wavelengths, respectively. The ratio of aerosol extinctions, R is defined as,

$$R = \frac{\beta_{440}}{\beta_{1050}} = \frac{\int_{r_1}^{r_2} \frac{dn(r)}{dr} Q(m, \lambda = 440, r) \pi r^2 dr}{\int_{r_1}^{r_2} \frac{dn(r)}{dr} Q(m, \lambda = 1050, r) \pi r^2 dr} \quad (4.19)$$

where r_1 and r_2 are the lower and upper radii limits of the integration and chosen such that the aerosol number density falls by 1×10^{-6} with respect to the maximum value in the size distribution. R values are plotted as function of r_m in Figure 4.16 for different σ values. It should be noted that the retrieved r_m is sensitive to the assumed σ value. For R greater than 2 an increase of 0.3 in σ will cause a decrease of about $0.05 \mu\text{m}$ in r_m and the uncertainty in r_m due to variation in σ increases with decreasing R . In the present work r_m values are determined separately from both curves corresponding to lognormal distribution of $\sigma = 1.86$ and ZOLD with $\sigma = 1.8$.

Figure 4.17 shows the measured aerosol extinction coefficients at 440 and 1050 nm at stratospheric altitudes and their ratio during October 1991. The aerosol extinctions are about 10^{-2} km^{-1} at these altitudes, which are about 2 orders of magnitude higher in comparison to the values obtained over Hyderabad in October 1985, a period considered to be volcanically quiescent [Jayaraman and Subbaraya, 1988]. Mode radii of the Pinatubo aerosols at these altitudes are determined from the aerosol extinction ratio as detailed above for the lognormal distribution and ZOLD (Figure 4.18). The mode radius of the aerosol layer is found to be around $0.22 \mu\text{m}$ with a prominent peak at 23 km with a value of $0.31 \mu\text{m}$ in the case of lognormal distribution and around $0.17 \mu\text{m}$ with a peak value of $0.195 \mu\text{m}$ in the case of ZOLD within the layer [Ramachandran et al., 1994c].

The effective radius, r_{eff} [Lenoble and Brogniez, 1984] described as

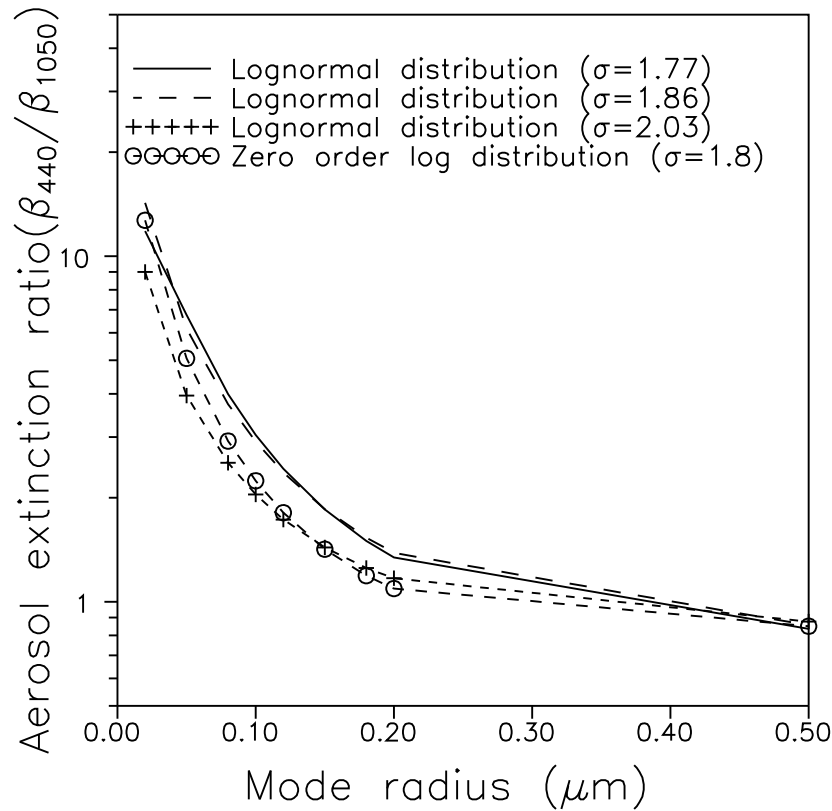


Figure 4.16: The aerosol extinction ratio as a function of the variable parameter r_m for lognormal ($\sigma = 1.77, 1.86$ and 2.03) and zero order logarithmic ($\sigma = 1.8$) distributions.

$$r_{\text{eff}} = \frac{\int_{r_1}^{r_2} r^3 \frac{dn(r)}{dr} dr}{\int_{r_1}^{r_2} r^2 \frac{dn(r)}{dr} dr} \quad (4.20)$$

is a more meaningful parameter for comparison, as it incorporates both r_m and σ . The corresponding r_{eff} computed using the above equation for LND and ZOLD are $0.58 \mu\text{m}$ and $0.57 \mu\text{m}$, respectively. Using balloonborne optical particle counters at Laramie, Wyoming (41°N), during July 1991, *Deshler et al.* [1992] have found $0.35 \mu\text{m}$ as a typical mode radius of the Pinatubo aerosols for a lognormal distribution of $\sigma = 1.6$ around 23 km. This gives an r_{eff} of $0.61 \mu\text{m}$ which is however slightly higher due to the fact that Deshler's measurements were made 3 months earlier to our measurements and about a month after the eruption.

4.5.5 Asymmetry factor

The asymmetry factor g is defined as the average of the cosine of the scattering angles for scattered radiation. Theoretically, the asymmetry factor can vary between -1 and $+1$. For

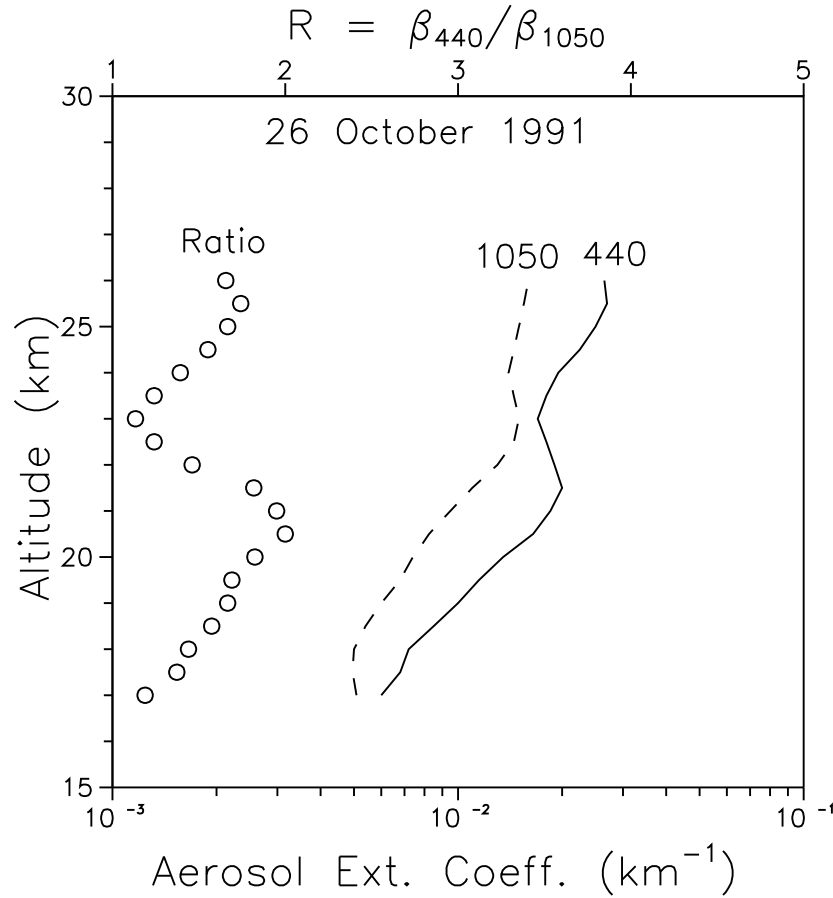


Figure 4.17: Aerosol extinction profiles at 440 (solid line) and 1050 (dashed line) nm and their ratios (circles) measured in October 1991, using balloon-borne Sun-tracking photometers over Hyderabad.

particles with isotropic scattering properties $g = 0$. The more the particles scatter in the forward direction, which is the case with larger particles the higher is the asymmetry factor. In the troposphere g is found to vary from 0.6 to 0.8 depending on the type of aerosols [d'Almeida *et al.*, 1991] for $\lambda = 500$ nm, but the distribution of g at the stratospheric altitudes is not well known, though an attempt was made over Alaska, using laser nephelometer measurements, in the altitude region of 11 to 13 km [Grams, 1981]. Here, an attempt has been made to obtain the vertical distribution of g at stratospheric altitudes, from the aerosol scattering phase function, derived from the scattered sky radiation measurements.

Though LND and ZOLD may describe better the stratospheric aerosol size distribution, for optically effective particles (in the size range of 0.05 to 10 μm) Junge power law can also be taken as a good representation [Volz and Sheehan, 1971] as the Mie scattering contribution

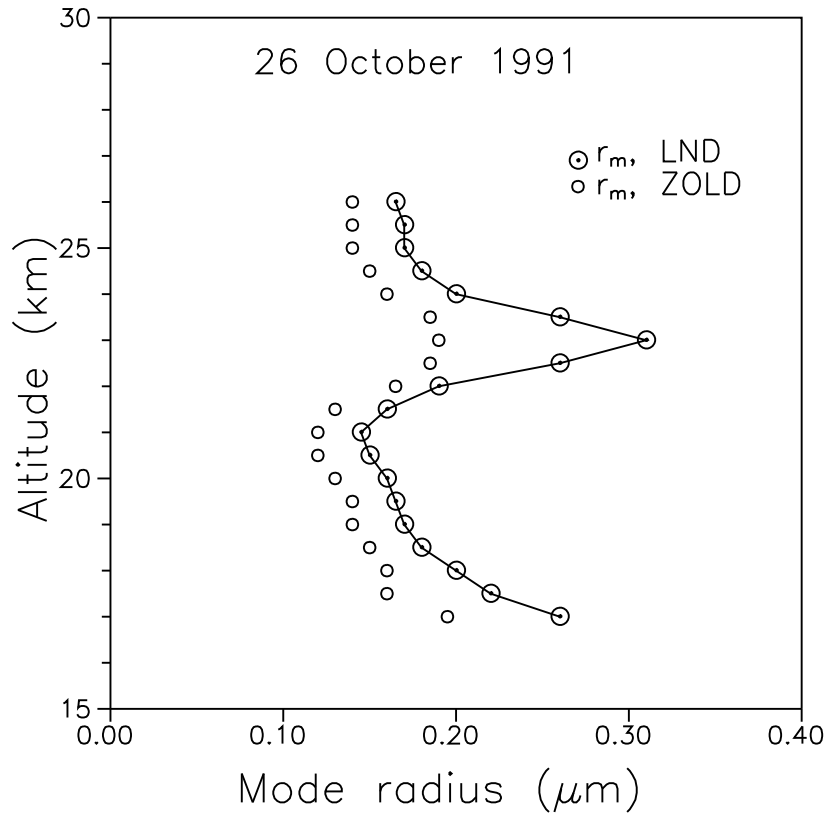


Figure 4.18: *The mode radius of the stratospheric aerosols obtained on 26 October 1991 using lognormal distribution (LND) and zero order logarithmic distribution (ZOLD).*

of the smaller particles (less than about $0.05 \mu\text{m}$) to the total integrated intensity is however marginal [Jayaraman, 1991]. The total extinction coefficient is found to increase only by 0.4% or less if the power law is truncated at $r_{\min} = 0.01 \mu\text{m}$ instead of $0.05 \mu\text{m}$ [Ramachandran *et al.*, 1994c]. Further, the advantage of the Junge power law is that only one parameter, ν , the slope of the power law curve best describes the size distribution, compared to LND and ZOLD where two parameters, r_m and σ are required to define the shape of the size distribution. Mie scattering computations are made to obtain the aerosol scattering phase functions at 500, 750 and 850 nm, for various ν values from 1 to 4, in steps of 0.2. The asymmetry factor g is determined from the aerosol phase functions $P_a(\lambda, \theta)$ using the expression

$$g = \frac{\int_0^\pi \cos\theta P_a(\lambda, \theta) d(\cos\theta)}{\int_0^\pi P_a(\lambda, \theta) d(\cos\theta)} \quad (4.21)$$

The theoretically obtained phase functions are used to fit the experimentally obtained scattering phase functions computed from the measured angular distribution of the scattered

radiation intensities from each altitude layer. The scattered radiation contribution from each layer is obtained by taking the difference between the values above and below. The obtained phase functions are also corrected for Rayleigh scattering. Attempt has been made to fit the data independently for the three photometer wavelengths and the mean values of the derived g and ν profiles alongwith standard deviation ($\pm 1\sigma$) are shown in Figures 4.19a and 4.19b. The uncertainty in determining asymmetry factor g is found to be about ± 0.05 .

As the particle size increases, the asymmetry factor g of the aerosol phase function increases and the slope ν of the power law curve fitted for the size distribution decreases and hence ν and g are anticorrelated, which is observed. In October 1991, it is interesting to note that while both ν and g show a large layer like structure above the local tropopause height, from 16 km to about 23 km the derived r_m values (Figure 4.18) show the peak at 23 km. Both the results are complementary to each other in the sense that while ν and g are representative of an ensemble of particles, r_m gives the mode radius at which the number of particles is maximum. Also, for the determination of r_m the width of the size distributions σ , for LND and ZOLD are assumed to be independent of altitude. In other words, while the bulk of the material produced after the eruption still remains at the 16 to 23 km region, the larger particles are formed at the expense of smaller particles. The aerosol extinction profiles also show that while the peak in the case of 440 nm occurs at the 21-22 km, in the 1050 nm extinction, which is sensitive to larger particles, the peak occurs at a slightly higher altitude of 23 km. In April 1992, two distinct layers are seen, consisting of larger particles, one with g values around 0.85, between 16 and 22 km and other with g values around 0.88, between 25 and 30 km. However, in comparison in October 1985, a volcanically quiescent period, g values are less than 0.7 in these altitudes.

Also an attempt has been made to intercompare the two independent techniques, namely, the estimation of r_m from the β_{440}/β_{1050} ratio, obtained from the direct radiation measurements and the estimation of g and ν profiles from the scattered radiation measurements, obtained during October 1991. Mie scattering computations are made using LND and ZOLD models with the r_m profiles of Figure 4.18 and g values are derived. It is found that though the exact shape (Figure 4.19a) could not be reproduced, the average g value for the Pinatubo layer obtained from both the techniques compare well with each other and is in the range of 0.83 ± 0.04 . Similarly using the Junge power law with the ν profile of Figure 4.19a, β_{440}/β_{1050} are computed and r_m values are derived using the calibration curve (Figure 4.16), for LND $\sigma = 1.86$. While the mean value of r_m derived from direct radiation measurements is 0.22 ± 0.05

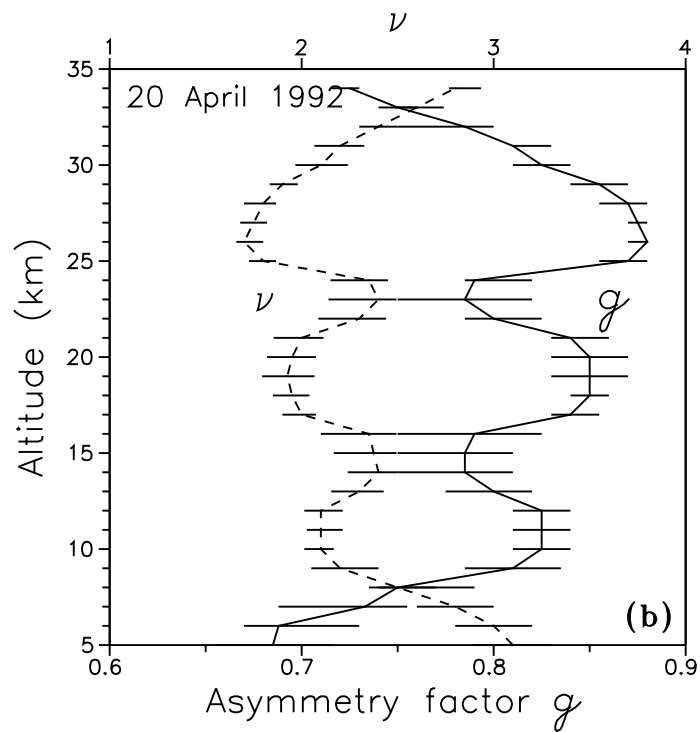
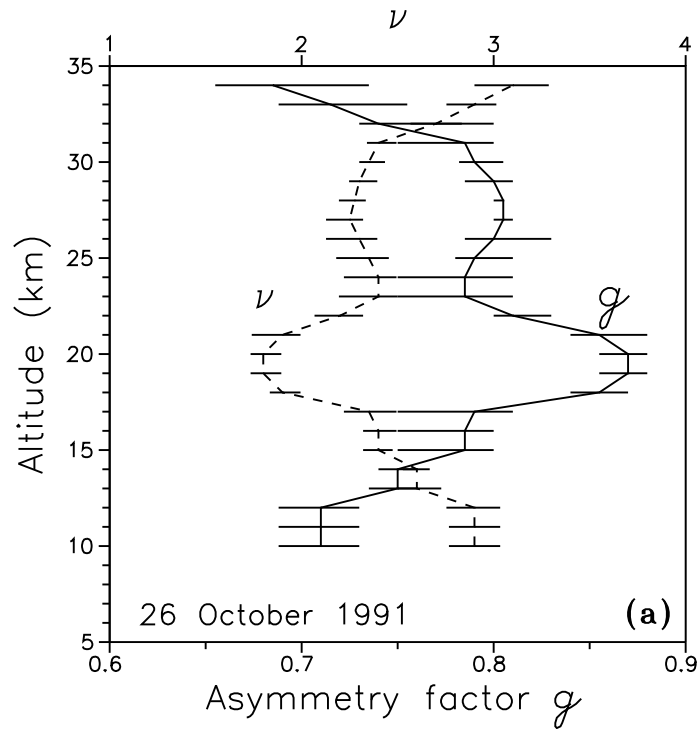


Figure 4.19: Vertical profiles of the asymmetry factor g and the aerosol size distribution parameter ν obtained on 26 October 1991 and 20 April 1992 from the measured angular distribution of the scattered radiation intensities.

μm for the layer, the mean r_m value derived from the Junge power law is found to be $0.20 \pm 0.01 \mu\text{m}$.

4.5.6 Mass density of Pinatubo aerosols

An attempt has been made to estimate the mass density (grams per cubic metre) of Pinatubo aerosols from the aerosol extinction profile of 500 nm, obtained during October 1991. Following *Jäger et al.* [1988] the mass densities (M) and extinction coefficients (β_{500}) are obtained using derived r_m (LND) and taking a density of 1.65 g cm^{-3} for 75% H_2SO_4 droplets. The obtained M/β_{500} ratios are multiplied with the measured β_{500} values to get the altitude variation of the mass density. The peak value at 23 km corresponding to peak r_m of $0.31 \mu\text{m}$ is found to be $22 \mu\text{gm}^{-3}$ which is slightly less than $28 \mu\text{gm}^{-3}$ the value reported by *Deshler et al.* [1992] for a mode radius of $0.35 \mu\text{m}$ for the late July 1991 period. The integrated value for the whole Pinatubo layer (17 to 26 km) is found to be about 0.053 gm^{-2} which is about 3.75 times higher than the value reported by *Jäger et al.* [1988] for El Chichon aerosol layer, obtained about 4 months after the eruption.

4.5.7 Comparison of Pinatubo results with previous major eruptions

In Figures 4.20a and b the results of aerosol concentration and ν are compared with the earlier results obtained over Hyderabad in October 1985 and over Thumba (8.5°N) in February 1980. These two cases are selected to show the effect of volcanic eruptions at stratospheric levels over the equatorial region. While the Thumba results are 3 months after the Sierra Negra volcanic eruption, the October 1985 result over Hyderabad is taken as typical of a volcanically quiet period. Though a volcanically produced aerosol layer is seen above about 15 km in the Thumba result [*Subbaraya and Jayaraman*, 1982], it is however much less significant compared to the recent Pinatubo results (Table 4.1). But the ν profiles (Figure 4.20b) show a decrease at the stratospheric level both after the Sierra Negra and Pinatubo eruptions, compared to the 1985 result indicating the presence of a layer having relatively a larger number of larger particles.

In Figure 4.21a a comparison between the aerosol extinction profile for 500 nm in the October flight and the SAGE II 525 nm extinction profile for the same period except at a higher latitude of 39.7°N [*Thomason and Osborn*, 1992] is attempted. A very good agreement is seen between the data sets in the 15 to 23 km region. The higher extinction values above 23 km over Hyderabad is the indication of the initial confinement of the aerosol particles over the

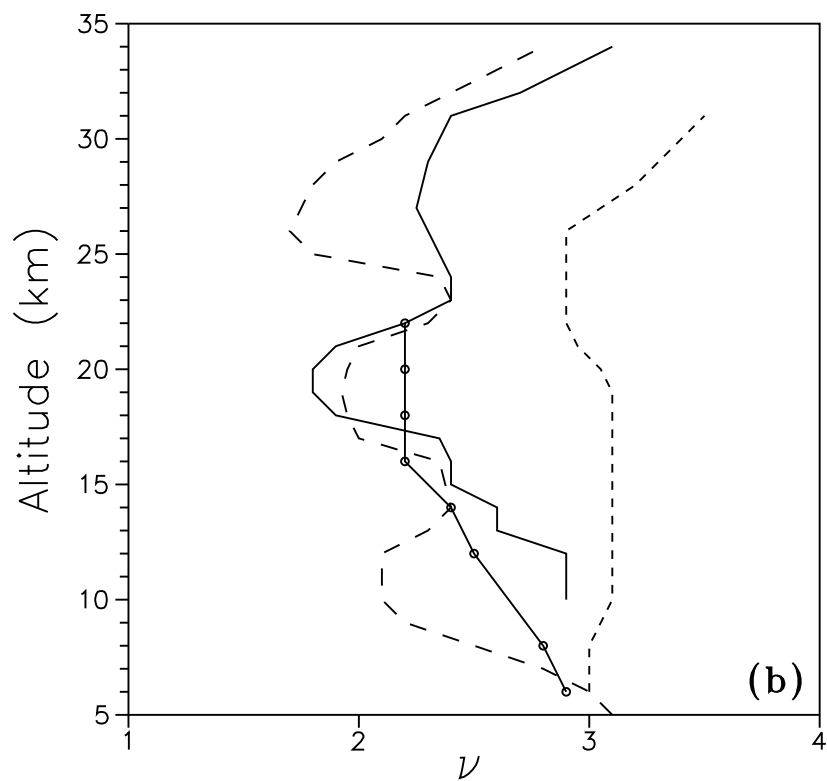
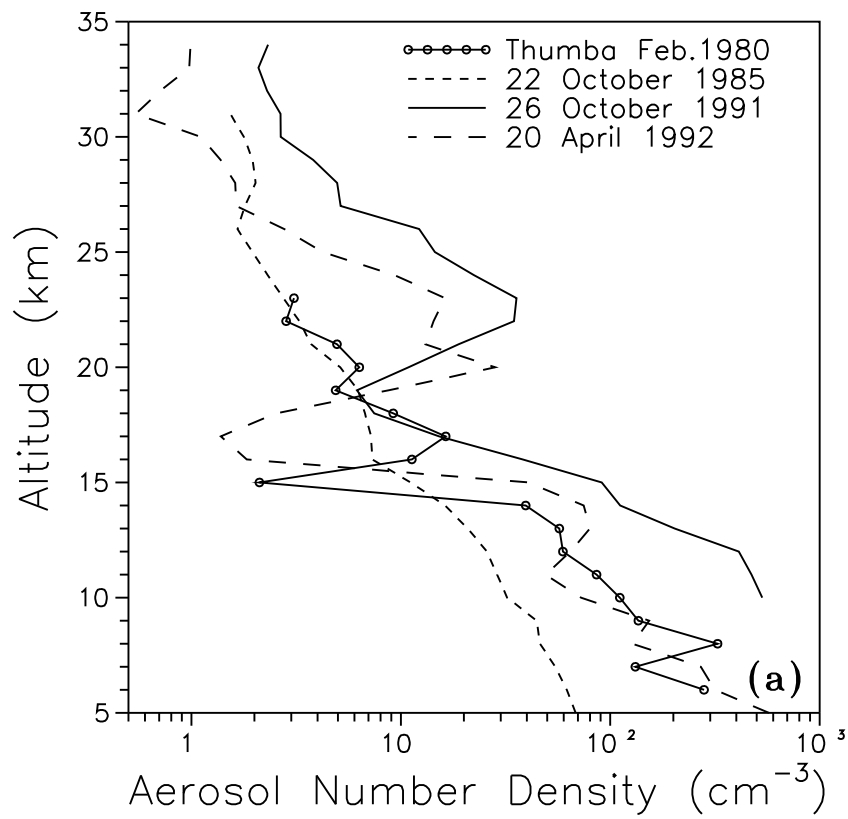


Figure 4.20: Comparison of the (a) aerosol number density and (b) aerosol size parameter data with the earlier results obtained during a volcanically perturbed period (Thumba, 1980) and a volcanically quiescent period (Hyderabad, 1985).

equatorial region, extending even above 30 km. In Figure 4.21b the 500 nm extinction values in the case of April flight are compared with the SAGE II results at 19°N during the same period and with the results of the Nd:YAG lidar experiment made at Ahmedabad (23°N), 2 weeks prior to the balloon experiment. The aerosol extinction values are obtained from the lidar backscattering coefficient by multiplying an altitude independent value of 50 which has the unit of steradian. Though an altitude dependent factor [Jäger *et al.*, 1988] can be more realistic, it can be shown that the error in the obtained extinction values are within 25%. A systematic increase in the extinction values is also seen above about 24 km with decreasing latitude indicating that the upper edge of the layer extends to higher altitudes in the equatorial region.

4.5.8 Synthesis of results

With an attempt to study the physical properties of the Pinatubo aerosols, Thomason [1992] has used the SAGE II aerosol extinction measurements and studied their ratios. Figure 4.22 is adopted from Thomason [1992] but for the present results, where the aerosols are classified into three modes, aerosols with low extinction and high extinction ratio representing smaller size background type aerosols (I), aerosols with high extinction and high extinction ratio representing the larger number of smaller particles representing an early volcanic period (II) and aerosols with high extinction and low extinction ratio representing higher number of larger particles representing post-volcanic aerosols (III). While Thomason [1992] has shown that immediately (1 month) after the eruption the aerosols exhibited high extinction but a small inferred particle size, corresponding to mode II in Figure 4.22, a transitional phase between the very small aerosols created by gas-to-particle conversion mechanism and the large sized post-volcanic aerosols that exhibit high extinction and low extinction ratio values corresponding to mode III. The balloon observations made in October 1991, 4 months after the eruption show mode III type particles. For comparison, SAGE results corresponding to October 1991 are shown for two different latitudes, one at 17.9°N, close to the balloon observation site and the other at a latitude of 39.7°N. A good agreement is seen between the SAGE and balloon derived ratios, all exhibiting the post-volcanic type aerosols. For comparison the extinction ratios (β_{450}/β_{1000}) obtained during 1985 over Hyderabad are shown which are found to represent mode I type particles corresponding to background aerosols.

It has been shown [Turco *et al.*, 1983] that condensation of sulphate aerosols would occur first on the large aerosols existing earlier and then on progressively smaller aerosols. Deshler

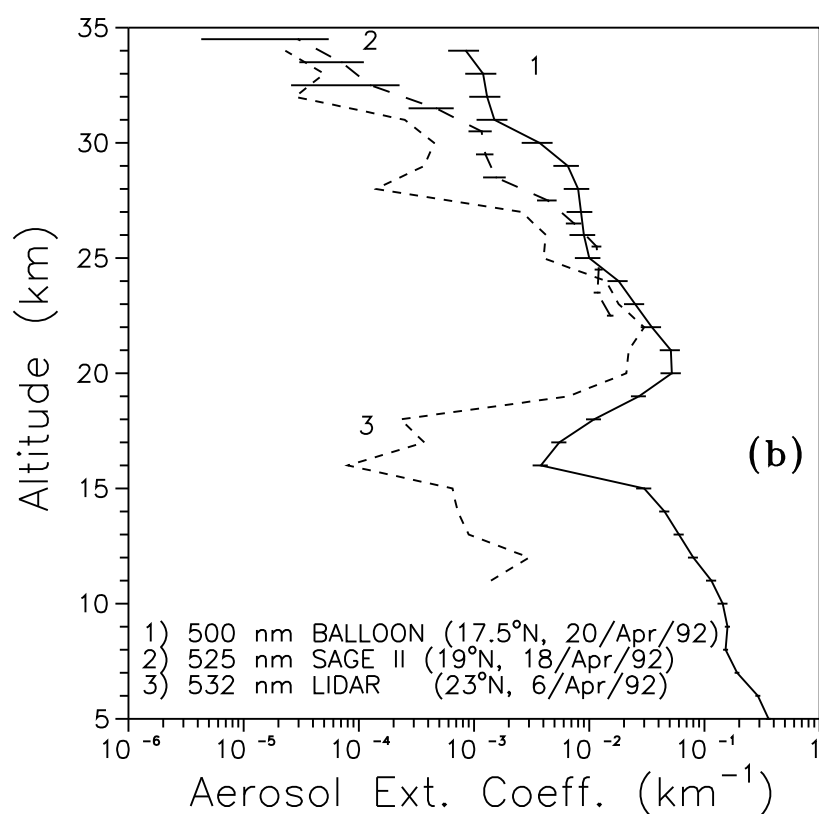
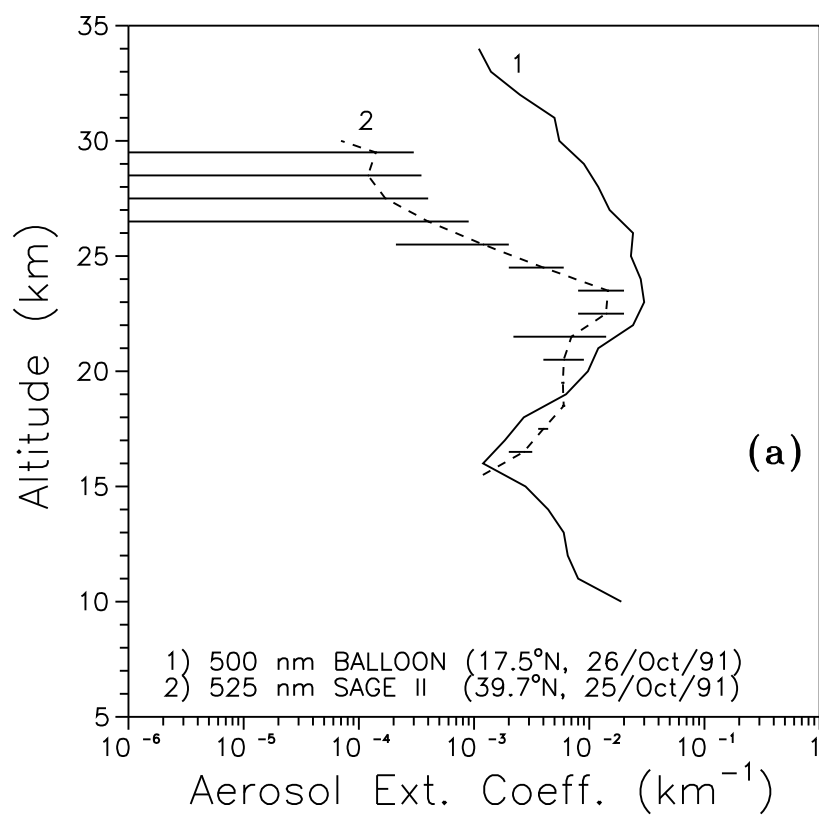


Figure 4.21: Comparison of the aerosol extinction at 500 nm with that of the SAGE II 525 nm results and with that of a Nd:YAG lidar experiment made in Ahmedabad (23°N) about 2 weeks prior to the balloon experiment in April 1992.

Table 4.1: *Comparison of the aerosol size parameter (ν) and number densities obtained on 22 October 1985, 26 October 1991 and 20 April 1992 over Hyderabad.*

Altitude (km)	Aerosol size parameter (ν)			Aerosol number density (cm^{-3})		
	22/10/85	26/10/91	20/04/92	22/10/85	26/10/91	20/04/92
5			3.10			572.80
6	3.00		3.00	62.01		316.71
7	3.00		2.80	54.59		270.48
8	3.00		2.50	46.19		127.83
9	3.05		2.20	44.55		153.43
10	3.10	2.90	2.10	32.18	531.26	72.53
11	3.10	2.90	2.10	28.82	472.61	49.15
12	3.10	2.90	2.10	25.76	411.25	64.58
13	3.10	2.60	2.30	20.86	202.87	79.90
14	3.10	2.60	2.40	16.27	111.45	74.68
15	3.10	2.40	2.38	11.13	91.10	40.49
16	3.10	2.40	2.35	7.31	38.12	1.84
17	3.10	2.35	2.00	7.20	15.22	1.38
18	3.10	1.90	1.95	6.73	7.46	2.54
19	3.10	1.80	1.93	6.26	6.17	8.75
20	3.05	1.80	1.95	5.13	10.90	28.19
21	2.95	1.90	2.00	3.73	18.90	13.06
22	2.90	2.20	2.30	3.27	34.65	14.32
23	2.90	2.40	2.40	2.75	35.66	16.27
24	2.90	2.40	2.35	2.31	22.31	9.30
25	2.90	2.35	1.80	1.96	14.54	4.23
26	2.90	2.30	1.70	1.66	12.23	2.77
27	3.05	2.25	1.75	1.80	5.15	1.63
28	3.20	2.28	1.80	2.03	4.96	1.62
29	3.30	2.30	1.90	1.96	3.81	1.28
30	3.40	2.35	2.10	1.78	2.67	1.11
31	3.50	2.40	2.20	1.53	2.66	0.54
32		2.70	2.40		2.29	0.71
33		2.90	2.60		2.09	0.98
34		3.10	2.80		2.32	0.99

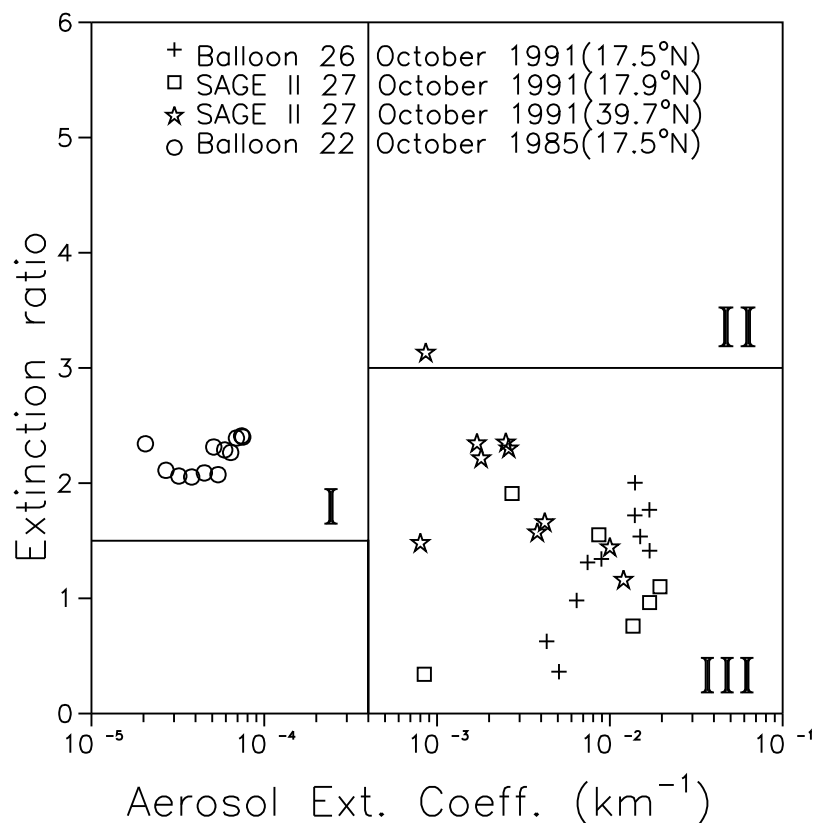


Figure 4.22: The scatter diagram, adopted from Thomason [1992], of the 525 to 1020 nm extinction ratio and 1020 nm extinction of SAGE II and the ratios of extinctions between 500 and 1050 nm and the extinction at 1050 nm of the balloon measurements made on 26 October 1991. The October 1985 balloon values over Hyderabad are also plotted for comparison. The scatter plot is divided into three regions (modes), the background type aerosols (mode I), the transition stage immediately after a major volcanic eruption (mode II) and the aged volcanic aerosols (mode III). See text for their characteristics.

et al. [1992] suggest that nucleation of new $\text{H}_2\text{SO}_4/\text{H}_2\text{O}$ aerosol occurred below 20 km during July and August 1991 over Laramie. Condensation on the already existing sulphate aerosol would increase the extinction and decrease the extinction ratio as the extinction becomes increasingly dominated by large aerosols whose scattering efficiency is almost the same at 500 nm and at 1050 nm. *Turco et al.* [1983] suggested in the case of Mt. St. Helens eruption, that if the concentration of sulphur dioxide is sufficiently large, conversion of H_2SO_4 produces large numbers of new small $\text{H}_2\text{SO}_4/\text{H}_2\text{O}$ aerosol and coagulation proceeds at a higher rate. In the case of Pinatubo eruption, the same phenomena would have occurred over the tropics between 20 and 25 km where the densest portions of the cloud were observed. Thus the condensation of H_2SO_4 vapour on the already existing $\text{H}_2\text{SO}_4/\text{H}_2\text{O}$ liquid droplets and subsequent coagulation is one of the major mechanisms, for the formation of larger aerosol particles at these altitudes. The high mode radius in the range of 0.2 to 0.3 μm obtained in October 1991 over Hyderabad and by *Deshler et al.* [1992] during July 1991 over Laramie, which was about 0.35 μm indicate the presence of aged volcanic aerosols, formed due to coagulation. In April 1992, a layer with ν values less than 2 is seen between 25 and 30 km, indicating the formation of larger aerosols from smaller aerosols due to coagulation and this phenomenon has subsequently reduced the total aerosol number density at these altitudes.

4.6 Nd:YAG backscatter lidar measurements

4.6.1 Lidar system specifications and Data collection

Lidar, analogous to radar, has become one of the most widely used techniques for atmospheric aerosol research, with the advent of high-power pulsed lasers, technological advance in the field of low level light detection and fast data processing methods. A continuous monitoring of the Pinatubo volcanic aerosol layer is essential to study the physical and chemical processes involved in the formation and decay of the layer, which will help in the assessment of its overall impact on climate [*Hofmann*, 1987; *Kiehl and Brieglab*, 1993]. A laser radar (lidar) system is an apt tool to conduct such a study. The Pinatubo aerosol layer has been continuously monitored by the newly set up Nd:YAG lidar operating at 532 nm at the Physical Research Laboratory (PRL), Ahmedabad (23°N, 72.5°E) since April 1992 [*Jayaraman et al.*, 1995a]. Results obtained on the vertical profiles of the scattering ratios, aerosol extinction coefficients and mass of the Pinatubo layer and its decay from April 1992 to May 1994 are reported here.

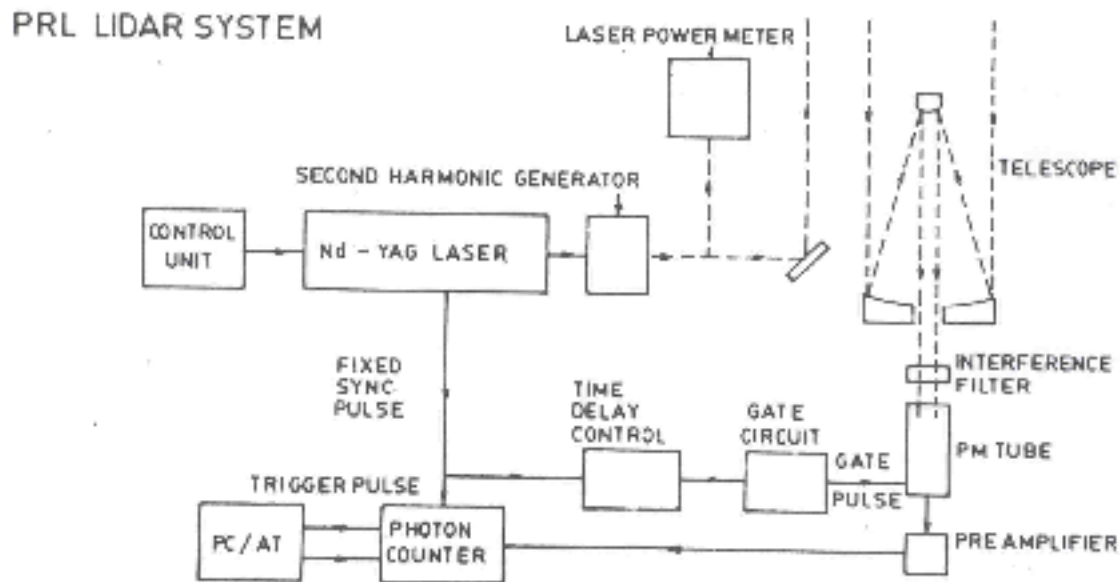


Figure 4.23: Block diagram of the Nd:YAG backscatter lidar system at PRL.

The specifications and the technical block diagram of the PRL lidar system used for the measurements are given in Table 4.2 and Figure 4.23, respectively. The system employs a transmitter consisting of a pulsed Nd:YAG laser, a 0.40 m diameter Cassegrain telescope which acts as the receiver, a thermoelectrically cooled photomultiplier tube operating in the photon counting mode, signal processing unit and data processor. The wavelength used for the measurement is 532 nm which is the second harmonic of Nd:YAG's fundamental wavelength of 1064 nm. The laser beam is transmitted vertically upwards with the help of a 45° incidence, 2-inch diameter ultrahard dielectric-coated high-energy laser mirror. The optical axis of the telescope is at a distance of 0.5 m from the transmitting optics. The field of view of the telescope is kept large in comparison to the laser beam divergence (Table 4.2) so as to accommodate the beam totally above a certain altitude, which is about 300 m in the present case. An interference filter having central wavelength at 532 nm with a bandwidth of 1 nm is used to reduce the background light noise in the collected backscattered signal. The backscattered photons are then detected by a gated photomultiplier which is cooled to below -25°C using a thermoelectric cooler. By gating process, the PMT is electrically switched OFF (by applying a reverse bias between the photo cathode and the first dynode) for a selected time, to avoid intense backscattered signals from low altitudes, which could cause saturation of the detector and can give rise to signal induced noise [Shimizu *et al.*, 1985]. In the present setup, the photomultiplier is turned ON for a time interval of 0.5 ms. A programmable time

Table 4.2: *Specifications of the PRL Lidar system.*

Item	Specifications
LASER	
(581C-10, Quantel, France)	
Material	Nd:YAG
Average output power	10 W
Output energy per pulse	440 mJ (532 nm)
Repetition rate	10 Hz
Pulse duration	7 ns
Beam diameter	9 mm
Beam divergence	0.3 mrad
RECEIVING OPTICS	
Telescope type	Cassegrain
Diameter	0.40 m
Field of view	6 mrad
Interference filter bandwidth	1 nm
Maximum λ	532 nm
Maximum transmission	48%
Photomultiplier	9813A (Thorn EMI, UK) (Photon counting mode)
SIGNAL PROCESSOR	
(SR430, Stanford Research Systems, USA)	
Bin width	640 ns (= 96 m alt. resolution) (with no interchannel dead time)
Integration	500 s (5000 records, typical)

delay pulse is used to switch ON the PMT from a desired altitude level. For the results presented here, a time delay of 60 μ s is used corresponding to an altitude of 9 km which is the starting altitude of the measurement. The signal is range detected using a scalar averager operating at 200 MHz count rate and integrated for 5000 laser shots. The signals are corrected for the counting loss [Donovan *et al.*, 1993] typical of the counting procedure. Background noise is estimated individually for each measurement, which is the observed photon count rate from altitudes where it does not decrease with altitude but takes more or less a constant value and subtracted from the signal. In general, the signal is about 40 times higher than the noise at 35 km (signal-to-noise-ratio of 40) and the factor reduces to about 10 at 45 km.

4.6.2 Data analysis

The range-corrected photon counts are normalised with model atmosphere [U. S. Standard Atmosphere, 1966] air density profiles in the altitude regions above 35 km, where the aerosol content is negligible. January 30°N air density profile is used for lidar observations taken during the 6 months from October to March and July 30°N profile is used for the months from April to September, taking into account the $\pm 7\%$ change in the air density values, between these two profiles, in the altitude region around 35 km.

The total backscattering coefficient β_z is obtained using the top to bottom inversion algorithm proposed by Klett [1985]

$$\beta_z = \frac{\exp(S - S_m)}{\frac{1}{\beta_m} + 2 \int_z^{z_m} \frac{\exp(S - S_m)}{B_a} dz} \quad (4.22)$$

where S and S_m are the logarithm of the range-corrected photon counts at any altitude z and at the maximum altitude of the obtained profile z_m , respectively. β_m is the backscattering coefficient at altitude z_m which is the Rayleigh backscattering coefficient at these altitudes in the absence of aerosols. B_a (sr^{-1}) is the ratio between aerosol backscattering and extinction coefficients. If B_a is taken as a constant and not dependent on altitude as it is done in the present work, then the above solution is similar to that obtained by Fernald [1984].

This top to bottom inversion procedure, proposed by Klett becomes an excellent choice for analysing the lidar data if backscattered signal can be measured well above the aerosol layers (35 km and above). Above 35 km the contribution from aerosol scattering to the total backscattering is negligible and hence β_m becomes the Rayleigh backscattering coefficient at the maximum altitude which can be readily computed from air density values. For a given wavelength, B_a depends on the aerosol size distribution which can be different at different

altitudes [Jayaraman and Subbaraya, 1988]. Using lidar and simultaneous balloonborne optical particle counter data Jäger and Hofmann [1991] have obtained values of B_a for 532 nm, for the El Chichon volcanic eruption. The values are found to be in the range between 0.016 and 0.03 with a mean value of about 0.02 in the lower stratosphere from 20 to 30 km. Recent results for Pinatubo by D'Altorio *et al.* [1993] using DIAL technique show that the ratio varies from 0.02 to 0.033 for 589 nm during the August 1991 to December 1992 period. In the present calculations, an altitude independent value of 0.02 sr^{-1} for B_a has been used for the retrieval of β_z . β_z values derived using three independent values for B_a , namely, 0.015, 0.02 and 0.025 show that the uncertainty in β_z increases from 1% at 30 km to about 25% at 20 km for a volcanically perturbed case such as after the Pinatubo eruption, while the uncertainty is well within 10% for background aerosol level for the same altitude region.

From the backscattering coefficient profiles the scattering ratio R is obtained as,

$$R = \frac{\beta_{\text{air}}(z) + \beta_{\text{aerosol}}(z)}{\beta_{\text{air}}(z)} \quad (4.23)$$

where $\beta_{\text{air}}(z)$ and $\beta_{\text{aerosol}}(z)$ are the air and aerosol backscattering coefficients at altitude z . Thus for an aerosol free Rayleigh atmosphere, R is unity and with increasing aerosol concentration R increases.

4.6.3 Lidar observations

The lidar observations are being made since April 1992, every fortnight, during clear nights, with breaks in the observations due to Indian monsoon which is active during June-September period over Ahmedabad. About 36 profiles have been chosen for the present study of the Pinatubo volcanic aerosol layer and its decay.

4.7 Results and Discussion

4.7.1 Scattering ratios

Figure 4.24 shows the variations in the obtained scattering ratio profiles with respect to time, starting from April 1992 until May 1994, a period corresponding to about 10 months after the Pinatubo eruption to about 3 years. The volcanic aerosol layer is seen very prominently as an increase in the scattering ratios from about 17 km (1 km above the local tropopause) to about 30 km. The layer peaks initially at 23 km and by May 1994, the peak has come down to 20 km. Also, the maximum scattering ratio is about 8 in April 1992, which increases to about

22 in May 1992 and decreases to about 3 in October 1992. During the rest of the observation period, though the Pinatubo layer is seen, the broad layer which was seen in the initial period reduces to an insignificant layer between 17 and 25 km, with a simultaneous decrease in peak scattering ratio to about 1.5 in May 1994. In the initial periods of the observations, two layers are seen, indicating inhomogeneities within the layer, which by the end of May 1992, merge to form one broad homogeneous layer. Similar observations of inhomogeneities within the layer which then disappeared by early 1992, have been reported by *Deshler et al.* [1993] using balloonborne optical particle counters over Laramie, Wyoming (41°N) and also by *Shibata et al.* [1994] using Nd:YAG lidar at Wakkanai (45.4°N), Japan.

4.7.2 Aerosol extinction coefficients

Figure 4.25 shows the derived vertical profiles of aerosol extinction coefficients from lidar measurements made during April 1992. The Pinatubo layer is seen between 17 and 30 km, with aerosol extinction in the range of $0.5 \times 10^{-5} \text{ km}^{-1}$ at 17 km which increases by more than 2 orders of magnitude to $0.3 \times 10^{-2} \text{ km}^{-1}$, between 20 and 25 km, where most of the aerosol cloud remained over the tropics. The assumption of a constant (altitude independent) extinction to backscatter ratio of 0.02 sr^{-1} used for the inversion of lidar data is found to introduce an error of about 1% in the derived extinction coefficient values at 30 km which increases to more than 25% at 20 km. The errors (horizontal bars) plotted in profile 1 of Figure 4.25 at every kilometre, however, do not look significant in the logarithmic scale. For comparison the Stratospheric Aerosol and Gas Experiment (SAGE) II satellite extinction profile obtained on 18 April 1992 at 19°N, 71.3°E has also been plotted. The lidar data agrees well with SAGE II data, between 22 and 29 km and differing beyond 29 km, where the SAGE II values are higher, indicating that the altitude extent of the layer increases to higher altitudes, even above 30 km over lower latitude regions. This feature has already been observed from balloon-borne observations of aerosol extinctions, made using Sun-tracking photometers over Hyderabad (17.5°N, 78.6°E), during April 1992. The aerosol backscattering coefficients obtained between 17 and 30 km, are integrated to study the decay of the Pinatubo layer and are plotted with respect to days after the eruption in Figure 4.26. An exponential fit to the data gives a $1/e$ folding time of 9 months compared to a value of about 7 months reported by *Grant et al.* [1994] for the tropical aerosol loading in a 10° latitude band centered on the densest aerosol region in 1991. As the Mt. Pinatubo eruption occurred in June 1991, situated at a latitude of 15.14°N, the low latitude region became the source of aerosols to higher latitude regions. The

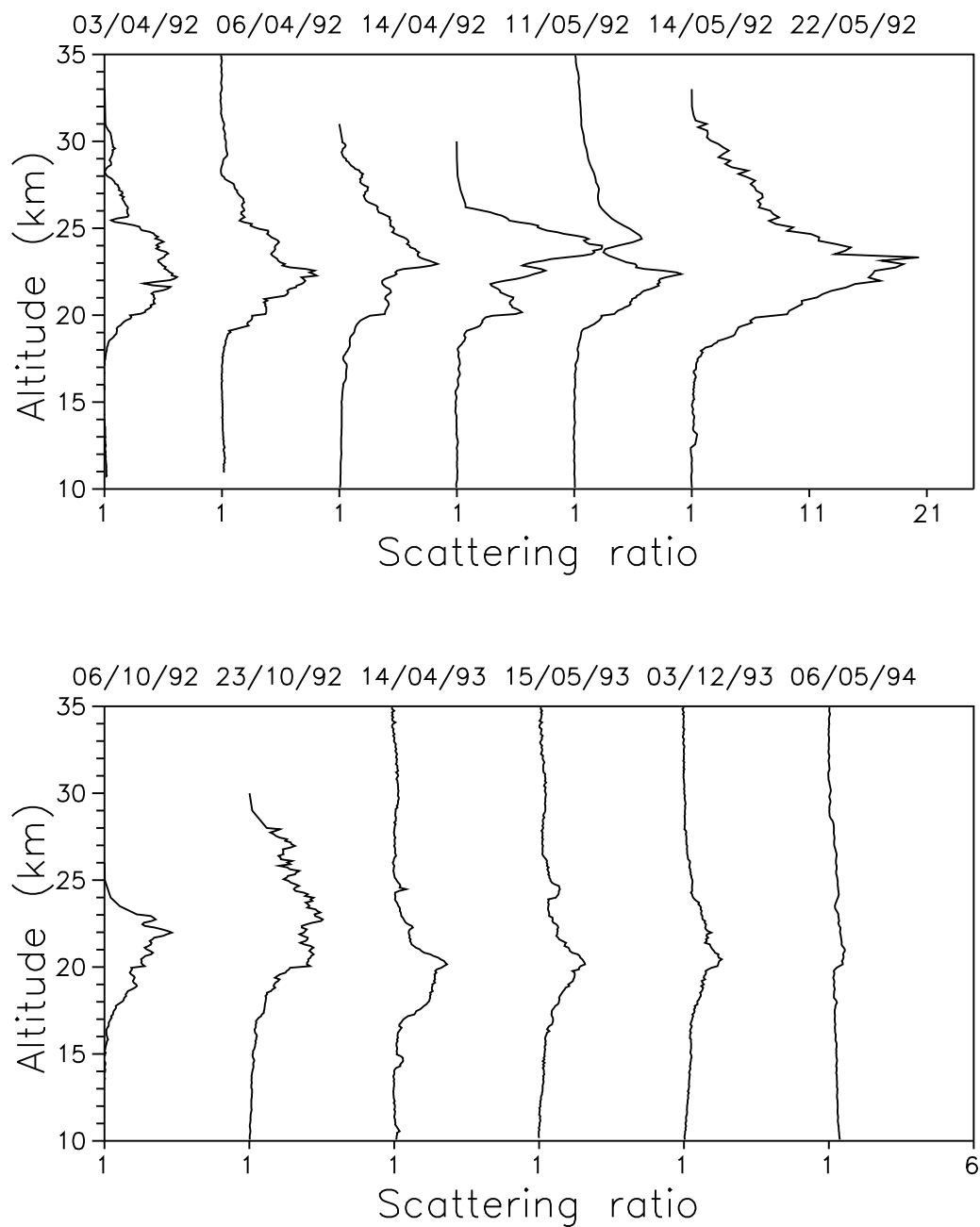


Figure 4.24: Sample profiles of the scattering ratio obtained during April 1992 to May 1994, showing the time evolution of the Pinatubo volcanic aerosol layer. The dates of measurements are given at the top as dd/mm/yy.

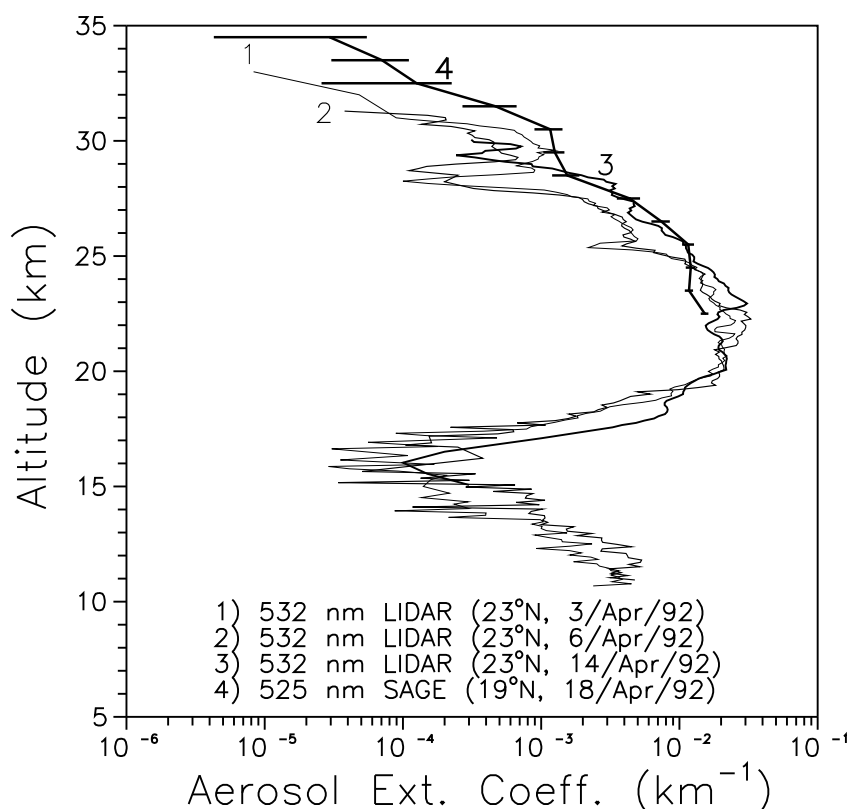


Figure 4.25: Profiles of aerosol extinction coefficients obtained over Ahmedabad (23°N , 72.5°E) during April 1992 using Nd:YAG lidar. SAGE II extinction profile for 19°N , 71.3°E is also plotted for comparison. The error in extinction coefficient values, which is of the order of 25% in the layer altitude and plotted in profile 1 at every km is, however, not quite visible.

poleward detrainment of particles was the dominant mechanism in distributing the particles at stratospheric altitudes, than the gravitational settling during the initial period after the eruption [Trepte *et al.*, 1993]. Earlier measurements made using balloon-borne Sun-tracking photometers after the El Chichon eruption in 1982, showed that the layer produced after the eruption decayed in about 3 years over the tropics [Jayaraman, 1991]. Since Mt. Pinatubo had put as much as 2 to 3 times more material into the stratosphere compared to El Chichon, it was not clear whether the lifetime of these aerosols will also be longer because of the larger number density of aerosols or, perhaps, the physical processes such as growth, coagulation and sedimentation will take place at a much faster rate to give more or less the same decay time. It is shown through model calculations [Pinto *et al.*, 1989] that as the mass of injected sulphur dioxide increases beyond 10 Mt, the aerosol microphysical processes of condensa-

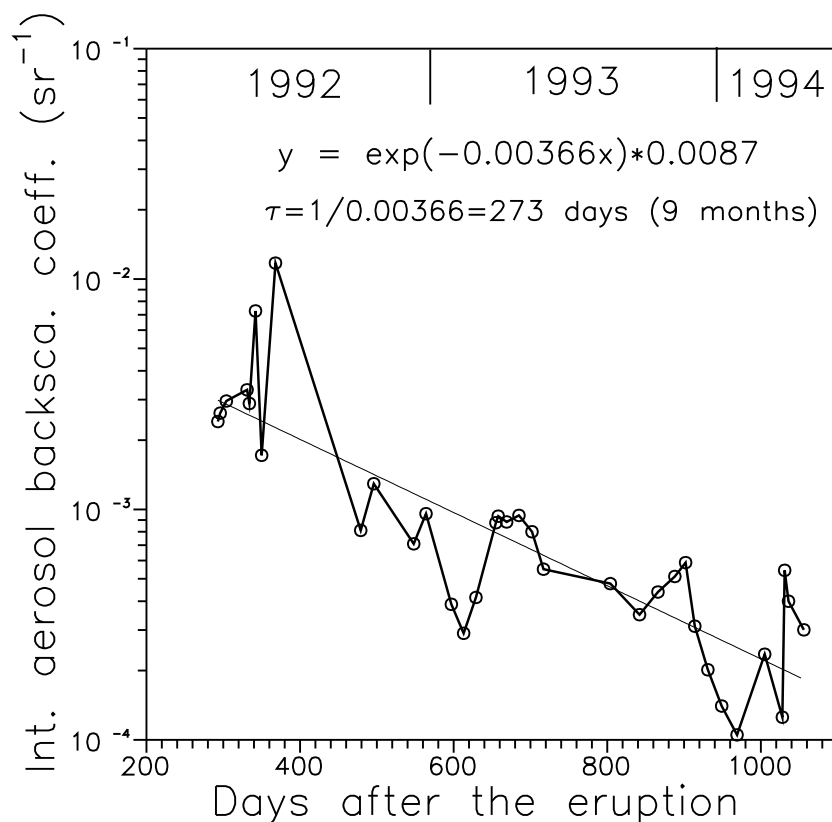


Figure 4.26: *The integrated aerosol backscatter (17 to 30 km) decay with time from April 1992 to May 1994.*

tion and coagulation produce larger particles as the SO_2 injection rate is increased rather than a larger number of particles of the same size, due to which the size of sulphate aerosols increases and the removal rate accelerates. Consequently, the residual sulphate masses could be quite similar after about 2 years for eruptions of widely different magnitudes. Interestingly, if the Pinatubo layer decays at the present rate, with a $1/e$ folding time of 9 months, then it could take about 4.5 years, to reach the background aerosol extinction coefficient value of about $2 \times 10^{-5} \text{ km}^{-1}$, a value representative of a volcanically quiescent period for the tropical stratosphere obtained from the balloon-borne measurements of stratospheric aerosols over Hyderabad [Jayaraman, 1991].

4.7.3 Decay of Pinatubo aerosol layer mass

The aerosol backscattering coefficient values are used to obtain the mass density (gm^{-3}) of the aerosols following the procedure described by Jäger and Hofmann [1991]. The mass den-

sities (M) and backscattering coefficients (β_{532}) are calculated for lognormal size distributions of aerosols with mode radii (r_m) 0.1, 0.2 and 0.3 μm having $\sigma = 1.86$ (value accepted in the literature for stratospheric aerosols [Pinnick *et al.*, 1976]) and taking a density of 1.65 g cm^{-3} for 75% H_2SO_4 droplets. Deshler *et al.* [1993] using balloonborne optical particle counters and fitting the obtained aerosol number density, with lognormal distributions have shown that the mode radius in the altitude region of 17 to 23 km is in the range of 0.1 to 0.5 μm , between July 1991 and January 1993. Also, our results on the mode radius obtained using balloonborne Sun-tracking photometers, during October 1991 [Ramachandran *et al.*, 1994c], show that it is in the range of 0.1 to 0.3 μm , in the 17 to 26 km altitude region. D'Altorio *et al.* [1993] using DIAL technique at L'Aquila (42°N), Italy, have shown that the mode radius in the 15 to 25 km altitude region lies in the range of 0.1 and 0.25 μm , during the August 1991 to December 1992 period. As in a monostatic lidar system like ours, it is not possible to retrieve r_m , calculations of aerosol mass densities are repeated for r_m values of 0.1, 0.2 and 0.3 μm .

The obtained M/β_{532} ratios for the mode radii, 0.1, 0.2 and 0.3 μm , are then multiplied with the lidar measured β_{532} values to get the altitude variation of the mass and are integrated between 17 and 30 km (Pinatubo layer). The variation of integrated mass density of the Pinatubo layer for the three mode radii is plotted in Figure 4.27 as a function of days after the eruption. The vertical bars show the variation in the derived mass due to different r_m values assumed. The continuous line is drawn through values corresponding to $r_m = 0.2 \mu\text{m}$ while the top and bottom values correspond to $r_m = 0.3$ and $0.1 \mu\text{m}$, respectively. Further, the obtained integrated aerosol backscattering coefficient for the layer is converted into mass (gm^{-2}) using the conversion table given by Jäger and Hofmann [1991]. The conversion model is based on a number of *in situ* aerosol measurements made during 1980 to 1987 which encompasses the El Chichon eruption. The conversion factors are taken from the table, taking into account the number of days elapsed after the eruption, in our case, the Mt. Pinatubo eruption. The results are shown as dashed line in Figure 4.27. A good agreement is seen with the result (continuous line) obtained from a more elaborate way of calculating the M/β_{532} ratio using Mie scattering theory and using the conversion values of Jäger and Hofmann (dashed line). The interesting feature is that the aerosol mass obtained using the conversion factor agrees better with the mass calculated using a mode radius value of 0.1 μm and also no considerable change is seen in the aerosol size distribution during the decay phase of the aerosol layer. However, there are at least two instances when the values agree better for a mode radius of 0.2 μm , one during May 1992 and the other in March-April 1994.

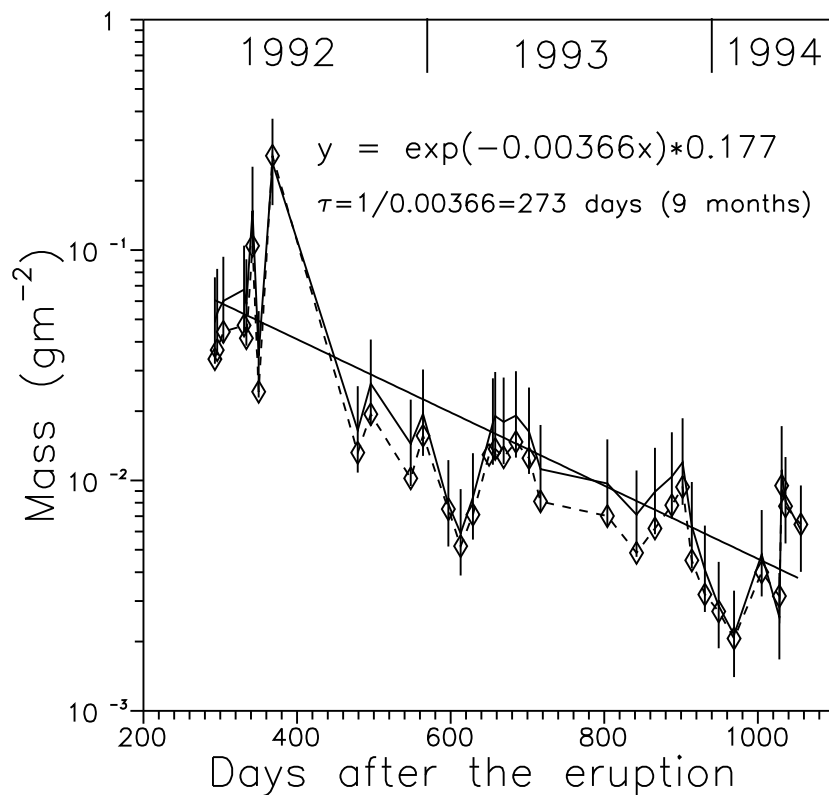


Figure 4.27: Time evolution of Pinatubo aerosol mass (integrated from 17 to 30 km) computed using the backscattering coefficient values. Vertical bars represent the variation in mass due to the r_m values taken as 0.1, 0.2 and 0.3 μm . Dashed line represents the mass value estimated using the conversion factors given by Jäger and Hofmann [1991].

On both the occasions, an increase in mass is also observed indicating a possibility of further input of particles of unknown origin into the stratosphere.

An increase in the aerosol backscatter and mass is seen at times during the decay phase which otherwise is quite smooth and uniform, with no considerable change in the aerosol size distribution. Jäger *et al.* [1995] and Uchino *et al.* [1995] from the results obtained while studying the evolution, spread and decay of Pinatubo aerosols in the northern hemisphere over a period of 3 years from 1991 to 1994 using lidars at Garmisch (47.5°N), Tsukuba (36.1°N) and Naha (26.2°N) have seen similar variations in the stratospheric aerosol optical depth, integrated aerosol backscatter and mass and attributed these seasonal changes to the tropopause height variations and due to the effective transport of aerosols from the equatorial reservoir to midlatitudes with planetary wave activity.

4.7.4 Aerosol mass decay at three stratospheric altitude regions

Aerosol layer mass at three altitude regions, namely, 15 to 20 km, 20 to 25 km and 25 to 30 km, is obtained from the vertical profiles of the integrated aerosol backscattering coefficient values and multiplied with the conversion factors given by *Jäger and Hofmann* [1991]. The monthly mean values for the three layers are shown in Figure 4.28 for the observation period. Exponential best fits are made for the three layers and $1/e$ decay times are estimated as 16.4, 8.8 and 5.4 months, respectively. As expected, the top layer shows a faster decay compared to

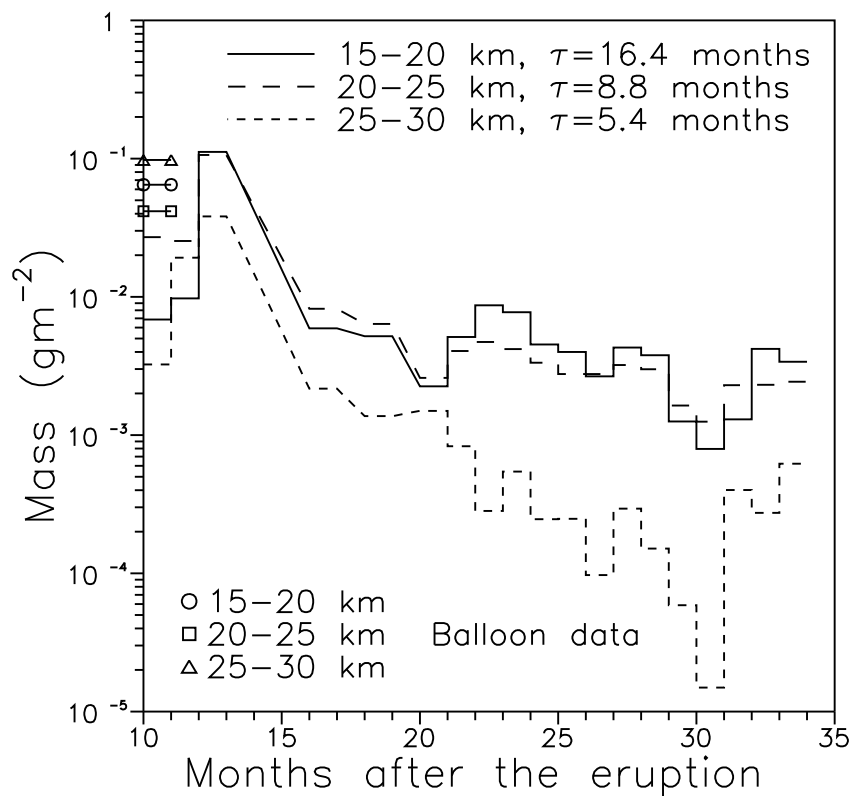


Figure 4.28: Mass of the Pinatubo volcanic aerosol layer estimated for three height regions 15–20 km, 20–25 km and 25–30 km, using the conversion factors given by *Jäger and Hofmann* [1991]. For comparison, masses estimated in the case of a balloon measurement made at Hyderabad (17.5° N) in April 1992 are also shown.

the bottom layers because the settling velocity of aerosols in the micron and submicron size ranges increases with increasing altitudes [*Lamb*, 1970]. It should be noted that the decrease in aerosol mass at a particular altitude layer is both due to removal of particles downward due to gravitational settling and horizontal dispersal to other latitudes. While a detailed dynami-

cal model is necessary to quantify the amount of material displaced by these two processes, qualitatively, the upper layer becomes the source of particles to the lower altitude regions. This further explains the faster decay pattern observed for the top layer, while the bottom two layers not only lose particles due to gravitational settling but also gain particles from the top layer and hence exhibit a slower decay. From April 1992 to February 1993, the 20-25 km layer has the maximum mass of particles. However, after this period the layer has a reduced mass with a subsequent gain in the lower layer, between 15 to 20 km. An increase seen in the aerosol mass in all the three layers about 30 months after the eruption could be due to the influx of particles into the stratosphere from an unknown source. For comparison, the mass of the Pinatubo layer is computed for the balloon-borne optical measurements data obtained over Hyderabad (17.5°N) in April 1992 [Ramachandran *et al.*, 1994b] and are shown for the three layers. The higher mass value obtained over Hyderabad indicates that at lower latitudes the layer has been broader and extends to higher altitudes as discussed earlier and these particles become the source to the higher latitude regions with time.

4.7.5 Peak scattering ratio

Figure 4.29 shows the variation in the peak scattering ratio, with values ranging from about 10 and above during April-May 1992 which declines to about 1.5 during May 1994. An exponential best fit gives a $1/e$ folding time of about 12.5 months, which is higher than a value of 9 months obtained in the case of integrated particulate backscattering or the mass of the layer. Similar differences between the estimated decay times have been observed earlier, both after the Fuego eruption as well as in the case of El Chichon eruption. In the case of Fuego, the $1/e$ folding times for the vertically integrated backscattering coefficient (IBC) and the peak scattering ratio have been 8 and 11 months, respectively [Russell and Hake, 1977]. In the case of El Chichon, the $1/e$ folding time for IBC is reported as 11.5 months [Jäger and Carnuth, 1987]. A value of 15.65 months as $1/e$ folding time was obtained for the peak scattering ratio of the El Chichon layer by plotting the scattering ratio values available in the literature [Hofmann, 1987] corresponding to a period from 200 to 1100 days after the eruption. Sedimentation removes the particles at low altitudes below the aerosol peak more effectively from the layer, while the major contribution to the vertically integrated particulate backscattering comes from these altitudes. Hence the total integrated aerosol backscattering or the mass of the whole layer shows a faster decay time than the decay time shown by the peak scattering ratio value alone. Similar argument has been given by Russell and Hake [1977] in explaining

the observed difference in the two decay times, in the case of Fuego eruption. This has implications in the calculation of the radiative effects of the volcanic aerosols. While for estimating the impact of stratospheric volcanic aerosol on surface temperature, the integrated value of aerosol scattering for the layer is sufficient, for a detailed calculation of the impact at stratospheric altitudes, the altitude variations of the extinction coefficients within the layer should also be taken into account whose decay patterns can be different as shown above.

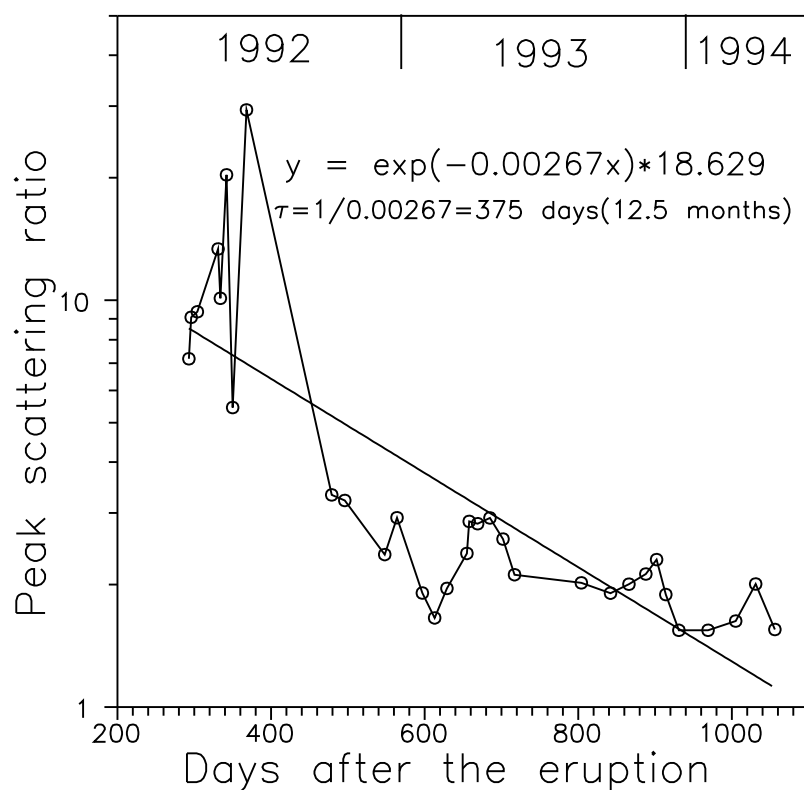


Figure 4.29: Time variation of the peak scattering ratio value from April 1992 to May 1994.

4.7.6 Comparison of results with El Chichon data

Table 4.3 shows a comparison between the mass of the aerosol layer as well as the IBC values obtained by *Jäger and Hofmann* [1991] for the case of El Chichon at 694.3 nm but corrected for 532 nm wavelength [*Jäger*, 1992] and the values obtained in the case of Mt. Pinatubo eruption. In both cases the results are integrated from tropopause +1 km to 30 km. In spite of the large latitudinal difference between the two measurement sites, Garmisch-Partenkirchen (47.5°N) and Ahmedabad (23°N) and a large difference in the quantity of mass injected by the

Table 4.3: *Comparison of the mass of the volcanic aerosol layer and the integrated aerosol backscattering coefficient (IBC) at 532 nm in the case of El Chichon eruption as reported by Jäger and Hofmann [1991] and in the case of Pinatubo eruption, the results of the present study.*

Time after eruption	El Chichon		Mt. Pinatubo	
	Mass (gm^{-2})	IBC (sr^{-1})	Mass (gm^{-2})	IBC (sr^{-1})
1 year	3.75×10^{-2}	2.25×10^{-3}	2.39×10^{-1}	1.17×10^{-2}
2 years	1.25×10^{-2}	6.88×10^{-4}	1.12×10^{-2}	5.50×10^{-4}
1056 days	6.00×10^{-3}	3.13×10^{-4}	6.11×10^{-3}	3.00×10^{-4}

two eruptions, the mass of the aerosol layer and the integrated backscattering coefficients become comparable, about 2 years after the eruption, as also shown by the model studies of *Pinto et al.* [1989].

4.8 Modeling studies of aerosol characteristics

4.8.1 A brief survey of existing aerosol models

Modeling of aerosols can be broadly classified on the basis of aerosol properties which they address to, namely optical and physical. The particle size distribution, shape and composition form usually the core of all serious optical models. These models find their application in the interpretation of data from both satellite and ground based remote optical sensors that monitor aerosols. The aerosol microphysical processes responsible for the formation, evolution, transport and removal of aerosols are the focal point of physical models, which are most often associated with chemical-radiative-dynamical effects. While there have been several attempts on both the fronts, with an emphasis on the global distribution, a recall of some important efforts would be in order, with a note that the focus of majority of these efforts has been on stratospheric aerosols.

Rosen et al. [1978] developed a one-dimensional steady-state i.e. during quiet periods stratospheric aerosol model which included the effects of sedimentation, diffusion, particle growth and coagulation. The results obtained indicated that the model was capable of describing many aspects of the stratospheric aerosol layer, such as the size distribution and the vertical profiles for particles $> 0.3 \mu\text{m}$ diameter. However the model could not incorporate the necessary input parameters to explain for example, the observed condensation nuclei

profiles.

Turco et al. [1979a] developed a time-dependent one-dimensional model, incorporating a wide range of basic physical and chemical processes to describe the stratospheric aerosols. The model could explain most of the observed experimental features regarding stratospheric aerosols such as sulphate mass, large particle ($r > 0.15 \mu\text{m}$) mixing ratio, ratio of particles $> 0.15 \mu\text{m}$ radius to those $\geq 0.25 \mu\text{m}$ radius etc. [*Toon et al.*, 1979] and in detail the sensitivity of the various processes were also discussed. The sensitivity tests and comparisons with observations suggested that coagulation controls the large particle mixing ratio. Some of the unresolved aerosol related problems in this model, included the role of volcanoes and other sulphur sources in maintaining the sulphate aerosol layer.

Capone et al. [1983] developed a two-dimensional model of sulphate photochemistry, transport and aerosol microphysics to study the evolution of El Chichon volcanic aerosols, for a period of 2 years. It was found that the residence time of the aerosol cloud in the stratosphere exceeded 2 years and also the model could reproduce the observed optical depth, lidar backscatter and infrared extinction coefficients if about 10 Mt of SO_2 was injected.

Hofmann and Rosen [1984] studied the stratospheric aerosol size and mass during the first 1.5 years after El Chichon eruption over Laramie and southern Texas ($27\text{--}29^\circ\text{N}$) using balloon-borne particle counters and compared the observations with the theory of particle growth in the stratosphere to characterise the sulphuric acid vapour temporal variations suggested by the data.

More recently, *Tie et al.* [1994] developed a two-dimensional model taking into account the coupling between dynamical, chemical, microphysical processes to simulate the observed results on El Chichon volcanic aerosols. The model could simulate most of the observations like aerosol size distributions, surface area, aerosol mass etc., quantitatively. It was also pointed out that the model substantially underestimated the aerosol load, if only gas phase SO_2 is considered to be ejected out of the eruption and so it was estimated that the direct ejection of sulphate particles is a very important process. The model calculations suggested that approximately 20% of the sulphate aerosols could have been provided by direct injection of aerosols during the eruption while the remaining 80% have been produced by the conversion of gas phase SO_2 . Also using the model developed they have studied the Pinatubo aerosols and their effect on the stratospheric ozone [*Tie et al.*, 1994]. The results showed that the highest surface area was found in the tropical region consistent with the observations. One year after the eruption the volcanic aerosols have been dispersed by transport processes. In Octo-

ber 1991 (4 months after the eruption), the largest amount of aerosol is located in the tropics and midlatitudes between 20 and 30 km. The calculated evolution and distribution of the aerosol surface areas were found to be in reasonable agreement with the observations.

Bekki and Pyle [1994] developed a global two-dimensional chemical-radiative-dynamical model, which contains a detailed treatment of sulphate aerosol microphysics and simulated the formation and temporal evolution of the sulphate aerosol cloud generated by Mt. Pinatubo, in June 1991. Though the model could simulate the observed SO_2 , due to the absence of homogeneous nucleation of aerosols in the model, there were discrepancies in the timing of the peak in aerosol loading and the magnitude of the surface area density, which made them to suggest that homogeneous nucleation plays an important role in the early stages of volcanic eruption in determining the average size of the volcanic sulphate particles and their residence times in the atmosphere. Also, the modeled aerosol layer had still not recovered to its background level 2 years after the eruption.

Pudykiewicz and Dastoor [1995] numerically simulated the global distribution of sulphate aerosol produced after a major volcanic eruption using a dynamic model and applied those results to Pinatubo eruption. Verification of results showed that the numerical model reproduced accurately the global distribution of sulphates and the aerosol optical depths derived for an eruption of magnitude Mt. Pinatubo matched well with experimentally observed results.

Recently *Zhao et al.* [1995] simulated the evolution of Pinatubo volcanic aerosols in the stratosphere and used the model to study the chemical, microphysical and radiative properties of volcanic aerosols. The model reproduced reasonably well the basic aerosol properties such as size distribution, total mass and concentration, temporal and altitude variation and radiative properties.

On the optical side, emphasis was given to the development of models based on a size distribution which will comply with direct measurements. *Pinnick et al.* [1976] proposed a simple exponential and lognormal size distribution function based on a large data base of directly measured submicrometer size aerosol. The model was utilised to compare particle concentration measurements observed with lidar backscattering. It was also used to estimate the dependence of aerosol extinction and backscatter on wavelength and to calculate the planetary albedo of stratospheric aerosols.

Toon and Pollack [1976] proposed a global stratospheric aerosol model based on a zero order logarithmic distribution (ZOLD) function, which is equivalent to a lognormal distribu-

tion, index of refraction and total optical depth consistent with several observations available then. The model was used in radiative transfer calculations to study long term climatic effects. Also for the first time, an attempt was made to model a volcanically perturbed stratosphere due to Agung eruption, with the data available at 20 km of *Mossop* [1964] and it was suggested that even under highly perturbed conditions the stratospheric sulphate aerosol size distribution may be similar to the ZOLD function proposed in the model. As tropospheric aerosols are composed of many diverse substances and as their sources and sinks are distributed nonuniformly in space and time, the tropospheric aerosol component is quite variable in addition to being complex. As only a few useful measurements of total aerosol optical depth were available then, it became a difficult task to model the tropospheric aerosols, even at one location, let alone globally, as the greatest restriction placed on the available data was temporal and geographical averaging and with all the variations observed in tropospheric aerosols, this assumption of averaging becomes meaningless, though an attempt was made by *Toon and Pollack* [1976].

There was an effort by *Russell et al.* [1981] to utilise all the existing aerosol size distributions in one unified approach. The optical model demonstrated the ability of deriving profiles of aerosol number density, extinction and backscatter obtained from satellites, lidars and dustsondes, during two extensive field measurements [*Russell et al.*, 1981, 1984].

Rosen and Hofmann [1986] developed a stratospheric optical model for direct measurements from dustsondes for the altitude range above the tropopause to 30 km, for an observation period covering both background and volcanically perturbed situations, for the midlatitudes. The proposed model could explain most of the experimental features on the aerosol number density, lidar backscatter and optical depth.

Jäger and Hofmann [1991] proposed an optical model for midlatitudes based on balloon-borne particle counter data from Laramie, Wyoming (41°N) and lidar backscatter data from Garmisch-Partenkirchen (47.5°N) obtained during the 1980-1987 period. The model essentially gave factors for conversion from aerosol backscatter to mass, area and extinction for the altitude range of 15 to 30 km, for three wavelengths 532, 694 and 1064 nm and two refractive indices 1.44/1.45. These conversion factors when applied to the lidar data of Garmisch gave very good results on optical depth, mass and area.

A global climatology of stratospheric aerosols was created by using SAM, SAGE I and SAGE II observations for about a decade by *Hitchman et al.* [1994] for the first time providing a global view of the long term average aerosol distributions on decadal, quasi-biennial and

seasonal timescales. The role of quasi-biennial oscillation on the stratospheric aerosols was discussed in detail and the dynamical effects of the aerosol distributions were attempted.

d'Almeida et al. [1991] from the data available on tropospheric aerosols constructed a global optical aerosol climatology model for a wide variety of aerosols ranging from Saharan dust to Antarctic. A wide variety of aerosol optical parameters including extinction, scattering, absorption, phase function, asymmetry factor and single scattering albedo for a large wavelength range from 0.3 to 40 μm and the variation of these parameters with relative humidity and their implications were discussed in detail.

4.8.2 Aerosol microphysical processes responsible for the formation and decay of stratospheric aerosol layer

The aerosol continuity equation can be written as

$$\frac{\partial n}{\partial t} = \left(\frac{\partial n}{\partial t} \right)_{\text{nuc}} + \left(\frac{\partial n}{\partial t} \right)_{\text{growth, evap.}} + \left(\frac{\partial n}{\partial t} \right)_{\text{coa.}} + \left(\frac{\partial n}{\partial t} \right)_{\text{sed.}} + \left(\frac{\partial n}{\partial t} \right)_{\text{diff.}} + \left(\frac{\partial n}{\partial t} \right)_{\text{washout}} \quad (4.24)$$

where the various terms refer to the rate of change of aerosol concentration due to processes such as nucleation, growth or evaporation, coagulation, sedimentation, diffusion and washout.

Nucleation refers to the formation of a new stable solid or liquid particle from a gas phase consisting of either gaseous species only (*homogeneous, homomolecular nucleation*) or involving two or more gaseous species, one of which most commonly is water (*homogeneous, heteromolecular nucleation*) or when two or more gaseous species condense onto preexisting particles (*heterogeneous, heteromolecular nucleation*) [*Hamill et al.*, 1977a]. The nucleation lifetime is of the order of a few days [*Turco et al.*, 1979a]. Immediately after the El Chichon as well as Mt. Pinatubo eruptions, high concentrations of aerosol droplets were observed suggesting that homogeneous nucleation is the most likely production mechanism of aerosols at the stratospheric altitudes [*Hofmann and Rosen*, 1983; *Deshler et al.*, 1992].

After nucleation the sulphuric acid-water solution droplets can grow by heteromolecular condensation of H_2SO_4 and H_2O vapours. At a given temperature, the water vapour equilibrium uniquely determines the weight percentage of H_2SO_4 in the solution and consequently the H_2SO_4 vapour pressure over the droplet. Accordingly, on the basis of H_2SO_4 vapour pressure, some of the sulphuric acid molecules incident on the droplet are absorbed or could be evaporated from the existing droplet [*Turco et al.*, 1979a].

Under stratospheric conditions, Brownian coagulation, which occurs when particles impinge during random thermal motions is important [*Turco et al.*, 1982]. The rate of change of

concentration of particles of radius r due to coagulation can be expressed as the difference between two integrals over the particle size distribution: one integral represents the production rate of particles of size r by the coagulation of two smaller particles and the second integral represents the loss rate of particles of size r by coagulation with all other particles. The coagulation integrals are calculated from *Turco et al.* [1979b]. The coagulation kernels for each pair of particles, is calculated based on *Fuchs* [1964] and *Hamill et al.* [1977b]. In our model, we have adopted a discrete formulation of the particle size distribution. In this formulation, coagulation is considered as an interaction process between pairs of particles whose sizes are limited to a finite set of discrete values. *Turco et al.* [1979b] state that even the continuous particle size distribution yields the same results for the average rates of particle coagulation, but the discrete formulation is much simpler to use.

The dynamical or transport (removal) mechanisms are diffusion (horizontal dilution i.e. spreading of aerosols to other latitudes and vertical diffusion) and gravitational sedimentation. When the aerosols grow to a few micron size, gravitational sedimentation, in which particles fall with respect to the air surrounding them and are returned to the troposphere, becomes important. The equation for settling velocity is given as

$$v_s = \frac{2\rho r^2 g}{9\eta} [1 + (\lambda/r)(A + B \exp\{-Cr/\lambda\})] \quad (4.25)$$

where ρ is the mass density of aerosols (1.65 g cm^{-3} for 75% H_2SO_4 droplets), g is the gravitational acceleration, λ is the mean free path and A , B and C are constants whose values are 1.249, 0.42 and 0.87, respectively [*Kasten*, 1968]. Using the above equation it is estimated that a particle of radius $1 \text{ }\mu\text{m}$ will fall from 20 to 10 km in less than a year but a $0.1 \text{ }\mu\text{m}$ particle will take about 10 years to fall the same distance. Therefore gravitational sedimentation is a significant removal mechanism for particles with radius $\geq 1 \text{ }\mu\text{m}$ and this accounts for the fact that the fraction of particles $\geq 1 \text{ }\mu\text{m}$ is smaller in the stratosphere than in the troposphere. Gravitational sedimentation is not a significant removal process for particles in the size range $\leq 0.1 \text{ }\mu\text{m}$ [*Hamill et al.*, 1977b].

4.9 A time dependent stratospheric aerosol layer model: Present work

In order to understand better the relative roles of the aerosol microphysical processes in influencing the stratospheric aerosol layer formation and decay, a simple model has been de-

veloped, taking into account the aerosol microphysical processes such as growth, coagulation and sedimentation, to explain the time evolution of the Pinatubo layer (17 to 30 km) and the results obtained have been compared with that of balloon and lidar measurements, as well as with the data for El Chichon available in literature.

4.9.1 Model specifications

As homogeneous-heteromolecular nucleation and heterogeneous-heteromolecular nucleation are the most important production mechanisms of aerosols only in the initial stages of volcanic eruption and also as the nucleation life time is of the order of a day (the process is almost instantaneous), the process of nucleation is not included in the model. *Hamill et al.* [1977a] showed through model calculations that the heterogeneous-heteromolecular nucleation rate is generally many orders of magnitude higher than the nucleation rate for any competing process. An analysis of the volcanic particles suggested that large numbers of sulphate particles have been formed by homogeneous nucleation in the early stages of Pinatubo volcanic eruption [*Sheridan et al.*, 1992; *Deshler et al.*, 1992]. Recent model studies of Pinatubo aerosol layer evolution by *Zhao et al.* [1995] showed that the new particle formation by homogeneous nucleation almost ceases in about a month after eruption. The enormous amount of SO_2 injected gets rapidly converted into H_2SO_4 in about 30 days, which is the chemical conversion time and the H_2SO_4 vapour thus formed build up very quickly to levels sufficient for homogeneous nucleation to occur. This chemical oxidation of SO_2 into H_2SO_4 is crucial for aerosol formation and evolution and the conversion rate is controlled by OH concentration. The H_2SO_4 vapour thus formed results in the nucleation of new particles followed by co-condensation with water to form the observed aerosol. *Winker and Osborn* [1992] estimate that one month after the eruption of Mount Pinatubo, about half the SO_2 had been converted into sulphate aerosols. Both experimental (TOMS [*Bluth et al.*, 1992] and MLS [*Read et al.*, 1993]) observations and model calculations [*Bekki and Pyle*, 1994] show that more than 90% of the conversion of SO_2 to sulphate aerosols was complete within 3 months after the Pinatubo eruption. In the case of El Chichon, the characteristic aerosol growth time was about 45 days [*Hofmann*, 1987].

Hence, in these calculations an aerosol size distribution is chosen which starts from $t + 45$ days and not at $t = 0$. Also, the process of aerosol evaporation due to the negative growth rate is not included. Average growth rates of aerosols for the altitude region of 20-30 km are taken from *Hofmann and Rosen* [1984] for a sulphuric acid concentration of 10^7 cm^{-3} (estimated

after 40 days of El Chichon eruption) and a water vapour mixing ratio of 3 ppmv.

In general, the sedimentation flux is calculated as

$$\left(\frac{\partial n}{\partial t} \right)_{\text{sed.}} = - \frac{\partial}{\partial z} (-v_s n) \quad (4.26)$$

where v_s is the settling velocity (cm s^{-1}) and n is the aerosol number density (cm^{-3}).

In the case of a layer (17-30 km), the total number of particles, n can be assumed to be distributed throughout the 13 (30–17) km regime of the stratosphere and hence the sedimentation flux becomes

$$\left(\frac{\partial n}{\partial t} \right)_{\text{sed.}} = \frac{(-v_s n)}{13} \quad (4.27)$$

A bimodal lognormal aerosol size distribution signifying an eruption of magnitude of El Chichon or Pinatubo with $r_1 = 0.02 \mu\text{m}$, $\sigma_1 = 2.2$, $N_1 = 5000 \text{ cm}^{-3}$ and $r_2 = 0.7 \mu\text{m}$, $\sigma_2 = 1.6$, $N_2 = 50 \text{ cm}^{-3}$, after 45 days of eruption, is taken as the initial boundary case (Model 2). Model 1 has a higher aerosol concentration by a factor of 10 when compared to Model 2 and Model 3 is lower by a factor of 10, while the mode radii and sigma are unchanged. This size distribution is taken, based on the optical particle counter data of stratospheric aerosols following El Chichon volcanic eruption by *Hofmann* [1988] and Mt. Pinatubo eruption by *Deshler et al.* [1993]. 15 size bins which cover the aerosols in the radius range of $0.01 \mu\text{m}$ to $15 \mu\text{m}$ are considered. The initial size distribution ($t + 45$ days) is made to undergo the physical processes of growth, coagulation and sedimentation and the evolution of the final size distribution after $t + 2$ months, $t + 3$ months, $t + 6$ months, $t + 1$ year, $t + 1.5$ years, $t + 1.8$ years, $t + 2$ years and $t + 3$ years is considered for the present study. In the current model no inflow of aerosols from the lower and upper altitudes i.e. from below 17 km and above 30 km is considered and hence an average aerosol size distribution representing the volcanically perturbed case in the stratosphere is taken. The initial size distribution ($t + 45$ days) has apart from the volcanically produced bimodal size distribution, embedded in it the background aerosol size distribution. The aerosol continuity equation in addition to the terms for growth, coagulation and sedimentation, has a contribution of aerosols from the background conditions, which is referred to as C here. Hence the equation becomes

$$\frac{\partial n}{\partial t} = \left(\frac{\partial n}{\partial t} \right)_{\text{growth}} + \left(\frac{\partial n}{\partial t} \right)_{\text{coa.}} + \left(\frac{\partial n}{\partial t} \right)_{\text{sed.}} + C \quad (4.28)$$

If the number density n becomes equal to the background aerosol size distribution which is in an equilibrium condition i.e. $n = n_{\text{eq}}$ then

$$\frac{\partial n}{\partial t} = \frac{\partial n_{eq}}{\partial t} \quad (4.29)$$

Therefore the contribution from the background, equilibrium condition C becomes

$$C = \left(\frac{\partial n_{eq}}{\partial t} - \frac{\partial n}{\partial t} \right)_{\text{growth}} - \left(\frac{\partial n}{\partial t} \right)_{\text{coa.}} - \left(\frac{\partial n}{\partial t} \right)_{\text{sed.}} \quad (4.30)$$

This contribution C is subtracted from the volcanic aerosol size distribution at each time step and hence, the volcanic stratospheric aerosol size distribution is corrected for the background, equilibrium aerosol size distribution, in this manner.

The horizontal and vertical diffusion of aerosols have not been considered due to the following reasons: lack of data on wind speed and movement of aerosols to other latitudes and as altitudinal dispersion of aerosols is not considered. Only gravitational settling of aerosols out of one vertical bin (17-30 km), which becomes the important and dominant removal mechanism for large aerosols, is considered here.

Since, washout is effective only below tropopause, it is not included in the model.

Figure 4.30 shows the evolution of volcanic aerosol size distribution after background corrections. Results corresponding to Model 2 aerosol size distribution are shown as an example. About 2 months after the eruption, the primary mode in the bimodal lognormal distribution grows to an average size of $0.08 \mu\text{m}$ and also the secondary mode is not prominent. About 3 months after the eruption the total number of particles starts to decay as a result of growth, coagulation and sedimentation. Aerosols in the size range $0.2\text{-}1 \mu\text{m}$ continue to grow through coagulation process, even for about an year or so, making the secondary mode to shift to a higher radius of about $1\text{-}2 \mu\text{m}$, with a subsequent reduction in the total number density. It is clearly seen, that as gravitational sedimentation is a very effective removal mechanism for larger aerosols in the range of a few microns, their removal rate is faster and in about 2-3 years, the size distribution returns to the background aerosol size distribution. Similar features of the evolved size distribution have been observed by *Tie et al.* [1994] while studying the El Chichon eruption over the equator as well as at midlatitudes.

4.9.2 Results and Discussion

The evolved size distributions are used to calculate the aerosol extinction coefficient at 500 nm (75% H_2SO_4 droplets, $m = 1.431 - i1 \times 10^{-8}$) and then integrated for the whole layer, to study the time evolution of the optical depth of the Pinatubo layer.

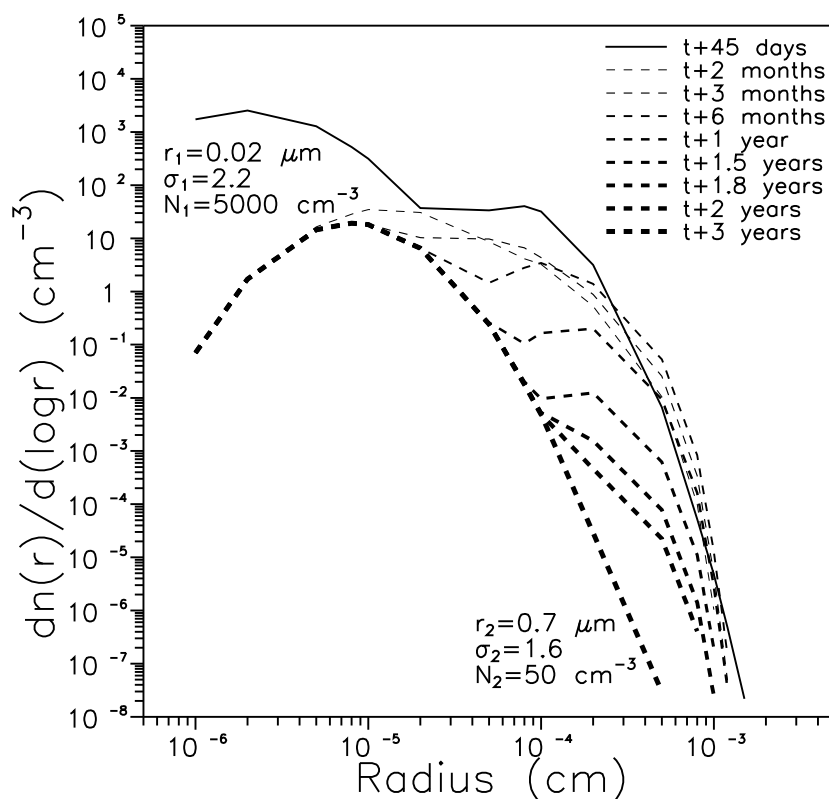


Figure 4.30: The final evolved size distributions after they have undergone the aerosol micro-physical processes of growth, coagulation and sedimentation and after applying background corrections. Model 2 size distribution is shown here as an example.

The percentage contribution of the different physical processes considered in the model namely growth, coagulation and sedimentation to the evolution of the aerosol size distribution show that coagulation dominates immediately after the eruption to about 150 days, whereafter growth and sedimentation become dominant (Figure 4.31). While condensational growth aids in producing larger particles, gravitational sedimentation becomes an effective removal mechanism for larger particles. Though the results shown are representative of Model 2 size distribution, they are found to be more or less similar for other size distributions also.

Sensitivity studies conducted by changing the growth rates and coagulation kernels by $\pm 10\%$ indicate that the percentage change in the calculated aerosol optical depth steadily increases from about $\pm 2\%$ to about $\pm 20\%$ in the case of growth rate, while due to coagulation, the change increases from about $\pm 0.5\%$ to about $\pm 8\%$, for a period corresponding from $t + 2$ months to $t + 14$ months (Figure 4.32). Afterwards, the percentage change in optical depth de-

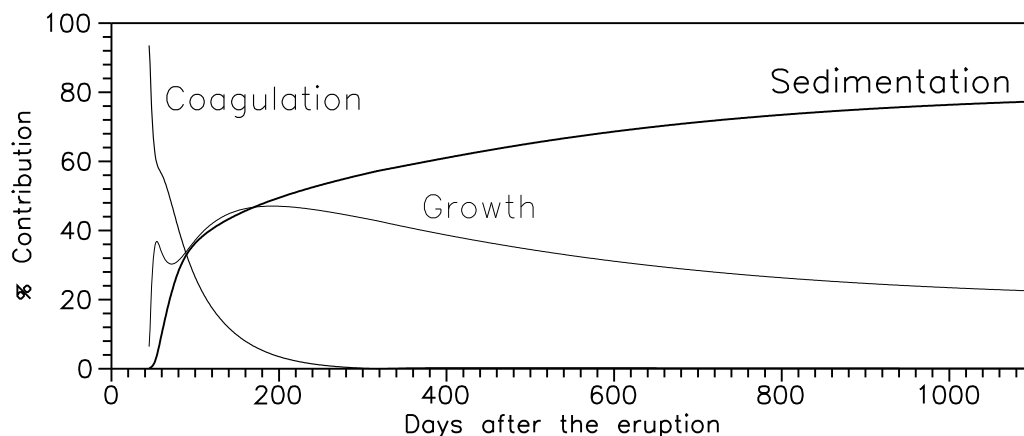


Figure 4.31: *Percentage contribution of the different physical processes to the evolution of aerosol size distribution at different times after a volcanic eruption.*

creases and becomes less than $\pm 1\%$ in about 2 years, indicating that the processes of growth and coagulation are important, in the first year of the eruption in maintaining the aerosol layer, whereafter when the particles grow sufficiently larger, of the order of a few microns, sedimentation becomes important. These results obtained with a change in the growth rates and coagulation kernels are in gross agreement with the results obtained from the percentage contribution calculations.

Figure 4.33a shows the aerosol optical depth obtained for the three model size distributions. The values decrease by about 5 to 9%, when calculated for 532 nm. Though in the initial stages of the eruption, eruptions of widely varying magnitudes, corresponding to the three model size distributions, used here, exhibit large differences in the optical depths, but after about 2 years, they are almost the same. The comparison of the model results with the experimental observations are done in 4.33b for both Pinatubo and El Chichon volcanic eruptions. The fact that nucleation and diffusion of aerosols have not been included in the model should be borne in mind while interpreting the results obtained. The October 1991 balloon data, measured 4 months after the Pinatubo eruption, lies very close to the third model and the April 1992 balloon data, measured 10 months after the eruption, lies close to the first model, indicating that the particles were still growing and coagulating to produce larger par-

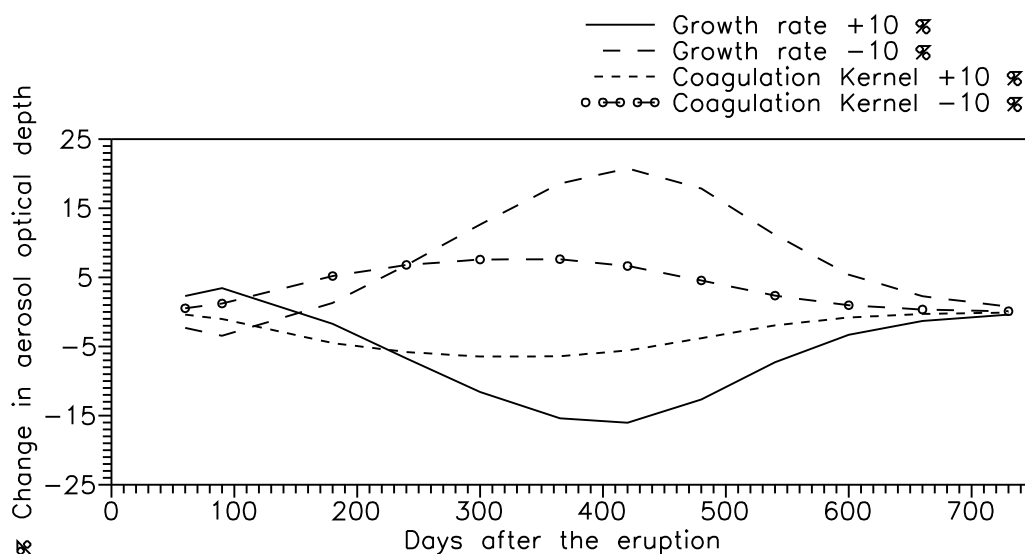


Figure 4.32: Results of sensitivity studies conducted by changing the growth rate and coagulation kernels by $\pm 10\%$.

ticles. The size parameter ν obtained during April 1992, indicates formation of larger particles at higher altitudes (25-30 km) by coagulation with a subsequent reduction in the total number density [Ramachandran *et al.*, 1994b]. The lidar optical depth values derived by multiplying the aerosol backscattering coefficient with an altitude independent value of 50 sr and then integrated for the layer (17-30 km) also exhibit a close correlation with all the models, in various stages.

The stratospheric aerosol optical depths obtained in the case of El Chichon by Jäger *et al.* [1988] and Robinson and DeFoor [1988] using lidars are included here to test the applicability of the model, in explaining the evolution of the aerosol layer formed after a major volcanic eruption. It is seen that the model reproduces the data obtained in both the cases. Though the model does not take into account the latitudinal dependence, as only conditions over tropics are considered, the data obtained by Jäger *et al.* [1988] in Garmisch-Partenkirchen at 47.5°N clearly shows that in the initial stages of the El Chichon aerosol layer, about an year or so, the optical depth obtained for the layer is much less when compared to the Mauna Loa (19.53°N) data of Robinson and DeFoor [1988]. In both the cases, the data obtained at 694 nm is wavelength corrected, for 532 nm using the values given by Jäger [1992]. In case of Mauna Loa data, the NonRayleigh BackScatter obtained for the stratospheric aerosol layer

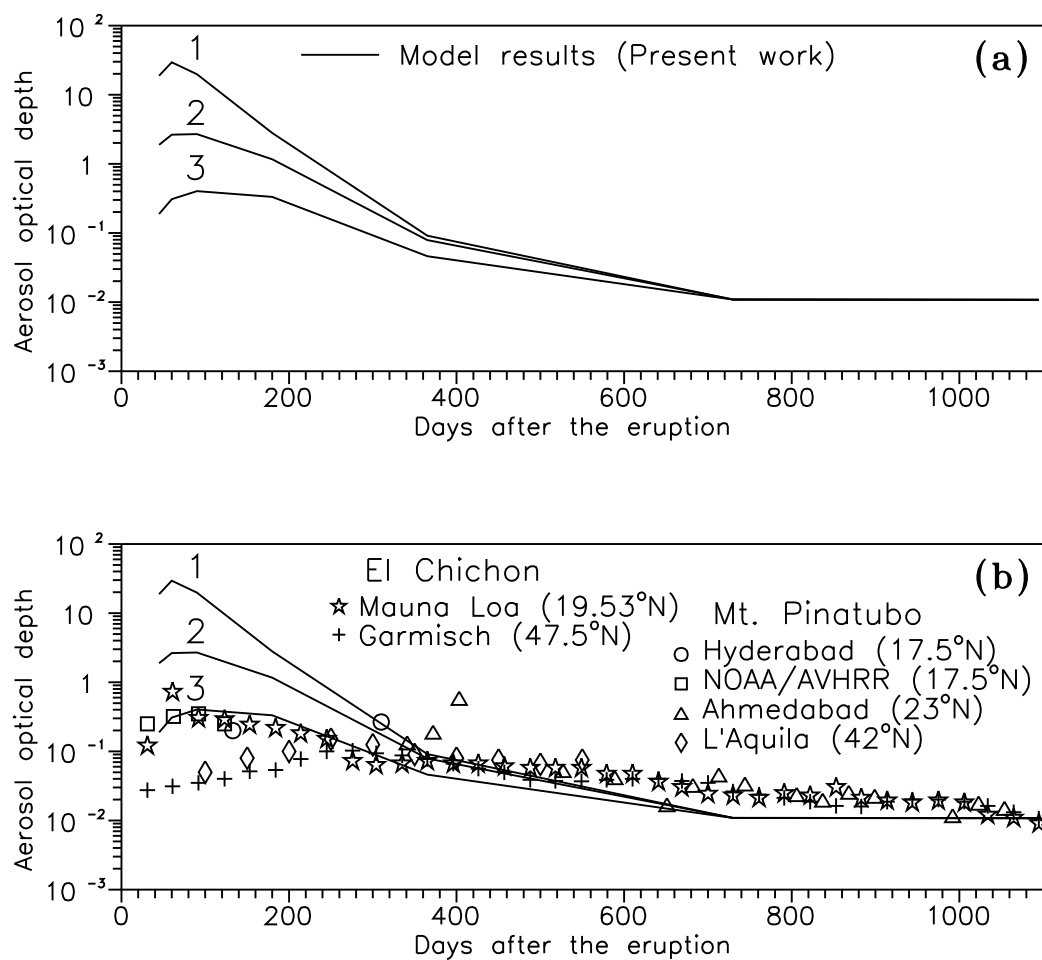


Figure 4.33: (a) The aerosol optical depths calculated for 500 nm for the three model aerosol size distributions used. (b) The aerosol optical depths obtained in the case of Pinatubo and El Chichon volcanic eruptions, using balloons, lidars and satellite are compared with the model results. See text for more details.

is multiplied by 50, to get the optical depth and then wavelength corrected. It is interesting to note that the same feature of latitudinal dependence is repeated in the case of Pinatubo eruption. The stratospheric aerosol optical depth (15-30 km) at L'Aquila (42°N), Italy obtained by *D'Altorio et al.* [1993] using DIAL measurements at 589 nm reproduces the same feature of the latitudinal dependence in the initial stages of the eruption. This feature was observed by using balloon-borne Sun-tracking photometers over Hyderabad during October 1991 and April 1992, about 4 and 10 months after Pinatubo eruption, where a systematic increase in the aerosol extinction coefficients was seen above 24 km with decreasing latitude, indicating that the upper edge of the layer extends to higher altitudes in the equatorial region [*Ramachandran et al.*, 1994b]. This feature is expected, as both El Chichon and Pinatubo, are in tropical latitudes and also for the first few months after the eruption, bulk of the aerosol cloud lay in the tropics [*Hofmann*, 1987; *Trepte et al.*, 1993] which were then carried to the higher latitudes. The aerosol optical depths obtained at 500 nm for Pinatubo layer using NOAA/AVHRR satellite data [*Minnis et al.*, 1993] at 17.5°N match very closely with Model 3. The NOAA/AVHRR data could be obtained only for the first 4 months after the Pinatubo eruption. In all the above results, only the monthly mean values are plotted. *Bekki and Pyle* [1994] using a global two-dimensional chemical-radiative-dynamical model, simulated the formation and temporal evolution of Pinatubo layer. Due to the absence of homogeneous nucleation of aerosols in the model, there were discrepancies in the timing of the peak in aerosol loading and the magnitude of surface area density, which made them to suggest that homogeneous nucleation plays an important role in the early stages of the volcanic eruption in determining the average size of the volcanic sulphate particles and their residence times in the atmosphere.

The decay of both the El Chichon and Pinatubo aerosol layers in about 3 years to values very close to background level, shows that though the mass injected by Pinatubo was more than 2 times as compared to El Chichon, faster growth rate and coagulation resulted in larger particles and due to faster removal rate, by sedimentation, the residual aerosol masses and hence the aerosol optical depths and the decay rates can remain the same (Table 4.3). This feature was also seen by *Pinto et al.* [1989] who through model calculations showed that when the mass of SO₂ injected increases beyond 10 Mt, the aerosol microphysical processes of condensation and coagulation produce larger particles, as the SO₂ injection rate is increased rather than a larger number of particles of the same size, due to which the size of sulphate aerosol increases and the removal rate accelerates. Consequently, the residual sul-

phate masses could be quite similar after about 2 years for eruptions of wide range of magnitudes, suggesting that volcanic effects may be self-limiting. Recently *Rosen et al.* [1994] from conjugate *in situ* observations of the stratospheric aerosol following Pinatubo eruption over Laramie, Wyoming (41°N) and Lauder (45°S), New Zealand, using balloonborne backscatter-sondes, showed that similar aerosol loading and decay rates occurred over both midlatitude stations. A comparison of the results obtained on El Chichon over Laramie indicated higher mixing ratios in the case of Pinatubo but very similar decay rates for both the eruptions.

When the models used were fitted with an exponential curve to study the $1/e$ folding times, they were found to be 4.1 months (Model 1), 5.6 months (Model 2) and 9 months (Model 3), showing that eruption of higher magnitude produces larger particles to give a faster decay time. This was experimentally verified by fitting an exponential fit to the Mauna Loa data, which gave a $1/e$ folding time of 11 months, for the El Chichon aerosol layer. For Pinatubo, an eruption which ejected 2 to 3 times more material into the stratosphere compared to El Chichon, a faster $1/e$ folding time of about 9 months, was found.

Some differences between the model and experimental results, could have been due to the assumption of average conditions, inside the layer, whereas it has been found using lidar data that the decay pattern can be different in different altitude regions [*Jayaraman et al.*, 1995b] as has been shown earlier. The integrated aerosol extinction coefficient obtained from lidar for three altitude regimes, namely, 15-20 km, 20-25 km and 25-30 km give $1/e$ folding times of 16.4, 8.8 and 5.4 months, respectively. It should be noted that the decrease in aerosol extinction coefficient at a particular altitude layer is both due to removal of particles downward due to gravitational settling and horizontal dispersion to other latitudes. Also, the lower layers have a slower decay pattern compared to the top layer, because they not only lose particles due to gravitational settling but also gain particles from above. Recent model studies of *Zhao et al.* [1995] indicate that the aerosol optical depth at 500 nm at different altitudes in the stratosphere can be different and hence an average picture for the stratosphere is not sufficient to explain the evolution.

Chapter 5

Summary and Scope for future work

This chapter holds in it the summary of the thesis with emphasis on the important results obtained. Suggestions for where work in the future direction should lead to, as an extension of the present work are also enlisted.

5.1 Summary of results obtained

5.1.1 Tropospheric aerosols

An automatic Sun-tracking photometer was developed and used to measure the columnar aerosol optical depths over Ahmedabad. Aerosol optical depths are found to exhibit diurnal, day to day and seasonal variations. Also, an increase in the values from January to May are found, indicating that the increase in surface temperature and winds induce more soil derived particles into the atmosphere. Results show that there are no appreciable changes in the aerosol optical depths which could be attributed to the Gulf oil fires indicating that the natural sources of aerosols over Ahmedabad, mainly wind blown dust dominated over the oil fire effluents. Other results [*Browning et al.*, 1991; *Bakan et al.*, 1991] using model calculations predicted that most of the smoke from the oil fires in Kuwait would remain in the lowest few kilometres of the troposphere. Airborne observations by *Johnson et al.* [1991] also confirmed the above findings. *Johnson et al.* [1991] concluded that although the effects may be significant on a regional scale, those on global scale including the Asian summer monsoon are likely to be insignificant. Also, according to *Bakan et al.* [1991] there was no indication of a weakening of the Indian summer monsoon. However, the spectral dependences show that the aerosol size distribution changed from bimodal in 1991 to monomodal in 1992, indicating that there are two sources (smoke particles from oil fires and local wind derived min-

eral particles) in 1991 when compared to one dominating source (wind blown dust) in 1992. Though the 1992 data are influenced by the Mt. Pinatubo volcanic eruption in June 1991, the aged volcanic aerosols are found to exhibit a monomodal size distribution with mode radius around $0.6 \mu\text{m}$ [Asano *et al.*, 1993], which could have been superimposed on the derived total columnar aerosol size distribution, with mode radius around $0.5 \mu\text{m}$ in the present work. The ozone column density values from Sun photometry measurements are consistently lower than the Dobson spectrophotometer values, by about 40-50 Dobson units. This observed difference could be due to the effects of high aerosol optical depths and their diurnal variations found over Ahmedabad. Hence, reliable estimation of ozone column amounts from UV extinction measurements is possible only in locations of low turbidity, unlike Ahmedabad. The increase in aerosol optical depth with decreasing relative humidity and increasing temperature, confirms that the increase in surface temperature reduces the soil moisture content, thus inducing more soil derived particles into the atmosphere. Secondly, since aerosols over Ahmedabad are mainly mineral, local wind derived particles which are nonhygroscopic, the aerosol optical depth is not directly related to relative humidity, unlike at a coastal station where the aerosol optical depth increases with an increase in relative humidity, because of the hygroscopic nature of maritime particles.

5.1.2 Stratospheric aerosols

a) Balloon-borne optical studies of Pinatubo aerosol layer over Hyderabad

An analysis of the direct and scattered radiation intensity measurements made over Hyderabad using Sun-tracking and Sun-scanning photometer systems onboard the balloons during October 1991 and April 1992 indicates a dense Pinatubo volcanic aerosol layer between 16 and 30 km. The aerosol extinction coefficients and number density values over Hyderabad are found to be the highest ever obtained during a decade of stratospheric aerosol measurements. The aerosol extinction coefficients obtained in 1991 and 1992 at all wavelengths are about 2 orders higher in magnitude at the peak altitude when compared with that of 1985 (background, volcanically quiescent) values over Hyderabad. The recent results showing the highest values ever obtained over the same site indicate the magnitude of Pinatubo eruption which is the strongest eruption in this century. The aerosol size distribution parameter derived from the scattered radiation intensities also shows layered structures. About 4 months after the eruption, in October 1991, the region between 17 and 23 km, is found to have ν values around 1.8, indicating the presence of larger aerosol particles. The size parameter ob-

tained during April 1992, about 10 months after the eruption, indicates formation of larger aerosols at higher altitudes by coagulation with a subsequent reduction in the aerosol number density. The aerosol layer peak was found to occur at 23 km in October 1991 with about 40 particles per cm^3 . In April 1992 the aerosol number densities have shown a decline, with a peak aerosol number density of about 20 particles per cm^3 at an altitude of about 20 km. Also, the October 1991 measurement revealed the existence of larger aerosol particles in the 17 and 26 km altitude range, with a mode radius of 0.2-0.3 μm , formed due to coagulation of sulphate aerosols. The derived asymmetry factor g also revealed the existence of larger particles which are qualitatively in agreement with the results on the size distribution parameter ν , the slope of Junge power law. The computed mass of the Pinatubo layer in October 1991, after 4 months of the eruption, is about 0.053 gm^{-2} , which is 3.75 times higher than the earlier reported value for El Chichon layer, at the same time of evolution. The obtained aerosol extinction profiles are found to agree well with that of an independent lidar measurement made over Ahmedabad and with SAGE II results.

b) Lidar studies of Pinatubo aerosol layer over Ahmedabad

A state-of-the-art Nd:YAG lidar commissioned in Ahmedabad (23°N) during April 1992 operating at 532 nm was employed to study the Pinatubo volcanic aerosol layer and its decay. 36 vertical profiles of scattering ratio obtained during April 1992 to May 1994, a period corresponding to 10 months after the Pinatubo eruption to about 3 years, every fortnight, have been used for the study. The volcanic aerosol layer is seen very prominently as an increase in the scattering ratios from about 17 km (1 km above the local tropopause) to about 30 km. Also, the scattering ratios which were about 10 during April-May 1992 have become about 1.5 in May 1994. The results obtained on the integrated mass densities and aerosol backscatter from 17 to 30 km give a $1/e$ folding time of 9 months, assuming a typical mode radius of aerosols to be in the range of 0.1 to 0.3 μm . Calculations show that if the layer decays at the same rate, then it may take about 4.5 years to attain the background aerosol backscattering coefficient for the tropical region. However, the peak scattering ratio value shows a longer decay time of 12.5 months as has been reported earlier in the case of Fuego and El Chichon eruptions. As the removal mechanisms of aerosol are faster below the peak, the integrated aerosol mass for the whole layer shows a faster decay than the decay time shown by the peak value alone. The average aerosol size distribution for the layer has not undergone any considerable change during the decay phase from 1 year after the eruption to about 3 years. After about 2 years,

the integrated mass and the backscattering coefficient in the case of Mt. Pinatubo are found to be in the same range as that of the El Chichon reported by *Jäger and Hofmann* [1991], as also shown by the model studies of *Pinto et al.* [1989] that the residual aerosol masses at stratospheric altitudes become comparable after about 2 years for eruptions of wide range of magnitudes.

c) Modeling studies of Pinatubo aerosol layer

Earlier results using balloon-borne Sun-tracking photometers for the El Chichon layer over Hyderabad, showed that the layer produced after the eruption decayed in about 3 years over the tropics [*Jayaraman*, 1991]. Since Mt. Pinatubo had injected as much as 2 to 3 times the material compared to El Chichon, it was not clear whether the lifetime of these aerosols will also be longer because of the larger number density of aerosols or, perhaps, the physical processes such as growth, coagulation and sedimentation will take place at a much faster rate to give more or less the same decay time and whether the residual aerosol masses would be similar, as shown through model calculations [*Pinto et al.*, 1989].

To understand better the relative roles of these processes in influencing the formation and decay of the stratospheric aerosol layer after major volcanic eruptions, a simple model was developed to study the time evolution of a volcanic aerosol layer (17-30 km) and aerosol size distribution using the microphysical processes of growth, coagulation and sedimentation. The results show that the Pinatubo aerosol layer has decayed to the background aerosol level in about 3 years, over the tropics. The experimental lidar data obtained continuously on the Pinatubo layer also gives this result. The latitudinal dependence of the aerosol layer is important only in the first few months after the eruption, as later on, low latitudes become the source of aerosols to higher latitudes. The data obtained in the case of El Chichon shows that the layer decayed in about 3 years. The latitudinal dependence in the case of El Chichon also is clearly seen only in the first few months after the eruption.

d) Conclusions

In conclusion, the balloon-borne, lidar and modeling studies have revealed the processes that are responsible for the formation of volcanic aerosol layer and its decay. Immediately after the eruption, within a day, homogeneous nucleation takes place giving rise to high concentrations of aerosol droplets. After nucleation the sulphuric acid-water solution droplets can grow by heterogeneous condensation of H_2SO_4 and H_2O vapours, the condensation occur-

ring first on large aerosols and then progressively on smaller aerosols. Condensation on the preexisting sulphate aerosols would increase the extinction and decrease the extinction ratio as the extinction becomes more and more dominated by large aerosols. If the amount of SO_2 injected is large, as in the case of Pinatubo, conversion of H_2SO_4 produces higher number of new small $\text{H}_2\text{SO}_4/\text{H}_2\text{O}$ aerosols and coagulation proceeds at a faster rate. Thus the condensation of H_2SO_4 on the already existing $\text{H}_2\text{SO}_4/\text{H}_2\text{O}$ droplets and subsequent coagulation is one of the principal mechanisms for the formation of larger aerosol particles. Once the aerosol grows to a few microns they are removed from the stratosphere by gravitational sedimentation. Sensitivity studies conducted using the model developed show that the processes of growth and coagulation are important, in the first year or so after the eruption in maintaining the aerosol layer, whereafter when the particles grow sufficiently larger, of the order of a few microns, sedimentation becomes important. The lidar obtained aerosol mass decay results show that the aerosol size distribution has not undergone any noticeable change throughout the decay phase from 1 year to 3 years after the eruption. It is also seen that aerosol mass decayed at various rates at different altitude regimes, indicating that dynamical removal processes such as gravitational settling and horizontal dispersal act differently depending on the particle size. The faster decay time for the mass of the layer in the 25-30 km region (Figure 4.28) further corroborates this fact. Also it is observed that the integrated backscattering coefficient (IBC) of the volcanic aerosol layer decays at a faster rate than the peak scattering ratio. The faster decay rate of IBC shows that due to sedimentation the particles at low altitudes below the aerosol peak are more effectively removed from the layer while the major contribution to IBC comes from these altitudes. Though the amount of SO_2 injected by Pinatubo is more than 2 times that of El Chichon, the model study showed that the aerosol microphysical processes of growth and coagulation, have taken place faster giving rise to larger particles and hence the removal rates of these large aerosols have been faster, giving the same decay times of 3 years to both the volcanic aerosol layers.

5.2 Scope for future work

5.2.1 Tropospheric aerosols

Tropospheric aerosols are much more variable on time and space scales because of the great diversity and wide distribution of sources and their short residence times, in many ways it is more difficult to study tropospheric aerosols than stratospheric aerosols and hence the

characterisation of tropospheric aerosols continues to pose a tougher challenge. Though certain characteristics have emerged recently the global trend on tropospheric aerosols remains highly uncertain. The studies on the tropospheric aerosol started with rejuvenated zeal after the recent work of *Charlson et al.* [1992] who suggested that the anthropogenic sulphate aerosol may be forcing climate in opposition to greenhouse warming with a comparable magnitude. Long term tropospheric aerosol measurements are limited to a few stations, to suggest any systematic trend on the climatic effects of aerosols. So in order to fully understand the climatic effects of aerosols, both due to natural and anthropogenic sources and to make model assessments it is very essential to have long term data on aerosol radiative properties, for example, optical depth and a better understanding of the physical and chemical processes going on at tropospheric levels. The emphasis should be given for the determination of physical and chemical properties of aerosols, by conducting coordinated measurements. As Sun photometers are versatile and easy to use devices to determine the aerosol optical depths, these measurements can be combined with collection of aerosol particles near simultaneously and can be used to determine the mass and the chemical composition of particles for different seasons to study the seasonal dependence of aerosols and the variation of aerosol mass with respect to seasons. These measurements when combined with multiwavelength lidar vertical profiles of aerosol extinction can give the size distribution of aerosols and the dominance of the aerosol particles of different sizes at different altitudes. All these information when combined can give an excellent data set of information on the physico-chemical processes that are responsible for the formation of aerosols and their settling times.

5.2.2 Stratospheric aerosols

Studies made after major volcanic eruptions such as Mt. St. Helens, El Chichon and Mt. Pinatubo have increased our scientific awareness on various processes which are responsible for the formation of aerosol layer at stratospheric altitudes, evolution and its decay and the radiative-chemical- dynamical influences, combined with technological advancements, in terms of techniques available to determine aerosol characteristics and fast computational facilities. This gives a confidence to say that now the volcanic aerosol layer formation and decay seems to be well understood. However, certain outstanding scientific issues regarding the properties of stratospheric aerosols and their roles in global change problems can be pointed out. First and foremost is regarding the background sulphate aerosol mass increase due to anthropogenic emissions, particularly due to high altitude commercial aircrafts [*Hofmann*,

1990]. Regarding volcanic aerosols, the precise composition of them is not known for evaluating heterogeneous chemistry in the stratosphere and do they act as nuclei for the formation of cirrus clouds in the upper troposphere, is also not clear.

Finally as has been commented upon earlier, large gaps exist in the knowledge of anthropogenic aerosols due to lack of data, which prevents quantification of their influence for use in climate models. Need of the hour therefore, is a study of coupling of the physical-chemical processes that produce them and the meteorological processes that distribute and remove them with the physical and optical characteristics that determine the radiative transfer and cloud microphysical effects.

- Items which are important but not studied in this thesis include:

1. Heterophase chemical reactions involving aerosols, which are important in the ozone depletion problem and the possibility of such reactions occurring in the tropical stratosphere.
2. The perturbations in the temperature profile which is very important to draw a conclusion on the radiative effects of aerosols. An aerosol-induced radiative heating can cause changes in the local energy balance and in atmospheric dynamics besides causing changes in the atmospheric temperature structure [*Ramaswamy, 1988a*]. Recent model studies of *Ramaswamy and Bowen* [1994] show that the lower stratospheric thermal profile is sensitive to the tropospheric aerosols and the rate of change of temperature is found to vary as a function of altitude and optical depth. The model calculations demonstrated that changes in the concentrations of radiatively active species including aerosols can contribute to a cooling of the lower stratospheric region. Also it is clear that in addition to being a significant climate change issue in its own right, the cooling of the lower stratosphere due to changes in radiatively active species has important climatic implications involving the stratospheric hydrological cycle [*Toon et al., 1986; Ramaswamy, 1988b*] and the chemical and dynamical processes leading to ozone depletion [*Austin et al., 1992; Mahlman et al., 1993*].
3. Role of cirrus clouds in altering aerosol properties, which in turn determine cooling or warming of the Earth's surface depending on optical depth.

References

- Acharya, Y.B., A. Jayaraman, and B.H. Subbaraya, A balloon-borne sun-tracking multichannel photometer for atmospheric aerosol measurements, *Adv. Space Res.*, 5, 65-68, 1985.
- Acharya, Y.B., S.K. Banerjee, K.S. Modh, B.H. Subbaraya, J.T. Vinchhi, K.S. Appu, M.D. Bhaskar, V. Narayanan, N.P. Raghavendrarao, K. Chatterjee, C.R. Sreedharan, S.C. Garg, Y.V. Somayajulu, P. Subramanyam, K.S. Zalpuri, V.D. Grinchinko, G.A. Khokin, V.A. Kononkov, I.S. Moshnikov, Bh.V. Ramanamurthy, A.M. Selvam, P. Sikka, and R. Vijayakumar, Indo-USSR ozonesonde intercomparison experiment at Thumba-Part II, *Sci. Rep. ISRO-IMAP-SR-24-85*, 51 pp., Indian Space Research Organisation, Bangalore, India, 1985.
- Ackerman, T.P., Aerosols in climate modeling, in *Aerosols and Climate*, edited by P. V. Hobbs and M. P. McCormick, pp. 335-348, A. Deepak Publishing, Virginia, USA, 1988.
- Alkezweeny, A.J., Trend analyses of sulfur dioxide emissions and sulfate concentrations and their application to global cooling, *Atmósfera*, 8, 91-97, 1995.
- d'Almeida, G.A., P. Koepke, and E.P. Shettle, *Atmospheric aerosols: Global climatology and radiative characteristics*, 561 pp., A. Deepak Publishing, Virginia, USA, 1991.
- Angreji, P.D., Revaluation of Total ozone measurements with Dobson Spectrophotometer at Mt. Abu/Ahmedabad during 1951-1985, *Sci. Rep. ISRO-PRL-SR-34-89*, 34 pp., Indian Space Research Organisation, Bangalore, India, 1989.
- Ångström, A., Techniques of determining the turbidity of the atmosphere, *Tellus*, 13, 214-223, 1961.
- Asano, S., A. Uchiyama, and M. Shiobara, Spectral optical thickness and size distribution of the Pinatubo volcanic aerosols as estimated by ground-based sunphotometry, *J. Meteorol. Soc. Japan*, 71, 165-173, 1993.

- Ashok, N.M., H.C. Bhatt, T. Chandrasekhar, and J.N. Desai, Twilight IR brightening over India due to El Chichón's eruption in Mexico, *Nature*, 300, 620-621, 1982.
- Austin, J., N. Butchart, and K.P. Shine, Probability of an Arctic ozone hole in a doubled CO₂ climate, *Nature*, 360, 221-225, 1992.
- Avdyushin, S.I., G.F. Tulinov, M.S. Ivanov, B.N. Kuzmenko, I.R. Mezhuev, B. Nardi, A. Hauchecorne, and M.-L. Chanin, 1. Spatial and temporal evolution of the optical thickness of the Pinatubo aerosol cloud in the northern hemisphere from a network of ship-borne and stationary lidars, *Geophys. Res. Lett.*, 20, 1963-1966, 1993.
- Bakan, S., A. Chlond, U. Cubasch, J. Feichter, H. Graf, H. Grassl, K. Hasselmann, I. Kirchner, M. Latif, E. Roeckner, R. Sausen, U. Schlese, D. Schrieffer, I. Schult, U. Schumann, F. Sielmann, and W. Welke, Climate response to smoke from the burning oil wells in Kuwait, *Nature*, 351, 367-371, 1991.
- Bekki, S., and J.A. Pyle, Two-dimensional modeling study of the volcanic eruption of Mount Pinatubo, *J. Geophys. Res.*, 99, 18,861-18,869, 1994.
- Bigg, E.K., Size distributions of stratospheric aerosols and their variations with altitude and time, *J. Atmos. Sci.*, 33, 1080-1086, 1976.
- Bluth, G.J.S., S.D. Doiron, A.J. Krueger, L.S. Walter, and C.C. Schnetzler, Global tracking of the SO₂ clouds from the June 1991 Mount Pinatubo eruptions, *Geophys. Res. Lett.*, 19, 151-154, 1992.
- Browning, K.A., R.J. Allam, S.P. Ballard, R.T.H. Barnes, D.A. Bennetts, R.H. Maryon, P.J. Mason, D. McKenna, J.F.B. Mitchell, C.A. Senior, A. Slingo, and F.B. Smith, Environmental effects from burning oil wells in Kuwait, *Nature*, 350, 363-367, 1991.
- Bullrich, K., Scattered radiation in the atmosphere, *Adv. Geophys.*, 10, 99-260, 1964.
- Cadle, R.D., and G.W. Grams, Stratospheric aerosol particles and their optical properties, *Rev. Geophys. Space Phys.*, 13, 475-501, 1975.
- Capone, L.A., O.B. Toon, R.C. Whitten, R.P. Turco, C.A. Riegel, and K. Santhanam, A two-dimensional model simulation of the El Chichon volcanic eruption cloud, *Geophys. Res. Lett.*, 10, 1053-1056, 1983.

- Charlson, R.J., S.E. Schwartz, J.M. Hales, R.D. Cess, J.A. Coakley, Jr., J.E. Hansen, and D.J. Hofmann, Climate forcing by anthropogenic aerosols, *Science*, 255, 423-430, 1992.
- Charlson, R.J., J.E. Lovelock, M.O. Andreae, and S.G. Warren, Oceanic phytoplankton, atmospheric sulphur, cloud albedo and climate, *Nature*, 326, 655-661, 1987.
- Chuan, R.L., Rapid measurement of particulate size distribution in the atmosphere, in *Fine particles: Aerosol Generation, Measurement, Sampling and Analysis*, edited by B. Y. H. Liu, pp. 763-775, Academic Press, New York, USA, 1976.
- Crutzen, P.J., The possible importance of CSO for the sulfate layer of the stratosphere, *Geophys. Res. Lett.*, 3, 73-76, 1976.
- Crutzen, P.J., The influence of nitrogen oxides on the atmospheric ozone content, *Quart. J. R. Meteorol. Soc.*, 96, 320-325, 1970.
- D'Altorio, A., F. Masci, V. Rizzi, G. Visconti, and M. Verdecchia, Continuous lidar measurements of stratospheric aerosols and ozone after the Pinatubo eruption Part II: Time evolution of ozone profiles and of aerosol properties, *Geophys. Res. Lett.*, 20, 2869-2872, 1993.
- Damle, S.V., TIFR National balloon facility - Evolution and usage, *Indian J. Radio Space Phys.*, 20, 161-168, 1991.
- Damle, S.V., G.S. Gokhale, and R.T. Redkar, Present status and new trends in scientific ballooning in India, *Adv. Space. Res.*, 3, 101-104, 1983.
- Davies, C.N., Size distribution of atmospheric particles, *J. Aerosol Sci.*, 5, 293-300, 1974.
- de Bary, E., and F. Rossler, Size distributions of atmospheric aerosols derived from scattered radiation measurements aloft, *J. Geophys. Res.*, 71, 1011-1016, 1966.
- Deepak, A., and R. Adams, Photography and photographic-photometry of the solar aureole, *Appl. Opt.*, 22, 1646-1654, 1983.
- DeFoor, T., E. Robinson, and S. Ryan, Early lidar observations of the June 1991 Pinatubo eruption plume at Mauna Loa observatory, Hawaii, *Geophys. Res. Lett.*, 19, 187-190, 1992.
- Deirmendjian, D., Scattering and polarization properties of water clouds and hazes in the visible and infrared, *Appl. Opt.*, 3, 187-196, 1964.

- Delmas, R.J., Environmental information from ice cores, *Rev. Geophys.*, 30, 1-21, 1992.
- Deshler, T., B.J. Johnson, and W.R. Rozier, Balloonborne measurements of Pinatubo aerosol during 1991 and 1992 at 41°N: Vertical profiles, size distribution, and volatility, *Geophys. Res. Lett.*, 20, 1435-1438, 1993.
- Deshler, T., D.J. Hofmann, B.J. Johnson, and W.R. Rozier, Balloonborne measurements of the Pinatubo aerosol size distribution and volatility at Laramie, Wyoming during the summer of 1991, *Geophys. Res. Lett.*, 19, 199-202, 1992.
- Devara, P.C.S., P.E. Raj, S. Sharma, and G. Pandithurai, Lidar-observed long-term variations in urban aerosol characteristics and their connection with meteorological parameters, *Int. J. Clim.*, 14, 581-591, 1994.
- Devara, P.C.S., and P.E. Raj, Study of atmospheric aerosols in a terrain-induced nocturnal boundary layer using bistatic lidar, *Atmos. Environ.*, 25, 655-660, 1991.
- Donovan, D.P., J. A. Whiteway, and A. I. Carswell, Corrections for non linear photon-counting effects in lidar system, *Appl. Opt.*, 32, 6742-6753, 1993.
- Dutton, E.G., and J.R. Christy, Solar radiative forcing at selected locations and evidence for global lower tropospheric cooling following the eruptions of El Chichón and Pinatubo, *Geophys. Res. Lett.*, 19, 2313-2316, 1992.
- Elterman, L., Vertical attenuation model with eight surface meteorological ranges 2 to 13 kilometers, *Rep. AFCRL-70-0200*, Air Force Cambridge Research Labs, Massachusetts, USA, 1970.
- Elterman, L., Aerosol measurement in the troposphere and stratosphere, *Appl. Opt.*, 5, 1769-1776, 1966.
- Farlow, N.H., G.V. Ferry, H.Y. Lem, and D.M. Hayes, Latitudinal variations of stratospheric aerosols, *J. Geophys. Res.*, 84, 733-743, 1979.
- Fernald, F.G., Analysis of atmospheric lidar observations: some comments, *Appl. Opt.*, 23, 652-653, 1984.
- Fiocco, G., and G. Grams, Observations of the aerosol layer at 20 km by optical radar, *J. Atmos. Sci.*, 21, 323-324, 1964.

- Flowers, E.C., R.A. McCormick, and K.R. Kurfis, Atmospheric turbidity over the United States, *J. Appl. Meteorol.*, 8, 1961-1966, 1969.
- Fuchs, N.A., *The mechanics of aerosols*, 408 pp., Pergamon press, New York, USA, 1964.
- Goodman, J., K.G. Snetsinger, R.F. Pueschel, G.V. Ferry, and S. Verma, Evolution of Pinatubo aerosol near 19 km altitude over western North America, *Geophys. Res. Lett.*, 21, 1129-1132, 1994.
- Grams, G.W., In-situ measurements of scattering phase functions of stratospheric aerosol particles in Alaska during July 1979, *Geophys. Res. Lett.*, 8, 13-14, 1981.
- Grant, W.B., E.V. Browell, J. Fishman, V.G. Brackett, R.E. Veiga, D. Nganga, A. Minga, B. Cros, C.F. Butler, C.S. Long, and L.L. Stowe, Aerosol-associated changes in the tropical stratospheric ozone following the eruption of Mount Pinatubo, *J. Geophys. Res.*, 99, 8197-8211, 1994.
- Grant, W.B., J. Fishman, E.V. Browell, V.G. Brackett, D. Nganga, A. Minga, B. Cros, R.E. Veiga, C. F. Butler, M.A. Fenn, and G.D. Nowicki, Observations of reduced ozone concentrations in the tropical stratosphere after the eruption of Mt. Pinatubo, *Geophys. Res. Lett.*, 19, 1109-1112, 1992.
- Griggs, M., Satellite measurements of tropospheric aerosols, *Adv. Space Res.*, 2, 109-118, 1983.
- Hamill, P., C.S. Kiang, and R.D. Cadle, The nucleation of $\text{H}_2\text{SO}_4\text{-H}_2\text{O}$ solution aerosol particles in the atmosphere, *J. Atmos. Sci.*, 34, 150-162, 1977a.
- Hamill, P., O.B. Toon, and C.S. Kiang, Microphysical processes affecting stratospheric aerosol particles, *J. Atmos. Sci.*, 34, 1104-1119, 1977b.
- Hänel, G., The properties of atmospheric aerosol particles as functions of the relative humidity at thermodynamic equilibrium with the surrounding moist air, *Adv. Geophys.*, 19, 73-188, 1976.
- Herman, B.M., S.R. Browning, and J.A. Reagan, Determination of aerosol size distributions from lidar measurements, *J. Atmos. Sci.*, 28, 763-771, 1971.
- Hitchman, M.H., M. McKay, and C.R. Trepte, A climatology of stratospheric aerosol, *J. Geophys. Res.*, 99, 20,689-20,700, 1994.

- Hofmann, D.J., S.J. Oltmans, W.D. Komhyr, J.M. Harris, J.A. Lathrop, A.O. Langford, T. Deshler, B.J. Johnson, A. Torres, and W.A. Matthews, Ozone loss in the lower stratosphere over the United States in 1992-1993: Evidence for heterogeneous chemistry on the Pinatubo aerosol, *Geophys. Res. Lett.*, *21*, 65-68, 1994.
- Hofmann, D.J., Twenty years of balloon-borne tropospheric aerosol measurements at Laramie, Wyoming, *J. Geophys. Res.*, *98*, 12,753-12,766, 1993.
- Hofmann, D.J., Increase in the stratospheric background sulfuric acid aerosol mass in the past 10 years, *Science*, *248*, 996-1000, 1990.
- Hofmann, D.J., and S. Solomon, Ozone destruction through heterogeneous chemistry following the eruption of El Chichon, *J. Geophys. Res.*, *94*, 5029-5041, 1989.
- Hofmann, D.J., Aerosols from past and present volcanic emissions, in *Aerosols and Climate*, edited by P. V. Hobbs and M. P. McCormick, pp. 195-214, A. Deepak Publishing, Virginia, USA, 1988.
- Hofmann, D.J., Perturbations to the global atmosphere associated with the El Chichon volcanic eruption of 1982, *Rev. Geophys.*, *25*, 743-759, 1987.
- Hofmann, D.J., and J.M. Rosen, On the temporal variation of stratospheric aerosol size and mass during the first 18 months following the 1982 eruptions of El Chichón, *J. Geophys. Res.*, *89*, 4883-4890, 1984.
- Hofmann, D.J., and J.M. Rosen, Stratospheric sulfuric acid fraction and mass estimate for the 1982 volcanic eruption of El Chichon, *Geophys. Res. Lett.*, *10*, 313-316, 1983.
- Hofmann, D.J., and J.M. Rosen, Balloon-borne observations of stratospheric aerosol and condensation nuclei during the year following the Mt. St. Helens eruption, *J. Geophys. Res.*, *87*, 11,039-11,061, 1982.
- Holland, A.C., and G. Gagne, The scattering of polarized light by polydisperse systems of irregular particles, *Appl. Opt.*, *9*, 1113-1121, 1970.
- Horvath, H., Atmospheric light absorption - A review, *Atmos. Environ.*, *27*, 293-317, 1993.
- Hudson, R.D., *Infrared system engineering*, 642 pp., Wiley Inter Science, New York, USA, 1969.
- Jaenicke, R., and L. Schütz, Comprehensive study of physical and chemical properties of the surface aerosols in the Cape Verde Islands region, *J. Geophys. Res.*, *83*, 3585-3599, 1978.

- Jäger, H., O. Uchino, T. Nagai, T. Fujimoto, V. Freudenthaler, and F. Homburg, Ground-based remote sensing of the decay of the Pinatubo eruption cloud at three northern hemisphere sites, *Geophys. Res. Lett.*, **22**, 607-610, 1995.
- Jäger, H., The Pinatubo eruption cloud observed by lidar at Garmisch-Partenkirchen, *Geophys. Res. Lett.*, **19**, 191-194, 1992.
- Jäger, H., and D.J. Hofmann, Midlatitude lidar backscatter to mass, area, and extinction conversion model based on *in situ* aerosol measurements from 1980 to 1987, *Appl. Opt.*, **30**, 127-138, 1991.
- Jäger, H., M. Littfass, D.J. Hofmann, and J.M. Rosen, Stratospheric extinction and mass variations after a major volcanic eruption, derived from lidar measurements at northern midlatitudes, in *Aerosols and Climate*, edited by P. V. Hobbs and M. P. McCormick, pp. 215-222, A. Deepak Publishing, Virginia, USA, 1988.
- Jäger, H., and W. Carnuth, The decay of the El Chichon stratospheric perturbation, observed by lidar at northern midlatitudes, *Geophys. Res. Lett.*, **14**, 696-699, 1987.
- Jayaraman, A., Y.B. Acharya, B.H. Subbaraya, and H. Chandra, Nd:YAG backscatter lidar at Ahmedabad (23°N, 72.5°E) for tropical middle atmospheric studies, *Appl. Opt.*, **34**, 6937-6940, 1995a.
- Jayaraman, A., S. Ramachandran, Y.B. Acharya, and B.H. Subbaraya, Pinatubo volcanic aerosol layer decay observed at Ahmedabad (23°N), India, using neodymium:yttrium/ aluminium /garnet backscatter lidar, *J. Geophys. Res.*, **100**, 23,209-23,214, 1995b.
- Jayaraman, A., Role of middle atmosphere coupling processes in ozone change, *Current Sci.*, **64**, 666-672, 1993.
- Jayaraman, A., and B.H. Subbaraya, Insitu measurements of aerosol extinction profiles and their spectral dependencies at tropospheric levels, *Tellus*, **45B**, 473-478, 1993a.
- Jayaraman, A., and B.H. Subbaraya, Monitoring of aerosol content over ocean surfaces using INSAT data, in *Advances in Tropical Meteorology: Monsoon variability, Satellite applications and Modelling*, edited by R. N. Keshavamurty and P. C. Joshi, pp. 356-365, Tata McGraw-Hill Publishing, New Delhi, India, 1993b.
- Jayaraman, A., and P. Koepke, Accounting for the multiple-scattering effect in radiation intensities at the top of the atmosphere, *Appl. Opt.*, **31**, 3473-3480, 1992.

- Jayaraman, A., Results on aerosol measurements from balloons, *Indian J. Radio Space Phys.*, 20, 290-294, 1991.
- Jayaraman, A., and B.H. Subbaraya, Rocket and balloon measurements of the vertical distribution of aerosols in the Indian tropical region, in *Aerosols and Climate*, edited by P. V. Hobbs and M. P. McCormick, pp. 117-124, A. Deepak Publishing, Virginia, USA, 1988.
- Jayaraman, A., B.H. Subbaraya, and Y.B. Acharya, The vertical distribution of aerosol concentration and size distribution function over the tropics and their role in radiation transfer, *Phys. Scr.*, 36, 358-361, 1987.
- Johnson, D.W., C.G. Kilsby, D.S. McKenna, R.W. Saunders, G.J. Jenkins, F.B. Smith, and J.S. Foot, Airborne observations of the physical and chemical characteristics of the Kuwait oil smoke plume, *Nature*, 353, 617-621, 1991.
- Joshi, M.N., Balloon flight operations, *Indian J. Radio Space Phys.*, 20, 176-181, 1991.
- Junge, C.E., Air chemistry and radioactivity, *Int. Geophys. Ser.*, 4, 111-208, 1963.
- Junge, C.E., and J.E. Manson, Stratospheric aerosol studies, *J. Geophys. Res.*, 66, 2163-2182, 1961.
- Junge, C.E., C.W. Chagnon, and J.E. Manson, Stratospheric aerosols, *J. Meteorol.*, 18, 81-108, 1961.
- Junge, C.E., Atmospheric Chemistry, *Adv. Geophys.*, 4, 1-108, 1958.
- Kasten, F., The falling speed of aerosol particles, *J. Appl. Meteorol.*, 7, 944-947, 1968.
- Kaufman, Y.J., R.S. Fraser, and R.L. Mahoney, Fossil fuel and biomass burning effect on climate-heating or cooling?, *J. Climate*, 4, 578-588, 1991.
- Kaufman, Y.J., R.S. Fraser, and R.A. Ferrare, Satellite measurements of large-scale air pollution: methods, *J. Geophys. Res.*, 95, 9895-9909, 1990.
- Kent, G.S., M.P. McCormick, and P.H. Wang, Validation of stratospheric aerosol and gas experiments I and II satellite aerosol optical depth measurements using surface radiometer data, *J. Geophys. Res.*, 99, 10,333-10,339, 1994.
- Kent, G.S., M.P. McCormick, and S.K. Schaffner, Global optical climatology of the free tropospheric aerosol from 1.0- μm satellite occultation measurements, *J. Geophys. Res.*, 96, 5249-5267, 1991.

- Kent, G.S., and M.P. McCormick, SAGE and SAM II measurements of the global stratospheric aerosol optical depth, *J. Geophys. Res.*, **89**, 5303-5314, 1984.
- Kerr, R.A., Study unveils climate cooling caused by pollutant haze, *Science*, **268**, 802, 1995.
- Khemani, L.T., Physical and chemical characteristics of atmospheric aerosols, in *Air pollution Control*, edited by P. N. Cheremisinoff, pp. 401-452, Vol. 2, Encyclopedia of Environmental control techniques, Gulf Publishing, USA, 1989.
- Khemani, L.T., G.A. Momin, M.S. Naik, R. Vijayakumar, and Bh.V. Ramanamurthy, Chemical composition and size distribution of atmospheric aerosols over the Deccan Plateau, India, *Tellus*, **34**, 151-158, 1982.
- Kiehl, J.T., and B.P. Briegleb, The relative roles by Sulfate aerosols and Greenhouse gases in Climate forcing, *Science*, **260**, 311-314, 1993.
- King, M.D., D.M. Byrne, B.M. Herman, and J.A. Reagan, Aerosol size distributions obtained by inversion of spectral optical depth measurements, *J. Atmos. Sci.*, **35**, 2153-2167, 1978.
- Kinne, S., O.B. Toon, and M.J. Prather, Buffering of stratospheric circulation by changing amounts of tropical ozone A Pinatubo case study, *Geophys. Res. Lett.*, **19**, 1927-1930, 1992.
- Kirchner, S., and R.J. Delmas, A 1000yr glaciochemical study at the South pole, *Ann. Glaciol.*, **10**, 80-84, 1988.
- Klett, J.D., Lidar inversion with variable backscatter/extinction ratios, *Appl. Opt.*, **24**, 1638-1643, 1985.
- Koepke, P., and M. Hess, Scattering functions of tropospheric aerosols: the effects of non-spherical particles, *Appl. Opt.*, **27**, 2422-2430, 1988.
- Kremser, H., P. Koepke, and H. Quenzel, Aerosol optical thickness from direct solar radiation: Improved Langley method applied to measured data, in *IRS '84: Current problems in atmospheric radiation, Proceedings of the International radiation Symposium*, pp. 46-49, A. Deepak Publishing, Virginia, USA, 1984.
- Krishna Moorthy, K., Prabha R. Nair, B.S.N. Prasad, N. Muralikrishnan, H.B. Gayathri, B. Narasimha Murthy, K. Niranjana, V. Ramesh Babu, G.V. Satyanarayana, V.V. Agashe, G.R. Aher, Risal Singh, and B.N. Srivastava, Results from the MWR network of IMA, *Indian J. Radio Space Phys.*, **22**, 243-258, 1993.

- Krishna Moorthy, K., Prabha R. Nair, and B.V. Krishna Murthy, Size distribution of coastal aerosols: Effects of local sources and sinks, *J. Appl. Meteorol.*, 30, 1844-1852, 1991.
- Krishna Moorthy, K., Prabha R. Nair, and B.V. Krishna Murthy, Multiwavelength solar radiometer network and features of aerosol spectral optical depth at Trivandrum, *Indian J. Radio Space Phys.*, 18, 194-201, 1989.
- Krishna Murthy, B.V., Aerosols and radiation budget in the middle atmosphere, *Indian J. Radio Space Phys.*, 17, 203-219, 1988.
- Krueger, A., M. Schoeberl, P. Newman, and R. Stolarski, The 1991 Antarctic ozone hole; TOMS observations, *Geophys. Res. Lett.*, 19, 1215-1218, 1992.
- Labitzke, K., and M.P. McCormick, Stratospheric temperature increases due to Pinatubo aerosols, *Geophys. Res. Lett.*, 19, 207-210, 1992.
- Lacis, A., J. Hansen, and M. Sato, Climate forcing by stratospheric aerosols, *Geophys. Res. Lett.*, 19, 1607-1610, 1992.
- Lal, S., B.H. Subbaraya, Y.B. Acharya, S.V. Ramani, R. Borchers, and P. Fabian, Vertical distribution of ozone over Hyderabad using a balloon-borne suntracking photometer, in *Ozone in the atmosphere*, edited by R. D. Bojkov and P. Fabian, pp. 136-139, A. Deepak publishing, Virginia, USA, 1989.
- Lamb, H.H., Volcanic dust in the atmosphere; with a chronology and assessment of its meteorological significance, *Philos. Trans. R. Soc. London A*, 266, 425-533, 1970.
- Lambert, A., R.G. Grainger, J.J. Remedios, C.D. Rodgers, M. Corney, and F.W. Taylor, Measurements of the evolution of the Mt. Pinatubo aerosol cloud by ISAMS, *Geophys. Res. Lett.*, 20, 1287-1290, 1993.
- Legrand, M., and R.J. Delmas, The ionic balance of Antarctic snow: A 10yr detailed record, *Atmos. Environ.*, 18, 1867-1874, 1984.
- Lenoble, J., and C. Brogniez, Information on stratospheric aerosol characteristics contained in the SAGE satellite multiwavelength measurements, *Appl. Opt.*, 24, 1054-1063, 1985.
- Lenoble, J., and C. Brogniez, A comparative review of radiation aerosol models, *Contr. Atmos. Phys.*, 57, 1-20, 1984.

- Mahlman, J.D., J.P. Pinto, and L.J. Umscheid, Transport, radiative and dynamical effects of the Antarctic ozone hole: A GFDL “SKYHI” model experiment, *J. Atmos. Sci.*, *51*, 489-508, 1993.
- Mani, A., and O. Chacko, Measurements of solar radiation and atmospheric turbidity with Ångström pyrhelimeters at Poona and Delhi during the I.G.Y., *Indian J. Meteorol. Geophys.*, *14*, 270-282, 1963.
- McCormick, M.P., and R.E. Veiga, SAGE II measurements of early Pinatubo aerosols, *Geophys. Res. Lett.*, *19*, 155-158, 1992.
- McCormick, M.P., P. Hamill, T.J. Pepin, W.P. Chu, T.J. Swissler, and L.R. McMaster, Satellite studies of the stratospheric aerosol, *Bull. Amer. Meteorol. Soc.*, *60*, 1038-1046, 1979.
- McPeters, R.D., The atmospheric SO₂ budget for Pinatubo derived from NOAA-11 SBUV/2 spectral data, *Geophys. Res. Lett.*, *20*, 1971-1974, 1993.
- Michalsky, J.J., E.W. Pearson, and B.A. LeBaron, An assessment of the impact of volcanic eruptions on the northern hemisphere's aerosol burden during the last decade, *J. Geophys. Res.*, *95*, 5677-5688, 1990.
- Minnis, P., E.F. Harrison, L.L. Stowe, G.G. Gibson, F.M. Denn, D.R. Doeling, and W.L. Smith, Jr., Radiative climate forcing by the Mount Pinatubo eruption, *Science*, *259*, 1411-1415, 1993.
- Molina, M.J., and F.S. Rowland, Stratospheric sink for chlorofluoromethanes: chlorine atom catalysed destruction of ozone, *Nature*, *249*, 810-812, 1974.
- Mossop, S.C., Volcanic dust collected at an altitude of 20 km, *Nature*, *203*, 824-827, 1964.
- Nardi, B., M.-L. Chanin, A. Hauchecorne, S.I. Avdyushin, G.F. Tulinov, M.S. Ivanov, B.N. Kuzmenko, and I.R. Mezhuev, 2. Morphology and dynamics of the Pinatubo aerosol layer in the northern hemisphere as detected from a ship-borne lidar, *Geophys. Res. Lett.*, *20*, 1967-1970, 1993.
- Negi, B.S., S. Sadasivan, and U.C. Mishra, Aerosol composition and sources in urban areas in India, *Atmos. Environ.*, *21*, 1259-1266, 1987.
- Newkirk, G., Jr., and J.A. Eddy, Light scattering particles in the upper atmosphere, *J. Atmos. Sci.*, *21*, 35-60, 1964.

- Nicolet, M., Solar spectral irradiances with their diversity between 120 and 900 nm, *Plan. Space Sci.*, 10, 1249-1289, 1989.
- Parameswaran, K., K.O. Rose, B.V. Krishna Murthy, M.T. Osborn, and L.R. McMaster, Comparison of Lidar and SAGE II data at a tropical station, *J. Geophys. Res.*, 96, 10,861-10,866, 1991.
- Parameswaran, K., K.O. Rose, and B.V. Krishna Murthy, Aerosol characteristics from bistatic lidar observations, *J. Geophys. Res.*, 89, 2541-2552, 1984.
- Penndorf, R., Tables of refractive index for standard air and the Rayleigh scattering co-efficient for the spectral region between 0.2 and 20.0 μm and their application to atmospheric optics, *J. Opt. Soc. America*, 47, 176-182, 1957.
- Pinker, R.T., G. Idemudia, and T.O. Aro, Characteristic aerosol optical depths during the Harmattan season on sub-Sahara Africa, *Geophys. Res. Lett.*, 21, 685-688, 1994.
- Pinnick, R.G., J.M. Rosen, and D.J. Hofmann, Stratospheric aerosol measurements, III: Optical model calculations, *J. Atmos. Sci.*, 33, 304-314, 1976.
- Pinto, J.P., R.P. Turco, and O.B. Toon, Self-limiting physical and chemical effects in volcanic eruption clouds, *J. Geophys. Res.*, 94, 11,165-11,174, 1989.
- Pollack, J.B., O.B. Toon, and D. Wiedman, Radiative properties of the background stratospheric aerosols and implications for perturbed conditions, *Geophys. Res. Lett.*, 8, 26-28, 1981.
- Prospero, J.M., R.J. Charlson, V. Mohnen, R. Jaenicke, A.C. Delany, J. Moyers, W. Zoller, and K. Rahn, The atmospheric aerosol system: An overview, *Rev. Geophys. Space Phys.*, 21, 1607-1629, 1983.
- Pudykiewicz, J.A., and P.A. Dastoor, On numerical simulation of the global distribution of sulfate aerosol produced by a large volcanic eruption, *J. Climate*, 8, 464-473, 1995.
- Pueschel, R.F., L. Machta, F.G. Cotton, E.C. Flowers, and J.T. Potterson, Normal incidence radiation trends on Mauna Loa, Hawaii, *Nature*, 240, 545-547, 1972.
- Quenzel, H., Passive remote sensing of aerosols from space now and in the future, *Adv. Space Res.*, 2, 19-28, 1983.

- Raj, P.E., and P.C.S. Devara, Some results of lidar aerosol measurements and their relationship with meteorological parameters, *Atmos. Environ.*, 23, 831-838, 1989.
- Ramachandran, S., A. Jayaraman, Y.B. Acharya, and B.H. Subbaraya, Features of aerosol optical depths over Ahmedabad as observed with a Sun-tracking photometer, *Contr. Atmos. Phys.*, 67, 57-70, 1994a.
- Ramachandran, S., A. Jayaraman, Y.B. Acharya, and B.H. Subbaraya, Balloon-borne photometric studies of the stratospheric aerosol layer after Mt. Pinatubo eruption, *J. Geophys. Res.*, 99, 16,771-16,777, 1994b.
- Ramachandran, S., A. Jayaraman, Y.B. Acharya, and B.H. Subbaraya, Mode radius and asymmetry factor of Mt. Pinatubo volcanic aerosols from balloon-borne optical measurements over Hyderabad during October 1991, *Geophys. Res. Lett.*, 21, 2011-2014, 1994c.
- Ramaswamy, V., and M. Bowen, Effect of radiatively active species upon the lower stratospheric temperatures, *J. Geophys. Res.*, 99, 18,909-18,921, 1994.
- Ramaswamy, V., Aerosol radiative forcing and model responses, in *Aerosols and Climate*, edited by P. V. Hobbs and M. P. McCormick, pp. 349-372, A. Deepak Publishing, Virginia, USA, 1988a.
- Ramaswamy, V., Dehydration mechanism in the Antarctic winter stratosphere, *Geophys. Res. Lett.*, 15, 863-866, 1988b.
- Rangarajan, S., Wavelength exponent for haze scattering in the tropics as determined by photoelectric photometers, *Tellus*, 24, 56-64, 1972.
- Read, W.G., L. Froidevaux, and J.W. Waters, Microwave Limb Sounder measurements of stratospheric SO₂ from the Mt. Pinatubo volcano, *Geophys. Res. Lett.*, 20, 1299-1302, 1993.
- Robinson, E., and T. DeFoor, Stratospheric aerosol conditions over Mauna Loa during recent quiescent volcanic periods, in *Aerosols and Climate*, edited by P. V. Hobbs and M. P. McCormick, pp. 325-334, A. Deepak publishing, Virginia, USA, 1988.
- Rosen, J.M., N.T. Kjöme, R.L. McKenzie, and J.B. Liley, Decay of Mount Pinatubo aerosol at midlatitudes in the northern and southern hemispheres, *J. Geophys. Res.*, 99, 25,733-25,739, 1994.

- Rosen, J.M., and D.J. Hofmann, Optical modeling of stratospheric aerosols: present status, *Appl. Opt.*, 25, 410-419, 1986.
- Rosen, J.M., D.J. Hofmann, and S.P. Singh, A steady-state stratospheric aerosol model, *J. Atmos. Sci.*, 35, 1304-1313, 1978.
- Rosen, J.M., D.J. Hofmann, and J. Laby, Stratospheric aerosol measurements II: the world-wide distribution, *J. Atmos. Sci.*, 32, 1457-1462, 1975.
- Rosen, J.M., The vertical distribution of dust to 30 kilometers, *J. Geophys. Res.*, 69, 4673-4676, 1964.
- Russell, P.B., M.P. McCormick, T.J. Swissler, J.M. Rosen, D.J. Hofmann, and L.R. McMaster, Satellite and correlative measurements of the stratospheric aerosol. III: Comparison of measurements by SAM II, SAGE, Dustsondes, Filters, Impactors and Lidar, *J. Atmos. Sci.*, 41, 1791-1800, 1984.
- Russell, P.B., T.J. Swissler, M.P. McCormick, W.P. Chu, J.M. Livingston, and T.J. Pepin, Satellite and correlative measurements of the stratospheric aerosol. I: An optical model for data conversions, *J. Atmos. Sci.*, 38, 1279-1294, 1981.
- Russell, P.B., and R.D. Hake, Jr., The post-Fuego stratospheric aerosol : Lidar measurements, with radiative and thermal implications, *J. Atmos. Sci.*, 34, 163-177, 1977.
- Sarkar, S.K., H.N. Dutta, P.K. Pasricha, and B.M. Reddy, *Atlas of tropospheric water vapour over the Indian subcontinent*, 164 pp., National Physical Laboratory, New Delhi, India, 1982.
- Sasi, M.N., and K. Sengupta, A reference atmosphere for Indian equatorial zone from surface to 80 km-1985, *Sci. Rep. SPL:SR:006:85*, 36 pp., Vikram Sarabhai Space Centre, Thumba, India, 1986.
- Sasi, M.N., and K. Sengupta, A model equatorial atmosphere over the Indian zone from 0 to 80 km, *Tech. Rep. VSSC-TR-46*, 45 pp., Vikram Sarabhai Space Centre, Thumba, India, 1979.
- Shaw, G.E., Sun photometry, *Bull. Ame. Meteorol. Soc.*, 64, 4-10, 1983.
- Shaw, G.E., Atmospheric ozone: Determination by Chappuis-Band absorption, *J. Appl. Meteorol.*, 10, 1335-1339, 1979.

- Shaw, G.E., Error analysis of multi-wavelength sun photometry, *Pure Appl. Geophys.*, 114, 1-14, 1976.
- Sheridan, P.J., R.C. Schnell, and D.J. Hofmann, Electron microscope studies of Mt. Pinatubo aerosol layers over Laramie, Wyoming during summer 1991, *Geophys. Res. Lett.*, 19, 203-206, 1992.
- Shettle, E.P., and R.W. Fenn, Models for the aerosols and the effects of humidity variations on their optical properties, *Pap. 675, AFGL-TR-079-0214*, 94 pp., Air Force Geophysics Laboratory, Massachusetts, USA, 1979.
- Shibata, T., T. Itabe, K. Mizutani, and K. Asai, Pinatubo volcanic aerosols observed by lidar at Wakkanai, Japan, *Geophys. Res. Lett.*, 21, 197-200, 1994.
- Shimizu, H., Y. Sasano, H. Nakane, N. Sugimoto, I. Matsui, and N. Takeuchi, Large scale laser radar for measuring aerosol distribution over a wide area, *Appl. Opt.*, 24, 617-626, 1985.
- Stowe, L.L., R.M. Carey, and P.P. Pellegrino, Monitoring of the Pinatubo aerosol layer with NOAA/11 AVHRR data, *Geophys. Res. Lett.*, 19, 159-162, 1992.
- Subbaraya, B.H., and A. Jayaraman, Aerosol concentrations and size distributions in the troposphere and lower stratosphere over Thumba, *Pure Appl. Geophys.*, 120, 407-421, 1982.
- Takamura, T., Y. Sasano, and T. Hayasaka, Tropospheric aerosol optical properties derived from lidar, sun photometer, and optical particle counter measurements, *Appl. Opt.*, 33, 7132-7140, 1994.
- Tanaka, M., T. Nakazawa, and M. Fukabori, Absorptions of the $\rho\sigma\tau$, $0.8\ \mu\text{m}$ and α bands of the water vapor, *J. Quant. Spec. Rad. Transfer*, 28, 463-470, 1982.
- Thekaekara, M.P., and A.J. Drummond, Standard values for the solar constant and its spectral components, *Nature Phy. Science*, 229, 6-9, 1971.
- Thomas, L., C.P. Chaloner, and S.K. Bhattacharyya, Laser-radar measurements in southern England of aerosols from Mount St Helens, *Nature*, 289, 473, 1981.
- Thomason, L.W., Observations of a new SAGE II aerosol extinction mode following the eruption of Mt. Pinatubo, *Geophys. Res. Lett.*, 19, 2179-2182, 1992.
- Thomason, L.W., and M.T. Osborn, Lidar conversion parameters derived from SAGE II extinction measurements, *Geophys. Res. Lett.*, 19, 1655-1658, 1992.

- Tie, X.X., G. Brasseur, B. Brieglab, and C. Granier, Two-dimensional simulation of Pinatubo aerosol and its effect on stratospheric ozone, *J. Geophys. Res.*, 99, 20,545-20,562, 1994.
- Tie, X.X., X. Lin, and G. Brasseur, Two-dimensional coupled dynamical/chemical/ micro-physical simulation of global distribution of El Chichón volcanic aerosols, *J. Geophys. Res.*, 99, 16,779-16,792, 1994.
- Toon, O.B., P. Hamill, R.P. Turco, and J.P. Pinto, Condensation of HNO_3 and HCl in the polar stratosphere, *Geophys. Res. Lett.*, 13, 1284-1287, 1986.
- Toon, O.B., R.P. Turco, P. Hamill, C.S. Kiang, and R.C. Whitten, A one-dimensional model describing aerosol formation and evolution in the stratosphere: II. Sensitivity and comparison with observations, *J. Atmos. Sci.*, 36, 718-736, 1979.
- Toon, O.B., and J.B. Pollack, A global average model of atmospheric aerosols for radiative transfer calculations, *J. Appl. Meteorol.*, 15, 225-246, 1976.
- Trepte R. T., L. W. Thomason, and G. S. Kent, Banded structures in stratospheric aerosol distributions, *Geophys. Res. Lett.*, 21, 2397-2400, 1994.
- Trepte, C.R., R.E. Veiga, and M.P. McCormick, The poleward dispersal of Mount Pinatubo volcanic aerosol, *J. Geophys. Res.*, 98, 18,563-18,573, 1993.
- Turco, R.P., K. Drdla, A. Tabazadeh, and P. Hamill, Heterogeneous chemistry of polar stratospheric clouds and volcanic aerosols, in *The role of the stratosphere in global change*, edited by M. -L. Chanin, pp. 65-134, Vol. 8, NATO ASI Series, Springer-Verlag, Berlin, Germany, 1993.
- Turco, R.P., O.B. Toon, R.C. Whitten, P. Hamill, and R.G. Keese, The 1980 eruptions of Mt. St. Helens: Physical and chemical processes in the stratospheric clouds, *J. Geophys. Res.*, 88, 5299-5319, 1983.
- Turco, R.P., R.C. Whitten, and O.B. Toon, Stratospheric aerosols: Observations and theory, *Rev. Geophys. Space Phys.*, 20, 233-279, 1982.
- Turco, R.P., P. Hamill, O.B. Toon, R.C. Whitten, and C.S. Kiang, A one-dimensional model describing aerosol formation and evolution in the stratosphere: I. Physical processes and mathematical analogs, *J. Atmos. Sci.*, 36, 699-717, 1979a.

- Turco, R.P., P. Hamill, O.B. Toon, R.C. Whitten, and C.S. Kiang, A one-dimensional model describing aerosol formation and evolution in the Stratosphere: I. Physical processes and computational analogs, *NASA Technical paper, 1362*, 94 pp., 1979b.
- Uchino, O., T. Nagai, T. Fujimoto, W.A. Matthews, and J. Orange, Extensive Lidar observations of the Pinatubo aerosol layers at Tsukuba (36.1°N), Naha (26.2°N), Japan and Lauder (45.0°S), New Zealand, *Geophys. Res. Lett.*, *22*, 57-60, 1995.
- U.S. Standard Atmosphere Supplements, 1966, NASA, 289 pp., U. S. Government Printing Office, Washington D.C., USA, 1966.
- Volz, F.E., and L. Sheehan, Skylight and Aerosol in Thailand During the Dry Winter Season, *Appl. Opt.*, *10*, 363-366, 1971.
- Volz, F.E., Spectral skylight and solar radiance measurements in the Caribbean: Maritime aerosols and Sahara dust, *J. Atmos. Sci.*, *27*, 1041-1047, 1970.
- Volz, F.E., and R.M. Goody, The intensity of the twilight and upper atmospheric dust, *J. Atmos. Sci.*, *19*, 385-406, 1962.
- Weller, M., and U. Leiterer, Experimental data on spectral aerosol optical thickness and its global distribution, *Contr. Atmos. Phys.*, *61*, 1-9, 1988.
- Whitby, K.T., The physical characteristics of sulfur aerosols, *Atmos. Environ.*, *12*, 135-159, 1978.
- Winker, D.M., and M.T. Osborn, Airborne lidar observations of the Pinatubo volcanic plume, *Geophys. Res. Lett.*, *19*, 167-170, 1992.
- Yue, G.K., and A. Deepak, Latitudinal and altitudinal variation of size distribution of stratospheric aerosols inferred from SAGE aerosol extinction coefficient measurements at two wavelengths, *Geophys. Res. Lett.*, *11*, 999-1002, 1984.
- Yue, G.K., and A. Deepak, Retrieval of stratospheric aerosol size distribution from atmospheric extinction of solar radiation at two wavelengths, *Appl. Opt.*, *22*, 1639-1645, 1983.
- Zhao, J.-X., R.P. Turco, and O.B. Toon, A model simulation of Pinatubo volcanic aerosols in the stratosphere, *J. Geophys. Res.*, *100*, 7315-7328, 1995.

List of Publications

1. **S. Ramachandran**, A. Jayaraman, Y.B. Acharya, and B.H. Subbaraya, Features of Aerosol optical depths over Ahmedabad as observed with a Sun-tracking photometer, *Contributions to Atmospheric Physics*, 67(1), 57-70, 1994a.
2. **S. Ramachandran**, A. Jayaraman, Y.B. Acharya, and B.H. Subbaraya, Balloon-borne photometric studies of the stratospheric aerosol layer after Mt. Pinatubo eruption, *Journal of Geophysical Research*, 99(D8), 16,771-16,777, 1994b.
3. **S. Ramachandran**, A. Jayaraman, Y.B. Acharya, and B.H. Subbaraya, Mode radius and asymmetry factor of Mt. Pinatubo volcanic aerosols from balloon-borne optical measurements over Hyderabad during October 1991, *Geophysical Research Letters*, 21(18), 2011-2014, 1994c.
4. Y.B. Acharya, A. Jayaraman, **S. Ramachandran**, and B.H. Subbaraya, Compact light-emitting-diode sun photometer for atmospheric optical depth measurements, *Applied Optics*, 34(7), 1209-1214, 1995.
5. A. Jayaraman, **S. Ramachandran**, Y.B. Acharya, and B.H. Subbaraya, Pinatubo volcanic aerosol layer decay observed at Ahmedabad (23°N), India, using neodymium:yttrium/aluminium/garnet backscatter lidar, *Journal of Geophysical Research*, 100(D11), 23,209-23,214, 1995.